2017

MECHANISMS OF HETEROGENEOUS OXIDATIONS AT MODEL AEROSOL INTERFACES BY OZONE AND HYDROXYL RADICALS

Elizabeth A. Pillar-Little
University of Kentucky, epillar86@gmail.com
Author ORCID Identifier:
 https://orcid.org/0000-0003-0444-2300
Digital Object Identifier: https://doi.org/10.13023/ETD.2017.269

Right click to open a feedback form in a new tab to let us know how this document benefits you.

MECHANISMS OF HETEROGENEOUS OXIDATIONS AT MODEL
AEROSOL INTERFACES BY OZONE AND HYDROXYL RADICALS

DISSERTATION

A dissertation submitted in partial fulfillment of the requirements for
the degree of Doctor of Philosophy in the College of Arts and Sciences
at the University of Kentucky

By

Elizabeth Ann Pillar-Little

Lexington, Kentucky

Director: Dr. Marcelo I. Guzman

Lexington, Kentucky

2017

ABSTRACT OF DISSERTATION

MECHANISMS OF HETEROGENEOUS OXIDATIONS AT MODEL AEROSOL INTERFACES BY OZONE AND HYDROXYL RADICALS

Atmospheric aerosols play an important role in climate by scattering and absorbing radiation and by serving as cloud condensation nuclei. An aerosol's optical or nucleation properties are driven by its chemical composition. Chemical aging of aerosols by atmospheric oxidants, such as ozone, alters the physiochemical properties of aerosol to become more hygroscopic, light absorbing, and viscous during transport. However the mechanism of these transformations is poorly understood. While ozone is a protective and beneficial atmospheric gas in the stratosphere, it is a potent greenhouse gas in the troposphere that traps heat near the Earth's surface. It also impacts human heath by irritating the respiratory tract and exacerbating cardiovascular diseases. Additionally, ozone can alter the ecosystem through oxidizing plant foliage which can lead to deforestation and crop losses as well. Both gases and aerosols in the troposphere can react with ozone directly and indirectly with hydroxyl radicals. While daytime aging is thought to be primarily driven by photochemical processes and hydroxyl radicals, ozone is thought to be a key player in nighttime or dark aging processes that can alter the physicochemical properties of aerosols. Measured concentrations of trace gases and aged aerosol components in the field are higher than values predicted based on laboratory studies and computer simulations. Consequently, new experimental approaches are needed to narrow the gaps between observations and mechanistic understandings.

In this dissertation, a plume of microdroplets was generated by pneumatically assisted aerosolization and then exposed to a flow of ozone before entering a mass spectrometer. This surface-specific technique allowed for the real-time analysis of reaction products and intermediates at the air-water interface. This work explores the *in situ* oxidation of iodide, a component of sea spray aerosols, by 0.05 – 13.00 ppmv ozone to explore how heterogeneous oxidation could enhance the production of reactive iodide species. Methods to study the reaction channels and intermediates were also established to not only determine a mechanism of iodide oxidation by ozone, but to enable the study of more complex systems. The developed approach was then applied to examine the oxidation of catechol and its substituted cousins, a family of compounds selected to model biomass burning and combustion emissions, at the air-water interface. While

literature suggested that the primary mechanism of catechol oxidation by ozone would be the cleavage of the C_1-C_2 bond, it was determined that this was only a minor pathway. An indirect oxidation channel dominated heterogeneous processes at the air-water interface, giving rise to hydroxyl and semiquinone radicals that recombine to produce polyhydroxylated aromatics and quinones. This new mechanism of aging represents an overlooked channel by which brown, light-absorbing carbon aerosols are produced in the atmosphere.

In addition, the work investigates how reactions on solid particulate aerosols proceed under variable relative humidity. Thin films were developed alongside a novel flow-through reactor to study of how aerosols are transformed by ozone and hydroxyl radicals when exposed to 50 ppbv - 800 ppmv of ozone. This system was employed to probe how catechol reacts with ozone under variable relative humidity. Further work was undertaken to model the adsorption process at the air-solid interface under variable humidity, permitting the estimation of the reactive uptake of ozone by the film at concentrations (50-200 ppbv) seen in rural and urban areas. Together, these results provide an increased understanding of how heterogeneous oxidation of aerosols contributes to aerosol aging processes as well as free radical production in the troposphere.

KEYWORDS: Aerosols, Atmospheric Chemistry, Hydroxyl Radical, Mass Spectrometry, Ozone.

Elizabeth A. Pillar-Little

07/02/17

MECHANISMS OF HETEROGENEOUS OXIDATIONS AT MODEL AEROSOL
INTERFACES BY OZONE AND HYDROXYL RADICALS

By

Elizabeth Ann Pillar-Little

Dr. Marcelo I. Guzman
Director of Dissertation

Dr. Mark A. Lovell
Director of Graduate Studies

07/02/17

For my parents Michael and Nancy Pillar and husband Timothy Pillar-Little

None of this would been possible without your unending love and support.

ACKNOWLEDGEMENTS

It is somewhat overwhelming to look back over the last six years at the immeasurable number of people who have supported me during my time in graduate school. I was originally very intimidated about moving to Lexington, but I quickly found an entire community of people who helped me a lot. These kind gestures of this community of people, their warm words, and acts of generosity made the long road to the Ph.D. a pleasurable and enriching experience.

During my time at the University of Kentucky, my advisor, Dr. Marcelo Guzman, has been a source of immense support, encouragement, and inspiration during my entire career. He has placed a lot of trust and faith in me over these six years by placing me in charge of several hundreds of thousands of dollars of equipment as we pursued mechanisms of aerosol processing. When research would get discouraging or overwhelming, he would be there with uplifting words or a few well-placed jokes to help me examine experimental difficulties from a new perspective. He always knew exactly what to say to get me headed off in the right direction, even if I was a bit slow moving at times. He constantly pushed me outside of my comfort zone to promote my growth as a scientist and as a person. I consider myself extremely lucky to have worked for such a wonderful mentor. I feel great pride in having worked for you; I hope I have done you proud as well.

Getting to know and work alongside members the Guzman group, past and present, has been one of the best aspects of my time in graduate school. No matter how long or short of a time I shared an office with Richa Althaye, Shasha Xia, Evie Zhou, Alexis Eugene, Elizabeth Bollinger, Nick English, Robert Camm, Samah Saad, Chris Ward, Sohel Rana,

shocked at receiving organic laboratory as a teaching assignment, and asking for her help and patience. With her guidance, I have grown into a mentor teaching assistant for the same course. The experience teaching in her labs has reinvigorated my love of teaching and has inspired me to pursue a career in teaching chemistry in a college setting. Thank you so much for everything. My fellow graduate students in the department have also been quite a joy to share this journey with. I think one of our best kept secrets at the University of Kentucky is how helpful all the grad students are whether it be working on cumes, bouncing research problems off each other during lunch, or being a sounding board when things are going poorly. In particular, Hope (and Jon) Abdallah, Dr. Surya Banks, Catherine Denning, Devin (and Chasity) Granger, Brittany Metts, Alexa Riddle, Dr. Aaron Swomley, and Brad Stewart shared in my successes and helped prevent me from giving up when everything seemed bleak. I would also like to thank my advisory committee, Dr. Jack Selegue, Dr. Bert Lynn, and Dr. Chris Matocha, for all of their helpful suggestions and advice over these six years.

In addition to all of the many great people I encountered in my academic career, I have enjoyed a great deal of support in my personal life as well. My parents Mike and Nancy Pillar have been my rock and greatest source of encourage throughout graduate school and through my life thus far. Whether it is helping me plan a wedding, renovate a condo, or just make me smile after a long day they would do anything to help lighten my load and help keep me on track. I love you both so much, thank you for all of the sacrifices you have made over the years. My "aunt" Peggy Kearney has also been there with me from when I was born in the house across the street, through graduations, illness, working together at Mercy Behavioral, Easters and Christmas, and so much more. You have been

such a great role model for me with how to balance being a woman and being career driven yet still have an enriching family life. Enjoy your retirement – you've earned it! Kyle Coval has been there for me every step of the way to like the sister I never had to share stories and stay up until ungodly hours of the morning just shooting the breeze. My extended family (the Williams, Pillar, and Little families) have been wonderful with their thoughtful cards and visits and patient with my intermittent absences from family functions.

Even though I don't get to see my friends Kristin and Willy Romanias and Ellen Gooodlet because we scattered like the wind after high school, I am always grateful for them encouraging me to dare to be different. At Mercyhurst, I also found kindred souls to share downtime between studies with discussing science, movies, games, sports, religion and everything else under the sun in Samuel (and Corinne) Romito, Allison Ozcko, Samuel Macklin, Brian Reddan, Erin (and Amy) Terrizzi. We've been through several relocations, employment changes, weddings, graduations, illnesses, and so much more together. You're a bunch of weirdos that never fail to make me laugh. Stay that way. I have also relied on a large network of folks all over the country and abroad that have offered an encouraging word or sympathetic ear. In particular, Elina Childs, Rod Combs, Michelle Costin, Andy Fite, Karen Gunther, Eleanna Skoula, Chris Sweeso, Melissa Tian, Adam and Lee Watson, and Ben White have always made time for me when I am struggling or went out of their way to make sure I felt loved during what can sometimes be a very isolating journey.

When I moved to Lexington, I knew no one. I have been blessed to get to know so many wonderful people who have not hesitated to welcome me into their families and

circles of friends so that Lexington soon felt like home. In particular, I would like to thank Gary and Liz Hansen, Tom and Fran D'Andrea, Eric Huffer and Susan Cohn, Dr. Ruth Baer, Sally McCord, Tim and Erica Emrick, Chris and Seanna LoBue, and Jeff Jones for adopting this grad student into their lives and making sure I was eating, sleeping, and surviving. For my young adult "focus group" comrades Robert Brown, Matt and Ashley Bryant Cheney, Shelby Kelly, Kres Neely and Audrey Bowlds, Josh and Meghan Riley-Graham, and Chuck and Puja Wright; thank you for often times saving me from being stuck in too much science and reminding me there is still indeed a larger world out there.

Lastly, I must thank Tim Pillar-Little who constantly has been my biggest cheerleader (and critic). You never cease to amaze me with the determination you show in your pursuit of your own PhD despite all of the hiccups, setbacks, and roadblocks you encounter. I am constantly inspired by your perseverance and strength. Never forget you are an amazing scientist on top of wonderful friend and husband. You always believed in me when I couldn't bring me to believe in myself. Thank you for giving me the opportunity to be your player two and teammate as we walk this journey together. I love how we make each new day an adventure, and I can't wait to see what the future holds with you by my side. For all of the people listed above, and those whom I may have forgotten, I am truly thankful for all of your love and support.

TABLE OF CONTENTS

LIST OF TABLES

LIST OF SCHEMES

LIST OF FIGURES

Chapter 1. Mechanistic Studies of Heterogeneous Reactions on Aerosol Surface Mimics

1.1 Synopsis

Atmospheric aerosols are important players in the radiative budget, or the interplay between incoming, absorbed, reflected, and outgoing radiation, of the planet through direct and indirect means.[1] Atmospheric components, such as aerosols, can have a net warming or cooling effect based on how they interact with radiation. Aerosols absorb radiation warming the planet, or scatter incoming radiation, increasing albedo (reflectivity) of Earth (cooling effect).[2] While the cooling properties of pure inorganic aerosols could be correctly modeled, the impact of organic aerosols on the radiative budget is unclear.[3, 4] Organic aerosols are transformed through chemical reactions during atmospheric transport.[5] The complex mixture resulting and their variable physical and chemical properties contribute to the uncertainty of these species for modulating incoming and outgoing solar radiation. Correlations between oxidative processing and increased absorptivity, hydroscopicity, and cloud condensation nuclei (CCN) activity have been observed but the mechanism behind this phenomenon is not well understood.[6] Heterogeneous interfaces are believed to be important in the processing of aerosols by promoting reaction pathways that might not be feasible in the gas-phase or in the bulk aerosol.[7] Thus investigating the mechanisms of heterogeneous oxidation at aerosol interfaces, is important to better understand how organic aerosols impact the radiative budget.

1.2 The Earth's Radiative Balance

The Earth's radiative balance is the energetic equilibrium between the incoming solar radiation, and what is absorbed or reflected back to space by the atmosphere or the surface. Radiative forcing is a measure of how much a particular atmospheric constituent traps (warms) or reflects (cools) outgoing terrestrial radiation.[8] The warming effect of methane, carbon dioxide, chlorofluorocarbons, and other greenhouse gases is widely understood and documented.[1] However, there is still a large degree of uncertainty in the net magnitude and direction of the contribution of aerosols to the radiative forcing budget, mainly attributable to their diversity in composition, size, optical properties, and hygroscopicity (Figure 1.1).[1]
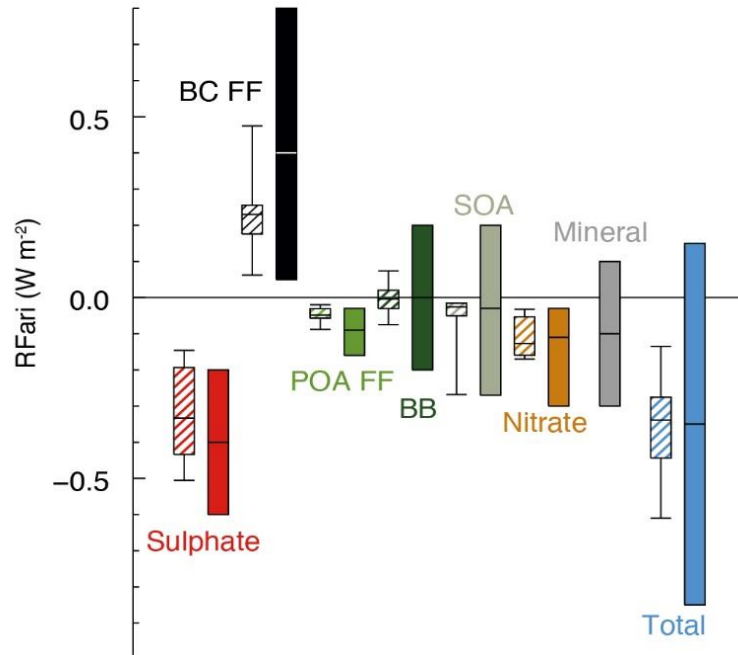
Figure 1.1. Annual mean top of the atmosphere radiative forcing due to aerosol-radiation interactions (RF$_{ari}$, in W m^{-2}) due to different anthropogenic aerosol types, for the 1750-2010 period. Hatched whisker boxes show median (line), 5th to 95th percentile ranges (box) and min/max values (whiskers) from AeroCom II models[9] corrected for the 1750-2010 period. Solid colored boxes show the AR5 best estimates and 90% uncertainty ranges. BC FF is for black carbon from fossil fuel and biofuel, POA FF is for primary organic aerosol from fossil fuel and biofuel, BB is for biomass burning aerosols and SOA is for secondary organic aerosols. Reproduced with permission from reference 1.

Inorganic CCN-active aerosols such as sulfates, nitrates, and sea salt aerosols are known to be excellent drivers of a net cooling radiative forcing because they promote enhanced cloud formation and thus heighten atmospheric reflectivity (Figure 1.1).[2] Many CCN are also extremely hydroscopic and increase the amount of water associated with inorganic aerosols. As water is a potent infrared absorber, the magnitude of cooling effects exerted on the atmosphere by inorganic aerosols may be diminished.[1] Mineral dusts, carried by winds from deserts like the Sahara, have been demonstrated to scatter incoming radiation to assist in cooling the planet.[10] However, particles including photoactive components such as iron and titanium oxides can increase the absorptive

power of sand and dust particles, resulting in a net neutral or slightly positive radiative forcing.[11]

Another important atmospheric aerosol constituent is black carbon (BC), which is produced from the incomplete combustion of fossil fuels, biofuels, and vegetation. BC is an efficient absorber of radiation, and thus contributes a net positive effect on aerosol radiative forcing (Figure 1.1).[12] This warming effect also continues once BC is deposited onto the Earth's surface, reducing the amount of radiation reflected back to outer space via absorption. This phenomenon is thought to be contributing to the acceleration of ice and snow melting in the polar regions through heat trapping in BC deposits.[13, 14]

1.3 Importance of Atmospheric Aerosols

Atmospheric aerosols, or the liquid and solid particulates suspended in the atmosphere, have many direct and indirect impacts on the health of the Earth's inhabitants and atmosphere.[15] The most obvious of these explicit effects are the deleterious health impacts observed from the inhalation of particulate matter with diameters less than 10 μM (PM_{10}). As the main component of urban smog, these small, ubiquitous particles pass into the lungs after being inhaled, leading to respiratory complications. Fine particulate matter with diameters smaller than 2.5 μM ($PM_{2.5}$) often enters the bloodstream and contributes to systemic inflammation that can lead to hypertension even after short exposure times.[16] Long term exposure to $PM_{2.5}$ has been linked to cardiovascular disease, respiratory diseases, asthma, low birth weight, lung cancer, stroke, and even diabetes.[17, 18] Additionally, aerosols can directly alter the radiation balance of the Earth via modifying the ability of the atmosphere to reflect, absorb or scatter solar radiation.[9] Hydrophilic

aerosols can serve as CCN, permitting the formation of cloud droplets.[19] Higher concentration of CCN also increases the albedo of clouds.[20, 21]

Unlike the extensive knowledge about inorganic and BC aerosols, far less information is available about the sources, sinks, and fates of organic aerosols (OA) in the atmosphere.[22-25] Models presently underestimate the OA loading in the troposphere, particularly from biomass burning sources, by 24% relative to field observations.[26] The OA loading and other key aerosol properties, such as optical absorptivity and hydroscopicity, seem to be driven by seasonal and regional variabilities.[26, 27] Oxidative aging of OA is also thought to increase hydroscopicity and improve their capability to act as CCN. Oxidation also amplifies the ability of OA to absorb radiation in the near ultraviolet range. These competing factors make assessing the impact of OA on the net radiative forcing budget complicated.[3, 4]

Reductions in greenhouse gas emissions have likewise cut the amounts of anthropogenic aerosols released to the atmosphere.[15] In fact, some of the warming observed by the end of this century might be attributable to smaller magnitudes of negative radiative forcing from aerosol-cloud and aerosol-radiation effects due to a reduction in the total atmospheric aerosol loading.[28-30] Consequently, it is important to understand how the dynamic composition of aerosols affects their optical and CCN properties to better constrain the radiative forcing of aerosols on Earth.

1.4 Formation of Primary versus Secondary Aerosols

Particles emitted directly to the atmosphere are called primary aerosols, and can originate from either natural or anthropogenic processes.[15] Wind-blown mineral dusts,

sea spray ejected from breaking waves, volcanic ash, pollen, and soils, among others are all examples of natural particulates in the atmosphere.[31] The inventories and trends of these species are generally well understood, allowing for predictions to be made on how they can shape the future climate.[15] Human activities such as fossil fuel burning, industrial development, and controlled agricultural burns can increase the amounts of sulfur, black carbon and organic aerosols in the atmosphere.[1]

Secondary aerosols are generated by conversion of volatile compounds into new particles or the transformation of existing primary particles in the atmosphere. These transformations can be carried out by either physical or chemical means. Most new particles are formed from the condensation or coagulation of gaseous or ultrafine particulate into larger particles, or the condensation of gases and volatile species onto pre-existing aerosols, such as black carbon or sea spray aerosols.[32] These processes most frequently occur with volatile organics emitted from plants and a wide host of anthropogenic sources, nitrogen oxide emissions from fossil fuel combustion, dimethyl sulfide emissions over the oceans, and sulfur dioxide emissions from fossil fuel combustion and volcanoes.[22, 32-34] These physical processes can alter the residence time of species in the atmosphere or change their optical and CCN properties. However, the natural aerosol loading of the planet can be modulated directly through anthropogenic emissions or indirectly by influencing biogeochemical cycles.[15, 35, 36]

Anthropogenic changes to the climate system, such as increased temperatures, carbon dioxide, or ozone levels[37, 38] can cause fluctuations in the natural emissions budget as well. For instance, rising global temperature and CO_2 concentrations cause an increase in biogenic volatile organic emissions (BVOCs).[39, 40] However, expected emissions of

BVOCs could be diminished because of deforestation, land usage changes, and losses of viable crop land due to aridification and salinification of soils.[41, 42] Surface ozone concentrations are expected to increase with growing BVOC emissions.[43] However, increasing atmospheric moisture driven by climbing global temperatures can partially counteract this trend by converting ozone into HO$^{\bullet}$.[43, 44] Elevated radical concentrations can facilitate production of highly absorptive brown carbon, and thus increase the positive radiative forcing component for OA.[43] Therefore, accounting for the impact of feedback loops on total organic loadings and trace gas species is important in predicting the effect of aerosols in the future climate.

Size is a major contributor to the atmospheric fate of particles because it dictates the residence time of aerosols against natural removal from the atmosphere through conversion or deposition. In the atmosphere, particles with diameters from 1 nm to 100 μm are observed. These can generally be grouped into four classes and some trends can be seen based on the source type. In nucleation mode (1-10 nm), aerosol physical processes, such as gas to particle conversion and the condensation of particles with water vapor, occur resulting in larger particles. Aitken mode particles are defined in the range of 10-100 nm in diameter and can undergo further coagulation and condensation to form accumulation mode particles which range from 0.1 to 1 μm in diameter. Windblown mineral dust, sea spray, pollen, and volcanic ash, as well as cloud-scavenged accumulation mode particles can range from 1 to 100 μm in size and are termed coarse mode aerosols.[32, 45]

Nucleation and Aitken particles have short lifetimes, from a few hours to a few days, because they undergo collisions that generate new particles. Coarse mode particles are

too heavy to persist in the atmosphere and undergo deposition in hours to a few days as well. This is why the 0.1-1 μm particles are given the name accumulation mode, because they tend to collect and linger in the atmosphere for 1-2 weeks before they are removed via deposition.[8, 32] Consequently, it is important to understand the composition, processing, and properties of these accumulation mode aerosols.

These new particles and some primary organic aerosols are prone to undergo multistep chemical reactions with trace atmospheric oxidizers (HO$^\bullet$, O$_3$, NO$_x$) and sunlight that alter their composition.[46-51] Each successive step of oxidation adds polar functional groups and decreases the volatility of the constituents.[22] This process leads to the partitioning of organics into the aqueous phase, where further processing can occur.[52, 53] These secondary organic aerosols along with organic aerosols generated from combustion or biomass burning events can absorb ultraviolet and visible radiation.[54] Studies have also demonstrated that as organic aerosols undergo subsequent stages of aging, they become increasingly water soluble and more absorbing.[55, 56] This absorptive organic aerosol fraction is often called brown carbon, after the light brown color of collected samples.[57] Field observations suggest that reactions taking place in clouds are critical for the secondary formation of brown carbon, which is thought to be an underrepresented source of positive radiative forcing.[4, 58]

The brown carbon contribution from secondary organic aerosols (SOA) has been identified to be one of the key uncertainties of the anthropogenic effect of aerosols on climate.[1] In order to better constrain the impacts of SOA on aerosol properties, better understanding needs to be obtained on the heterogeneous processing of aerosols, the

products of these reactions, and how these products will transform the optical and hydroscopic properties of the SOA.

1.5 Chemical Processing at Atmospheric Interfaces

Much of the chemical processing of aerosols occurs at the air-particle interface. These regions take three main forms, gas-solid, gas-semisolid and gas-liquid. Different products may result from reactions on each interface.[59] The interaction and uptake of a gas molecule by an aerosol particle occurs in a similar manner regardless of the phase, but additional parameters are needed to describe the processes on solid or semisolid interfaces, which are summarized in Figure 1.2.
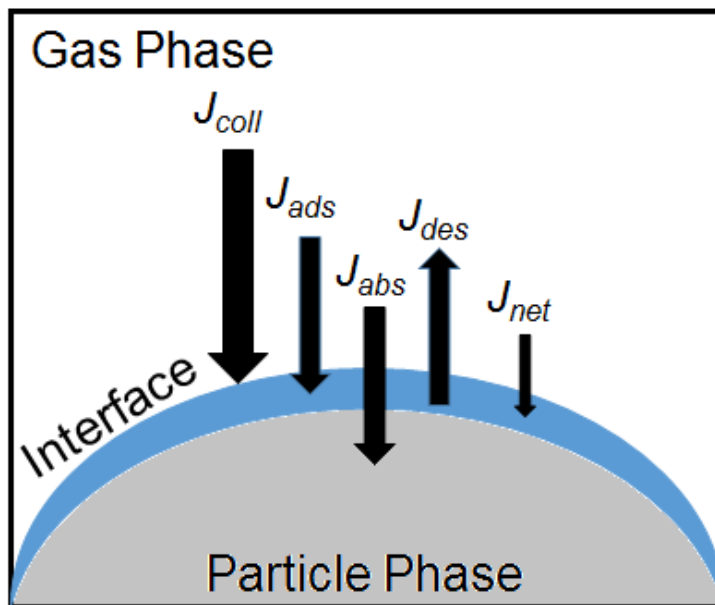
Figure 1.2: Illustration of key processes occurring at the interface between aerosols and the atmosphere.

An aerosol surface interacts with a number of gas molecules colliding on it. This collisional flux can be defined as

$$J_{coll} = \frac{v[X]_g}{4} \qquad \text{(Eq. 1.1)}$$

where $[X]_g$ is the concentration of the species X in the gas phase and v is the mean thermal velocity of X.[60] As gas molecules collide with the aerosol surface, a portion of these equilibrate with the surface. This accommodation process is dictated by the temperature, composition, and pressure of the gas as well as the phase and state of the surface.[61] Experimental observations are often corrected with a thermal accommodation coefficient, α_t, which can be described by the relationship

$$\alpha_t = \frac{E_{in} - E_{re}}{E_{in} - E_w} \qquad \text{(Eq. 1.2)}$$

where E_{in} is the incident energy flux, E_{re} is the reflected energy flux, and E_w is the flux of emitted molecules if they were in thermal equilibrium with the surface.[61-63] Molecules that do not immediately bounce off the surface can be held by van der Waals interactions or hydrogen bonds. This process, known as adsorption, is often termed physisorption because it represents the contribution of physical processes to the sticking of gaseous species to the interface. The adsorption flux can be estimated by the relationship

$$J_{ads} = \frac{\alpha_s v}{4(1-\theta)[X]_g} \qquad \text{(Eq. 1.3)}$$

where α_s is the surface accommodation coefficient, or the ratio of accommodated molecules to the number of molecular collisions and θ is the fractional surface coverage by the species of interest.[60, 64]

From this point, the adsorbed molecules can have three different fates: 1) absorption, 2) chemisorption, and 3) desorption. A portion of the adsorbed molecules are taken up and accommodated into the aerosol. This process is called absorption and this flux can be defined as

$$J_{abs} = \alpha_b J_{coll} \qquad \text{(Eq. 1.4)}$$

where α_b is the bulk accommodation coefficient,[60] which is determined by the relationship

$$\alpha_b = \alpha_s \frac{k_{sb}}{k_{sb} + k_{des}}. \qquad \text{(Eq. 1.5)}$$

In equation 1.5, k_{sb} and k_{des} are the surface to bulk transfer rate constant and the desorption rate constants, respectively.[64] Adsorbed molecules can become chemisorbed to the aerosol if they undergo chemical reactions with other adsorbed species or with aerosol constituents. Chemisorptive processes such as these are apparent through a hyperbolic relationship between the concentration of the gas the and reaction rate. This is often described by the Langmuir-Hinshelwood adsorption mechanism, which provides information regarding the partitioning of the reactant gas between the gas phase and the

particle phase followed by the reaction between the adsorbed gas and species in and on the aerosol.[64, 65]

Finally, a portion of the adsorbed molecules can detach or desorb from the surface back into the gas-phase. The desorption flux can be expressed as

$$J_{des} = [X]_g \, \tau_d^{-1} \qquad \text{(Eq. 1.6)}$$

where τ_d is the desorption lifetime.[60] The net uptake into the aerosols, J_{net}, is described as the difference between the adsorption (J_{ads}) and desorption (J_{des}) fluxes. However, it is extremely challenging to isolate and measure any of the individual processes needed to define the adsorption and desorption fluxes. Therefore, many studies have focused on determining the reactive uptake of gases by aerosol surfaces (γ). This quantity describes the overall uptake for all surface processes combined, regardless if they are physical or chemical in nature.[66, 67] While γ cannot be measured directly, it can be described using the experimentally observed reactive uptake of a gas into the interfacial region, γ_{eff} (Eq. 1.7).

$$\frac{1}{\gamma_{eff}} = \frac{1}{\Gamma_g} + \frac{1}{\gamma} \qquad \text{(Eq. 1.7)}$$

Where Γ_g is a correction factor defined as

$$\Gamma_g = 8 D_g \nu^{-1} d_p^{-1} \qquad \text{(Eq. 1.8)}$$

that includes the gas-phase diffusion coefficient for the compound of interest (D_g) and the particle diameter (d_p).[60] Therefore J_{net}, or the net flux between a gas and the surface of an aerosol,[67] can also be defined as

$$J_{net} = \gamma\, J_{coll} \qquad\qquad\qquad\qquad\qquad\qquad\qquad \text{(Eq. 1.9)}$$

In order to better comprehend the oxidative aging processes that aerosols undergo, it is imperative to understand how oxidants can interact with aerosol surfaces.[67, 68] Competition between chemical reactions during adsorption and absorption can lead to radical chemistry in both the bulk and the interface.[59] This complex interaction between aerosols and the atmosphere gives rise to many varied pathways of reaction "in" and "on" aerosols, leading to the complex compositions observed in field observations.[59] With a deeper understanding of how the processes occur at the surface of aerosols, the resulting physical and chemical outcomes can reveal optical and chemical transformations.

1.6 Aging of Aerosols in the Atmosphere

The atmospheric processing of aerosols is of great interest to atmospheric chemists and climate scientists because of its ability to impact aerosol properties.[7] Gas-phase reactions between atmospheric oxidizers and volatile organic species have been studied extensively. In general, common atmospheric oxidants, like ozone, nitric oxide, and peroxides react with gas-phase organics to generate less volatile and more polar products that partition to the particle phase, forming SOA.[22, 68, 69] Understanding how SOA behaves as it is transported through the atmosphere is an important issue to explain how

urban pollution becomes more oxygenated (higher O/C ratio) during the aging process.[69] Despite the varied sources of organic aerosols, oxalic acid has been identified as a pervasive component of aged SOA.[70] Thus, there must be a common mechanism of oxidative chemical processing that generates oxalic acid as an end product.[47, 70-75] In order to elucidate a mechanism of oxidative aging, it is imperative to understand the major routes atmospheric aerosol processing can take and how they can contribute to aerosol complexity. Even though physical processing (Section 1.4) drives the formation of new aerosols from primary emissions of natural and anthropogenic particles, the fate of these newborn particles during transport can be extremely complex due to the many forces acting on them.

The chemical processing of SOA to generate aged SOA can proceed through oxidative pathways, non-oxidative pathways, or photochemistry.[5] In oxidative processing, trace gases react with organic species on the surface of the aerosol (Section 1.5) to produce alkyl radicals (Figure 1.3). Molecular oxygen (O_2) then adds to the radical to form the highly reactive alkylperoxy radical which then can undergo reactions with a host of atmospheric radicals (NO, NO_2, RO_2, HO_2, NO_3).[5] These reactions result in the addition of polar functional groups, such as hydroperoxyl (-OOH), nitrate ($-NO_3$), nitro ($-NO_2$), hydroxyl (-OH), carboxylic acid (-COOH), ketones, among others.[76] These added polar groups, in addition to increasing hygroscopicity, decrease molecule volatility.[77] These oxidatively induced aerosol properties encourage further SOA formation via condensation and coagulation.
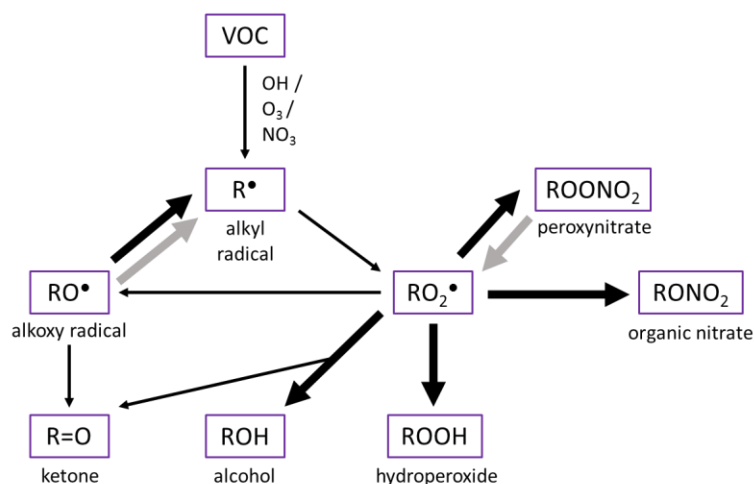
Figure 1.3. Simplified mechanism for the atmospheric oxidation of a generic VOC. Thick black arrows denote reactions that can lead to a substantial decrease in volatility; gray arrows denote reactions that can lead to a substantial volatility increase. Figure adapted from reference 5.

Semi-volatile species produced from oxidation reactions can undergo accretion reactions in aerosols to form heavier species after partitioning into the particle phase.[5, 78] This non-oxidative pathway can take many forms, but most if not all accretion reactions involve polymerization or radical recombination of organic compounds. The resulting heavier, nonvolatile products are complex oligomeric species unlikely to be formed oxidatively in the gas phase. Based on field studies, it has been inferred that accretion reactions are enhanced in acidic aerosols by acid-catalyzed nucleophilic additions to aldehydes, carbonyls, and alcohols.[78] Additionally, alkenes, such as limonene, have also been show to more readily undergo accretion reactions such as dimerization in the presence of strong acids.[79, 80] As many atmospheric aerosols are comprised of acidic components, these reactions represent a common pathway for the formation of non-volatile species in aerosols.[81]

In addition to chemical reactions, sunlight can also catalyze oxidative and accretion chemistry in and on aerosols.[49-51, 72, 73] Organic and inorganic molecules can act as chromophores, or light absorbing moieties, that absorb visible and ultraviolet radiation. These compounds, such as conjugated double bonds or carbonyls, lead to the formation of excited state molecules that can undergo homolytic bond cleavage, radical recombination, electron transfer, decomposition, hydrogen abstraction, and photosensitization.[72, 73, 82-84] The resulting products, which are similar to what is observed with particle-phase accretion chemistry, dehydrate or cyclize during the night to form polymers or supramacromolecular structures. When the sun rises the next day, photons are absorbed by these complexes, leading to their dissociation. This pattern of diurnal cycling is commonly seen with α-dicarbonyls, which are prevalent in aged OA, and is a possible source of positive radiative forcing from OA.[72, 73]

Sunlight can also accomplish aerosol processing indirectly via the photochemical production of hydroxyl radical (HO$^\bullet$), which is one of the most abundant tropospheric oxidizers.[85] Volatile organics often first undergo gas-phase oxidation by HO$^\bullet$, decreasing volatility and encouraging coagulation to form SOA. Photochemistry can also alter the balance of available trace oxidizers such as ozone and nitrogen dioxide through the cycling of halogen radicals.[86] Therefore, photochemical processes are an important factor in the direct and indirect production of SOA through oxidative and non-oxidative means.

All these different aerosol processes mentioned above can change the physiochemical properties of SOA. It has been demonstrated that higher O/C ratios in aerosols enhances hydroscopicity due to its greater hydrophilic character from a larger amount of polar functional groups.[22] Highly oxygenated SOA can serve as CCN at lower RH whereas

more hydrophobic OA can only do this in very moist environments. Diminished compound volatility has also been observed relative to an elevated O/C ratio. As aging proceeds, volatility can be altered further via oligomerization and fragmentation.[87] All of these processes can amplify the number of light absorbing functional groups, which increase the absorbing power of aged SOA.[49] Oligomerization is also thought to be a contributing factor into the creation of light absorbing brown carbon in humic-like substances (HULIS).[88, 89] Through understanding the interplay between chemical processing and aerosol properties, more complete mechanistic models can be developed to describe the evolution of aerosols, including their composition and absorptivity.[5, 49]

1.7 Heterogeneous Studies of Relevance to the Atmosphere

While the physical and chemical processes that lead to aerosols formation in the environment are a current focus of study, it remains very unclear how the compositional complexity observed in field measurements is generated. Gas and aqueous phase bulk studies have proven to be useful in predicting the mechanisms and products of interfacial reactions, but often underestimate the variety of possible products and pathways that could be important.[46, 47, 74] Cloud chambers,[90-92] Knudsen cells,[93, 94] droplet train flow reactors,[95-97] flow tube reactors,[98-101] and molecular dynamics simulations[102] have been used to investigate different properties of aerosols and the results of atmospheric processing. However, these methods do not always provide atmospherically relevant models reflecting aerosol surface to volume ratios, interfacial diffusion rates and mass accommodation, organic coatings, water associated with particles, and hydrophobicity.[59]

Collected aerosols from field studies have been characterized using aerosol time of flight mass spectrometers, [103-105] electron microscopy, [106, 107] X-ray diffraction, [108, 109] and many other methods to determine the outcome of aging. These methods provide insight into the composition of the aerosol, but do not permit tracking of how the particles arrived to that state. Therefore, new instrumental methods are demonstrated in this thesis[46, 47, 74, 110] which provide mechanistic insight into the aging process (Section 1.6). Two questions explored are what reaction pathways predominate in the interface of air with water[46, 47, 75] or with a solid?[74] How do different reactive channels contribute to changes in optical properties?[49, 50, 72, 73] In order to tackle these problems, analytical systems were developed to probe the heterogeneous oxidative aging of aerosol proxies at the air-water and air-solid interface.

The oxidation of aqueous aerosols have been investigated using droplet generation systems paired with in-line detection systems to allow for the observation of intermediates that might be lost in traditional collection and offline processing methods. Nebulizers coupled to flow tubes interfaced with mass spectrometers, particle sizers, and infrared spectrometers have been employed to examine how transformations might occur in clouds.[98, 111] However, interfacial reactions often proceed too quickly to capture reactive intermediates in these systems. To bridge this gap, nebulizing systems have been interfaced with an electrospray mass spectrometer (ESI MS) to provide a novel instrumental set up to create aqueous microdroplets that can probe reactions at the air-water interface with shortened analysis times.[46, 47]

Pneumatically assisted electrospray uses a high flow rate of carrier gas to rapidly desolvate the solvent jet as it leaves the capillary.[112] Ions and molecules are ejected off

the droplet surfaces to relieve excess charge as the droplets are sheared and desolvated by the carrier gas. As a result, this analytical method allows for selective sampling of the reactants and products in the droplet interface.[113] Further customizing the instrument allows for the delivery of oxidant gases to examine the *in situ* oxidation of inorganic and organic species on the surface of aqueous microdroplets under atmospherically relevant conditions (Figure 1.4).[46, 47]
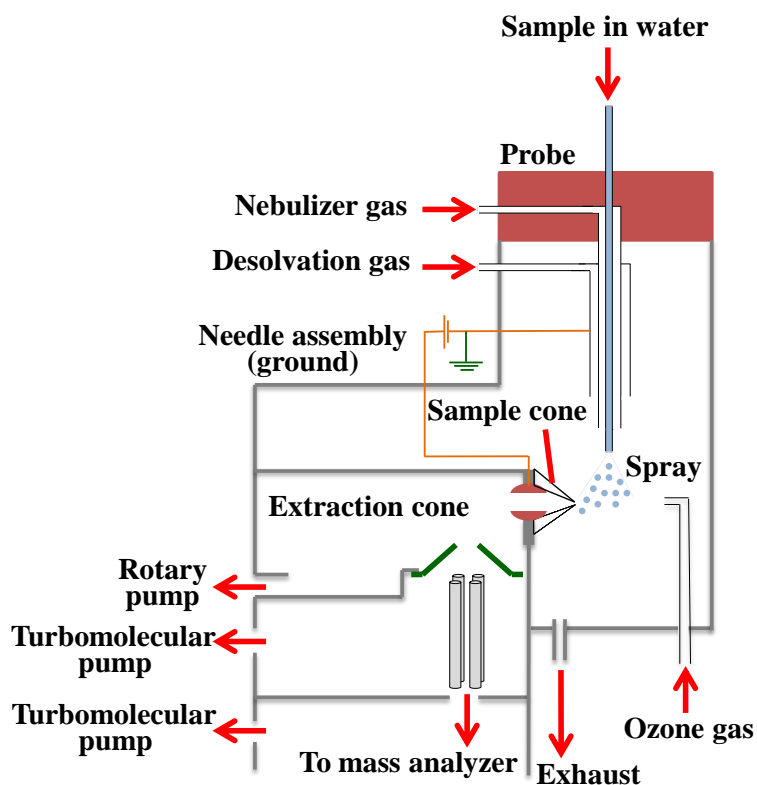
Figure 1.4. Schematic of pneumatically assisted electrospray ionization mass spectrometry set-up utilized to probe reactions at the air-water interface. Reproduced with permission from reference 47.

Studying reactions on solid aerosols in the laboratory have utilized thin films or solid particles as proxies to investigate the uptake of gases on solid aerosols and how this transforms their composition. Aerosol chambers and flow tubes[114-118] use gas phase

19

reactions to generate SOA in controlled environments. The resulting aerosols are analyzed by different techniques, such as optical spectroscopy, before they are collected for further characterization by chromatography and mass spectrometry.[115] Variations in the physical state of the aerosol, reaction time, size, and the procedure for measuring rate of loss can lead to disparate reaction rates and uptake coefficients between different groups studying the same molecules.[59] These approaches capture the variations in composition in the early stages of aging but are not representative of the extended aging periods experienced during transport.[74]

More recently, thin films have been used to simulate aerosol surface reactions at the air-particle interface.[98, 119, 120] This approach has proven quite useful to monitor the degradation of the proxy materials and evolution of condensed and gas phase products in gas cells or environmental chambers.[121] While ultrafast processes at the air-water interface were studied in a developed customized set-up described previously,[47] it is possible that some products that form over longer time scales are missed. Therefore, an additional system was needed to study oxidative processing on surfaces that could pair real-time monitoring with offline compositional analysis.[74]

A flow-through reaction chamber was designed for providing a clear picture of reactions on solid aerosols (Figure 1.5).[48, 110] Stainless steel infrared holders were designed with chemically inert optical windows and placed into a reaction chamber designed to allow for easy access to the samples inside. Humid ozone was circulated through the reactor at a constant rate, and samples were regularly scanned to monitor the oxidation process. Protocols were also developed to extract the reacted films and analyze their products by chromatography and mass spectrometry. Not only did this experimental

design validate findings using the air-water interface technique, but also provides further details of intermediates and products that escaped detection at the air-water interface.[48, 110]
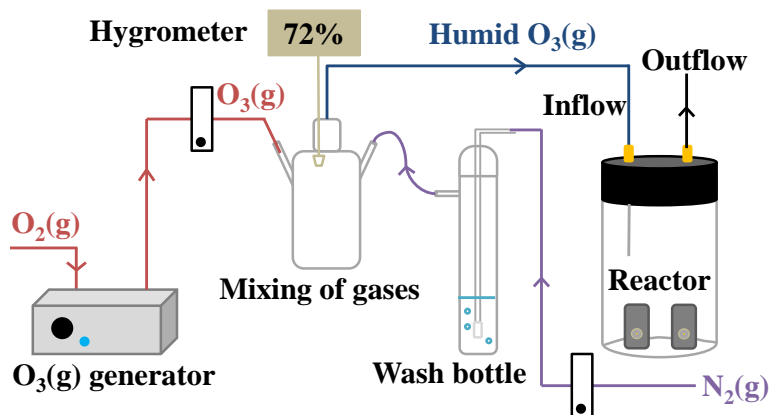
Figure 1.5. Flow-through reactor system with mixing of dry and wet gases. Reproduced with permission from reference 49.

1.8 Research Objectives

SOA and biomass burning aerosols (BBA) contribute the largest portions of uncertainty to the aerosol-radiation component of radiative forcing.[1] Most of previous attempts to constrain uncertainties from OA have focused on the formation of SOA from biogenic sources, such as isoprene and several terpenes.[122] To increase the certainty in future global temperature and climate forecasts made by climate models, knowledge of the fate of anthropogenically driven organic compounds in the atmosphere is needed.[123] In addition, better inventories of sources and sinks of atmospheric oxidizers are necessary to predict how oxidation contributes to aerosol aging.[15, 124] through investigating the transformations of overlooked sources of SOA, such as BBA and polycyclic aromatic hydrocarbons (PAHs) under atmospherically relevant conditions, information to diminish the uncertainties of OA to radiative forcing can be contributed.[47, 74, 75]

Chapter 2 explains the conversion of iodide to hypoiodous acid and molecular iodine in aqueous microdroplets exposed to ozone and reveals the role of reactions occurring on the surface of sea spray aerosols and their importance in tropospheric ozone depletion.[46] Previous studies demonstrated that iodide can be significantly enriched at the air-water interface, as it happens in sea spray aerosols formed during bubble bursting and wave breaking processes.[112] In turn, tropospheric ozone should react with the surface available iodide to produce reactive halogen species (RHS), molecular iodine and hypoiodous acid. This mechanism of RHS production is proposed to help close the gap between RHS predicted by models and those same species measured during field campaigns.

Chapter 3 studies the oxidation of catechol by ozone and hydroxy radicals at the air-water interface, applying the technique developed in Chapter 2.[47] Catechol, a dihydroxybenzene found in biomass burning emissions, was previously thought to primarily undergo ring-opening reactions when exposed to ozone.[120] However, this work demonstrates that electron transfers initiates an indirect oxidation pathway. So in addition to observing the expected catechol ozonolysis products,[125] the indirect oxidation channel leads to the production of polyhydroxylated aromatic (PHA) compounds and quinones.[47] This mechanism provides an explanation for the production of light absorbing brown carbon along with how complex mixtures of organic compounds are generated.[47, 48, 110]

In Chapter 4, the heterogeneous oxidation of catechol at the air-solid interface was investigated. Similar product mixtures as observed at the air-water interface were characterized using infrared spectroscopy and mass spectrometry.[48] The heterogeneous oxidation of catechol at the air-solid interface gave rise to organic acids from direct ozonolysis, and PHAs, bi- and terpheynls products via the crosslinking of reactive

semiquinone intermediates. Relative humidity was also found to be a key driver in the reaction rate, suggesting that adsorbed water facilitates ring cleavage and electron transfer as observed in Chapter 3.

In Chapter 5, a series of substituted catechols is employed to serve as a proxy to explore how anthropogenically emitted phenols can be oxidized at the air-water interface.[75] As seen in Chapter 3, dicarboxylic acids and polyphenols were produced during the heterogeneous reactions of ozone and these compounds at the air-water interface.[75] However, it was noticed that the increased electron density in the aromatic system from electron donating moieties lead to an increase in product formation.[75] Chapter 6 (Conclusion) outlines the outcomes of these projects and their potential impact on research in aerosol and atmospheric science.

1.9 References

1. Boucher, O.; Randall, D.; Artaxo, P.; Bretherton, C.; Feingold, G.; Forster, P.; Kerminen, V.-M.; Kondo, Y.; Liao, H.; Lohmann, U.; Rasch, P.; Satheesh, S. K.; Sherwood, S.; Stevens, B.; Zhang, X. Y., Clouds and Aerosols. In *Climate Change 2013: The Physical Science Basis. Contribution of Working Group I to the Fifth Assessment Report of the Intergovernmental Panel on Climate Change*, Stocker, T. F.; Qin, D.; Plattner, G.-K.; Tignor, M.; Allen, S. K.; Boschung, J.; Nauels, A.; Xia, Y.; Bex, V.; Midgley, P. M., Eds. Cambridge University Press: Cambridge, United Kingdom and New York, NY, USA, 2013; pp 571−658.

2. Petters, M. D.; Kreidenweis, S. M. A Single Parameter Representation of Hygroscopic Growth and Cloud Condensation Nucleus Activity. *Atmos. Chem. Phys.* **2007,** *7* (8), 1961-1971.

3. Duplissy, J.; DeCarlo, P. F.; Dommen, J.; Alfarra, M. R.; Metzger, A.; Barmpadimos, I.; Prevot, A. S. H.; Weingartner, E.; Tritscher, T.; Gysel, M.; Aiken, A. C.; Jimenez, J. L.; Canagaratna, M. R.; Worsnop, D. R.; Collins, D. R.; Tomlinson, J.; Baltensperger, U. Relating Hygroscopicity and Composition of Organic Aerosol Particulate Matter. *Atmos. Chem. Phys.* **2011,** *11* (3), 1155-1165.

4. Liu, J.; Scheuer, E.; Dibb, J.; Ziemba, L. D.; Thornhill, K. L.; Anderson, B. E.; Wisthaler, A.; Mikoviny, T.; Devi, J. J.; Bergin, M.; Weber, R. J. Brown Carbon in the Continental Troposphere. *Geophys. Res. Lett.* **2014,** *41* (6), 2191-2195.

5. Kroll, J. H.; Seinfeld, J. H. Chemistry of Secondary Organic Aerosol: Formation and Evolution of Low-Volatility Organics in the Atmosphere. *Atmos. Environ.* **2008,** *42* (16), 3593-3624.

6. Rudich, Y.; Donahue, N. M.; Mentel, T. F. Aging of Organic Aerosol: Bridging the Gap between Laboratory and Field Studies. *Ann. Rev. Phys. Chem.* **2007,** *58* (1), 321-352.

7. George, I. J.; Abbatt, J. P. D. Heterogeneous Oxidation of Atmospheric Aerosol Particles by Gas-Phase Radicals. *Nature Chem.* **2010,** *2* (9), 713-722.

8. Jacobs, D. J., *Introduction to Atmospheric Chemistry*. Princeton University Press: Princeton, New Jersey, 1999; p 280.

9. Myhre, G.; Samset, B. H.; Schulz, M.; Balkanski, Y.; Bauer, S.; Berntsen, T. K.; Bian, H.; Bellouin, N.; Chin, M.; Diehl, T.; Easter, R. C.; Feichter, J.; Ghan, S. J.; Hauglustaine, D.; Iversen, T.; Kinne, S.; Kirkevåg, A.; Lamarque, J. F.; Lin, G.; Liu, X.; Lund, M. T.; Luo, G.; Ma, X.; van Noije, T.; Penner, J. E.; Rasch, P. J.; Ruiz, A.; Seland, Ø.; Skeie, R. B.; Stier, P.; Takemura, T.; Tsigaridis, K.; Wang, P.; Wang, Z.; Xu, L.; Yu, H.; Yu, F.; Yoon, J. H.; Zhang, K.; Zhang, H.; Zhou, C. Radiative Forcing of the Direct Aerosol Effect from Aerocom Phase Ii Simulations. *Atmos. Chem. Phys.* **2013,** *13* (4), 1853-1877.

10. Usher, C. R.; Michel, A. E.; Grassian, V. H. Reactions on Mineral Dust. *Chem. Rev.* **2003,** *103* (12), 4883-4940.

11. Sokolik, I. N.; Winker, D. M.; Bergametti, G.; Gillette, D. A.; Carmichael, G.; Kaufman, Y. J.; Gomes, L.; Schuetz, L.; Penner, J. E. Introduction to Special Section: Outstanding Problems in Quantifying the Radiative Impacts of Mineral Dust. *J. Geophys. Res. Atmos.* **2001,** *106* (D16), 18015-18027.

12. Ramanathan, V.; Carmichael, G. Global and Regional Climate Changes Due to Black Carbon. *Nature Geosci.* **2008,** *1* (4), 221-227.

13. Flanner, M. G. Arctic Climate Sensitivity to Local Black Carbon. *J. Geophys. Res. Atmos.* **2013,** *118* (4), 1840-1851.

14. AMAP. *The Impact of Black Carbon on the Arctic Climate.*; Arctic Monitoring and Assessment Programme (AMAP): Oslo, 2011.

15. von Schneidemesser, E.; Monks, P. S.; Allan, J. D.; Bruhwiler, L.; Forster, P.; Fowler, D.; Lauer, A.; Morgan, W. T.; Paasonen, P.; Righi, M.; Sindelarova, K.; Sutton, M. A. Chemistry and the Linkages between Air Quality and Climate Change. *Chem. Rev.* **2015,** *115* (10), 3856-3897.

16. Brook, R. D.; Rajagopalan, S. Particulate Matter, Air Pollution, and Blood Pressure. *J. Am. Soc. Hypertens.* **2009,** *3* (5), 332-350.

17. Pope, C. A.; Burnett, R. T.; Thun, M. J. Lung Cancer, Cardiopulmonary Mortality, and Long-Term Exposure to Fine Particulate Air Pollution. *J. Am. Med. Assoc.* **2002,** *287* (9), 1132-1141.

18. World Health Organization. *Review of Evidence on Health Aspects of Air Pollution (Revihaap) Project*; Copenhagen, 2013.

19. Albrecht, B. A. Aerosols, Cloud Microphysics, and Fractional Cloudiness. *Science* **1989,** *245* (4923), 1227-1230.

20. Liu, J.; Li, Z. Estimation of Cloud Condensation Nuclei Concentration from Aerosol Optical Quantities: Influential Factors and Uncertainties. *Atmos. Chem. Phys.* **2014,** *14* (1), 471-483.

21. Kravitz, B.; Wang, H.; Rasch, P. J.; Morrison, H.; Solomon, A. B. Process-Model Simulations of Cloud Albedo Enhancement by Aerosols in the Arctic. *Phil. Trans. R. Soc. A* **2014,** *372* (2031).

22. Hallquist, M.; Wenger, J. C.; Baltensperger, U.; Rudich, Y.; Simpson, D.; Claeys, M.; Dommen, J.; Donahue, N. M.; George, C.; Goldstein, A. H.; Hamilton, J. F.; Herrmann, H.; Hoffmann, T.; Iinuma, Y.; Jang, M.; Jenkin, M. E.; Jimenez, J. L.; Kiendler-Scharr, A.; Maenhaut, W.; McFiggans, G.; Mentel, T. F.; Monod, A.; Prévôt, A. S. H.; Seinfeld, J. H.; Surratt, J. D.; Szmigielski, R.; Wildt, J. The Formation, Properties and Impact of Secondary Organic Aerosol: Current and Emerging Issues. *Atmos. Chem. Phys.* **2009,** *9* (14), 5155-5236.

23. Johnson, D.; Utembe, S. R.; Jenkin, M. E.; Derwent, R. G.; Hayman, G. D.; Alfarra, M. R.; Coe, H.; McFiggans, G. Simulating Regional Scale Secondary Organic Aerosol Formation During the Torch 2003 Campaign in the Southern UK. *Atmos. Chem. Phys.* **2006,** *6* (2), 403-418.

24. Robinson, A. L.; Donahue, N. M.; Shrivastava, M. K.; Weitkamp, E. A.; Sage, A. M.; Grieshop, A. P.; Lane, T. E.; Pierce, J. R.; Pandis, S. N. Rethinking Organic Aerosols: Semivolatile Emissions and Photochemical Aging. *Science* **2007,** *315* (5816), 1259.

25. Heald, C. L.; Jacob, D. J.; Park, R. J.; Russell, L. M.; Huebert, B. J.; Seinfeld, J. H.; Liao, H.; Weber, R. J. A Large Organic Aerosol Source in the Free Troposphere Missing from Current Models. *Geophys. Res. Lett.* **2005,** *32* (18), L18809.

26. Kaiser, J. W.; Heil, A.; Andreae, M. O.; Benedetti, A.; Chubarova, N.; Jones, L.; Morcrette, J. J.; Razinger, M.; Schultz, M. G.; Suttie, M.; van der Werf, G. R. Biomass Burning Emissions Estimated with a Global Fire Assimilation System Based on Observed Fire Radiative Power. *Biogeosci.* **2012,** *9* (1), 527-554.

27. Tosca, M. G.; Randerson, J. T.; Zender, C. S. Global Impact of Smoke Aerosols from Landscape Fires on Climate and the Hadley Circulation. *Atmos. Chem. Phys.* **2013,** *13* (10), 5227-5241.

28. Naik, V.; Horowitz, L. W.; Fiore, A. M. Impact of Preindustrial to Present-Day Changes in Short-Lived Pollutant Emissions on Atmospheric Composition and Climate Forcing. *J. Geophys. Res. Atmos.* **2013,** *118* (14), 8086-8110.

29. Levy, H.; Horowitz, L. W.; Schwarzkopf, M. D.; Ming, Y.; Golaz, J.-C.; Naik, V.; Ramaswamy, V. The Roles of Aerosol Direct and Indirect Effects in Past and Future Climate Change. *J. Geophys. Res. Atmos.* **2013,** *118* (10), 4521-4532.

30. Rotstayn, L. D.; Collier, M. A.; Chrastansky, A.; Jeffrey, S. J.; Luo, J. J. Projected Effects of Declining Aerosols in RCP4.5: Unmasking Global Warming? *Atmos. Chem. Phys.* **2013,** *13* (21), 10883-10905.

31. Andreae, M. O. Aerosols before Pollution. *Science* **2007,** *315* (5808), 50-51.

32. Seinfeld, J. H.; Pandis, S. N., *Atmospheric Chemistry and Physics: From Air Pollution to Climate Change*. Second Edition ed.; Wiley: 2006; p 1232.

33. Woodhouse, M. T.; Mann, G. W.; Carslaw, K. S.; Boucher, O. Sensitivity of Cloud Condensation Nuclei to Regional Changes in Dimethyl-Sulphide Emissions. *Atmos. Chem. Phys.* **2013,** *13* (5), 2723-2733.

34. Alexander, B.; Park, R. J.; Jacob, D. J.; Li, Q. B.; Yantosca, R. M.; Savarino, J.; Lee, C. C. W.; Thiemens, M. H. Sulfate Formation in Sea-Salt Aerosols: Constraints from Oxygen Isotopes. *J. Geophys. Res. Atmos.* **2005,** *110* (D10), D10307.

35. Setyan, A.; Song, C.; Merkel, M.; Knighton, W. B.; Onasch, T. B.; Canagaratna, M. R.; Worsnop, D. R.; Wiedensohler, A.; Shilling, J. E.; Zhang, Q. Chemistry of New Particle Growth in Mixed Urban and Biogenic Emissions – Insights from CARES. *Atmos. Chem. Phys.* **2014,** *14* (13), 6477-6494.

36. Paasonen, P.; Asmi, A.; Petaja, T.; Kajos, M. K.; Aijala, M.; Junninen, H.; Holst, T.; Abbatt, J. P. D.; Arneth, A.; Birmili, W.; van der Gon, H. D.; Hamed, A.; Hoffer, A.; Laakso, L.; Laaksonen, A.; Richard Leaitch, W.; Plass-Dulmer, C.; Pryor, S. C.; Raisanen, P.; Swietlicki, E.; Wiedensohler, A.; Worsnop, D. R.; Kerminen, V.-M.; Kulmala, M. Warming-Induced Increase in Aerosol Number Concentration Likely to Moderate Climate Change. *Nature Geosci.* **2013,** *6* (6), 438-442.

37. Wu, S.; Mickley, L. J.; Jacob, D. J.; Rind, D.; Streets, D. G. Effects of 2000–2050 Changes in Climate and Emissions on Global Tropospheric Ozone and the Policy-Relevant Background Surface Ozone in the United States. *J. Geophys. Res. Atmos.* **2008,** *113* (D18).

38. Ammann, M.; Klimont, Z.; Wagner, F. Regional and Global Emissions of Air Pollutants: Recent Trends and Future Scenarios. *Annu. Rev. Environ. Resour.* **2013,** *38* (1), 31-55.

39. Guenther, A.; Karl, T.; Harley, P.; Wiedinmyer, C.; Palmer, P. I.; Geron, C. Estimates of Global Terrestrial Isoprene Emissions Using MEGAN (Model of Emissions of Gases and Aerosols from Nature). *Atmos. Chem. Phys.* **2006,** *6* (11), 3181-3210.

40. Sanderson, M. G.; Jones, C. D.; Collins, W. J.; Johnson, C. E.; Derwent, R. G. Effect of Climate Change on Isoprene Emissions and Surface Ozone Levels. *Geophys. Res. Lett.* **2003,** *30* (18).

41. Wiedinmyer, C.; Tie, X.; Guenther, A.; Neilson, R.; Granier, C. Future Changes in Biogenic Isoprene Emissions: How Might They Affect Regional and Global Atmospheric Chemistry? *Earth Interact.* **2006,** *10* (3), 1-19.

42. Lathière, J.; Hauglustaine, D. A.; Friend, A. D.; De Noblet-Ducoudré, N.; Viovy, N.; Folberth, G. A. Impact of Climate Variability and Land Use Changes on Global Biogenic Volatile Organic Compound Emissions. *Atmos. Chem. Phys.* **2006,** *6* (8), 2129-2146.

43. Wang, Y.; Shen, L.; Wu, S.; Mickley, L.; He, J.; Hao, J. Sensitivity of Surface Ozone over China to 2000–2050 Global Changes of Climate and Emissions. *Atmos. Environ.* **2013,** *75*, 374-382.

44. Doherty, R. M.; Wild, O.; Shindell, D. T.; Zeng, G.; MacKenzie, I. A.; Collins, W. J.; Fiore, A. M.; Stevenson, D. S.; Dentener, F. J.; Schultz, M. G.; Hess, P.; Derwent, R. G.; Keating, T. J. Impacts of Climate Change on Surface Ozone and Intercontinental Ozone Pollution: A Multi-Model Study. *J. Geophys. Res. Atmos.* **2013,** *118* (9), 3744-3763.

45. Whitby, K. T. The Physical Characteristics of Sulfur Aerosols. *Atmos. Environ.* **1978,** *12* (1–3), 135-159.

46. Pillar, E. A.; Guzman, M. I.; Rodriguez, J. M. Conversion of Iodide to Hypoiodous Acid and Iodine in Aqueous Microdroplets Exposed to Ozone. *Environ. Sci. Technol.* **2013,** *47* (19), 10971-10979.

47. Pillar, E. A.; Camm, R. C.; Guzman, M. I. Catechol Oxidation by Ozone and Hydroxyl Radicals at the Air–Water Interface. *Environ. Sci. Technol.* **2014,** *48* (24), 14352-14360.

48. Pillar, E. A.; Zhou, R.; Guzman, M. I. Heterogeneous Oxidation of Catechol. *J. Phys. Chem. A* **2015,** *119* (41), 10349-10359.

49. Rincón, A. G.; Guzmán, M. I.; Hoffmann, M. R.; Colussi, A. J. Optical Absorptivity Versus Molecular Composition of Model Organic Aerosol Matter. *J. Phys. Chem. A* **2009,** *113* (39), 10512-10520.

50. Rincón, A. G.; Guzmán, M. I.; Hoffmann, M. R.; Colussi, A. J. Thermochromism of Model Organic Aerosol Matter. *J.Physical Chem. Lett.* **2010,** *1* (1), 368-373.

51. Guzmán, M. I.; Colussi, A. J.; Hoffmann, M. R. Photoinduced Oligomerization of Aqueous Pyruvic Acid. *J. Phys. Chem. A* **2006,** *110* (10), 3619-3626.

52. Pankow, J. F. An Absorption Model of the Gas/Aerosol Partitioning Involved in the Formation of Secondary Organic Aerosol. *Atmos. Environ.* **1994,** *28* (2), 189-193.

53. Chan, A. W. H.; Kroll, J. H.; Ng, N. L.; Seinfeld, J. H. Kinetic Modeling of Secondary Organic Aerosol Formation: Effects of Particle- and Gas-Phase Reactions of Semivolatile Products. *Atmos. Chem. Phys.* **2007,** *7* (15), 4135-4147.

54. Andreae, M. O.; Gelencsér, A. Black Carbon or Brown Carbon? The Nature of Light-Absorbing Carbonaceous Aerosols. *Atmos. Chem. Phys.* **2006,** *6* (10), 3131-3148.

55. Updyke, K. M.; Nguyen, T. B.; Nizkorodov, S. A. Formation of Brown Carbon Via Reactions of Ammonia with Secondary Organic Aerosols from Biogenic and Anthropogenic Precursors. *Atmos. Environ.* **2012,** *63*, 22-31.

56. Cappa, C. D.; Che, D. L.; Kessler, S. H.; Kroll, J. H.; Wilson, K. R. Variations in Organic Aerosol Optical and Hygroscopic Properties Upon Heterogeneous Oh Oxidation. *J. Geophys. Res. Atmos.* **2011,** *116* (D15).

57. Bond, T. C. Spectral Dependence of Visible Light Absorption by Carbonaceous Particles Emitted from Coal Combustion. *Geophys. Res. Lett.* **2001,** *28* (21), 4075-4078.

58. Chung, C. E.; Ramanathan, V.; Decremer, D. Observationally Constrained Estimates of Carbonaceous Aerosol Radiative Forcing. *Proc. Natl. Acad. Sci.* **2012,** *109* (29), 11624-11629.

59. Kolb, C. E.; Cox, R. A.; Abbatt, J. P. D.; Ammann, M.; Davis, E. J.; Donaldson, D. J.; Garrett, B. C.; George, C.; Griffiths, P. T.; Hanson, D. R.; Kulmala, M.; McFiggans, G.; Pöschl, U.; Riipinen, I.; Rossi, M. J.; Rudich, Y.; Wagner, P. E.; Winkler, P. M.; Worsnop, D. R.; O' Dowd, C. D. An Overview of Current Issues in the Uptake of Atmospheric Trace Gases by Aerosols and Clouds. *Atmos. Chem. Phys.* **2010,** *10* (21), 10561-10605.

60. Pöschl, U.; Rudich, Y.; Ammann, M. Kinetic Model Framework for Aerosol and Cloud Surface Chemistry and Gas-Particle Interactions - Part 1: General Equations, Parameters, and Terminology. *Atmos. Chem. Phys.* **2007,** *7* (23), 5989-6023.

61. Rader, D. J.; Grasser, T. W.; Castaneda, J. N.; Trott, W. M.; Torczynski, J. R., *Measurements of Thermal Accommodation Coefficients*. United States. Department of Energy: 2005.

62. Davidovits, P.; Worsnop, D. R.; Jayne, J. T.; Kolb, C. E.; Winkler, P.; Vrtala, A.; Wagner, P. E.; Kulmala, M.; Lehtinen, K. E. J.; Vesala, T.; Mozurkewich, M. Mass

Accommodation Coefficient of Water Vapor on Liquid Water. *Geophys. Res. Lett.* **2004,** *31* (22).

63. Vieceli, J.; Roeselová, M.; Potter, N.; Dang, L. X.; Garrett, B. C.; Tobias, D. J. Molecular Dynamics Simulations of Atmospheric Oxidants at the Air−Water Interface: Solvation and Accommodation of Oh and O₃. *J. Phys. Chem. B* **2005,** *109* (33), 15876-15892.

64. Crowley, J. N.; Ammann, M.; Cox, R. A.; Hynes, R. G.; Jenkin, M. E.; Mellouki, A.; Rossi, M. J.; Troe, J.; Wallington, T. J. Evaluated Kinetic and Photochemical Data for Atmospheric Chemistry: Volume V – Heterogeneous Reactions on Solid Substrates. *Atmos. Chem. Phys.* **2010,** *10* (18), 9059-9223.

65. Najera, J. J.; Percival, C. J.; Horn, A. B. Infrared Spectroscopic Studies of the Heterogeneous Reaction of Ozone with Dry Maleic and Fumaric Acid Aerosol Particles. *Phys. Chem. Chem. Phys.* **2009,** *11* (40), 9093-9103.

66. Davidovits, P.; Kolb, C. E.; Williams, L. R.; Jayne, J. T.; Worsnop, D. R. Update 1 Of: Mass Accommodation and Chemical Reactions at Gas−Liquid Interfaces. *Chem. Rev.* **2011,** *111* (4).

67. Ammann, M.; Pöschl, U. Kinetic Model Framework for Aerosol and Cloud Surface Chemistry and Gas-Particle Interactions - Part 2: Exemplary Practical Applications and Numerical Simulations. *Atmos. Chem. Phys.* **2007,** *7* (23), 6025-6045.

68. Finlayson-Pitts, B. J. Reactions at Surfaces in the Atmosphere: Integration of Experiments and Theory as Necessary (but Not Necessarily Sufficient) for Predicting the Physical Chemistry of Aerosols. *Phys. Chem. Chem. Phys.* **2009,** *11* (36), 7760-7779.

69. Rudich, Y.; Donahue, N. M.; Mentel, T. F. Aging of Organic Aerosol: Bridging the Gap between Laboratory and Field Studies. *Annu. Rev. Phys. Chem.* **2007,** *58* (1), 321-352.

70. Kawamura, K.; Tachibana, E.; Okuzawa, K.; Aggarwal, S. G.; Kanaya, Y.; Wang, Z. F. High Abundances of Water-Soluble Dicarboxylic Acids, Ketocarboxylic Acids and α-Dicarbonyls in the Mountaintop Aerosols over the North China Plain During Wheat Burning Season. *Atmos. Chem. Phys.* **2013,** *13* (16), 8285-8302.

71. Mkoma, S. L.; Kawamura, K. Molecular Composition of Dicarboxylic Acids, Ketocarboxylic Acids, α-Dicarbonyls and Fatty Acids in Atmospheric Aerosols from Tanzania, East Africa During Wet and Dry Seasons. *Atmos. Chem. Phys.* **2013,** *13* (4), 2235-2251.

72. Eugene, A. J.; Xia, S.-S.; Guzman, M. I. Aqueous Photochemistry of Glyoxylic Acid. *J. Phys. Chem. A* **2016,** *120* (21), 3817-3826.

73. Eugene, A. J.; Guzman, M. I. Reactivity of Ketyl and Acetyl Radicals from Direct Solar Actinic Photolysis of Aqueous Pyruvic Acid. *J. Phys. Chem. A* **2017,** *121*, 2924-2935.

74. Pillar, E. A.; Zhou, R.; Guzman, M. I. Heterogeneous Oxidation of Catechol. *J.Phys. Chem. A* **2015,** *119* (41), 10349-10359.

75. Pillar, E. A.; Guzman, M. I. Oxidation of Substituted Catechols at the Air–Water Interface: Production of Carboxylic Acids, Quinones, and Polyphenols. *Environ. Sci. Technol.* **2017,** *51*, 4951-4959.

76. Atkinson, R.; Arey, J. Atmospheric Degradation of Volatile Organic Compounds. *Chem. Rev.* **2003,** *103* (12), 4605-4638.

77. Pankow, J. F.; Asher, W. E. Simpol.1: A Simple Group Contribution Method for Predicting Vapor Pressures and Enthalpies of Vaporization of Multifunctional Organic Compounds. *Atmos. Chem. Phys. Discuss.* **2007,** *7* (4), 11839-11894.

78. Barsanti, K. C.; Pankow, J. F. Thermodynamics of the Formation of Atmospheric Organic Particulate Matter by Accretion Reactions—Part 1: Aldehydes and Ketones. *Atmos. Environ.* **2004,** *38* (26), 4371-4382.

79. Li, Y. J.; Cheong, G. Y. L.; Lau, A. P. S.; Chan, C. K. Acid-Catalyzed Condensed-Phase Reactions of Limonene and Terpineol and Their Impacts on Gas-to-Particle Partitioning in the Formation of Organic Aerosols. *Environ. Sci. Tech.* **2010,** *44* (14), 5483-5489.

80. Liggio, J.; Li, S.-M.; Brook, J. R.; Mihele, C. Direct Polymerization of Isoprene and α-Pinene on Acidic Aerosols. *Geophys. Res. Lett.* **2007,** *34* (5), L05814.

81. Williams, M. B.; Michelsen, R. R. H.; Axson, J. L.; Iraci, L. T. Uptake of Acetone, Acetaldehyde and Ethanol in Cold Sulfuric Acid Solutions Containing Organic Material: Carbon Accretion Mechanisms. *Atmos. Environ.* **2010,** *44* (9), 1145-1151.

82. Canonica, S.; Kohn, T.; Mac, M.; Real, F. J.; Wirz, J.; von Gunten, U. Photosensitizer Method to Determine Rate Constants for the Reaction of Carbonate Radical with Organic Compounds. *Environ. Sci. Technol.* **2005,** *39* (23), 9182-9188.

83. Vione, D.; Maurino, V.; Minero, C.; Pelizzetti, E.; Harrison, M. A. J.; Olariu, R.-I.; Arsene, C. Photochemical Reactions in the Tropospheric Aqueous Phase and on Particulate Matter. *Chem. Soc. Rev.* **2006,** *35* (5), 441-453.

84. Eugene, A. J.; Xia, S.-S.; Guzman, M. I. Negative Production of Acetoin in the Photochemistry of Aqueous Pyruvic Acid. *Proc. Natl. Acad. Sci.* **2013,** *110* (46), E4274-E4275.

85. Gligorovski, S.; Strekowski, R.; Barbati, S.; Vione, D. Environmental Implications of Hydroxyl Radicals ($^{\bullet}$OH). *Chem. Rev.* **2015,** *115* (24), 13051–13092.

86. Carpenter, L. J.; MacDonald, S. M.; Shaw, M. D.; Kumar, R.; Saunders, R. W.; Parthipan, R.; Wilson, J.; Plane, J. M. C. Atmospheric Iodine Levels Influenced by Sea Surface Emissions of Inorganic Iodine. *Nature Geosci.* **2013,** *6* (2), 108-111.

87. Kroll, J. H.; Smith, J. D.; Che, D. L.; Kessler, S. H.; Worsnop, D. R.; Wilson, K. R. Measurement of Fragmentation and Functionalization Pathways in the Heterogeneous Oxidation of Oxidized Organic Aerosol. *Phys. Chem. Chem. Phys.* **2009,** *11* (36), 8005-8014.

88. Zheng, G.; He, K.; Duan, F.; Cheng, Y.; Ma, Y. Measurement of Humic-Like Substances in Aerosols: A Review. *Environ. Pollut.* **2013,** *181*, 301-314.

89. Sharpless, C. M.; Aeschbacher, M.; Page, S. E.; Wenk, J.; Sander, M.; McNeill, K. Photooxidation-Induced Changes in Optical, Electrochemical, and Photochemical Properties of Humic Substances. *Environ. Sci. Technol.* **2014,** *48* (5), 2688-2696.

90. Wagner, P. E. A Constant-Angle Mie Scattering Method (CAMS) for Investigation of Particle Formation Processes. *J. Colloid Interface Sci.* **1985,** *105* (2), 456-467.

91. Kupc, A.; Winkler, P. M.; Vrtala, A.; Wagner, P. E. Unusual Temperature Dependence of Heterogeneous Nucleation of Water Vapor on Ag Particles. *Aerosol Sci. Technol.* **2013,** *47* (9), i-iv.

92. Vesala, T.; Kulmala, M.; Rudolf, R.; Vrtala, A.; Wagner, P. E. Models for Condensational Growth and Evaporation of Binary Aerosol Particles. *J. Aerosol Sci.* **1997,** *28* (4), 565-598.

93. Quinlan, M. A.; Reihs, C. M.; Golden, D. M.; Tolbert, M. A. Heterogeneous Reactions on Model Polar Stratospheric Cloud Surfaces: Reaction of Dinitrogen Pentoxide on Ice and Nitric Acid Trihydrate. *J. Phys. Chem.* **1990,** *94* (8), 3255-3260.

94. Caloz, F.; Fenter, F. F.; Tabor, K. D.; Rossi, M. J. Paper I: Design and Construction of a Knudsen-Cell Reactor for the Study of Heterogeneous Reactions over the Temperature Range 130–750 K: Performances and Limitations. *Rev. Sci. Instrum.* **1997,** *68* (8), 3172-3179.

95. Worsnop, D. R.; Zahniser, M. S.; Kolb, C. E.; Gardner, J. A.; Watson, L. R.; Van Doren, J. M.; Jayne, J. T.; Davidovits, P. The Temperature Dependence of Mass Accommodation of Sulfur Dioxide and Hydrogen Peroxide on Aqueous Surfaces. *J. Phys. Chem.* **1989,** *93* (3), 1159-1172.

96. Li, Y. Q.; Davidovits, P.; Kolb, C. E.; Worsnop, D. R. Mass and Thermal Accommodation Coefficients of $H_2O(g)$ on Liquid Water as a Function of Temperature. *J. Phys. Chem. A* **2001,** *105* (47), 10627-10634.

97. Worsnop, D. R.; Shi, Q.; Jayne, J. T.; Kolb, C. E.; Swartz, E.; Davidovits, P. Gas-Phase Diffusion in Droplet Train Measurements of Uptake Coefficients. *J. Aerosol Sci.* **2001,** *32* (7), 877-891.

98. Ryder, O. S.; Campbell, N. R.; Morris, H.; Forestieri, S.; Ruppel, M. J.; Cappa, C. D.; Tivanski, A.; Prather, K.; Bertram, T. H. Role of Organic Coatings in Regulating N_2O_5 Reactive Uptake to Sea Spray Aerosol. *J. Phys. Chem. A* **2015,** *119* (48), 11683-11692.

99. Thornberry, T.; Abbatt, J. P. D. Heterogeneous Reaction of Ozone with Liquid Unsaturated Fatty Acids: Detailed Kinetics and Gas-Phase Product Studies. *Phys. Chem. Chem. Phys.* **2004,** *6* (1), 84-93.

100. McCabe, J.; Abbatt, J. P. D. Heterogeneous Loss of Gas-Phase Ozone on n-Hexane Soot Surfaces: Similar Kinetics to Loss on Other Chemically Unsaturated Solid Surfaces. *J. Phys. Chem. C* **2009,** *113* (6), 2120-2127.

101. Arangio, A. M.; Slade, J. H.; Berkemeier, T.; Pöschl, U.; Knopf, D. A.; Shiraiwa, M. Multiphase Chemical Kinetics of OH Radical Uptake by Molecular Organic Markers of Biomass Burning Aerosols: Humidity and Temperature Dependence, Surface Reaction, and Bulk Diffusion. *J. Phys. Chem. A* **2015,** *119* (19), 4533-4544.

102. Garrett, B. C.; Schenter, G. K.; Morita, A. Molecular Simulations of the Transport of Molecules across the Liquid/Vapor Interface of Water. *Chem. Rev.* **2006,** *106* (4), 1355-1374.

103. Washenfelder, R. A.; Attwood, A. R.; Brock, C. A.; Guo, H.; Xu, L.; Weber, R. J.; Ng, N. L.; Allen, H. M.; Ayres, B. R.; Baumann, K.; Cohen, R. C.; Draper, D. C.; Duffey, K. C.; Edgerton, E.; Fry, J. L.; Hu, W. W.; Jimenez, J. L.; Palm, B. B.; Romer, P.; Stone, E. A.; Wooldridge, P. J.; Brown, S. S. Biomass Burning Dominates Brown Carbon Absorption in the Rural Southeastern United States. *Geophys. Res. Lett.* **2015,** *42* (2), 653-664.

104. DeCarlo, P. F.; Kimmel, J. R.; Trimborn, A. M.; Northway, M. J.; Jayne, J. T.; Aiken, A. C.; Gonin, M.; Fuhrer, K.; Horvath, T.; Docherty, K. S.; Worsnop, D. R.; Jimenez, J. L. Field-Deployable, High-Resolution, Time-of-Flight Aerosol Mass Spectrometer. *Anal.Chem.* **2006,** *78* (24), 8281-8289.

105. Canagaratna, M. R.; Jayne, J. T.; Jimenez, J. L.; Allan, J. D.; Alfarra, M. R.; Zhang, Q.; Onasch, T. B.; Drewnick, F.; Coe, H.; Middlebrook, A.; Delia, A.; Williams, L. R.; Trimborn, A. M.; Northway, M. J.; DeCarlo, P. F.; Kolb, C. E.; Davidovits, P.; Worsnop, D. R. Chemical and Microphysical Characterization of Ambient Aerosols with the Aerodyne Aerosol Mass Spectrometer. *Mass Spectrom. Rev.* **2007,** *26* (2), 185-222.

106. Pósfai, M.; Axisa, D.; Tompa, É.; Freney, E.; Bruintjes, R.; Buseck, P. R. Interactions of Mineral Dust with Pollution and Clouds: An Individual-Particle Tem Study of Atmospheric Aerosol from Saudi Arabia. *Atmos. Res.* **2013,** *122*, 347-361.

107. O'Brien, R. E.; Wang, B.; Kelly, S. T.; Lundt, N.; You, Y.; Bertram, A. K.; Leone, S. R.; Laskin, A.; Gilles, M. K. Liquid–Liquid Phase Separation in Aerosol Particles: Imaging at the Nanometer Scale. *Environ. Sci. Technol.* **2015,** *49* (8), 4995-5002.

108. Satsangi, P. G.; Yadav, S. Characterization of Pm$_{2.5}$ by X-Ray Diffraction and Scanning Electron Microscopy–Energy Dispersive Spectrometer: Its Relation with Different Pollution Sources. *Int. J. Environ. Sci. Technol.* **2014,** *11* (1), 217-232.

109. Sakata, K.; Sakaguchi, A.; Tanimizu, M.; Takaku, Y.; Yokoyama, Y.; Takahashi, Y. Identification of Sources of Lead in the Atmosphere by Chemical Speciation Using X-Ray Absorption near-Edge Structure (Xanes) Spectroscopy. *J. Environ. Sci.* **2014,** *26* (2), 343-352.

110. Pillar, E. A.; Eugene, A. J.; Guzman, M. I. *In Preparation* **2016**.

111. Katrib, Y.; Biskos, G.; Buseck, P. R.; Davidovits, P.; Jayne, J. T.; Mochida, M.; Wise, M. E.; Worsnop, D. R.; Martin, S. T. Ozonolysis of Mixed Oleic-Acid/Stearic-Acid Particles: Reaction Kinetics and Chemical Morphology. *J. Phys. Chem. A* **2005,** *109* (48), 10910-10919.

112. Guzman, M. I.; Athalye, R. R.; Rodriguez, J. M. Concentration Effects and Ion Properties Controlling the Fractionation of Halides During Aerosol Formation. *J. Phys. Chem. A* **2012,** *116* (22), 5428-5435.

113. Iribarne, J. V.; Thomson, B. A. On the Evaporation of Small Ions from Charged Droplets. *J. Chem. Phys.* **1976,** *64* (6), 2287-2294.

114. Bertram, T. H.; Thornton, J. A.; Riedel, T. P. An Experimental Technique for the Direct Measurement of N$_2$o$_5$ Reactivity on Ambient Particles. *Atmos. Meas. Tech.* **2009,** *2* (1), 231-242.

115. Morris, J. W.; Davidovits, P.; Jayne, J. T.; Jimenez, J. L.; Shi, Q.; Kolb, C. E.; Worsnop, D. R.; Barney, W. S.; Cass, G. Kinetics of Submicron Oleic Acid Aerosols with Ozone: A Novel Aerosol Mass Spectrometric Technique. *Geophys. Res. Lett.* **2002,** *29* (9), 711-714.

116. Sage, A. M.; Weitkamp, E. A.; Robinson, A. L.; Donahue, N. M. Reactivity of Oleic Acid in Organic Particles: Changes in Oxidant Uptake and Reaction Stoichiometry with Particle Oxidation. *Phys. Chem. Chem. Phys.* **2009,** *11* (36), 7951-7962.

117. Ziemann, P. J. Aerosol Products, Mechanisms, and Kinetics of Heterogeneous Reactions of Ozone with Oleic Acid in Pure and Mixed Particles. *Faraday Discuss.* **2005,** *130*, 469-490.

118. Docherty, K. S.; Ziemann, P. J. Reaction of Oleic Acid Particles with No$_3$ Radicals: Products, Mechanism, and Implications for Radical-Initiated Organic Aerosol Oxidation. *J. Phys. Chem. A* **2006,** *110* (10), 3567-3577.

119. Last, D. J.; Najera, J. J.; Percival, C. J.; Horn, A. B. A Comparison of Infrared Spectroscopic Methods for the Study of Heterogeneous Reactions Occurring on Atmospheric Aerosol Proxies. *Phys. Chem. Chem. Phys.* **2009,** *11* (37), 8214-8225.

120. Barnum, T. J.; Medeiros, N.; Hinrichs, R. Z. Condensed-Phase Versus Gas-Phase Ozonolysis of Catechol: A Combined Experimental and Theoretical Study. *Atmos. Environ.* **2012,** *55*, 98-106.

121. Leng, C.; Hiltner, J.; Pham, H.; Kelley, J.; Mach, M.; Zhang, Y.; Liu, Y. Kinetics Study of Heterogeneous Reactions of Ozone with Erucic Acid Using an Atr-Ir Flow Reactor. *Phys. Chem. Chem. Phys.* **2014,** *16* (9), 4350-4360.

122. Moise, T.; Flores, J. M.; Rudich, Y. Optical Properties of Secondary Organic Aerosols and Their Changes by Chemical Processes. *Chem Rev* **2015,** *115* (10), 4400-4439.

123. Zhang, R.; Wang, G.; Guo, S.; Zamora, M. L.; Ying, Q.; Lin, Y.; Wang, W.; Hu, M.; Wang, Y. Formation of Urban Fine Particulate Matter. *Chem. Rev.* **2015,** *115* (10), 3803-3855.

124. Pusede, S. E.; Steiner, A. L.; Cohen, R. C. Temperature and Recent Trends in the Chemistry of Continental Surface Ozone. *Chem. Rev.* **2015,** *115* (10), 3898-3918.

125. von Sonntag, C.; von Gunten, U., *Chemistry of Ozone in Water and Wastewater Treatment*. IWA Publishing: 2012.

Chapter 2. Conversion of Iodide to Hypoiodous Acid and Iodine in Aqueous Microdroplets Exposed to Ozone
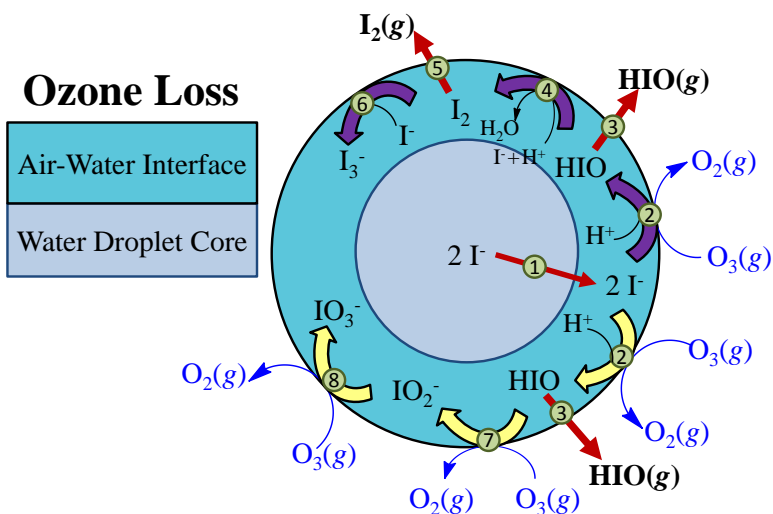
Scheme 2.1 Synopsis TOC

2.1 Synopsis

Halides are incorporated into aerosol sea spray, where they start the catalytic destruction of ozone (O_3) over the oceans and affect the global troposphere. Two intriguing environmental problems undergoing continuous research are 1) to understand how reactive gas phase molecular halogens are directly produced from inorganic halides exposed to O_3, and 2) to constrain the environmental factors that control this interfacial process. This paper presents a laboratory study of the reaction of O_3 at variable iodide (I^-) concentration (0.010-100 μM) for solutions aerosolized at 25 °C, which reveal remarkable differences in the reaction intermediates and products expected in sea spray for low tropospheric [O_3]. The ultrafast oxidation of I^- by O_3 at the air-water interface of microdroplets is evidenced by the appearance of hypoiodous acid (HIO), iodite (IO_2^-), iodate (IO_3^-), triiodide (I_3^-), and molecular iodine (I_2). Mass spectrometry measurements reveal an enhancement (up to 28%) in the dissolution of gaseous O_3 at the gas-liquid interface when increasing the concentration of NaI or NaBr from 0.010 to 100 μM. The production of iodine species such as HIO and I_2 from NaI aerosolized solutions exposed to 50 ppbv O_3 can occur at the air-water interface of sea spray, followed by their transfer to the gas-phase, where they contribute to the loss of tropospheric ozone.

2.2 Introduction

Increasing levels of greenhouse gases in the atmosphere over the past 160 years have led to a significant climate perturbation in the present timescale.[1] Ozone, $O_3(g)$, near the tropopause is an important greenhouse gas. Thus, a better understanding of the anthropogenic effects on climate requires the full characterization of the pathways of

production and destruction of tropospheric $O_3(g)$. Ozone molecules also play a key role in tropospheric chemistry, absorb infrared radiation, and have adverse effects in air quality and public health. The major source of ozone in the lower atmosphere is the oxidation of organic compounds and carbon monoxide in the presence of nitrogen oxides occurring over the continents, followed by a minor contribution from stratospheric influx.[2, 3] Ozone is transported from continental regions to the marine boundary layer (MBL), where major ozone loss occurs, primarily due to photolysis in the presence of water. However, the ozone loss calculated with all known losses, excluding halogens, accounts for only about 50% of the observed loss.[4]

Similarly to the stratospheric destruction of ozone by chlorine and bromine, halogen species emitted from surface waters, can contribute to the global decrease of ozone levels.[4] The destruction of tropospheric $O_3(g)$[5, 6] occurs at air-water and air-ice interfaces, mediated by heterogeneous reactions[7-10] catalyzed by organic species.[11-13] The activation of halogens such as Br_2 and I_2 to participate in the photochemical depletion of tropospheric ozone remains poorly understood.[14] It is well known that marine macroalgae in coastal regions produce I_2, rather than iodine-containing organic compounds, which is transferred to the atmosphere and photo-activated to release iodine atoms.[15, 16] However, measurements over the open ocean cannot be explained by this mechanism of O_3 loss.[17] Perhaps, a major contribution to the loss of tropospheric ozone over the open ocean originates from inert halide ions (e.g. Br^-, and I^-)[18, 19] or oxyanions (e.g., IO_3^-),[20] which are somehow converted into molecular halogens (e.g., Br_2 and I_2), and reactive halogen species, RHS (e.g., $Br^\bullet$, $BrO^\bullet$, and $IO^\bullet$). RHS deplete the level of $O_3(g)$ (~50 ppbv) during early spring in the Artic troposphere.[5, 21-23] The production of $I_2(g)$ and $HOI(g)$ from

submicromolar levels of aqueous I⁻ reacting with $O_3(g)$ in the top micrometer surface layer of the ocean ($pH_{ocean} \sim 8$)[24] functions as a source of IO• radicals independent of the bulk pH.[23]

The process of sea spray formation generates negatively charged droplets that contain dissolved halides salts,[25] and establishes a negative current into the atmospheric boundary layer.[26, 27] Previously it was shown how the fractionation of halides species occurring at the air-water interface[28, 29] during aerosol formation depends mainly on the concentration of species present in surface waters that is strongly biased by the size of the ions.[18] However, the remaining question to be answered is: How do those aerosolized inert halide salts are later oxidized to become RHS in the air?[14, 30] Thus, it is crucial to identify the mechanisms of production of halogen oxides in the tropical MBL.[1, 31-34] Electrospray ionization mass spectrometer (ESI-MS) was recently used at high temperature (350 °C) to propose that interfacial reactivity patterns exist in microdroplets.[35, 36] However, experiments at lower temperature are needed together with a detailed analysis of the direct reaction products and intermediates for the reaction of iodide at variable ozone concentration to model the loss of ozone. In this article, we investigate a widespread effect of halides reactions with ozone to produce I_2 and reactive species at the air-water interface at 25 °C to simulate the non-photochemical processes occurring in the MBL. This study reports the enhanced dissolution of O_3 in aerosolized microdroplets with increasing sodium halide (X^-: Br^-, I^-) concentration (10 nM − 100 μM). In addition, this study examined the cycle of ozone destruction on microdroplets by freshly produced iodine species such as HIO, HIO_2, HIO_3, the effect of polysorbate 20 surfactant to

enhance or suppress the production of iodine species, and detect for the first time the reaction intermediate HI_2O^- for the production of I_2.

2.3 Experimental Section

2.3.1 Preparation of Solutions

Sodium salts NaI (99.99%) from Fisher Scientific and NaBr (99.5%) from Acros were used. A 1.00 mM stock solution of each salt was freshly made and used to prepare 0.040, 0.400, 4.00, 40.0, 200.0, and 400.0 μM solutions. Previous solutions underwent a 4 time dilution during infusion to a final concentration of 0.010, 0.100, 1.00, 10.0, 50.0, and 100.0 μM of each halide. Solutions were prepared in ultrapure water (18.2 MΩ-cm, <5 ppb organics (TOC), <1 CFU/mL, Elga Purelab flex-Veolia), methanol, or acetonitrile (both 99.9%, Fisher Optima). We use the convention that all species are in the aqueous state, i.e., $I^-(aq) \equiv I^-$, unless indicated otherwise. Polysorbate 20 (100%, Sigma Aldrich) and samples with halides present in surface seawater[37-40] were also prepared.

The same normalized ion counts were observed for solutions at pH 6.2, 6.8, and 8.1. The pH of solutions was adjusted with 0.01 M NaOH and measured with a pH-meter (Mettler Toledo) calibrated at pH 4.01 and 7.00 or 7.00 and 10.01 with buffer solutions (Orion). Interfacial reactions 1 and 5 (Table 10.1), under the conditions investigated, may be the main pathway for the oxidation of iodine species in atmospheric particles (below pH ≈ 8). The lower pH studied (6.2) belongs to the range where the emissions of HIO(g) and I_2(g) would remain unaffected. At lower pHs also existing in the atmosphere, proton transfer at the interface may occur facilitated by weak acids and fulvic acids[12, 13] supplying the protons consumed by reactions 1 and 5, which otherwise rise the bulk pH

of the particles.[13] Therefore, an unchanged production of I_2 and HIO for the pH range studied is expected.

2.3.2 Instrument Description

The process of electrospray-ionization, ESI, has been extensively used to aerosolize nonvolatile molecules to the gas-phase region of a mass spectrometer.[41] In our ESI system (Scheme 10.2) described in more detail before,[18] a solution of electrolytes is nebulized into an atmospheric-pressure ion source region. Pneumatically assisted electrospray converts the solution into small microdroplets by the combination of a strong electric potential (i.e., 2.5 kV) between a stainless steel needle (127 μm internal diameter) and counter-electrode located at the entrance cone, and a high-flow of N_2 nebulizing gas (P = 70 psi, flow = 12 L min^{-1}). The larger velocity of the N_2 nebulizing gas over the liquid forming the plume of droplets (v_{gas} / v_{liquid} = 1.19 × 10^3) contributes to the formation of fine aerosol droplets.

The operation of the ESI probe in the negative-ion mode generates small negatively charged droplets which subsequently form a plume of solvated molecular ions that travel to the entrance cone. Neutral solvent molecules undergo evaporation from the surface of the charged droplets, causing the droplets to shrink in size, shortening the distance of the negative charges at the surface of the newly formed smaller droplets. Thus, the ions are sputtered off the surface as the charge builds up, making the experiment surface sensitive.[29] The first generation daughter droplets of smaller size experience charge crowding on the surface that generates repulsion forces that overcome the surface tension of the liquid. In consequence, the parent droplets disintegrate into daughter microdroplets that are 10-times smaller. The ionized species are attracted towards the lower pressure

orifice of the entrance cone. The ions travel through the entrance capillary at lower pressure to a quadrupole mass analyzer (accurate to 0.17 amu), for detection at specific m/z^- ratios.

Scheme 2.2. Reactor Diagram
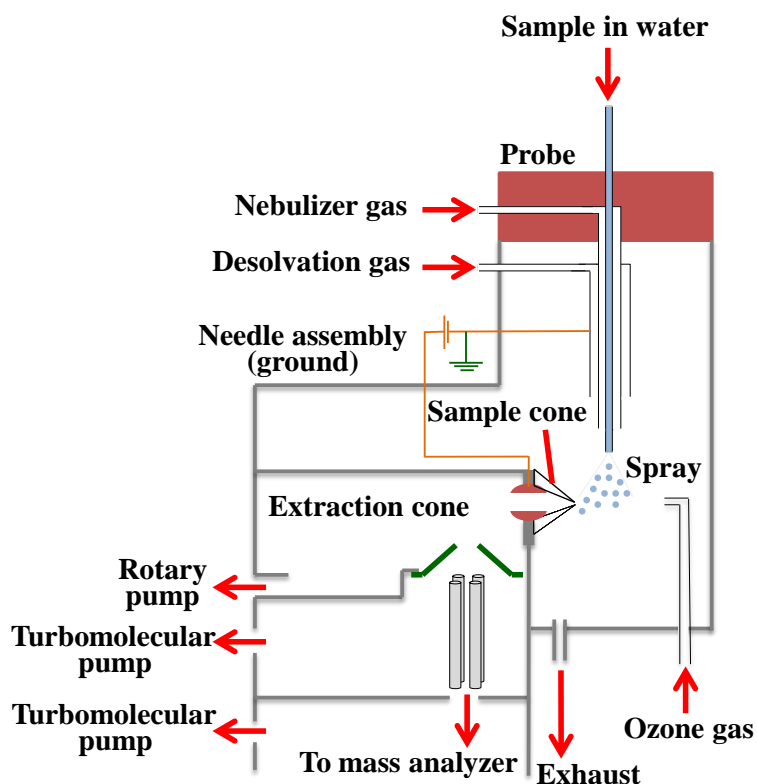
A spark discharge ozone generator (Ozone Solutions) fed with 0.1-2.0 L min^{-1} O$_2$(*g*) (ultrahigh purity, Scott-Gross) generates O$_3$(*g*) that is diluted with 1.0-5.0 L min^{-1} dry N$_2$(*g*) (ultrahigh purity, Scott-Gross). Ozone is quantified by UV absorption spectrophotometry (Evolution Array UV-Visible Spectrophotometer, Thermo Scientific) in a fused silica cuvette (10.00 cm optical path, Starna Cell) using absorption cross

sections $\sigma_{250\ nm} = 1.1 \times 10^{-17}$ cm^2 molecule^{-1}, and $\sigma_{300\ nm} = 3.9 \times 10^{-19}$ cm^2 molecule^{-1} at room temperature.[42] After dilution, ozone concentrations are fixed in the range 500 ppbv - 1000 ppmv. Then, the mixture of gases is transported to a 2 mm internal diameter stainless steel tube, which exhaust is positioned 32 mm far from the entrance cone with a 60° angle to the needle and at 12 mm distance from its center. The final flow of $O_3(g)$ is fixed at 0.200 L min^{-1} with a flow meter before encountering the aerosolized microdroplets produced from the top. The [$O_3(g)$] registered in the UV (0.2 L min^{-1}) is diluted 61-times while mixing with the $N_2(g)$ nebulizing gas (12.0 L min^{-1}), what brings a typical experimental concentration in the figures to be in the order of atmospheric relevant conditions. An experimental reading of 3 ppmv $O_3(g)$ in the UV-visible spectrophotometer is actually reported as 49 ppbv after final dilution in the chamber. Therefore, the experiments at variable ozone concentration yield fundamental mechanistic information that cover the low [$O_3(g)$] found in the troposphere. The encounter of $O_3(g)$ with the microdroplets containing iodide produces the oxidized species presented in the next section. The overall time from the formation of original droplets, transport through the ozone plume, and ion detection is <1 millisecond. However, the contact time between $O_3(g)$ and the plume of microdroplets is τ ~1 microsecond.

The nebulizer voltage of the ESI probe was optimized to 2.5 kV for maximum ion count. The cone voltage, capable of producing collisional induced dissociation (CID) of the ions, was optimized for each species to obtain the highest ion count possible for all ions. In summary, the experimental conditions were (unless indicated otherwise in a figure): Drying gas temperature, 25 °C; nebulizer voltage, –2.5 kV; cone voltage, –70 V;

and nebulizer pressure, 70 psi. Mass spectra were acquired between 25 and 440 amu, and the desired peaks were monitored. The solvent background was subtracted from the mass spectrum of the sample acquired at fixed time intervals (e.g., time $\geq$ 1 min). The flow of a solvent pump (Lab Alliance) at 150 µL/min, stabilized with a back pressure regulator, was mixed through a T connector with a 50 µL/min flow of the sample in a syringe pump (Harvard Apparatus), and directed to the ESI-MS (Thermo Scientific, MSQ Plus).

A solution composed of 1.3 mM NaI, 0.05 mM KI, and 0.02 mM CsI, in 50:50 water:2-propanol (100%, Fisher Optima) solvent, was used to calibrate the mass spectrometer within the mass range m/z^- 22.9898-1971.6149 amu. The calibration conditions were: Drying gas temperature, 350 °C; nebulizer voltage, 3 kV; cone voltage, 75 V; and nebulizer pressure 70 psi.

2.4 Results and Discussion

2.4.1 Reactions of Ozone with Iodide at the Air-Water Interface

Figure 2.1 shows electrospray mass spectra of aerosolized NaI aqueous solutions exposed to a flow of 0.2 L min^{-1} (A) $N_2(g)$, (B) 50 ppbv, (C) 130 ppbv, (D) 492 ppbv, and (E) 1.393 ppmv ppmv $O_3(g)$ at pH = 6.2. In the absence of ozone (Figure 2.1A) only I^- (m/z = 127) is detected. Upon addition of 50 ppbv $O_3(g)$, significant changes are observed (Figure 2.1B), the ion count of I^- decreases and new peaks appear: IO^- (m/z = 143, the conjugate base of HIO) and its hydrate $H_2O \cdot IO^-$ (m/z = 161), a trace of IO_2^- (m/z = 159),[43] I_2 (detected as $I_2^{-\cdot}$ at m/z = 254) becomes the dominant peak,[44] HI_2O^- (m/z = 271) the short lived reaction intermediate for the production of I_2, a practically imperceptible trace of NaI_2^- (m/z = 277) cluster,[45] and I_3^- (m/z = 381).[46] The same products are observed for

130 ppbv $O_3(g)$ (Figure 2.1C). A farther increase to 492 ppbv $O_3(g)$ clearly shows (1) the appearance of additional peaks (Figure 2.1D) for aqueous O_3 (detected as $O_3^{-\cdot}$ at $m/z = 48$), IO_3^- ($m/z = 175$), (2) an enhancement in the ion count of IO^-, IO_2^-, $H_2O\cdot IO^-$, (3) a decrease of I^-, I_2, I_3^-, and (4) the complete loss of HI_2O^-. An increase in the production of IO_3^- is detected at 1.393 ppmv $O_3(g)$ (Figure 2.1E).
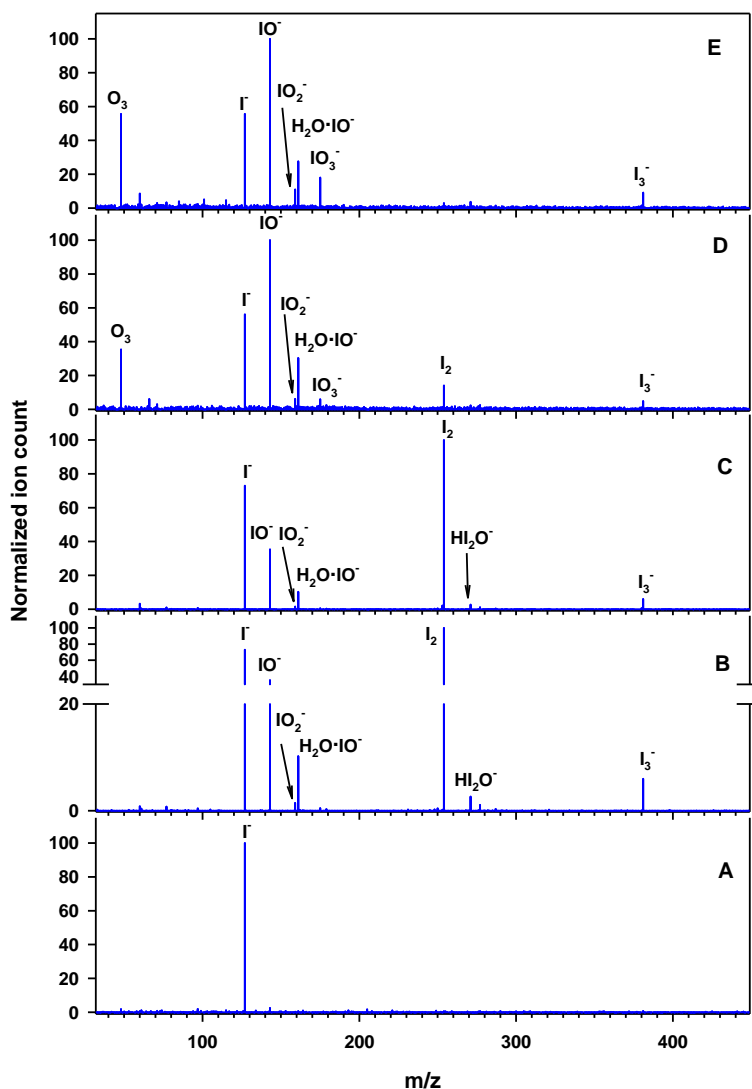
Figure 2.1. Spectra of ESI-MS of 50 μM solution of NaI at pH = 6.2 exposed to a 0.200 L min^{-1} flow (A) 1 atm $N_2(g)$, (B) 50 ppbv, (C) 130 ppbv, (D) 492 ppbv, and (E) 1.393 ppmv $O_3(g)$. Ion count values are normalized relative to the most intense peak in the mass spectrum.

The fact that neutral species such as O_3, and I_2 are detected implies that a mechanism of charge transfer is operative. Because $m/z = 48$ is not detected in a control without water, we propose that (1) $O_3(g)$ dissolves in the droplet containing ions in the early stage of aerosolization, (2) droplet evaporation occurs accompanied by fission in smaller droplets, and (3) finally the production of $O_3^{\bullet-}$ takes place from the latest progeny droplets that are the direct precursor to form the ions that reach the detector. Solvent and gas molecules are pumped away in the intermediate vacuum stage between the ESI probe and analyzer. Charge transfer to $O_3(aq)$ occurs in the last step of ion formation, and *a posteriori* of the observed reactions. Therefore, the detected $O_3^{\bullet-}$ does not play a role as a reagent in this system, and the reactions observed are from the direct interaction of I^- with molecular O_3. Otherwise, different chemistry would have resulted from $O_3^{\bullet-}$ that quickly generates $HO^{\bullet}$ in water, which could neither predict the abundance of I_3^- observed nor the formation of IO_3^-.[47]

Figure 2.2 shows how the ion count of I^-, I_2, IO^-, $H_2O \bullet IO^-$, I_3^-, IO_2^-, and IO_3^- exponentially rise to a maximum for increasing initial $[I^-]$ at constant $[O_3(g)]$. Note that although I_2 is the largest peak at 130 ppbv $O_3(g)$ (Figure 2.2A), this observation cannot be interpreted as a higher $[I_2]$ than $[I^-]_0$. Simple stoichiometry shows that for a ~20% loss of $[I^-]_0 = 100$ μM, a theoretical maximum of 10 μM I_2 could be produced. Indeed, the production of other iodine species establishes a lower yield for the production of I_2. The large ion count of I_2 can be interpreted as being correlated to the high tendency of this species to partition into the gas phase and form ions.[48] Furthermore, the chemical species are enriched or depleted at the air-water interface depending not only on their relative concentrations but also on size.[18] Under low $O_3(g)$ conditions, I_2 reacts farther to generate

I$_3^-$ (Scheme 2.3, reaction 6). An increase to 492 ppbv O$_3$(g) (Figure 2.2B) produces a dominant IO$^-$ peak and its hydrate, capable of evolving to the gas phase as HIO given its high pK_a. HIO and its hydrate are also unstable and undergo farther processing through two channels for the production of (1) I$_3^-$ and (2) IO$_3^-$. The mechanism is shifted to produce the IO$_2^-$ intermediate conducting to IO$_3^-$ final product at 1.393 ppmv O$_3$(g) (Figure 2.2C). While at 50 and 130 ppbv I$_3^-$ is a final reaction product (Figure 2.1B and C) the mechanism must shift somehow at 1.393 ppm because this species appears to be less abundant than IO$_3^-$.

The results in Figures 2.1 and 2.2 are summarized in Scheme 2.3. The experiments at variable O$_3$(g) concentration may proceed at the interface by the exothermic reaction: I$^-$ + O$_3$ → IOOO$^-$ → IO$^-$ + O$_2$.[23] The progression of the data in Figures 2.1 and 2.2, and the dependence with ozone partial pressure, P_{O_3}, indicate that the detection of the unstable intermediate IOOO$^-$ seems unlikely in these experiments. However, if the intermediate is present even at very low concentration, its mass spectrum would overlap the major isomeric IO$_3^-$ product at m/z = 175, making it undistinguishable for this technique. For relevant pH values in sea spray aerosols and surface ocean waters (pH + 2 < $pK_{a,\text{HIO}}$ = 10.4),[49] the fully undissociated hypoiodous acid, HIO, is practically the only species in the acid-base equilibrium, and therefore the precursor of I$_3^-$ and IO$_3^-$. Thus, the reaction rate equations for the consumption of the conjugate base IO$^-$ with O$_3$(g) and I$^-$ can be neglected.
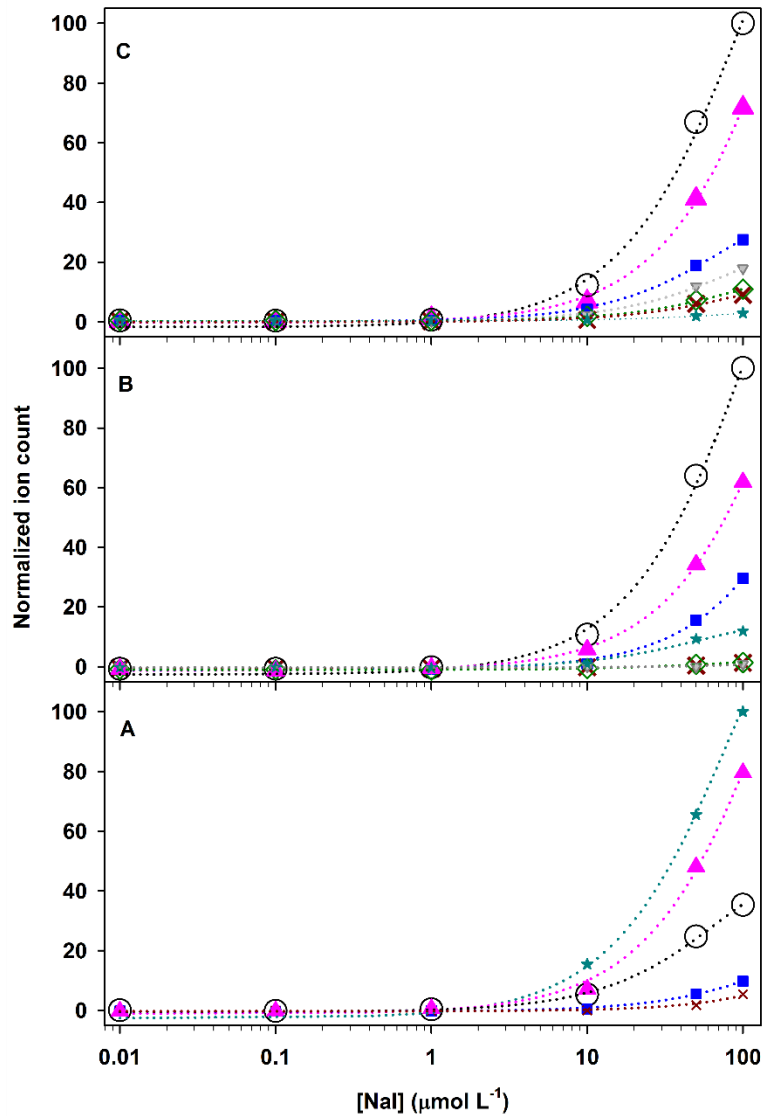
Figure 2.2. Semi-logarithmic plots of normalized ion count for ($\blacktriangle$) I⁻, ($\bigstar$) I_2, ($\bigcirc$) IO⁻, ($\blacksquare$) $H_2O \bullet IO^-$, ($\times$) I_3^-, ($\Diamond$) IO_2^-, and ($\blacktriangledown$) IO_3^- in the ESI mass spectra as a function of increasing [NaI] at pH = 6.2. Aerosolized solutions are exposed to (A) 130 ppbv, (B) 492 ppbv, and (C) 1.393 ppmv $O_3(g)$.

Scheme 2.3. Reactions of iodide in aqueous microdroplets exposed to $O_3(g)$.
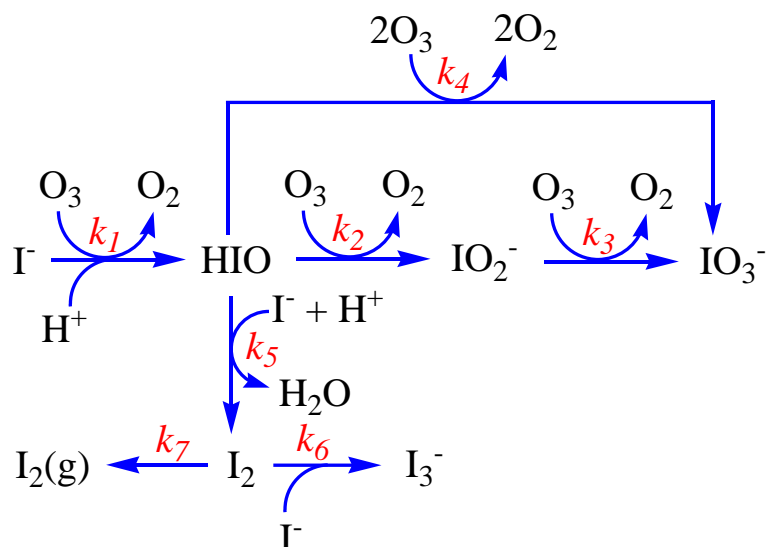
In more detail, at low ozone concentrations (Figures 2.1B, C and 2.2A), the iodide solution is converted to I_3^- through reactions 1, 5, and 6 (see Table 2.1) during aerosolization. From the viewpoint of an environmentally relevant process, reaction 1 plays a major role to feed the transfer of RHS to the gas-phase, as recently demonstrated by Carpenter *et al.*, who reported a large emission ratio $HIO(g)/I_2(g) \approx 10$, using a model with a reacto-diffusive length of ~ 1 μm undergoing processing during hours,[24] which should not be compared to the experimental δ and τ used herein. Alternatively, the fate of iodide can be the production of iodate (IO_3^-) (Figure 2.1E) at higher ozone levels. For high P_{O_3}, HIO undergoes oxidation to IO_3^- in a sequential process described by reactions 2 and 3 (Table 2.1). Because HIO is produced at the interface, its tendency to escape to the gas-phase should be higher than predicted[50] for typical bulk processes. The IO_3^- production pathway, with unknown reaction rate constants, is summarized by overall

reaction 4 (Scheme 2.3). Although the rate constant for the oxidation of IO_2^-, reaction 3, is unknown, it should proceed faster than the preceding reaction 2, and therefore is not the rate limiting step.

Table 2.1

Chemical reactions, kinetic and equilibrium constants in water at room temperature

Reaction number	Reaction	Rate or equilibrium constant	Ref.
R1	$I^- + O_3 + H^+ \rightarrow HIO + O_2$	$k_1 = 2.4 \times 10^9$ M^{-1} s^{-1}	[51]
R2	$HIO + O_3 \rightarrow IO_2^- + O_2 + H^+$	^{a}	
R3	$IO_2^- + O_3 \rightarrow IO_3^- + O_2$	^{a}	
R4	$HIO + 2\,O_3 \rightarrow IO_3^- + 2\,O_2 + H^+$	$k_4 = 3.6 \times 10^4$ M^{-1} s^{-1}	[43]
R5	$HIO + I^- + H^+ \rightarrow I_2 + H_2O$	$k_5 = 4.4 \times 10^{12}$ M^{-2} s^{-1}	[44]
R6	$I_2 + I^- \rightleftharpoons I_3^-$	$K_6 = 721$ M^{-1}, $k_6 = 6.2 \times 10^9$ M^{-1} s^{-1},	[46]
		$k_{-6} = 8.5 \times 10^6$ s^{-1}	
R7	$I_2 \rightleftharpoons I_2(g)$	$K_7 = 0.33$ atm M^{-1}	[48]
R8	$HIO \rightleftharpoons HIO(g)$	$K_8 = 5.34 \times 10^{-3}$ atm M^{-1}	[50]

All species are aqueous or liquids unless otherwise indicated. ^{a} unknown

2.4.2 Ozone Concentration Effect

Figure 2.3A shows the linear dependence for the branching ratio $[IO_3^-]/[I_3^-]$ when 100 μM I^- reacts with increasing $[O_3(g)]$, in agreement with the mechanism in Scheme 2.3. The branching ratio is directly derived from the data in panels C and D of Figure 2.3. The loss of $[I^-]$ in microdroplets appears to reach steady state conditions for $[O_3(g)]$, 1.64 ppmv (Figure 2.3B). The reactions of I^- and its follow-up products occur so quickly that other reactions of I^-, such as with HO$^\bullet$ radicals, can be disregarded.[47]

49

Figure 2.3 also shows that above 3.28 and 1.20 ppmv $O_3(g)$ the respective HIO and I_2 species reach a stationary state production in our continuous flow reactor. Remarkably, the high abundance of the intermediate HIO for all $[O_3(g)]$ range above 130 ppbv, which has the largest ion count relative to the other species, reaches a maximum at 1.47 ppmv, while it is further oxidized in the microdroplets or transferred to the gas-phase. However, the higher counts for the peak at *m/z* = 254 (Figure 2.3E) than for *m/z* = 143 (panel F) below 130 ppbv $O_3(g)$ suggests that I_2 should be considered in models that describe the chemistry over surface ocean waters. At low ozone concentration, I_2 reaches a maximum, when the production of HIO is growing from its minimum, but decays exponentially at high $[O_3(g)]$. The production of IO_3^- and I_3^- (Table 2.1, Reactions 4 and 6) in thin slabs occurs simultaneously with the fast replenishment of I^- loss from a contiguous internal layer, resulting in product yields that exceed unity at the interface even at room temperature. This surprising result agrees with the observations made by Enami and coworkers at very high temperature (T ≥ 340 °C) in a different instrumental setup.[35, 36] Thus, the experiments support the proposal that classical bulk solution models cannot be applied to explain the kinetics and mechanisms of reactions at the interface of microdroplets and sea spray aerosols.[22] Therefore, these observations need to be taken into account in future models that describe ozone loss mediated by iodine species emitted from sea spray aerosol.
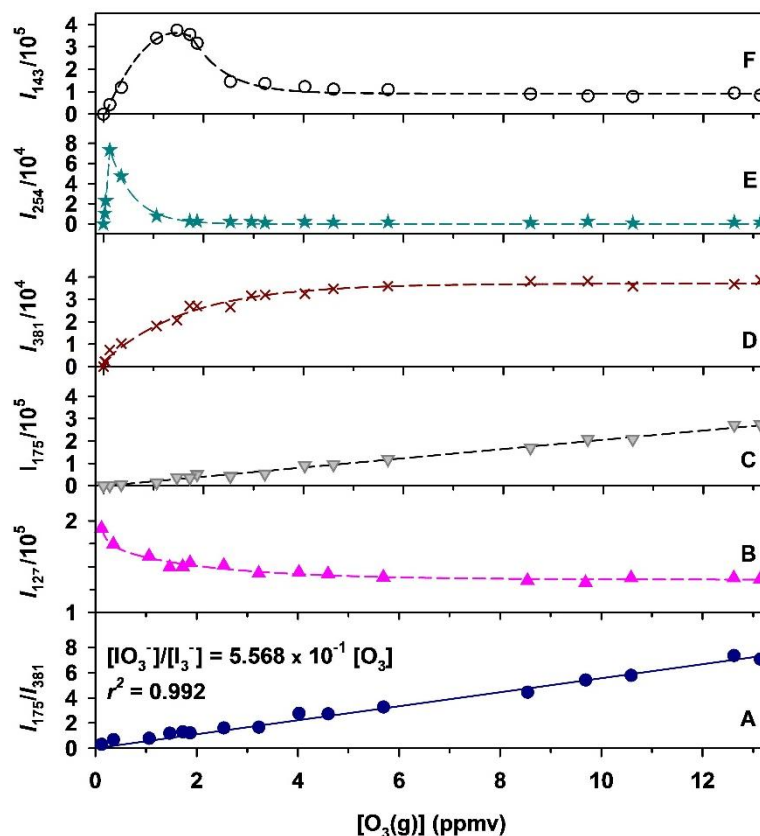
Figure 2.3. (A) Ratio of production of ions IO_3^- and I_3^-, I_{175}/I_{381}, as a function of $[O_3(g)]$ for $[I^-]_0 = 100$ μM at pH = 6.2. The data is fitted with a linear regression curve through the origin. Ion count, $I_{m/z}$, for the loss of (B) I^-, and production of (C) IO_3^-, (D) I_3^-, (E) I_2, and (F) IO^- with increasing $[O_3(g)]$.

Diffusion of iodide through an ultrathin interface occurs from the core of the droplet with diffusion coefficient $D > 2 \times 10^{-5}$ cm^2 s^{-1} in water. In a microsecond contact time ($\tau \approx 1$ μs) $O_3(g)$ interacts with the electrolytes on a nanoscopic interface of thickness $\delta \approx 1$ nm. The thickness of the interfacial reactive layer assumed ($\delta \approx 1$ nm) agrees well with previous related experiments using ESI-MS.[29] In more detail, this number was also constrained during studies that measured the availability of protons at the air-water interface that assumed the concentration of a gas-phase species reached its bulk value at

51

an interfacial depth of $\delta \approx 1.0$ nm below the Gibbs dividing surface,[52, 53] at which the interfacial water density is half its bulk value.

The duration of encounters between $O_3(g)$ and I^-, the time that the microdroplets are effectively exposed to ozone, can be estimated from the concentration of ozone by assuming it reaches the bulk value at an interface of thickness δ as described previously [52]. For example, for $\delta = 1$ nm, the effective time τ that the interfacial layer is exposed to $O_3(g)$ can be estimated from the ratio of the surface density of ozone (S_{O_3}) to the water surface collision rate (f):[52] $\tau = S_{O_3}/f$. For example, at 50 ppbv $O_3(g)$, assuming that S_{O_3} is given by $[O_3]_{interface} \times \delta = 3.225 \times 10^{11}$ molecules cm^{-3} $\times$ 1×10^{-7} cm $= 3.226 \times 10^4$ molecules cm^{-2}, and if f is given by $f = \frac{1}{4} (\gamma_w \, \upsilon_{O_3} \, n) = \frac{1}{4} (1.10 \times 10^{-2} \; 3.94$ cm s$^{-1} \; 1.231 \times 10^{12}$ molecule cm$^{-3}) = 5.34 \times 10^{10}$ molecules cm^{-2} s^{-1}, where $\gamma_w < 1$ is the uptake coefficient [9], υ_{O_3} is the mean molecular speed of the gas at 298 K, and n is the number of ozone molecules per cm^3 at 50 ppbv mixing ratio. Hence, $\tau < 3.226 \times 10^4$ molecules cm^{-2}/5.34×10^{10} molecules cm^{-2} s$^{-1} = 0.6$ μs. The same calculation for a thickness range 5-10 nm yields an effective time range of 3-6 μs, what indicates that present reactions occur in faster time scales than the 1 ms time needed from droplet formation to ion detection. Therefore, this analysis corroborates that the thickness of the interfacial layers are in the order of a few nanometers or below, supporting the assumptions that $\delta \approx 1$ nm and $\tau \approx 1$ μs.

A rigorous mathematical solution to the system under investigation requires working with differential equations describing the reaction kinetics, including diffusion through a sharp boundary.[54] However, classical methods for fixed volume batch reactors may not

be valid to model present experiments with microdroplets,[55] where the transport of species by diffusion is neither occurring over lengths that are much larger than the mean free paths, nor homogeneous.[18]

Considering that equilibrium is reached for the dissolution of $O_3(g) \rightleftharpoons O_3$, the ion count for aqueous O_3, I_{48}, is directly proportional to the recorded absorbance of $O_3(g)$ in the UV spectrophotometer. In other words, the concentration of ozone in the liquid phase is directly proportional to the partial pressure of the gas and can be retrieved from Henry's law, $[O_3] = H_0 P_{O_3}$. The proportionality Henry's law constant H_0 depends on pH, temperature, composition, and more remarkably on salt concentration. A first approximation can be applied by modeling the system as a 1-D flow reactor under equilibrium for the dissolution of O_3. In this reactor, reactant loss in a layer is quickly replenished by mass inflow from a contiguous underlying layer. Therefore, the instantaneous chemical loss and transport of I^- in the localized interfacial layers of the microdroplets can be approximately described by the equation:

$$\frac{d[I^-]}{dt} = \frac{D}{\delta \, \xi} \frac{[I^-]_0 - [I^-]}{} - k_1[O_3][I^-]$$ (Eq. 2.1)

where $[I^-]_0$ is the initial concentration of iodide, δ is the interfacial thickness defined earlier, and $\xi = 100$ cm s^{-1} relates the length over which the intradroplet concentration gradient per unit of time is established for a local process occurring with rate constant k_1 under constant ozone input. The loss of iodide is a complex process that can be described, at constant contact time, to exponentially decay with increasing ozone levels (Figure 2.3B). The solution to Equation 2.1 is:

$$[I^-] = [I^-]_0 \left(\frac{D + (1 + \delta \, \xi \, k_1 \, [O_3] - D) \, e^{-\left(\frac{1}{\delta \xi} + k_1 [O_3]\right)t}}{1 + \delta \, \xi \, k_1 \, [O_3]} \right) \qquad\qquad \text{(Eq. 2.2)}$$

The fact that Figure 2.3B levels off indicates the lack of diffusion controlled limitations. Because I^- diffuses in a few nanoseconds through the $\delta = 1$ nm layer, a stationary state ($d[I^-]/dt = 0$) is quickly established during our measurements. Assuming that the final products IO_3^- and I_3^- are generated at faster rates than the previous intermediates IO_2^- and I_2, $k_2 << k_3$ and $k_5 << k_6$, Scheme 2.3 predicts the linearity observed in Figure 2.3A between the ion count for both final products and $[O_3]$. Remarkably, due to the contribution of intradroplet diffusion to the detected interfacial $[I^-]$, the outer layer of the droplet behaves as an open reactor, in agreement with other studies.[35, 56] Therefore, present observations of products with high yields, exceeding unity values from bulk reagent concentration, occur because iodide is continuously replenished after interacting with $O_3(g)$ in the flow-through reactor.

Guzman *et al.* studied how equimolar and seawater mimic solutions of seven different anions (including Cl^-, Br^-, I^-, and IO_4^-) are enriched or depleted at the interface of the microdroplets depending on their concentration with a strong bias given by the inverse square of the size (r) of the species.[18] Therefore, although parallel calibrations are needed for a quantitative statement to assert which one is the most abundant, the high abundance of the ion IO^- ($r = 250$ pm)[57] that is smaller than the product I_3^- ($r = 470$ pm)[57] and of comparable size to the molecule of iodine (with a I-I bond distance of 267 ppm)[58] suggests that IO^- is generally the most enriched intermediate at the interface in the timescale of our measurements. However this trend is reverted for environmental relevant conditions (left hand-side of Figure 2.3E and F), because below 130 ppbv the ion count

for $m/z = 254$ is larger than for $m/z = 143$. For example a comparison of the ion counts ($I_{m/z}$) in panels E and F below 130 ppmv $O_3(g)$ yields the ratio for uncalibrated intermediates of comparable size $\phi = I_{254}/I_{143}$ to be between 1.6 and 3.2 at 120 and 50 ppbv $O_3(g)$, respectively.

2.4.3 Effect of Solvent: Solutions in Acetonitrile and Methanol

Solutions of NaI prepared in pure acetonitrile or methanol were aerosolized to compare any solvent dependent changes in the reaction mechanism in water. The experiments provide a better understanding of the interfacial reactivity of I^- with $O_3(g)$. The unique properties of each solvent represent possible differences existing in the surface coverage of marine aerosols. Sum-frequency generation vibrational spectroscopy measurements showed that the outer layer of the methanol-air interface is covered by methyl groups instead of the –OH found in water.[59] The methanol-air interface has the polar –OH group pointing into the core of the droplets. In contrast, the configuration of acetonitrile in the liquid-air interface is composed of single disordered molecules with a significant tendency to form antiparallel dipole pairs.[60] All anions present during the reaction are oriented to minimize the distortion of both interfaces.[18]

No evaluation of the species generated during the ozonolysis of iodide in methanol was reported for the branching ratio $[IO_3^-]/[I_3^-]$.[28] Therefore, the objective of Figures 2.4-2.6 is to display the identity of the reaction products in acetonitrile and methanol versus water for three different $[O_3(g)]$. For example, the key peak at $m/z = 143$ for hypoiodite is reported here for the first time in water, methanol, and acetonitrile.
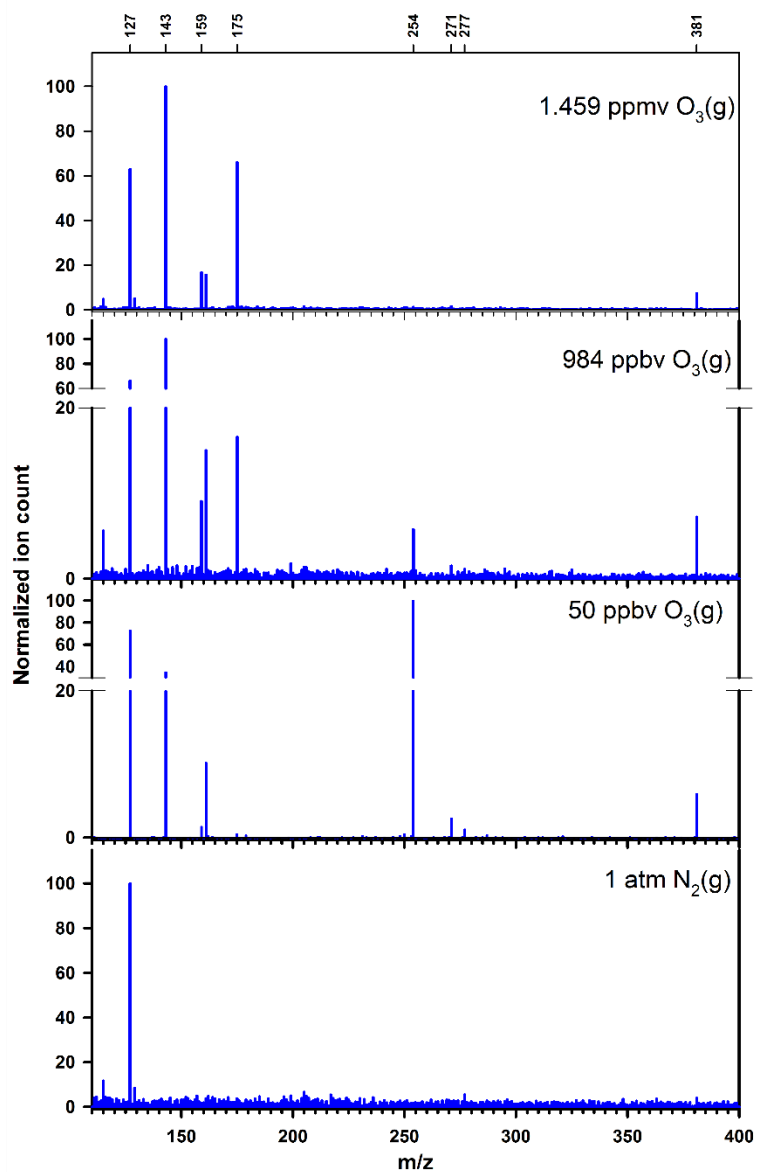
Figure 2.4. Spectra of ESI-MS of 50 μM solution of NaI at pH = 6.2 in water exposed to 1 atm $N_2(g)$, 50 ppbv $O_3(g)$, 984 ppbv $O_3(g)$, and 1.459 ppmv $O_3(g)$. Ion count values are normalized relative to the most intense peak in each mass spectrum.
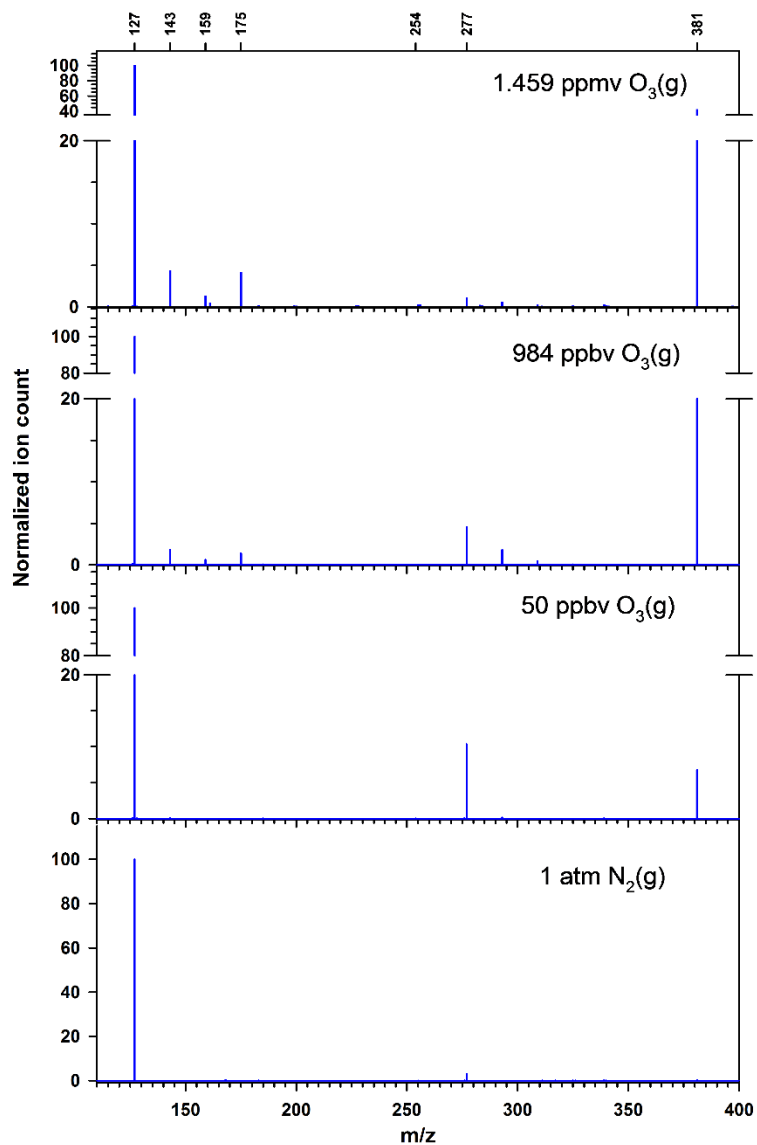
Figure 2.5. Spectra of ESI-MS of 50 μM solution of NaI in acetonitrile exposed to 1 atm N$_2$(*g*), 50 ppbv O$_3$(*g*), 984 ppbv O$_3$(*g*), and 1.459 ppmv O$_3$(*g*). Ion count values are normalized relative to the most intense peak in each mass spectrum.
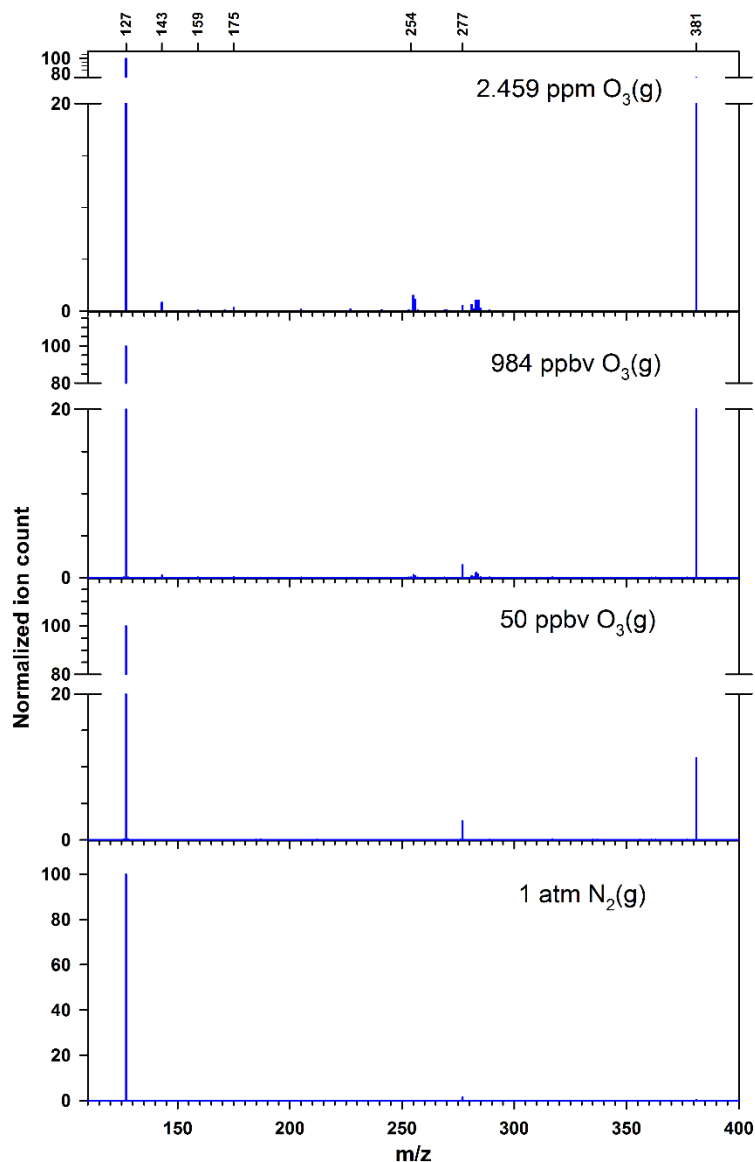
Figure 2.6. Spectra of ESI-MS of 50 μM solution of NaI in methanol exposed to 1 atm $N_2(g)$, 50 ppbv $O_3(g)$, 984 ppbv $O_3(g)$, and 2.459 ppmv $O_3(g)$. Ion count values are normalized relative to the most intense peak in each mass spectrum.

The fact that $O_3(g)$ reacts with I^- in acetonitrile and methanol to form the same products observed in water suggests a common oxidation mechanism. When a NaI solution in acetonitrile reacts with 2.459 ppmv $O_3(g)$, the relative ion count for the production of IO^-, IO_2^-, and IO_3^- drops 25, 14, and 29 times, respectively, relative to water (Figures 2.4 and

2.5). Therefore, the anion IO⁻ can undergo direct oxidation even under aprotic conditions. Furthermore, for 2.459 ppmv $O_3(g)$ reacting with I⁻ in methanol, the three oxyanions are 111, 85, and 220 times less abundant than in water (Figures 2.4 and 2.6). Remarkably, the production of $H_2O \cdot IO^-$ (m/z = 161) and the intermediate HI_2O^- (m/z = 271) in methanol and acetonitrile is not observed in the timescale of our measurements. Therefore, we propose that hydrated hypoiodous acid is a key intermediate for the production of iodine oxyanions, while naked HIO is a main precursor of I_2 and I_3^-.

The different relative abundances for oxyanion products registered in organic solvents also suggests a shorter droplet lifetime together with a more favorable liquid-to-gas transfer for species that do not contain oxygen atoms (Figures 2.4–2.6). The gradual volatility increase accompanying the simultaneous decrease in boiling temperatures $T_{b,water} > T_{b,acetonitrile} > T_{b,methanol}$ (100 > 82 > 65 °C) and surface tension $\gamma_{water} > \gamma_{acetonitrile} > \gamma_{methanol}$ (72 > 29 > 22 dyn cm⁻¹),[61] results in a shorter contact time between O_3, I⁻, and their products in the droplets.[62] Possibly, the shorter lifetime of the organic droplets favors the reaction of first generation oxidation product HIO with nearby and more abundant I⁻ to generate I_2 and later enhance the intradroplet concentration of I_3^-. The unfavorable channel of IO_3^- production presumably requires a longer contact time for the reaction with O_3 and/or the presence of $H_2O \cdot IO^-$.

2.4.4 Enhanced Dissolution of Ozone by Electrolytes

The dissolution of $O_3(g)$ in microdroplets for increasing [NaI] and [NaBr] is quantified from the single ion monitoring (SIM) MS at *m/z* = 48, background subtracted from the ion count registered in pure water, and finally converted to aqueous solubility by Henry's law (Figure 2.7). The Henry's law constant H_0 = 0.011 M atm⁻¹ [63], the vapor pressure of

water $P_{H_2O} = 0.0312$ atm[61] at 298 K, and $P_{O_3} = 2.459$ ppmv are used in the conversion. The Henry's law constant H remains practically equal to its value in pure water H_0 in the presence of dilute electrolytes. Figure 2.7 also represents the percentage increase of O_3 dissolution by aqueous microdroplets containing electrolytes.
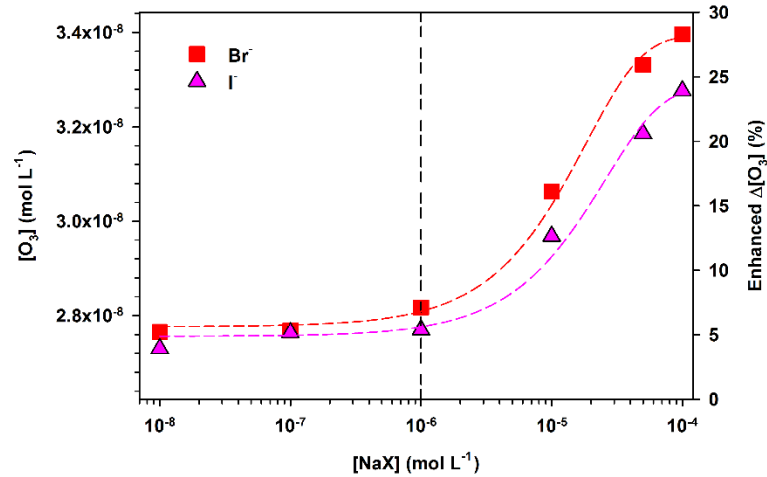
Figure 2.7. Solubility of ozone, $[O_3]$, in microdroplets for increasing concentration of (■) NaBr and (▲) NaI relative to ultrapure water. Data processed using Henry's law constant,[63] single ion monitoring MS of peak $m/z = 48$, and $O_3(g)$ absorption at 250 nm. $P_{O_3} = 2.459$ ppmv. The scale to the right hand-side of the plot shows the percentage of $[O_3]$ enhancement in the presence of individual electrolytes.

Since the Sechenov equation[64, 65] at constant temperature and pH fails to explain the behavior of O_3 observed in Figure 2.7, a modified equation is introduced for simple dilute electrolytes ($[NaX] \to 0$). Equation 2.3 predicts the solubility increment of the gas in short lived micrometer size water droplets:

$$[O_3] = [O_3]_0 + [O_3]_{100\,\mu M}\,(1 - exp^{-(K_G[NaX])})$$ (Eq. 2.3)

where $[O_3]_{100 \mu M}$ indicates the amplitude in Figure 2.7, K_G is a constant, and $[O_3]_0$ is the offset from zero. Indeed, the experimental results reflect the uptake of O_3 at the air-water interface in $\tau = 1$ µs. The best fitting parameters describing Figure 10.7 with Equation 2.3 for each halide are $[O_3]_{Br^-} = 2.78 \times 10^{-2} + 6.16 \times 10^{-1} (1 - exp^{-5.43 \times 10^{-2}[NaBr]})$ and $[O_3]_{I^-} = 2.76 \times 10^{-2} + 5.27 \times 10^{-1} (1 - exp^{-3.85 \times 10^{-2}[NaI]})$, both with coefficient of correlation $r^2 \geq 0.990$.

Present measurements represent a steady state ($d[O_3]/dt = 0$) at the interface because no accumulation occurs over time. The mass transfer of gaseous ozone below 1 µM sodium halide is practically constant for both species, and suddenly increases above this concentration indicated by a perpendicular dashed line in Figure 2.7. Therefore, the mass transfer of $O_3(g)$ into the aqueous phase is the most important phenomena affecting the experiment in Figure 2.7, followed by the reactivity of O_3 with I^-, because other individual halides remain inert. A simple comparison of the amplitude in Figure 2.7 shows that $[O_3]_{100 \mu M}$ in I^- is only a 14% lower than in Br^-.

The measured $[O_3]$ depends on time, the liquid film mass transfer coefficient, and the interfacial area of the microdroplets.[66] The rate of autodecomposition of ozone in the interfacial layer can be neglected in the ultrafast contact time of our measurements. Therefore, the observable $[O_3]$ cannot be related to the solubility concentration in a bulk solution that is typically less than the equilibrium concentration due to autodecomposition. Instead, the enhanced change in $[O_3]$, expressed as a percentage, represents the actual solubility concentration in the interfacial region where mass transfer takes place. In other words, since the MS monitors the process occurring on the outer

layers of the microdroplets,[18] the interfacial concentration $[O_3]_{interface}$ is assumed equal to the equilibrium concentration $[O_3]$.

The uptake of ozone by water implies several steps related to properties of the interface, gas- and condensed-phases. The uptake process starts with the diffusion of $O_3(g)$ molecules toward the water interface, followed by the mass transfer across the interface (accommodation process), diffusion and reaction with iodide in the condensed phase, and desorption of the gas-phase reaction products. The surface density of ozone molecules in the interface, S_{O_3} (molecules cm^{-2}), can be estimated from the concentration of dissolved ozone $[O_3]$ (molecules cm^{-3}) in the thin slab of thickness $\delta = 1 \times 10^{-7}$ cm from the equation

$$S_{O_3} = \delta \, [O_3] = v_{O_3} \tau \, \gamma_w \, [O_3(g)]/4 \qquad \text{(Eq. 2.4)}$$

where $v_{O_3} = 3.94$ cm s^{-1} is the mean thermal velocity of gaseous ozone at 298 K, $[O_3(g)]$ is the concentration of ozone molecules striking the liquid microdroplets with a contact time $\tau = 1 \times 10^{-6}$ s, and γ_w is the uptake coefficient of ozone in water. Considering the uptake in Figure 2.7, for dilute 100 μM NaBr aerosolized solution for microdroplets exposed to $P_{O_3} = 2.459$ ppmv yields $\gamma_w = 4.45 \times 10^{-7}$, a low limit that is comparable to the value obtained at interfaces for bromide[62] or anthracene.[67]

2.4.5 Effect of Surfactant

Many organic compounds present in surface ocean water are surfactant agents also emitted to the atmosphere as part of sea spray aerosol. Therefore, it is important to explore the effect of surfactants on the oxidation of iodide. Figure 2.8 shows that the

nonionic surfactant polysorbate 20 has a minor effect during the ozonolysis of iodide

below [polysorbate 20] = 10^{-5} mol L^{-1}. The addition of the surfactant below the critical

micelle concentration (CMC)[68] to the NaI solution exposed to 2.705 ppmv $O_3(g)$

decreases the total ion count and alters the interface. The surfactant forms micelles at the

CMC,[68] 8.0×10^{-5} M of polysorbate 20.[69] For low surfactant concentration the

normalized ion count in the presence of surfactant, are close to their values in water as

indicated by the proximity of the experimental points to the horizontal dashed line. The

highest ion count corresponds always to HIO for the whole [polysorbate 20] interval. At

this [$O_3(g)$], the ion IO^- covers the majority of the interfacial layer for surfactant and

surfactant-free solutions.
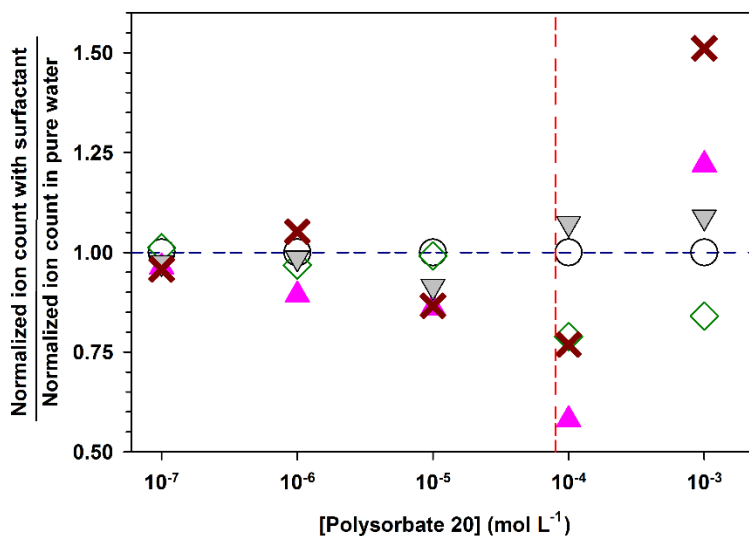
Figure 2.8. Ratios of normalized ion count in the presence and absence of surfactant for $[I^-]_0 = 50$ μM at pH = 6.2 and 2.705 ppmv $O_3(g)$, at variable concentration of polysorbate 20: (▲) I^-, (◯) IO^-, (×) I_3^-, (◇) IO_2^-, and (▽) IO_3^-. The red dashed vertical line indicates the critical micelle concentration,[69] and the blue dashed horizontal line represents no change in the presence of surfactant relative to pure water microdroplets.

The results for low [polysorbate 20] indicate the fast bulk accommodation of $O_3(g)$[9] is still the controlling factor for reaction 1. Under these conditions, polysorbate 20 behaves as a nonreactive amphiphile,[10] with a behavior similar to a short chained permeable surfactant such as undissociated nonanoic acid (C_9),[10] which minimally affects the uptake coefficient of O_3 ($\gamma_w = 1.1 \times 10^{-2}$ for deliquesced KI particles).[10] However, a different behavior may occur in the presence of reactive organic species that can compete with I^- to react with $O_3(g)$, such as amphiphilic fulvic acids that can transfer $H^+_{interface}$ through weak carboxylic acids moieties, and enhance the emission of $I_2(g)$ from submicrometer particles.[12, 13]

Significant changes occur above the CMC (vertical red dashed line in Figure 2.8). For [polysorbate 20] $= 10^{-4}$ M, there is an abrupt interfacial depletion of $I^- < I_3^- < IO_2^-$, and a minor enrichment in the production of IO_3^- in the reactive surface layers. In the presence of 1 mM surfactant, I_3^-, I^-, and IO_3^- become approximately 50, 20, and 7% more enriched than in water. At high surfactant loading, the ions compete for the surface sites based on their relative concentration in a process strongly influenced by their size, polarizability, and geometry.[18] The surfactant produces a salting out or salting in of the ions relative to the hydrophobic groups of polysorbate 20.[68] At 1 mM, the hydrophobic groups of the surfactant are not in contact with the aqueous phase in the micellar form, favoring the salting out of the largest I_3^- ion. The strong salt out of even low amounts of I_3^- reflects its ability to highly alter interfacial water structure.[68] However, the presence of surfactant does not prevent the loss of ozone and the production of I_2 and HIO.

2.4.6 Atmospheric Implications

The mechanism investigated here indicates that inorganic processes in sea salt spray could also be an important source of halogens, particularly gaseous I_2 and HIO, in the MBL. Both photoactive species HIO and I_2 produce iodine atoms in the gas-phase, capable of forming the iodine monoxide radical (IO$^\bullet$), and regenerate I$^\bullet$ by different pathways of ozone loss.[70] This was pointed out using processes at the air-sea interface as a source,[24] and here we expand the potential sources to sea spray. This process occurs throughout the ocean, and thus impacts the global tropospheric ozone budget. The interaction of $O_3(g)$ with nano- and micromolar solutions of I$^-$ in the presence of Cl$^-$, Br$^-$, and surfactants generate reactive iodine species even at nighttime.[71] In sea spray at low [I$^-$], considerable [HIO] can be produced *in situ* in interfacial reactions that facilitate its transfer to the gas-phase.

One-dimensional models of the MBL[24] have been used to estimate the source from the sea for a given set of average conditions. However, the actual source will vary geographically. Production of sea spray will be very sensitive to local conditions, particularly surface winds. The production of iodine (Scheme 2.3) will depend on temperature, humidity, pH, the concentration of halogen species in the liquid phase, and droplet size. Finally, the balance between transport of ozone from the continents to the ocean, and its loss in the MBL is best simulated by global three-dimensional models which include complete gas phase chemistry and long-range transport.

Future modeling efforts should apply first a chemistry-diffusion-evaporation model of the droplet to derive pseudo first order rates for the "net" source processes described in reactions 1 and 5 (Scheme 2.3 and Table 2.1). Reaction 1 constitutes a direct loss of

ozone on the gas-phase surface, in addition to contributing to iodine production, which also leads to ozone destruction. Scheme 2.3 also suggests another heterogeneous loss of O_3 through (net) reaction 4 (Table 2.1). We expect that all the above parameterizations will include a dependence on temperature, humidity, pH and possibly droplet size, resulting from such dependencies of the relevant Henry's law constant, evaporation rates, and aqueous reactions. Such parameterizations exist for some of the chlorine and bromine reactions[42] that take place in polar stratospheric clouds and which contribute to the formation of the ozone hole.

2.5 Acknowledgement

2.6 References

1. Forster, P.; Ramaswamy, V.; Artaxo, P.; Berntsen, T.; Betts, R.; Fahey, D. W.; Haywood, J.; Lean, J.; Lowe, D. C.; Myhre, G.; Nganga, J.; Prinn, R.; Raga, G.; Schulz, M.; Van Dorland, R., Changes in Atmospheric Constituents and in Radiative Forcing. In *Climate Change 2007: The Physical Science Basis. Contribution of Working Group I to the Fourth Assessment Report of the Intergovernmental Panel on Climate Change*, Solomon, S.; Qin, D.; Manning, M.; Chen, Z.; Marquis, M.; Averyt, K. B.; Tignor, M.; Miller, H. L., Eds. Cambridge University Press: Cambridge, United Kingdom and New York, NY, USA, 2007.

2. Denman, K. L.; Brasseur, G.; Chidthaisong, A.; Ciais, P.; Cox, P. M.; Dickinson, R. E.; Hauglustaine, D.; Heinze, C.; Holland, E.; Jacob, D.; Lohmann, U.; Ramachandran, S.; da Silva Dias, P. L.; S.C.;, W.; Zhang, X., Couplings between Changes in the Climate System and Biogeochemistry. In *Climate Change 2007: The Physical Science Basis. Contribution of Working Group I to the Fourth Assessment Report of the Intergovernmental Panel on Climate Change*, Solomon, S.; Qin, D.; Manning, M.; Chen, Z.; Marquis, M.; Averyt, K. B.; Tignor, M.; Miller, H. L., Eds. Cambridge University Press: Cambridge, United Kingdom and New York, NY, USA, 2007.

3. Murphy, D. M.; Fahey, D. W. An Estimate of the Flux of Stratospheric Reactive Nitrogen and Ozone into the Troposphere. *J. Geophys. Res.-Atmos.* **1994,** *99* (D3), 5325-5332.

4. Read, K. A.; Mahajan, A. S.; Carpenter, L. J.; Evans, M. J.; Faria, B. V. E.; Heard, D. E.; Hopkins, J. R.; Lee, J. D.; Moller, S. J.; Lewis, A. C.; Mendes, L.; McQuaid, J. B.; Oetjen, H.; Saiz-Lopez, A.; Pilling, M. J.; Plane, J. M. C. Extensive Halogen-Mediated Ozone Destruction over the Tropical Atlantic Ocean. *Nature* **2008,** *453* (7199), 1232-1235.

5. Barrie, L. A.; Bottenheim, J. W.; Schnell, R. C.; Crutzen, P. J.; Rasmussen, R. A. Ozone Destruction and Photochemical Reactions at Polar Sunrise in the Lower Arctic Atmosphere. *Nature* **1988,** *334* (6178), 138-141.

6. Carpenter, L. J.; Hopkins, J. R.; Jones, C. E.; Lewis, A. C.; Parthipan, R.; Wevill, D. J.; Poissant, L.; Pilote, M.; Constant, P. Abiotic Source of Reactive Organic Halogens in the Sub-Arctic Atmosphere? *Environ. Sci. Technol.* **2005,** *39* (22), 8812-8816.

7. Wren, S. N.; Donaldson, D. J. Glancing-Angle Raman Spectroscopic Probe for Reaction Kinetics at Water Surfaces. *Phys. Chem. Chem. Phys.* **2010,** *12* (11), 2648-2654.

8. Reeser, D. I.; Donaldson, D. J. Influence of Water Surface Properties on the Heterogeneous Reaction between $O_3(g)$ and $I^-(aq)$. *Atmos. Environ.* **2011,** *45* (34), 6116-6120.

9. Rouvière, A. l.; Sosedova, Y.; Ammann, M. Uptake of Ozone to Deliquesced Ki and Mixed KI/NaCl Aerosol Particles. *J. Phys. Chem. A* **2010,** *114* (26), 7085-7093.

10. Rouvière, A.; Ammann, M. The Effect of Fatty Acid Surfactants on the Uptake of Ozone to Aqueous Halogenide Particles. *Atmos. Chem. Phys.* **2010,** *10* (23), 11489-11500.

11. Hayase, S.; Yabushita, A.; Kawasaki, M.; Enami, S.; Hoffmann, M. R.; Colussi, A. J. Heterogeneous Reaction of Gaseous Ozone with Aqueous Iodide in the Presence of Aqueous Organic Species. *J. Phys. Chem. A* **2010,** *114* (19), 6016-6021.

12. Hayase, S.; Yabushita, A.; Kawasaki, M.; Enami, S.; Hoffmann, M. R.; Colussi, A. J. Weak Acids Enhance Halogen Activation on Atmospheric Water's Surfaces. *J. Phys. Chem. A* **2011,** *115* (19), 4935-4940.

13. Hayase, S.; Yabushita, A.; Kawasaki, M. Iodine Emission in the Presence of Humic Substances at the Water's Surface. *J. Phys. Chem. A* **2012,** *116* (24), 5779-5783.

14. Simpson, W. R.; von Glasow, R.; Riedel, K.; Anderson, P.; Ariya, P.; Bottenheim, J.; Burrows, J.; Carpenter, L. J.; Frieß, U.; Goodsite, M. E.; Heard, D.; Hutterli, M.; Jacobi, H. W.; Kaleschke, L.; Neff, B.; Plane, J.; Platt, U.; Richter, A.; Roscoe, H.; Sander, R.; Shepson, P.; Sodeau, J.; Steffen, A.; Wagner, T.; Wolff, E. Halogens and Their Role in Polar Boundary-Layer Ozone Depletion. *Atmos. Chem. Phys.* **2007,** *7* (16), 4375-4418.

15. Huang, R. J.; Seitz, K.; Buxmann, J.; Pöhler, D.; Hornsby, K. E.; Carpenter, L. J.; Platt, U.; Hoffmann, T. *In Situ* Measurements of Molecular Iodine in the Marine

Boundary Layer: The Link to Macroalgae and the Implications for O_3, IO, OIO and NO_x. *Atmos. Chem. Phys.* **2010,** *10* (10), 4823-4833.

16. Huang, R. J.; Thorenz, U. R.; Kundel, M.; Venables, D. S.; Ceburnis, D.; Ho, K. F.; Chen, J.; Vogel, A. L.; Küpper, F. C.; Smyth, P. P. A.; Nitschke, U.; Stengel, D. B.; Berresheim, H.; O'Dowd, C. D.; Hoffmann, T. The Seaweeds *Fucus Vesiculosus* and *Ascophyllum Nodosum* Are Significant Contributors to Coastal Iodine Emissions. *Atmos. Chem. Phys.* **2013,** *13* (10), 5255-5264.

17. von Glasow, R. Atmospheric Chemistry: Sun, Sea, and Ozone Destruction. *Nature* **2008,** *453* (7199), 1195-1196.

18. Guzman, M. I.; Athalye, R. R.; Rodriguez, J. M. Concentration Effects and Ion Properties Controlling the Fractionation of Halides During Aerosol Formation. *J. Phys. Chem. A* **2012,** *116* (22), 5428-5435.

19. Garland, J. A.; Curtis, H. Emission of Iodine from the Sea Surface in the Presence of Ozone. *J. Geophys. Res.-Oceans* **1981,** *86* (C4), 3183-3186.

20. Saunders, R. W.; Kumar, R.; MacDonald, S. M.; Plane, J. M. C. Insights into the Photochemical Transformation of Iodine in Aqueous Systems: Humic Acid Photosensitized Reduction of Iodate. *Environ. Sci. Technol.* **2012,** *46* (21), 11854-11861.

21. Liao, J.; Sihler, H.; Huey, L. G.; Neuman, J. A.; Tanner, D. J.; Friess, U.; Platt, U.; Flocke, F. M.; Orlando, J. J.; Shepson, P. B.; Beine, H. J.; Weinheimer, A. J.; Sjostedt, S. J.; Nowak, J. B.; Knapp, D. J.; Staebler, R. M.; Zheng, W.; Sander, R.; Hall, S. R.; Ullmann, K. A Comparison of Arctic Bro Measurements by Chemical Ionization Mass Spectrometry and Long Path-Differential Optical Absorption Spectroscopy. *J. Geophys. Res.-Atmos.* **2011,** *116*, D00R02.

22. Hunt, S. W.; Roeselová, M.; Wang, W.; Wingen, L. M.; Knipping, E. M.; Tobias, D. J.; Dabdub, D.; Finlayson-Pitts, B. J. Formation of Molecular Bromine from the Reaction of Ozone with Deliquesced Nabr Aerosol: Evidence for Interface Chemistry. *J. Phys. Chem. A* **2004,** *108* (52), 11559-11572.

23. Sakamoto, Y.; Yabushita, A.; Kawasaki, M.; Enami, S. Direct Emission of I_2 Molecule and IO Radical from the Heterogeneous Reactions of Gaseous Ozone with Aqueous Potassium Iodide Solution. *J. Phys. Chem. A* **2009,** *113* (27), 7707-7713.

24. Carpenter, L. J.; MacDonald, S. M.; Shaw, M. D.; Kumar, R.; Saunders, R. W.; Parthipan, R.; Wilson, J.; Plane, J. M. C. Atmospheric Iodine Levels Influenced by Sea Surface Emissions of Inorganic Iodine. *Nature Geosci.* **2013,** *6* (2), 108-11.

25. Reiter, R. Charges on Particles of Different Size from Bubbles of Mediterranean Sea Surf and from Waterfalls. *J. Geophys. Res.-Atmos.* **1994,** *99* (D5), 10807-10812.

26. Bhattacharyya, I.; Maze, J. T.; Ewing, G. E.; Jarrold, M. F. Charge Separation from the Bursting of Bubbles on Water. *J. Phys. Chem. A* **2011,** *115* (23), 5723-5728.

27. Blanchard, D. C. Electrically Charged Drops from Bubbles in Sea Water and Their Meteorological Significance. *J. Meteorology* **1958,** *15* (4), 383-396.

28. Cheng, J.; Hoffmann, M. R.; Colussi, A. J. Anion Fractionation and Reactivity at Air/Water:Methanol Interfaces. Implications for the Origin of Hofmeister Effects. *J. Phys. Chem. B* **2008,** *112* (24), 7157-7161.

29. Cheng, J.; Vecitis, C. D.; Hoffmann, M. R.; Colussi, A. J. Experimental Anion Affinities for the Air/Water Interface. *J. Phys. Chem. B* **2006,** *110* (51), 25598-25602.

30. Platt, U.; Honninger, G. The Role of Halogen Species in the Troposphere. *Chemosphere* **2003,** *52* (2), 325-338.

31. O'Dowd, C. D.; Jimenez, J. L.; Bahreini, R.; Flagan, R. C.; Seinfeld, J. H.; Hameri, K.; Pirjola, L.; Kulmala, M.; Jennings, S. G.; Hoffmann, T. Marine Aerosol Formation from Biogenic Iodine Emissions. *Nature* **2002,** *417* (6889), 632-636.

32. Thomas, J. L.; Jimenez-Aranda, A.; Finlayson-Pitts, B. J.; Dabdub, D. Gas-Phase Molecular Halogen Formation from NaCl and NaBr Aerosols: When Are Interface Reactions Important? *J. Phys. Chem. A* **2006,** *110* (5), 1859-1867.

33. McMurdo, C. J.; Ellis, D. A.; Webster, E.; Butler, J.; Christensen, R. D.; Reid, L. K. Aerosol Enrichment of the Surfactant PFO and Mediation of the Water−Air Transport of Gaseous PFOA. *Environ. Sci. Technol.* **2008,** *42* (11), 3969-3974.

34. Finlayson-Pitts, B. J. Halogens in the Troposphere. *Anal. Chem.* **2009,** *82* (3), 770-776.

35. Enami, S.; Vecitis, C. D.; Cheng, J.; Hoffmann, M. R.; Colussi, A. J. Global Inorganic Source of Atmospheric Bromine. *J. Phys. Chem. A* **2007,** *111* (36), 8749-8752.

36. Enami, S.; Vecitis, C. D.; Cheng, J.; Hoffmann, M. R.; Colussi, A. J. Mass Spectrometry of Interfacial Layers During Fast Aqueous Aerosol/Ozone Gas Reactions of Atmospheric Interest. *Chem. Phys. Lett.* **2008,** *455* (4–6), 316-320.

37. Stumm, W.; Morgan, J. J., *Aquatic Chemistry*. 3rd ed.; Wiley: 1996; p 1040.

38. Fukushi, K.; Watanabe, K.; Takeda, S.; Wakida, S. I.; Yamane, M.; Higashi, K.; Hiiro, K. Determination of Bromide Ions in Seawater by Capillary Zone Electrophoresis Using Diluted Artificial Seawater as the Buffer Solution. *J. Chromatogr. A* **1998,** *802* (1), 211-217.

39. Wong, G. T. F.; Zhang, L. S. Seasonal Variations in the Speciation of Dissolved Iodine in the Chesapeake Bay. *Estuar. Coast. Shelf Sci.* **2003,** *56* (5-6), 1093-1106.

40. Martinelango, P. K.; Tian, K.; Dasgupta, P. K. Perchlorate in Seawater - Bioconcentration of Iodide and Perchlorate by Various Seaweed Species. *Anal. Chim. Acta* **2006,** *567* (1), 100-107.

41. Cody, R. B., Electrospray Ionization Mass Spectrometry: History, Theory, and Instrumentation. In *Applied Electrospray Mass Spectrometry*, 1st ed.; Pramanik, B. N.; Ganguly, A. K.; Gross, M. L., Eds. Taylor & Francis: New York, 2002; p 464.

42. Sander, S. P.; Abbatt, J.; Barker, J. R.; Burkholder, J. B.; Friedl, R. R.; Golden, D. M.; Huie, R. E.; Kolb, C. E.; Kurylo, M. J.; Moortgat, G. K.; Orkin, V. L.; Wine, P. H., Chemical Kinetics and Photochemical Data for Use in Atmospheric Studies: Evaluation Number 17. In Jet Propulsion Laboratory, California Institute of Technology, Pasadena, CA, http://jpldataeval.jpl.nasa.gov: 2011.

43. Bichsel, Y.; von Gunten, U. Oxidation of Iodide and Hypoiodous Acid in the Disinfection of Natural Waters. *Environ. Sci. Technol.* **1999,** *33* (22), 4040-4045.

44. Eigen, M.; Kustin, K. The Kinetics of Halogen Hydrolysis. *J. Am. Chem. Soc.* **1962,** *84* (8), 1355-1361.

45. Hao, C.; March, R. E.; Croley, T. R.; Smith, J. C.; Rafferty, S. P. Electrospray Ionization Tandem Mass Spectrometric Study of Salt Cluster Ions. Part 1— Investigations of Alkali Metal Chloride and Sodium Salt Cluster Ions. *J. Mass. Spec.* **2001,** *36* (1), 79-96.

46. Troy, R. C.; Kelley, M. D.; Nagy, J. C.; Margerum, D. W. Non-Metal Redox Kinetics: Iodine Monobromide Reaction with Iodide Ion and the Hydrolysis of Ibr. *Inorg. Chem.* **1991,** *30* (25), 4838-4845.

47. von Sonntag, C.; von Gunten, U., *Chemistry of Ozone in Water and Wastewater Treatment: From Basic Principles to Applications*. IWA Publishing: 2012; p 302.

48. Palmer, D. A.; Ramette, R. W.; Mesmer, R. E. The Hydrolysis of Iodine: Equilibria at High Temperatures. *J. Nucl. Mater.* **1985,** *130* (0), 280-286.

49. Bichsel, Y.; von Gunten, U. Hypoiodous Acid: Kinetics of the Buffer-Catalyzed Disproportionation. *Water Res.* **2000,** *34* (12), 3197-3203.

50. Lin, C.-C. Volatility of Iodine in Dilute Aqueous Solutions. *J. Inorg. Nucl. Chem.* **1981,** *43* (12), 3229-3238.

51. Magi, L.; Schweitzer, F.; Pallares, C.; Cherif, S.; Mirabel, P.; George, C. Investigation of the Uptake Rate of Ozone and Methyl Hydroperoxide by Water Surfaces. *J. Phys. Chem. A* **1997,** *101* (27), 4943-4949.

52. Enami, S.; Hoffmann, M. R.; Colussi, A. J. Proton Availability at the Air/Water Interface. *J. Phys. Chem. Lett.* **2010,** *1* (10), 1599-1604.

53. Petersen, P. B.; Saykally, R. J. Probing the Interfacial Structure of Aqueous Electrolytes with Femtosecond Second Harmonic Generation Spectroscopy. *J. Phys. Chem. B* **2006,** *110* (29), 14060-14073.

54. van Elk, E. P. Gas-Liquid Reactions - Influence of Bulk and Mass Transfer on Process Performance. Ph.D., University of Twente, Enschede, 2001.

55. Benson, S. W., *The Foundations of Chemical Kinetics*. McGraw-Hill: New York, 1960; p 736.

56. Enami, S.; Vecitis, C. D.; Cheng, J.; Hoffmann, M. R.; Colussi, A. J. Electrospray Mass Spectrometric Detection of Products and Short-Lived Intermediates in Aqueous Aerosol Microdroplets Exposed to a Reactive Gas. *J. Phys. Chem. A* **2007,** *111* (50), 13032-13037.

57. Markus, Y., *Ion Properties*. Marcel Dekker: New York, 1997; p 272.

58. House, J. E.; House, K. A., *Descriptive Inorganic Chemistry*. 2nd ed.; Academic Press: Burlington, 2010; p 592.

59. Liu, W.-T.; Zhang, L.; Shen, Y. R. Interfacial Structures of Methanol:Water Mixtures at a Hydrophobic Interface Probed by Sum-Frequency Vibrational Spectroscopy. *J. Chem. Phys.* **2006,** *125* (14), 144711-144716.

60. Ding, F.; Hu, Z.; Zhong, Q.; Manfred, K.; Gattass, R. R.; Brindza, M. R.; Fourkas, J. T.; Walker, R. A.; Weeks, J. D. Interfacial Organization of Acetonitrile: Simulation and Experiment. *J. Phys. Chem. C* **2010,** *114* (41), 17651-17659.

61. *CRC Handbook of Chemistry and Physics*. 93rd ed.; CRC Press/Taylor and Francis: Boca Raton, Fl., **2013**; p 2664.

62. Oldridge, N. W.; Abbatt, J. P. D. Formation of Gas-Phase Bromine from Interaction of Ozone with Frozen and Liquid Nacl/Nabr Solutions: Quantitative Separation of Surficial Chemistry from Bulk-Phase Reaction. *J. Phys. Chem. A* **2011,** *115* (12), 2590-2598.

63. Standard Reference Database 69: The Nist Chemistry Webbook. In Mallard, W. G.; Linstrom, P. J., Eds. National Institute of Standards and Technology: http://webbook.nist.gov. Gaithersburg, MD, 2000; Vol. 2012.

64. Rhim, J. A. Equilibrium Concentration and Overall Henry's Law Constant of the Dissolved Ozone. *Env. Eng. Res.* **2004,** *9* (2), 88-95.

65. Rischbieter, E.; Stein, H.; Schumpe, A. Ozone Solubilities in Water and Aqueous Salt Solutions. *J. Chem. Eng. Data* **2000,** *45* (2), 338-340.

66. Roth, J. A.; Sullivan, D. E. Solubility of Ozone in Water. *Ind. Eng. Chem. Fund.* **1981,** *20* (2), 137-140.

67. Mmereki, B. T.; Donaldson, D. J. Direct Observation of the Kinetics of an Atmospherically Important Reaction at the Air−Aqueous Interface. *J. Phys. Chem. A* **2003,** *107* (50), 11038-11042.

68. Rosen, M. J., *Surfactants and Interfacial Phenomena*. 3 ed.; Wiley: Hoboken, 2004; p 444.

69. Kim, C.; Hsieh, Y.-L. Wetting and Absorbency of Nonionic Surfactant Solutions on Cotton Fabrics. *Colloids Surf. A Physicochem. Eng. Asp.* **2001,** *187–188*, 385-397.

70. Saiz-Lopez, A.; Plane, J. M. C.; Baker, A. R.; Carpenter, L. J.; von Glasow, R.; Gómez Martín, J. C.; McFiggans, G.; Saunders, R. W. Atmospheric Chemistry of Iodine. *Chem. Rev.* **2011,** *112* (3), 1773-1804.

71. Saiz-Lopez, A.; von Glasow, R. Reactive Halogen Chemistry in the Troposphere. *Chem. Soc. Rev.* **2012,** *41* (19), 6448-6472.

2.7 Supporting Information For: Conversion of Iodide to Hypoiodous Acid and Iodine

in Aqueous Microdroplets Exposed to Ozone

Content   **Page**

Explanation of Latimer Diagrams in Context of this Work

The magnitude and sign of the electromotive forces (E) participating in a redox reaction can indicate a great deal about its thermodynamic properties.[1] Reactions with a positive E result in a spontaneous reaction, as the solution to the relationship between E and Gibbs free energy (ΔG) will be negative, described by the equation

$$\Delta G = -nFE \qquad\qquad\qquad \text{(Eq. 2.5)}$$

where n represents the number of electrons transferred, and F is Faraday's constant. A Latimer diagram is used to concisely display the E values for a series of transitions between oxidation states for a species of interest.[1] These values can be utilized to determine which oxidation states are stable or unstable. If the value to the left of the oxidation state is larger than the value to the right, it will be thermodynamically stable. If the value on the right is larger, the species will tend to disproportionate into the species on either side.[1]
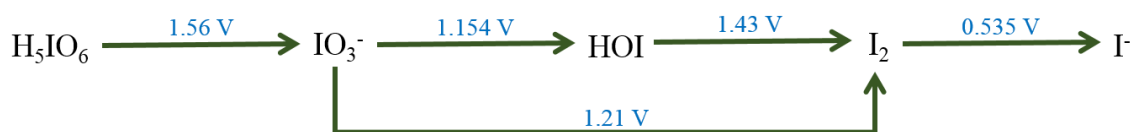
Figure S1. Latimer diagram for iodide illustrating the standard reduction potential for conversion between oxidation states under acidic conditions ([H$^+$] = 1 M, pH 0).[2]
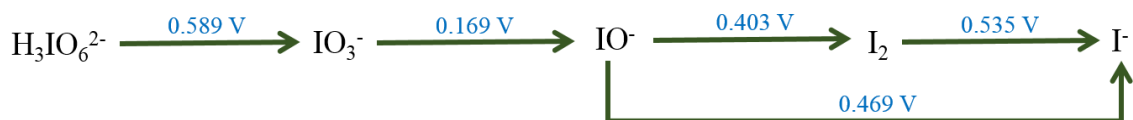
Figure S2. Latimer diagram for iodide illustrating the standard reduction potential for conversion between oxidation states under basic conditions ([OH$^-$] = 1 M, pH 14).[2]

While examining the scenario under acidic conditions (Figure S1), the only unstable species is HIO. This would disproportionate into IO_3^- and I_2. However, under basic conditions (Figure S2), IO$^-$ is stable and would likely diminish the rate of HIO disproportionation. In contrast, IO_3^- and I_2 are unstable in basic conditions and stable in acidic media.

References

1. Huheey, J. E.; Keiter, E. A.; Keiter, R. L., *Inorganic Chemistry: Principles of Structure and Reactivity*. Pearson Education 1993.

2. Bratsch, S. G. Standard Electrode Potentials and Temperature Coefficients in Water at 298.15 K. *J. Phys. Chem. Ref. Data* **1989,** *18* (1), 1-21.

Chapter 3. Catechol Oxidation by Ozone and Hydroxyl Radicals at the Air-Water Interface
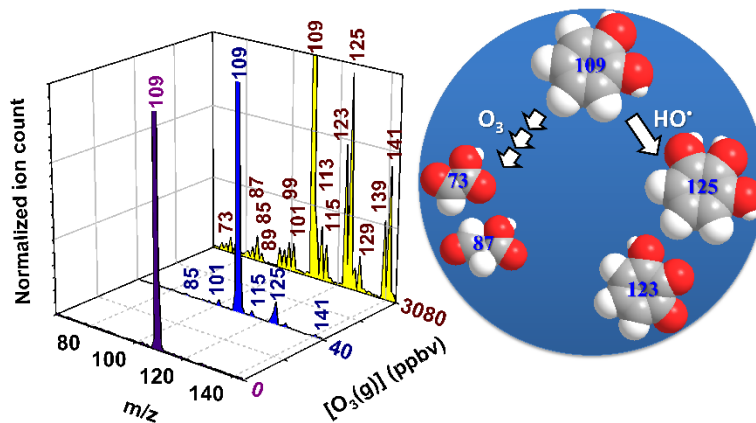
Scheme 3.1 Synopsis TOC

3.1 Synopsis

Anthropogenic emissions of aromatic hydrocarbons promptly react with hydroxyl radicals undergoing oxidation to form phenols and polyphenols (e.g., catechol) typically identified in the complex mixture of humic-like substances (HULIS). Because further processing of polyphenols in secondary organic aerosols (SOA) can continue mediated by a mechanism of ozonolysis at interfaces, a better understanding about how these reactions proceed at the air-water interface is needed. This work shows how catechol −a molecular probe of the oxygenated aromatic hydrocarbons present in SOA− can contribute interfacial reactive species that enhance the production of HULIS under atmospheric conditions. Reactive semiquinone radicals are quickly produced upon the encounter of 40 ppbv – 6.0 ppmv $O_3(g)$ with microdroplets containing [catechol] = 1-150 μM. While the previous pathway results in the instantaneous formation of mono- and poly-hydroxylated aromatic rings (PHA) and chromophoric mono- and poly-hydroxylated quinones (PHQ), a different channel produces oxo- and di-carboxylic acids of low molecular weight (LMW). The cleavage of catechol occurs at the 1,2-carbon-carbon bond at the air-water interface through the formation of 1) an ozonide intermediate, 2) a hydroperoxide, and 3) *cis,cis*-muconic acid. However, variable [catechol] and [$O_3(g)$] can affect the ratio of the primary products (*cis,cis*-muconic acid and trihydroxybenzenes) and higher-order products observed (PHA, PHQ, and LMW oxo- and di-carboxylic acids). Secondary processing is confirmed by mass spectrometry showing the production of crotonic, maleinaldehydic, maleic, glyoxylic, and oxalic acids. The proposed pathway can contribute precursors to aqueous SOA (AqSOA) formation

converting aromatic hydrocarbons into polyfunctional species widely found in tropospheric aerosols with light-absorbing brown carbon.

3.2 Introduction

Aerosol particles play a key role in climate by scattering and absorbing sunlight and to a lesser extent by absorbing, scattering and re-emitting terrestrial radiation.[1] In addition, aerosols can serve as cloud condensation nuclei and ice nuclei upon which cloud droplets and ice crystals form.[1] The mechanisms of production and the properties of secondary organic aerosols (SOA) from laboratory and field studies have been reviewed.[2-3] Atmospheric transport and *in situ* photo-oxidative surface processing of the species found in aerosols contribute to the large complexity of these systems, making the quantification of photo-oxidative aging complicated.[4] In this context, recent field measurements of the concentration of water soluble organic compounds (WSOC) including dicarbonyls (e.g., glyoxal), oxocarboxylic acids (e.g., glyoxylic and 3-oxopropoanoic acids), dicarboxylic acids (e.g., oxalic acid), and unsaturated carboxylic acids (e.g., fumaric and maleic acids) suggested common natural sources and/or similar formation pathways.[5] Similarly, measurements of the distribution ratio of oxalic acid to levoglucosan over the open ocean suggested that photo-oxidative mechanisms control the chemical composition of marine SOA.[6-7] The high levels of dicarbonyls, oxo- and di-carboxylic acids quantified in aerosols at dissimilar locations such as the Brazilian Amazon, Singapore, and the summit (1534 m a.s.l.) of Mount Tai in central East China far exceeded those reported in Chinese megacities at ground levels,[8-10] demanding an explanation to the origin of these important SOA species.

Correlations between the content of WSOC and the transport of biomass burning products as well as with photooxidative processing during atmospheric transport were established at different sites.[8-10] The photooxidation of species such as glyoxylic acid results in the final production of oxalic acid in the aerosol aqueous phase.[8] Catechol, hydroquinone, and resorcinol are typically the major gas-phase organic constituents (~50 ppbv) resulting from biomass burning.[11] Interestingly, cloud water rich in light absorbing compounds was also collected at Mount Tai and characterized to contain aromatic species such as phenol and catechol with $-CH_3$, $-NO_2$, and $-C=O$ substituents.[12] These ubiquitous surface active species are enriched in interfacial regions[13] of atmospheric aerosols and susceptible to photo-oxidation,[14] as they reside at the air-water interface.

The heterogeneous ozonolysis of catechol has been the subject of recent studies focused on monitoring the reaction products by FTIR on the surface of 1) thin solid films under high relative humidity (RH),[15] and 2) reactant adsorbed over NaCl and Al_2O_3 particles that produce *cis,cis*-muconic acid and traces of oxalic acid.[16] The ring-opening of catechol and the formation of unsaturated carboxylic acid was observed in an aerosol flow reactor.[17] A maximum uptake coefficient of 5.6×10^{-5} was measured at RH = 81 % for $[O_3(g)] = 4$ ppmv at 298 K.[15] The theoretical rate constant for the ozonolysis of catechol, $k_{O_3+cat} = 3.4 \times 10^{-25}$ cm^3 molecules^{-1} s^{-1}, and associated lifetimes of 4.3 h on NaCl and 18 h in Al_2O_3 were estimated for typical unpolluted tropospheric conditions ($[O_3(g)] = 40$ ppbv).[16] However, the typical methods employed for studying heterogeneous reactions (DRIFTS- and ATR-FTIR) require several minutes resulting in the oversight of structural information at the early stages of ozonolysis.[17] The ozonolysis of thin films of catechol at high relative humidity monitored by FTIR is discussed further

in the Supporting Information. However, the importance of ozonolysis remains uncertain, and no mechanistic comparison with OH-initiated chemistry was considered. Therefore, further *in situ* studies providing fast mechanistic information ($\sim 10^{-6}$ < timescale < 10^{-3} s) of the interfacial oxidation of catechol are needed to comprehend better the fate of biomass burning emissions.

In this article, catechol is used as a molecular probe to study the ozonolysis of surface active organic matter present in atmospheric aerosols. A customized electrospray (ESI) mass spectrometry (MS) system is used to study reactions at the air-water interface with ultrafast contact ($\tau_c \sim 1$ µs) and detection ($\tau_d \sim 1$ ms) times.[18-19] Spectroscopic features reveal the interfacial production of short lived species that agree with observations in bulk water[20] but escaped detection in experiments at the air-water interface.[15] Experiments reveal two reactive channels are operative at the air-water interface, 1) hydroxylation and 2) oxidative cleavage of the aromatic ring.[21] The first channel operates through semiquinone radicals that are instantaneously converted to mono- and poly-hydroxylated aromatic rings (PHA) and mono- and poly-hydroxylated quinones (PHQ). The second channel is the ultrafast cleavage of the 1,2-carbon-carbon bond of catechol, which proceeds through the consecutive formation of 1) a moloozonide, 2) a hydroperoxide, and 3) *cis,cis*-muconic acid (MA). Furthermore, experiments with variable [catechol] and [$O_3(g)$] modify the ratio of primary products (MA, and mono-hydroxylated-catechol). Additional evidence of secondary processing is registered by MS measurements that confirm the production of methacrylic acid, maleinaldehydic acid, maleic acid, glyoxylic acid, oxalic acid, PHA, and PHQ. This work shows that tropospheric humic-like substances (HULIS)[22] precursors can be produced by interfacial

reactions of hydroxylated aromatics that contribute reactive chemical species *in situ* produced in atmospheric particles.[21]

3.3 Experimental Section

Solutions of catechol (Sigma-Aldrich, 99.9%) were prepared daily in ultrapure water (18.2 MΩ cm, Elga Purelab flex, Veolia) and infused into a calibrated ESI-MS (Thermo Scientific, MSQ Plus). Experiments were performed between pH 5 and 10. Figures report the ion count ($I_{m/z}$) at specific mass-to-charge (m/z) ratios for experiments at pH 8.0, unless otherwise indicated. The pH of solutions was adjusted with 0.01 M NaOH (Fisher, 99.3%) and measured with a calibrated pH-meter (Mettler Toledo). In selected experiment, KOH (Acros, ACS grade) or LiOH (LiOH•H_2O, Fisher, laboratory grade) were used to adjust the pH and verify that the species reported are not clusters that could include alkali metals. All species are in the aqueous state, unless indicated otherwise.

The ESI-MS experimental setup to study the instantaneous formation of short-lived intermediates at the liquid-gas interface was previously described in detail.[18-19] In order to prepare solutions of catechol to be tested, a typical mixing ratio range of $P_{catechol}$ = 5-50 ppbv from biomass burning emissions is considered,[11] together with the vapor pressure of water P_{H_2O} = 0.0312 atm (at 298 K),[23] and Henry's law constant $H_o^{catechol}$ = 4600 M atm^{-1} (at 298 K). Therefore, a broad range of $22 \leq$ [catechol] ≤ 223 μM is obtained as an estimate for atmospheric waters in contact with pollution from biomass burning. In present experiments, a solution of 1–150 μM catechol is pneumatically aerosolized into fine micrometer size droplets at atmospheric pressure and encounters a 0.2 L min^{-1} flow of 40 ppbv $\leq$ [O_3(g)] $\leq$ 6.0 ppmv, both interacting during a contact time of the few

microseconds.[18-19] A spark discharge ozone generator (Ozone Solutions) fed with $O_2(g)$ (Scott-Gross, UHP) is used for $O_3(g)$ production. $O_3(g)$ is diluted with $N_2(g)$ (Scott Gross, UHP) and monitored in a 10-cm path length cuvette (Starna cell) by UV absorption spectrophotometry.[24] Gaseous ozone is transported to a stainless steel tube, where a final 61-times dilution with the $N_2(g)$ nebulizing gas (12.0 L min^{-1}) occurs to yield information that covers the low $[O_3(g)]$ found in the troposphere.

The encounter of $O_3(g)$ with the microdroplets containing catechol produces oxidized species reported as anions for specific *m/z* values. The overall time from the formation of droplets, transport through the $O_3(g)$ plume, and ion detection is τ_d <1 ms. However, the contact time (τ_c) between $O_3(g)$ and the plume of microdroplets was previously described to be in the order of a few microseconds.[19] In summary, the experimental conditions were: Drying gas temperature, 250 °C; nebulizer voltage, -1.9 kV; cone voltage, -50 V; and nebulizer pressure, 70 psi. Ion counts reported correspond to processed data after solvent background subtraction from the raw sample mass spectral data acquired at fixed time intervals (e.g., time $\geq$ 30 s). All identified species are indicated by their *m/z* values in the text and schemes. Reported data are the average of duplicate experiments with error bars corresponding to one standard deviation.

3.4 Results and Discussion

3.4.1 Reactions of Catechol at the Air-Water Interface

The ozonolysis of micromolar concentrations of catechol at the air-water interface was monitored under variable $[O_3(g)]$. Figure 3.1 shows ESI mass spectra of aerosolized solutions of catechol in water at pH = 8.0 exposed to a flow of 0.2 L min^{-1} (A) 1 atm

N$_2$(g) (bottom purple trace), (B) 40 ppbv O$_3$(g) (center blue trace), and (C) 3.08 ppmv

O$_3$(g) (top yellow trace). The control measurement in the absence of ozone (bottom trace

in Figure 3.1) only displays the detectable monoanion of catechol C$_6$H$_4$(OH)O$^-$ (m/z 109)

and a minor accompanying peak corresponding to the cluster of catechol anion with two

water molecules (m/z 145). Major changes are observed upon addition of 40 ppbv O$_3$(g)

(central trace) that results in the appearance of several small peaks due to the immediate

oxidation of catechol that does not require an induction period longer than the contact

time. The ion count of these new peaks generally increases as the ozone level rises to

3.08 ppmv O$_3$(g) (top trace), and a few additional peaks appear.
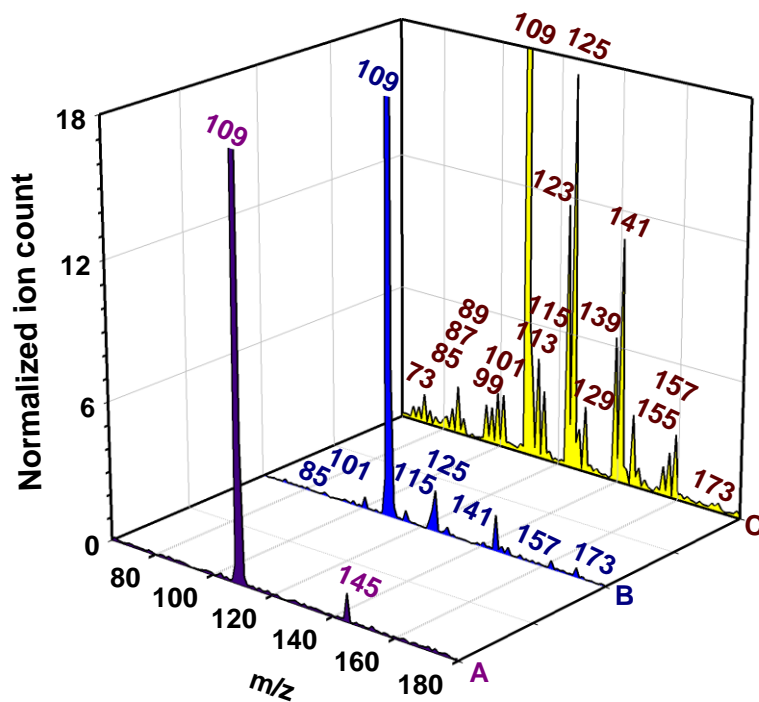
Figure 3.1. Spectra of ESI-MS of 100 µM solution of catechol in H$_2$O at pH = 8.0
exposed to a 0.200 L min^{-1} flow of (A) 1 atm N$_2$(g) (bottom purple trace), (B) 40 ppbv
O$_3$(g) (center blue trace), and (C) 3.08 ppmv O$_3$(g) in H$_2$O (top yellow trace). Ion count
values are normalized percentages relative to I_{109}, the most intense peak in the mass
spectrum, and the scale only shows signals up to 18%.

Previous studies of the ozonolysis of catechol in bulk water did not address all the uncertainties existing in the mechanism,[20, 25] but are helpful to assign the products in Figure 3.1. These products correspond to: glyoxylic acid detected as its anion (*m/z* 73), crotonic acid (*m/z* 85) or an isomer such as 4-hydroxycrotonaldehyde, 3-oxopropanoic acid (*m/z* 87), oxalic acid (*m/z* 89), maleinaldehydic acid (*m/z* 99), 4-hydroxy-2-butenoic acid (*m/z* 101), 5-oxo-3-pentenoic acid (*m/z* 113), maleic acid (*m/z* 115), 3-hydroxy-*o*-quinone or 4-hydroxy-*o*-quinone (*m/z* 123), 1,2,3- and 1,2,4-tryhydroxybenzene (*m/z* 125), glutaconic acid (*m/z* 129), 3,4-dihydroxy-*o*-quinone or 3,6-dihydroxy-*o*-quinone (*m/z* 139), *cis,cis*-muconic acid, 1,2,3,4- and 1,2,4,5-tetrahydroxybenzene (*m/z* 141), 3,4,5-tridihydroxy-*o*-quinone and 3,4,6-tridihydroxy-*o*-quinone (*m/z* 155), pentahydroxybenzene (*m/z* 157), and hexahydroxybenzene (*m/z* 173). Scheme 3.2 shows the proposed routes starting from catechol to form the identified PHA and PHQ products.

Scheme 3.2. Proposed Mechanism for the Direct Ozonolysis for the Direct Ozonolysis of Catechol at the Air-Water Interface. Reaction numbers and observed *m/z* values are given in red and blue font, respectively.
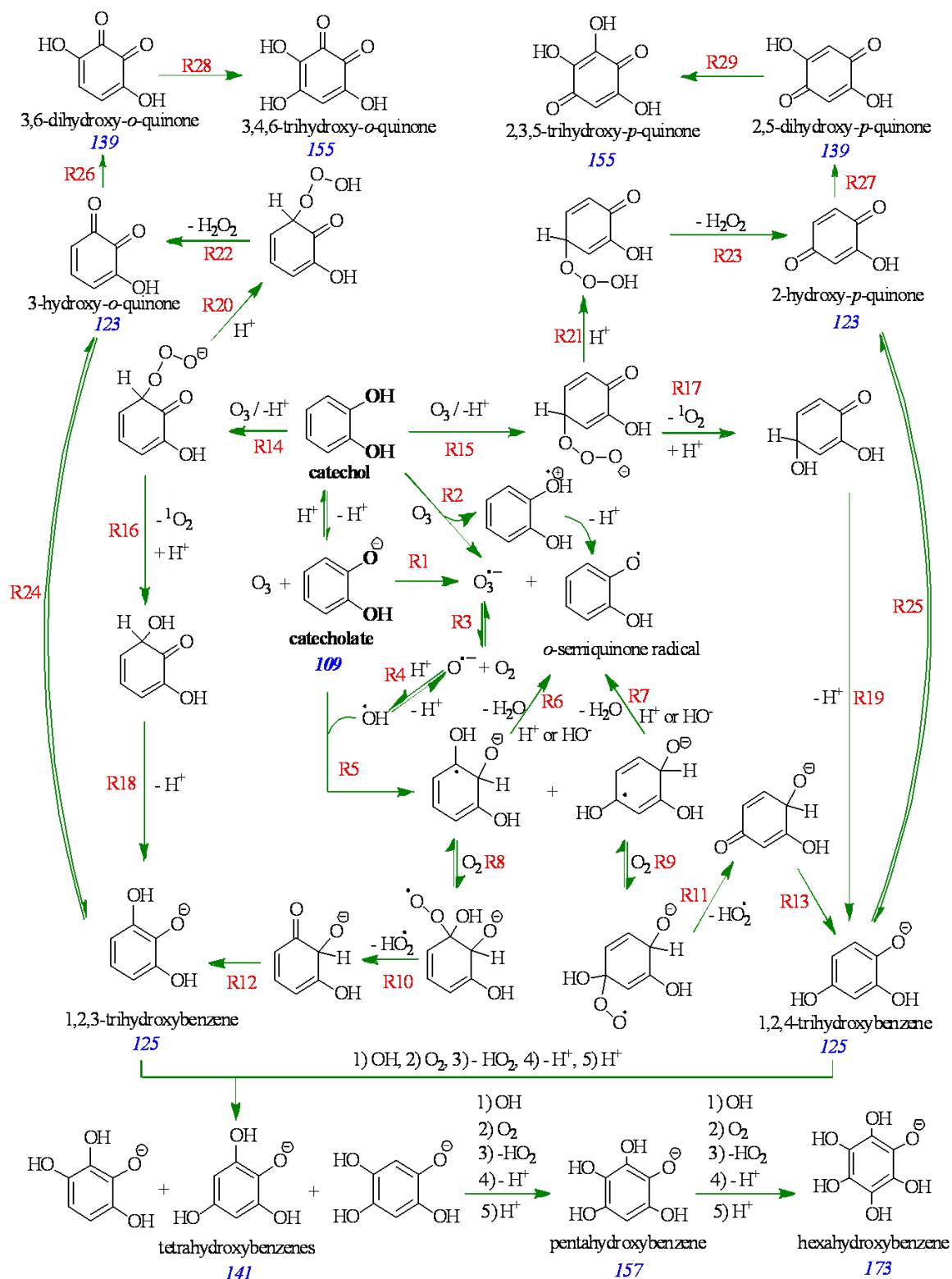
Figure 3.2 shows how the relative ion count of catechol to its initial value ($I_{109}/I_{109,0}$) exponentially drops for increasing [$O_3(g)$] in experiments with $1 \leq$ [catechol] ≤ 150 μM. The behavior observed in Figure 3.2 agrees with the first order reaction on both [O_3] and [catechol] in bulk water.[26] $O_3(g)$ molecules diffuse toward the interface and after the accommodation process they react with catechol available in the external layer. Catechol loss at the interface is quickly replenished by diffusion of the molecule from its internal reservoir in the core of the microdroplets. The heterogeneous reactions take place within the contact time $\tau_c \approx 1$ μs on a nanoscopic interface of thickness $\delta \approx 1$ nm, as observed also for the reaction of O_3 with iodide.[19] The surface density of O_3 molecules in the interface, S_{O_3}, can be estimated from the dissolved [O_3] in the thin interfacial slab using the equation 3.1:

$$S_{O_3} = \delta\,[O_3] = v_{O_3}\tau_c\,\gamma_{O_3}[O_3(g)]/4 \qquad \text{(Eq. 3.1)}$$

where $v_{O_3} = 3.94 \times 10^4$ cm s^{-1} is the mean thermal velocity of $O_3(g)$ at 298 K, [$O_3(g)$] is the concentration of ozone molecules striking the liquid microdroplets of diameter $D = 10$ μm with $\tau_c = 1 \times 10^{-6}$ s, and γ_{O_3} is the uptake coefficient of $O_3(g)$ in water. The dimensionless Henry's law constant $H_{0,O_3} = 0.269$ (at 298 K),[27] can be used to evaluate the reactive uptake coefficient of the gas, $\gamma_{O_3} = (4\,\delta\,H_0)/(v_{O_3}\tau_c) = 2.73 \times 10^{-6}$. This γ_{O_3} value is 20-times smaller than the maximum measured for solid films of catechol exposed to $O_3(g)$ at 81% relative humidity.[15] Complete $O_3(g)$ dissolution occurs on the thin interfacial slab faster than τ_c for all [$O_3(g)$] employed. Diffusion controlled limitations can be neglected because $I_{109}/I_{109,0}$ in Figure 3.2 levels off due to the few

nanoseconds needed by the solute to diffuse through the $\delta = 1$ nm interface and to establish stationary conditions (d[catechol]/$dt = 0$) in the open reactor that continuously replenishes the reagent after it reacts with O_3.[19, 28-29]
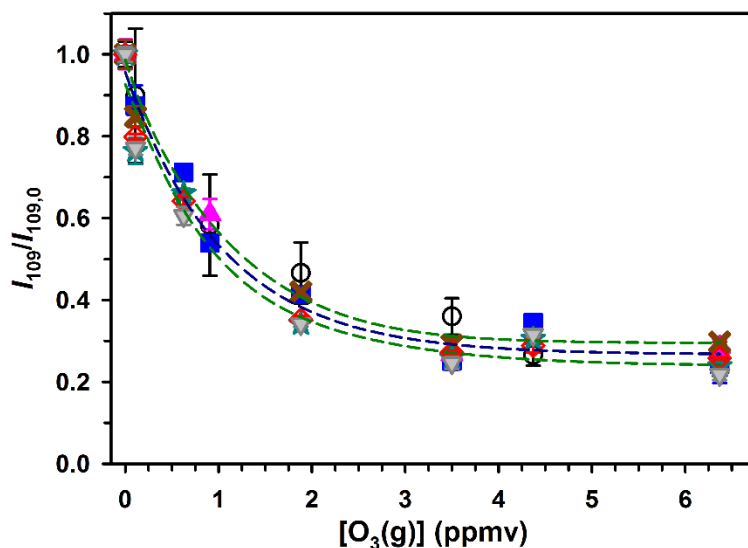
Figure 3.2. Relative ion count of catechol ($m/z = 109$) to its initial value, $I_{109}/I_{109,0}$, in the ESI mass spectra for aerosolized solutions of [catechol]$_0$ = 1 (open black circle), 10 (blue square), 25 (pink triangle), 50 (brown cross), 100 (teal blue star), 125 (red open diamond), and 150 μM (gray inverted triangle) as a function of increasing [O_3(g)] at pH = 7.8. The overall nonlinear regression (dashed blue trace) with a 95% confidence interval (dashed green traces) decays exponentially as $I_{109}/I_{109,0} = 0.267 + 0.690 \times e^{-0.948\,[\text{catechol}]}$ with $r^2 = 0.971$.

3.4.2 Reactivity Driven by Hydroxyl Radicals

The thermodynamically favorable ($\Delta E = +0.48$ V) electron transfer reaction R1 (Scheme 3.2) between catecholate and dissolved O_3, with redox potentials $E_{\text{catechol}} = 0.53\,V$ and $E_{O_3} = 1.01\,V$ (at pH = 7), produces a semiquinone radical (p$K_a = 5$)[30] directly.[31] The same reaction can proceed indirectly from molecular catechol through reaction R2 after the very acidic radical cation (p$K_a = $ -1.62)[32] formed deprotonates in picoseconds. The ozonide radical $O_3^{\bullet-}$ coexists in equilibrium R3 ($K_{eq} = 5.5 \times 10^{-7}$ M at

20 °C)[33] with the strong base O$^{\cdot-}$ (pK_a = 11.8).[33] Therefore, at pH ≤ 10.8, O$^{\cdot-}$ will be present as its fully associated conjugated acid (equilibrium R4) HO$^{\cdot}$. Accordingly, it is important to consider how this *in situ* generated HO$^{\cdot}$ can contribute to the initial degradation of catechol and other phenols/polyphenols in aerosols and at other environmental interfaces such as the sea surface microlayer of the ocean.

Experiments with catechol at pH = 10 provide important information to rationalize the two mechanisms of formation of *o*-semiquinone radicals: 1) from reactions R1 and R2 and 2) from the resonance-stabilized 1,2,3- or 1,2,4-trihydroxycyclohexadienyl radical formed by R5 after fast base-catalyzed water elimination via reactions R6 and R7. The dehydration reaction of related dihydroxycyclohexadienyl radicals ($k' \sim 10^9$ M^{-1} s^{-1}) can only compete with the fast addition of O$_2$ to the dihydroxycyclohexadienyl radicals under acid or base catalysis.[34] Therefore, the base catalyzed dehydration of trihydroxycyclohexadienyl radicals by reactions R6 and R7[35] competes with the production of trihydroxycyclohexadienyl peroxy radicals by reactions R8 and R9 (also k $\sim 10^9$ M^{-1} s^{-1})[35] at pH = 10 (Figure S1, Supporting Information). Considering the partial pressure of oxygen in the system, P_{O_2} = 0.01639 atm (H_{0,O_2} = 0.0013 $M\ atm^{-1}$ at 25 °C),[27] there is [O$_2$] = 21.3 μM under equilibrium conditions to compete for the intermediate.

Under pH = 5 (Figure S1, Supporting Information), catechol appears to be relatively stable during the microsecond contact time. However, for the pH interval from 6 to 9, the formation of products at *m/z*, 123 (hydroxyquinones), 125 (trihydroxybenzenes), 139 (dihydroxyquinones), and 141 (trihydroxybenzenes) is observed. The results of this study show that the complexity of the heterogeneous ozonolysis of catechol at neutral and even

slightly basic or acidic pH is higher than previously considered.[15] Figure 3.3 displays how the main products observed for the loss of catechol (pK_{a1} = 9.34 and pK_{a2} = 12.60 at 298 K)[23] change with [$O_3(g)$]. The fast production of HO• is evidenced by the quick appearance of 1,2,3- and/or 1,2,4-trihydroxybenzene (I_{125}) during the interfacial ozonolysis of 1 ≤ [catechol] ≤ 150 μM (Figure 3A). The maximum value of I_{125} is reached at 626 ppbv $O_3(g)$ for the electrophilic addition of HO• to the *ortho-* and *para-* positions of catechol via R5 + R8 + R10 + R12 and R5 + R9 + R11 + R13, respectively. For higher [$O_3(g)$], I_{125} decays smoothly due to its conversion into other products.

Figure 3.3 also shows that trihydroxybenzene signals grow faster than for all other species and dominate the products at the low [$O_3(g)$] for the pH range in which HO• is quickly produced. Even under acidic conditions of pH 6 the production of trihydroxybenzenes is observed and starts vanishing for pH ≤ 5 (Figure S1, Supporting Information). Acid and base catalysis should promote reactions R6 and R7, but at pH 7, the addition of superoxide radicals (introduced below), $O_2^{•-}$, to the trihydroxycyclohexadienyl radicals would stop the production of trihydroxybenzenes. The reactivity of 1,2,3- or 1,2,4-trihydroxycyclohexadienyl radicals towards abundant $O_2(g)$ to produce 1,2,3-trihydroxybenzene and 1,2,4-trihydroxybenzene simultaneously results in the release of hydroperoxyl radicals $HO_2^•$ during R10 and R11. The equilibrium between conjugated $HO_2^•$ acid (pK_a = 4.8)[36] and superoxide radical $O_2^{•-}$ is shifted towards the formation of the dissociated species in these experiment.
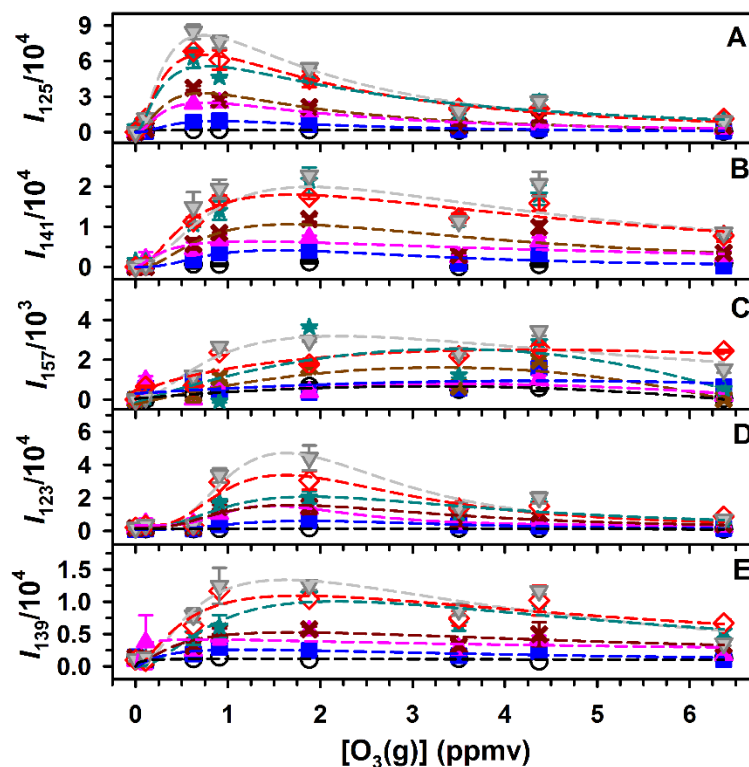
Figure 3.3. Ion count, $I_{m/z}$, of (A) 1,2,3- and 1,2,4-trihydroxybenzene ($m/z = 125$), (B) *cis,cis*-muconic acid, 1,2,3,4- and 1,2,4,5-tetrahydroxybenzene ($m/z = 141$), (C) pentahydroxybenzene ($m/z = 157$), (D) 3-hydroxy- and 4-hydroxy-*o*-quinone ($m/z = 123$), and (E) 3,4-dihydroxy- and 3,6-dihydroxy-*o*-quinone ($m/z = 139$) produced from exposing aerosolized catechol solutions in Figure 2A to increasing [O$_3$(g)]. Dashed lines connecting points are meant to guide the eye and do not represent curve fittings.

In principle, the reaction $O_2^{\bullet-} + O_3 \rightleftharpoons O_3^{\bullet-} + O_2$ ($k_{O_2^{\bullet-} + O_3} = 1.5 \times 10^9$ M^{-1} s^{-1})[37] can produce $O_3^{\bullet-}$, which regenerates HO$^{\bullet}$ through reactions R3 + R4.[37] Nevertheless, the recycling of $O_2^{\bullet-}$ should be unimportant at high pH, as explained next. Although the rate constant for the reaction of catecholate with O_3 is unknown, it should be in the order of typical diffusion controlled reactions under present conditions: $k_{O_3 + \text{catecholate}} \simeq 10^{10} M^{-1} s^{-1}$. Therefore, considering that [catecholate] $\gg$ [O$_2^{\bullet-}$], the rate of reaction R1 is orders of magnitude larger than the rate of reaction of $O_2^{\bullet-}$ with O_3:[38]

$$Rate\ R_1 \gg Rate\ R_{O_2^{\bullet-}+O_3} \tag{Eq. 3.2}$$

$$k_{O_3+catecholate}\ [\text{catecholate}][O_3] \gg k_{O_2^{\bullet-}+O_3}\ [O_2^{\bullet-}]\ [O_3] \tag{Eq. 3.3}$$

$$\sim 10^{10} M^{-1} s^{-1}\ [\text{catecholate}]\ [O_3] \gg 1.5 \times 10^9\ M^{-1}\ s^{-1}\ [O_2^{\bullet-}]\ [O_3] \tag{Eq. 3.4}$$

For example, for [catechol] = 25 μM at pH = 10 ($\alpha_{C_6H_4(OH)O^-}$ = 81.9%), catecholate scavenges the interfacial O_3[19] by reaction R1 more efficiently than the much less abundant $O_2^{\bullet-}$, making the superoxide radical pathway for indirect $HO^{\bullet}$ production negligible. In addition to the indirect oxidation of catechol with $HO^{\bullet}$ described above, Scheme 3.2 includes other channels for the production of 1,2,3- and 1,2,4-trihydroxybenzene (*m/z* 125) presented in Figure 3.3A. The direct attack of O_3 to positions 3 and 6 of catechol to produce 1,2,3- and 1,2,4-trihydroxybenzene should proceed with the release of $O_2(^1\Delta_g)$ through reactions R14 + R16 + R18 and R15 + R17 + R19, respectively.[39] Chemiluminescent emissions of the hydroxytrioxide anion intermediates by R16 and R17 were observed during the ozonolysis of catechol.[40]

The net increase of I_{141} in Figure 3B remains lower than I_{125} and reaches a maximum at 1.88 ppmv $O_3(g)$. Because $I_{125} > I_{141}$, the results at low $[O_3(g)]$ strongly suggest that 1,2,3- and 1,2,4-trihydroxybenzene are produced earlier than the species at *m/z* 141. In addition, the tetrahydroxybenzene products should decay faster than the trihydroxybenzenes precursors because they are more prone to undergo further oxidation. However, the sequential conversion of the ozonide of catechol into a hydroperoxide intermediate results in the generation of *cis,cis*-muconic acid as reported in bulk water.[20]

Cis,cis-muconic acid also contributes to the signal at *m/z* 141, a product discussed below in terms of the direct cleavage of catechol. The same mechanistic steps producing trihydroxybenzenes from catechol are invoked at the bottom of Scheme 3.2 to explain the generation of tetrahydroxybenzenes (*m/z* 141) from trihydroxybenzenes, pentahydroxybenzene (*m/z* 157, Figure 11.3C) from tetrahydroxybenzenes, and hexahydroxybenzene from pentahydroxybenzene. In Figure 3.3C, I_{157} reaches a plateau for $[O_3(g)] = 880$ ppbv, indicating steady state conditions for these species assigned to 1,2,3,4-, 1,2,3,5, and 1,2,4,5-tetrahydroxybenzene in Scheme 3.2.

Figure 3.3D shows the production of 3-hydroxy-*o*-quinone and/or 2-hydroxy-*p*-quinone (I_{123}). These species can be easily produced from 1) the action of semiquinone radicals and 2) the elimination of H_2O_2 after O_3 attack to positions 3 and 4 of catechol. In the first case, the corresponding 1,2,3- and 1,2,4-trihydroxybenzenes generated from 1,3- and 1,4-addition of ozone to catechol react directly with the *in situ* formed *o*-semiquinone radical to generate 3-hydroxy-*o*-quinone and 2-hydroxy-*p*-quinone, respectively. Because the participation of the *o*-semiquinone radical that regenerates catechol seems less likely to contribute to the formation of quinones than the pathways from H_2O_2 elimination, the former reactions are only depicted in Scheme S1 (Supporting Information). These reactions could proceed through a cyclic ozonide intermediate. Although the reaction was studied for phenol, the several steps involved are complex, and no complete mechanistic understanding was reached yet.[38] In the second case, the production of 3-hydroxy-*o*-quinone and/or 2-hydroxy-*p*-quinone is given by the sequences R14 + R20 + R22 and R15 + R21 + R23, respectively.

Theoretically, the disproportionation of two semiquinone radicals of the hydroxyquinones may interconvert the species with m/z 125 and 123 via R24 and R25 (Scheme 3.2), although its probability seems low as it depends on the encounter of two such radicals at the interface of short lived droplets. The pH dependence for R25, the fast redox conversion of 1,2,4-trihydroxybenzene to 2-hydroxy-p-quinone in bulk water, is provided in Figure S2 (Supporting Information) and has also been observed during studies of denitrifying bacteria.[41]

Figure 3.3E presents the production of isomers such as 3,6-dihydroxy-o-quinone and 2,5-dihydroxy-p-quinone with m/z 139, which may be produced in reactions R26 and R27 by hydroxylation of 3-hydroxy-o-quinone and 2-hydroxy-p-quinone, respectively. The interconversion of quinone (m/z 123) and hydroquinone (m/z 125) redox pair 123:125 described above by R24 and R25 could be considered also for the pairs 139:141 and 155:157, which under typical oxidizing conditions are shifted toward the quinone form. The related production of trihydroxyquinones by R28 and R29 is included in Scheme 3.2.

In summary, because some catechol is dissociated into catecholate ($\alpha_{C_6H_4(OH)O^-}$ = 4.4% and $\alpha_{C_6H_4(OH)_2}$ = 95.6%) at pH 8, a reactive channel with in situ generated HO$^\bullet$ radicals enhances the loss of total catechol.[31] While at low pH the electrophilic attack of O$_3$ to catechol dominates the mechanism, radical-radical reactions are also observed at neutral and basic pHs. At slightly basic and even at pH = 7, hydroxyl radicals become a considerable oxidizing agent that simultaneously attacks the ring of catechol. The rate constant for the reaction of aqueous catechol with HO$^\bullet$ (measured at pH = 9), $k_{HO^\bullet+catechol} = 1.1 \times 10^{10} \ M^{-1}s^{-1}$,[42] is 2×10^4 times larger than for its reaction with O$_3$, $k_{O_3+catechol} = 5.2 \times 10^5 \ M^{-1}s^{-1}$ (available only at pH = 7).[38] Because the rate of

HO• production increases for higher pHs, the loss of catechol (Figure 3.2) and the generation of products (Figure 3.3) includes contributions from both O_3 and HO• oxidizing agents. However, the rate of catechol loss should not be described with typical bulk kinetics,[26] but by a Langmuir-Hinshelwood mechanism[43] that considers the adsorption isotherms of the oxidizers.[16] The reactive uptake coefficients of $O_3(g)$ (γ_{O_3}= 2.73×10^{-6} estimated herein) and OH radical (γ_{OH} is unavailable) on catechol at the air-water interface should be considered to account for the number of collisions leading to reaction. Because for species such as 4-methyl-5-nitrocatechol and levoglucosan $\gamma_{OH} > 10^{-2}$,[44] it is expected that $\gamma_{OH} \gg \gamma_{O_3}$ for catechol.

3.4.3 Direct Oxidation Reaction Driven by Ozone

In the previous discussion of Figure 3.1 several multifunctional carboxylic acids were listed, but the mechanism to account for their generation differs from that presented in Scheme 3.2. The generation of glyoxylic acid (*m/z* 73), crotonic acid (*m/z* 85), 3-oxopropanoic acid (*m/z* 87), oxalic acid (*m/z* 89), maleinaldehydic acid (*m/z* 99), 4-hydroxy-2-butenoic acid (*m/z* 101), 5-oxo-2-pentenoic acid (*m/z* 113), maleic acid (*m/z* 115), glutaconic acid (*m/z* 129), and *cis,cis*-muconic acid (*m/z* 141) must result from the direct electrophilic attack of ozone to the 1,2 carbon-carbon bond of catechol. The production pathways and *m/z* values for all species detected are respectively given in red and blue font in Scheme 3.3. Ring cleavage was proposed to proceed through a phenoxide anion for the related molecule of phenol in water,[45] or through the phenoxide radical produced from the first order reaction of ozone with the phenoxide anion.[46] The lower levels of direct ozonolysis products clearly distinguished in Figure 3.1 are due to

the microseconds contact time in the setup,[19] which does not allow to accumulate secondary oxidation products.

Scheme 3.3 implies that catechol undergoes the electrophilic attack of O_3 to the bond between carbons 1 and 2 through a primary ozonide by reaction R30 forming consecutively the first Criegee intermediate (CI) by R31, a hydroperoxide intermediate by R32, and *cis,cis*-muconic acid (*m/z* 141) after a loss of H_2O_2 by R33.[25] The production of *cis,cis*-muconic acid in Scheme 3.3 should be favored at lower pH, because at higher pH the channel of $O_2(^1\Delta_g)$ elimination by R16 and R17 (Scheme 11.2) is preferred from the stabilized hydroxytrioxide anions generating 1,2,3- and 1,2,4-trihydroxybenzene at *m/z* = 125. In Scheme 3.3 the unsaturated species *cis,cis*-muconic acid, the primary product of catechol direct ozonolysis, is further processed to form other organic acids.[47] The ozonide resulting from R34 can decompose in two different sets of products, 1) maleinaldehydic acid (*m/z* 99) and a second Criegee intermediate (CI II) by R35, and 2) glyoxylic acid (*m/z* 73) and a third Criegee intermediate (CI III) by R43. The aldehyde group in maleinaldehydic acid is susceptible to ozone attack by R36 and further oxidation to maleic acid (*m/z* 115). The oxidation of the unsaturated bond of maleic acid also results in the production of glyoxylic acid and CI II by R37 + R38.

Scheme 3.3. Proposed mechanism for the direct ozonolysis of catechol at the air-water interface. Reaction numbers and observed *m/z* values are given in red and blue font, respectively.
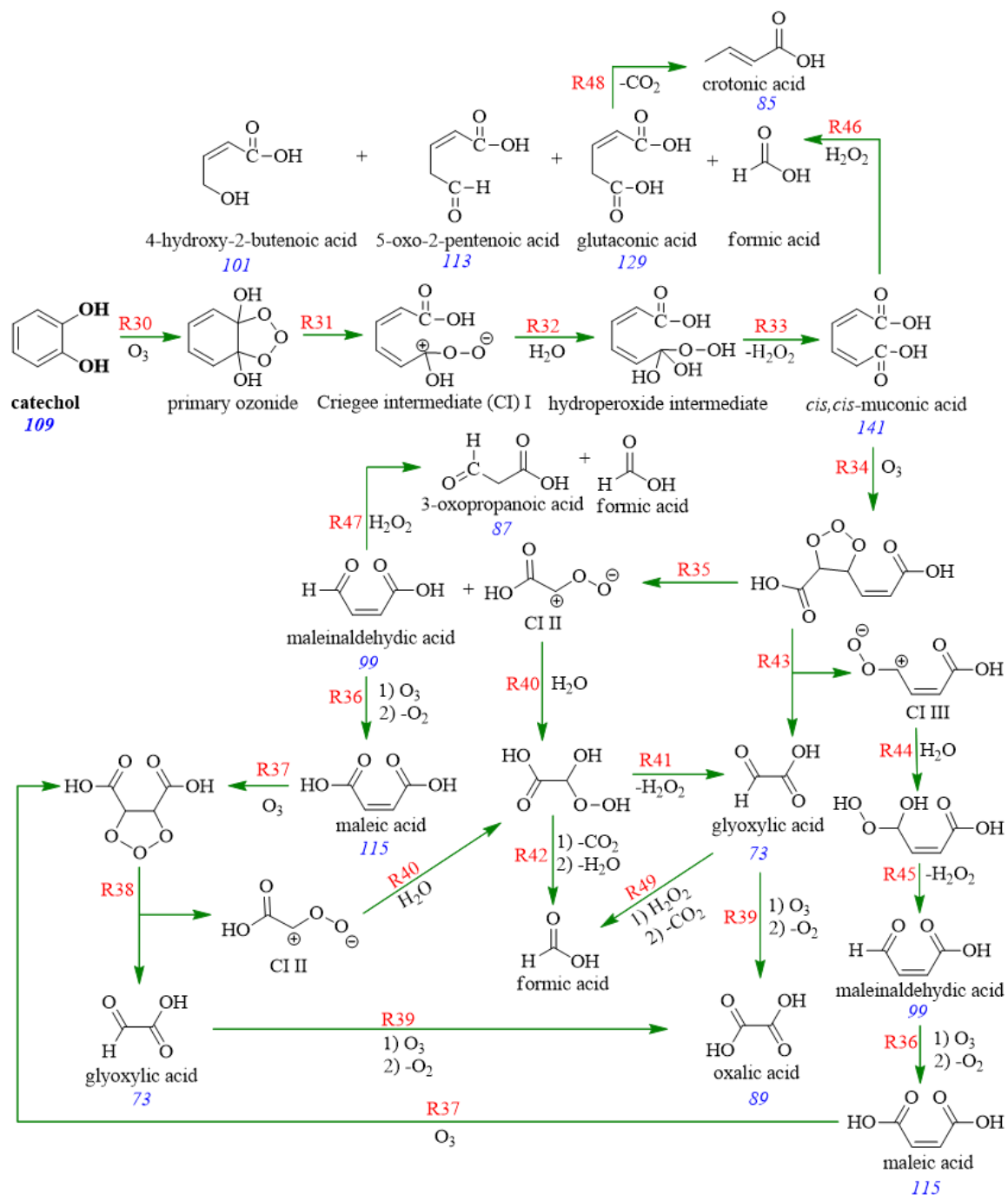
The common oxidative fate of glyoxylic acid (from R38 and R43 in Scheme 3.3) is oxalic acid (m/z 89) by R39. A hydroperoxide is formed after hydration of CI II by R40, which can yield H_2O_2 to the medium generating also glyoxylic acid by R41, or decarboxylate into formic acid by R42. A different pathway for the formation of maleinaldehydic acid from CI III by R44 + R45 merges with the production of maleic acid by R36, and glyoxylic acid by R37 + R38. Scheme 3.3 accounts for the formation of 4-hydroxy-2-butenoic acid (m/z 101), 5-oxo-3-penteneoic acid (m/z 113), and glutaconic acid (m/z 129), by the Baeyer-Villiger (BV) oxidation of *cis,cis*-muconic acid reaction R46.[48] Similarly, Scheme 3.3 also shows the BV oxidation of maleinaldehydic acid to 3-oxopropanoic acid (m/z 87) by R47 and of glutaconic acid to crotonic acid (m/z 87) or an isomer after decarboxylation via R48.

The results of spiked analysis with standards and the deconvolution of a 45 % of I_{141} arising from 25 μM *cis,cis*-muconic acid exposed to 3.18 ppmv $O_3(g)$ at pH = 8 (Figure S1) is provided in the Supporting Information. Based on this specific case, the predominant products of interfacial ozonolysis depicted in Scheme 11.3 are [glyoxylic acid] = 200 nM > [oxalic acid] = 174 nM > [*cis,cis*-muconic acid] = 129 nM > [3-oxopropanoic acid] = 109 nM. Some reaction products (e.g., the dicarbonyl species glyoxal, CO_2, and H_2O_2)[25] remain undetected by this technique. In this regard, the support for Baeyer-Villiger promoted reactions[48] from the generated H_2O_2[49] arises from the *in situ* oxidation of products that results in glyoxylic acid by R49.[50] The latter reaction resulting in formic acid involves ozone attack to a double bond conjugated to a carbonyl. Considering that glyoxylic acid generates CO_2 and formic acid, it is reasonable to propose that maleinaldehydic, glutaconic, and *cis,cis*-muconic acids could be the

precursor of peaks at m/z 85, 87, 101, 113 and 129 in Figure 3.1 as indicated in Scheme 3.3.

3.4.4 Atmospheric Implications

Catechol undergoes fast oxidation at the air-water interface by several competing pathways. Hydroxylation and cleavage of the aromatic ring of catechol occur at the air-water interface. The initial oxidation reaction of polyphenols is governed by HO$^\bullet$ radicals formed at high yields under atmospheric conditions. The rate constant for the reaction of catechol with HO$^\bullet$ in the gas-phase under dry conditions is $k_{\text{catechol+HO}} = 1.04 \times 10^{-10}$ cm^3 molecules^{-1} s^{-1}.[51] For an average tropospheric [HO$^\bullet$] = 1.6×10^6 radicals cm^{-3},[52] the residence time $(\tau_i = k^{-1}[\text{oxidizer}]^{-1})$ of catechol against HO$^\bullet$ is $\tau_{\text{catechol+HO}} = 1.7$ h. The rate constant of catechol reacting with O$_3$(g) on the surface of NaCl at RH = 2 % is $k^{NaCl}_{\text{catechol+O}_3} = 6.3 \times 10^{-17}$ cm^3 molecule^{-1} s^{-1}.[16] Assuming standard pressure and 40 ppbv O$_3$(g) $\equiv$ [O$_3$(g)] $= 9.85 \times 10^{11}$ molecules cm^{-3}, the residence time against loss by ozone is $\tau_{\text{catechol+O}_3} = 4.5$ h, which is 6.9-times shorter than in the gas-phase.[51] A 27 % of the total loss of catechol can be contributed by heterogeneous ozonolysis to a mechanism that is largely dominated by gas-phase HO$^\bullet$ during daytime.

A simple analysis can assess the importance of gaseous O$_3$ and $^\bullet$OH interfacial driven chemistry under timescales shorter than the residence time of catechol against both oxidizers. This analysis considers the same particle, $i.e.$, the same surface (A) of a 100-nm diameter particle covered by catechol molecules, reacts with O$_3$(g) or OH(g). The ratio for the rate of loss of molecules by [O$_3$(g)] $= 9.85 \times 10^{11}$ molecules cm^{-3} and [OH(g)] $= 1.6 \times 10^6$ molecules cm^{-3} can be bracketed in the particle using the kinetic theory of gases:[53]

$$1 \leq (\gamma_{O_3}[O_3(g)] \, \upsilon_{O_3} A/4)/(\gamma_{OH}[OH(g)] \, \upsilon_{OH} A/4) \leq 100 \qquad \text{(Eq. 3.5)}$$

where room temperature is assumed, $\gamma_{O_3} = 2.73 \times 10^{-6}$, $0.01 < \gamma_{OH} < 1$, and the mean thermal velocity of OH radicals is $\upsilon_{OH} = 6.61 \times 10^4 \, cm \, s^{-1}$. Therefore, this comparison suggests that the loss of catechol by O_3 may be up to 100-times faster than for OH radicals during interfacial reactions. However, because this analysis did not consider the interfacial production of OH radicals reported in this work, future research should try to assess the contribution from *in situ* produced radicals to the loss of catechol.

Hydroxylation contributes to enhance the reactivity of biomass burning emissions toward atmospheric oxidants as well as the absorptivity[54-56] of airborne species. After the initial processing of aromatic species by abundant HO˙, direct ozonolysis becomes a competitive mechanism for the loss of produced PHA and chromophoric PHQ compounds at the air-water interface. Considering the shorter $\tau_{catechol+HO}$ and $\tau_{catechol+O_3}$ than the residence time of biomass burning plumes and tropospheric aerosols against deposition (~1 week),[52] the mechanisms described contribute to the aging of particles during transport. Moreover, the chain of oxidation reactions generates LMW oxo- and unsaturated di-carboxylic acids, precursors to tropospheric HULIS.[22] This work provides a plausible explanation to the mechanisms by which high levels of dicarbonyls, oxo- and di-carboxylic acids are produced in aerosols[7-10] from biomass burning products.[11-12] The mechanisms have direct global implication because they provide new pathways for AqSOA formation of brown carbon species with low volatility.[57]

3.5 Acknowledgement

3.6 References

1. Boucher, O.; Randall, D.; Artaxo, P.; Bretherton, C.; Feingold, G.; Forster, P.; Kerminen, V.-M.; Kondo, Y.; Liao, H.; Lohmann, U.; Rasch, P.; Satheesh, S. K.; Sherwood, S.; Stevens, B.; X.Y. Zhang, X. Y. Clouds and Aerosols. In *Climate Change 2013: The Physical Science Basis. Contribution of Working Group I to the Fifth Assessment Report of the Intergovernmental Panel on Climate Change*, Stocker, T. F.; Qin, D.; Plattner, G.-K.; Tignor, M.; Allen, S. K.; Boschung, J.; Nauels, A.; Xia, Y.; Bex, V.; Midgley, P. M., Eds. Cambridge University Press: Cambridge, United Kingdom and New York, NY, USA, 2013.

2. Hallquist, M.; Wenger, J. C.; Baltensperger, U.; Rudich, Y.; Simpson, D.; Claeys, M.; Dommen, J.; Donahue, N. M.; George, C.; Goldstein, A. H.; Hamilton, J. F.; Herrmann, H.; Hoffmann, T.; Iinuma, Y.; Jang, M.; Jenkin, M. E.; Jimenez, J. L.; Kiendler-Scharr, A.; Maenhaut, W.; McFiggans, G.; Mentel, T. F.; Monod, A.; Prevot, A. S. H.; Seinfeld, J. H.; Surratt, J. D.; Szmigielski, R.; Wildt, J. The Formation, Properties and Impact of Secondary Organic Aerosol: Current and Emerging Issues. *Atmos. Chem. Phys.* **2009**, *9*, 5155-5236.

3. Finlayson-Pitts, B. J. Reactions at Surfaces in the Atmosphere: Integration of Experiments and Theory as Necessary (but Not Necessarily Sufficient) for Predicting the Physical Chemistry of Aerosols. *Phys. Chem. Chem. Phys.* **2009**, *11*, 7760-7779.

4. Rudich, Y.; Donahue, N. M.; Mentel, T. F. Aging of Organic Aerosol: Bridging the Gap between Laboratory and Field Studies. *Annu. Rev. Phys. Chem.* **2007**, *58*, 321-352.

5. Mkoma, S. L.; Kawamura, K. Molecular Composition of Dicarboxylic Acids, Ketocarboxylic Acids, A-Dicarbonyls and Fatty Acids in Atmospheric Aerosols from Tanzania, East Africa During Wet and Dry Seasons. *Atmos. Chem. Phys.* **2013**, *13*, 2235-2251.

6. Fu, P.; Kawamura, K.; Usukura, K.; Miura, K. Dicarboxylic Acids, Ketocarboxylic Acids and Glyoxal in the Marine Aerosols Collected During a Round-the-World Cruise. *Mar. Chem.* **2013**, *148*, 22-32.

7. Mochida, M.; Kawamura, K.; Umemoto, N.; Kobayashi, M.; Matsunaga, S.; Lim, H. J.; Turpin, B. J.; Bates, T. S.; Simoneit, B. R. T. Spatial Distributions of Oxygenated Organic Compounds (Dicarboxylic Acids, Fatty Acids, and Levoglucosan) in Marine Aerosols over the Western Pacific and Off the Coast of East Asia: Continental Outflow of Organic Aerosols During the Ace-Asia Campaign. *J. Geophys. Res. Atmos.* **2003**, *108*, 8638.

8. Kawamura, K.; Tachibana, E.; Okuzawa, K.; Aggarwal, S. G.; Kanaya, Y.; Wang, Z. F. High Abundances of Water-Soluble Dicarboxylic Acids, Ketocarboxylic Acids and A-Dicarbonyls in the Mountaintop Aerosols over the North China Plain During Wheat Burning Season. *Atmos. Chem. Phys.* **2013**, *13*, 8285-8302.

9. Kundu, S.; Kawamura, K.; Andreae, T. W.; Hoffer, A.; Andreae, M. O. Molecular Distributions of Dicarboxylic Acids, Ketocarboxylic Acids and α-Dicarbonyls in Biomass Burning Aerosols: Implications for Photochemical Production and Degradation in Smoke Layers. *Atmos. Chem. Phys.* **2010**, *10*, 2209-2225.

10. Yang, L.; Nguyen, D. M.; Jia, S.; Reid, J. S.; Yu, L. E. Impacts of Biomass Burning Smoke on the Distributions and Concentrations of C_2–C_5 Dicarboxylic Acids and Dicarboxylates in a Tropical Urban Environment. *Atmos. Environ.* **2013**, *78*, 211-218.

11. Veres, P.; Roberts, J. M.; Burling, I. R.; Warneke, C.; de Gouw, J.; Yokelson, R. J. Measurements of Gas-Phase Inorganic and Organic Acids from Biomass Fires by Negative-Ion Proton-Transfer Chemical-Ionization Mass Spectrometry. *J. Geophys. Res.-Atmos.* **2010**, *115*.

12. Desyaterik, Y.; Sun, Y.; Shen, X.; Lee, T.; Wang, X.; Wang, T.; Collett, J. L. Speciation of "Brown" Carbon in Cloud Water Impacted by Agricultural Biomass Burning in Eastern China. *J. Geophys. Res.-Atmos.* **2013**, *118*, 7389-7399.

13. Dharaiya, N.; Bahadur, P. Phenol Induced Growth in Triton X-100 Micelles: Effect of pH and Phenols' Hydrophobicity. *Colloid Surface A* **2012**, *410*, 81-90.

14. Latif, M. T.; Brimblecombe, P. Surfactants in Atmospheric Aerosols. *Environ. Sci. Technol.* **2004**, *38*, 6501-6506.

15. Barnum, T. J.; Medeiros, N.; Hinrichs, R. Z. Condensed-Phase Versus Gas-Phase Ozonolysis of Catechol: A Combined Experimental and Theoretical Study. *Atmos. Environ.* **2012**, *55*, 98-106.

16. Woodill, L. A.; O'Neill, E. M.; Hinrichs, R. Z. Impacts of Surface Adsorbed Catechol on Tropospheric Aerosol Surrogates: Heterogeneous Ozonolysis and Its Effects on Water Uptake. *J. Phys. Chem. A* **2013**, *117*, 5620-5631.

17. Ofner, J.; Krüger, H. U.; Zetzsch, C. Time Resolved Infrared Spectroscopy of Formation and Processing of Secondary Organic Aerosol *Z. Phys. Chem.* **2010**, *224*, 1171-1183.

18. Guzman, M. I.; Athalye, R. R.; Rodriguez, J. M. Concentration Effects and Ion Properties Controlling the Fractionation of Halides During Aerosol Formation. *J. Phys. Chem. A* **2012**, *116*, 5428-5435.

19. Pillar, E. A.; Guzman, M. I.; Rodriguez, J. M. Conversion of Iodide to Hypoiodous Acid and Iodine in Aqueous Microdroplets Exposed to Ozone. *Environ. Sci. Technol.* **2013**, *47*, 10971-10979.

20. Yamamoto, Y.; Niki, E.; Shiokawa, H.; Kamiya, Y. Ozonation of Organic Compounds. 2. Ozonation of Phenol in Water. *J. Org. Chem.* **1979**, *44*, 2137-2142.

21. Guzman, M. I.; Pillar, E. A. Ozonation of Aromatic Hydrocarbon Probes at the Air-Water Interface In *248th ACS National Meeting & Exposition*, American Chemical Society: San Francisco, CA, 2014; pp COLL-93.

22. Graber, E. R.; Rudich, Y. Atmospheric Hulis: How Humic-Like Are They? A Comprehensive and Critical Review. *Atmos. Chem. Phys.* **2006**, *6*, 729-753.

23. *Crc Handbook of Chemistry and Physics*, 93rd ed.; CRC Press/Taylor and Francis: Boca Raton, Fl., **2013**, p 2664.

24. Sander, S. P.; Abbatt, J.; Barker, J. R.; Burkholder, J. B.; Friedl, R. R.; Golden, D. M.; Huie, R. E.; Kolb, C. E.; Kurylo, M. J.; Moortgat, G. K.; Orkin, V. L.; Wine, P. H. Chemical Kinetics and Photochemical Data for Use in Atmospheric Studies: Evaluation Number 17 Jet Propulsion Laboratory, California Institute of Technology, Pasadena, CA, http://jpldataeval.jpl.nasa.gov: 2011.

25. Bailey, P. S. *Ozonation in Organic Chemistry*; Academic Press: New York, 1982; Vol. 2. p 272.

26. Gurol, M. D.; Nekouinaini, S. Kinetic Behavior of Ozone in Aqueous Solutions of Substituted Phenols. *Ind. Eng. Chem. Fund.* **1984**, *23*, 54-60.

27. Standard Reference Database 69: The NIST Chemistry Webbook Mallard, W. G.; Linstrom, P. J., Eds. National Institute of Standards and Technology: http://webbook.nist.gov. Gaithersburg, MD, 2000; Vol. 2012.

28. Enami, S.; Vecitis, C. D.; Cheng, J.; Hoffmann, M. R.; Colussi, A. J. Global Inorganic Source of Atmospheric Bromine. *J. Phys. Chem. A* **2007**, *111*, 8749-8752.

29. Enami, S.; Vecitis, C. D.; Cheng, J.; Hoffmann, M. R.; Colussi, A. J. Electrospray Mass Spectrometric Detection of Products and Short-Lived Intermediates in Aqueous Aerosol Microdroplets Exposed to a Reactive Gas. *J. Phys. Chem. A* **2007**, *111*, 13032-13037.

30. Steenken, S.; O'Neill, P. Oxidative Demethoxylation of Methoxylated Phenols and Hydroxybenzoic Acids by the Hydroxyl Radical. An in Situ Electron Spin Resonance, Conductometric Pulse Radiolysis and Product Analysis Study. *J. Phys. Chem.* **1977**, *81*, 505-508.

31. Flyunt, R.; Leitzke, A.; Mark, G.; Mvula, E.; Reisz, E.; Schick, R.; von Sonntag, C. Determination of $^{\bullet}OH$, $O_2^{\bullet-}$, and Hydroperoxide Yields in Ozone Reactions in Aqueous Solution. *J. Phys. Chem. B* **2003**, *107*, 7242-7253.

32. Steenken, S.; Neta, P. Properties of Phenoxyl Radicals. In *The Chemistry of Phenols*, Rappoport, Z., Ed. John Wiley & Sons: New York, 2003; p 1000.

33. Elliot, A. J.; McCracken, D. R. Effect of Temperature on O$^{\bullet-}$ Reactions and Equilibria: A Pulse Radiolysis Study. *Rad. Phys. Chem.* **1989**, *33*, 69-74.

34. Mvula, E.; Schuchmann, M. N.; von Sonntag, C. Reactions of Phenol-OH-Adduct Radicals. Phenoxyl Radical Formation by Water Elimination vs. Oxidation by Dioxygen. *J. Chem. Soc. Perk. T. 2* **2001**, 264-268.

35. Adams, G. E.; Michael, B. D. Pulse Radiolysis of Benzoquinone and Hydroquinone. Semiquinone Formation by Water Elimination from Trihydroxy-Cyclohexadienyl Radicals. *T. Faraday Soc.* **1967**, *63*, 1171-1180.

36. Bielski, B. H. J.; Cabelli, D. E.; Arudi, R. L.; Ross, A. B. Reactivity of HO$_2$/O$_2^-$ Radicals in Aqueous-Solution. *J. Phys. Chem. Ref. Data* **1985**, *14*, 1041-1100.

37. Neta, P.; Huie, R. E.; Ross, A. B. Rate Constants for Reactions of Inorganic Radicals in Aqueous Solution. *J. Phys. Chem. Ref. Data* **1988**, *17*, 1027-1284.

38. Mvula, E.; von Sonntag, C. Ozonolysis of Phenols in Aqueous Solution. *Org. Biomol. Chem.* **2003**, *1*, 1749-1756.

39. von Sonntag, C.; von Gunten, U. *Chemistry of Ozone in Water and Wastewater Treatment: From Basic Principles to Applications*; IWA Publishing, 2012, p 302.

40. Iwaki, R.; Kamiya, I. Chemiluminescent Reaction between Polyphenols and Ozone in Acetic Acid. *B. Chem. Soc. Jpn.* **1969**, *42*, 855-863.

41. Philipp, B.; Schink, B. Evidence of Two Oxidative Reaction Steps Initiating Anaerobic Degradation of Resorcinol (1,3-Dihydroxybenzene) by the Denitrifying Bacterium Azoarcus Anaerobius. *J. Bacteriol.* **1998**, *180*, 3644-3649.

42. Buxton, G. V.; Greenstock, C. L.; Helman, W. P.; Ross, A. B. Critical Review of Rate Constants for Reactions of Hydrated Electrons, Hydrogen Atoms and Hydroxyl Radicals ($^{\bullet}$OH/$^{\bullet}$O^{-}) in Aqueous Solution. *J. Phys. Chem. Ref. Data* **1988**, *17*, 513-886.

43. Atkins, P.; de Paula, J. *Elements of Physical Chemistry*, 6th ed.; W. H. Freeman: New York, 2013, p 630.

44. Slade, J. H.; Knopf, D. A. Multiphase Oh Oxidation Kinetics of Organic Aerosol: The Role of Particle Phase State and Relative Humidity. *Geophys. Res. Lett.* **2014**, *41*, 5297-5306.

45. Augugliaro, V.; Rizzuti, L. The Ph Dependence of the Ozone Absorption Kinetics in Aqueous Phenol Solutions. *Chem. Eng. Sci.* **1978**, *33*, 1441-1447.

46. Konstantinova, M. L.; Razumovskii, S. D.; Zaikov, G. E. Kinetics and Mechanism of the Reaction of Ozone with Phenol in Alkaline Media. *B. Acad. Sci. USSR, Div. Chem. Sci.* **1991**, *40*, 266-270.

47. Ramseier, M. K.; von Gunten, U. Mechanisms of Phenol Ozonation-Kinetics of Formation of Primary and Secondary Reaction Products. *Ozone Sci. Eng.* **2009**, *31*, 201-215.

48. ten Brink, G. J.; Arends, I. W. C. E.; Sheldon, R. A. The Baeyer−Villiger Reaction: New Developments toward Greener Procedures. *Chem. Rev.* **2004**, *104*, 4105-4124.

49. Criegee, R. Mechanism of Ozonolysis. *Angew. Chem. Int. Ed.* **1975**, *14*, 745-752.

50. Kolsaker, P.; Bernatek, E.; Johanson, R.; Hytta, R. Glyoxylic Acid as a Reductant in Ozonolysis. *Acta Chem. Scand.* **1973**, *27*, 1526-1530.

51. Tomas, A.; Olariu, R. I.; Barnes, I.; Becker, K. H. Kinetics of the Reaction of O_3 with Selected Benzenediols. *Int. J. Chem. Kinet.* **2003**, *35*, 223-230.

52. Seinfeld, J. H.; Pandis, S. N. *Atmospheric Chemistry and Physics: From Air Pollution to Climate Change*, 2nd ed.; Wiley: New York, 2006, p 1232.

53. George, I. J.; Abbatt, J. P. D. Heterogeneous Oxidation of Atmospheric Aerosol Particles by Gas-Phase Radicals. *Nat. Chem.* **2010**, *2*, 713-722.

54. Rincón, A. G.; Guzmán, M. I.; Hoffmann, M. R.; Colussi, A. J. Optical Absorptivity Versus Molecular Composition of Model Organic Aerosol Matter. *J. Phys. Chem. A* **2009**, *113*, 10512-10520.

55. Rincón, A. G.; Guzmán, M. I.; Hoffmann, M. R.; Colussi, A. J. Thermochromism of Model Organic Aerosol Matter. *J. Phys. Chem. Lett.* **2010**, *1*, 368-373.

56. Saleh, R.; Robinson, E. S.; Tkacik, D. S.; Ahern, A. T.; Liu, S.; Aiken, A. C.; Sullivan, R. C.; Presto, A. A.; Dubey, M. K.; Yokelson, R. J.; Donahue, N. M.; Robinson, A. L. Brownness of Organics in Aerosols from Biomass Burning Linked to Their Black Carbon Content. *Nature Geosci.* **2014**, *7*, 647-650.

57. Saleh, R.; Hennigan, C. J.; McMeeking, G. R.; Chuang, W. K.; Robinson, E. S.; Coe, H.; Donahue, N. M.; Robinson, A. L. Absorptivity of Brown Carbon in Fresh and Photo-Chemically Aged Biomass-Burning Emissions. *Atmos. Chem. Phys.* **2013**, *13*, 7683-7693.

3.7. Supporting Information for Catechol Oxidation by Ozone and Hydroxyl Radicals at the Air-Water Interface

Content   **Pages**

This material presents the Supporting Information explaining how catechol undergoes fast oxidation at the air-water interface by two competing pathways in the presence of O_3. Hydroxylation and cleavage of the 1,2 position of the aromatic ring of catechol occurs at the air-water interface in agreement with observations made in bulk water for phenol.[1] The previously observed formation of $HO^\bullet$ (~22% yield)[2] in the reaction of phenol (pK_a = 9.99)[3] with ozone[4] in the presence of *ter*-butanol and dimethyl sulfoxide (DMSO) scavengers[4-5] supports this work. The chain of oxidation reactions from direct O_3 action generates *cis,cis*-muconic acid and low molecular weight (LMW) oxocarboxylic acids and unsaturated dicarboxylic acids under tropospheric conditions. Under atmospheric conditions, the initial oxidation reaction of polyphenols is governed by $HO^\bullet$ radicals formed at high yields. For polluted conditions of high $[O_3(g)]$, the production of mono- and poly-hydroxylated aromatic hydrocarbons (PHA), and mono- and poly-hydroxylated quinones (PHQ) from the hydroxylation channel should contribute to enhance the reactivity of biomass burning emissions toward atmospheric oxidants. The ozonolysis of catechol at variable pH described in the main text of the article is presented below in Figure S1.
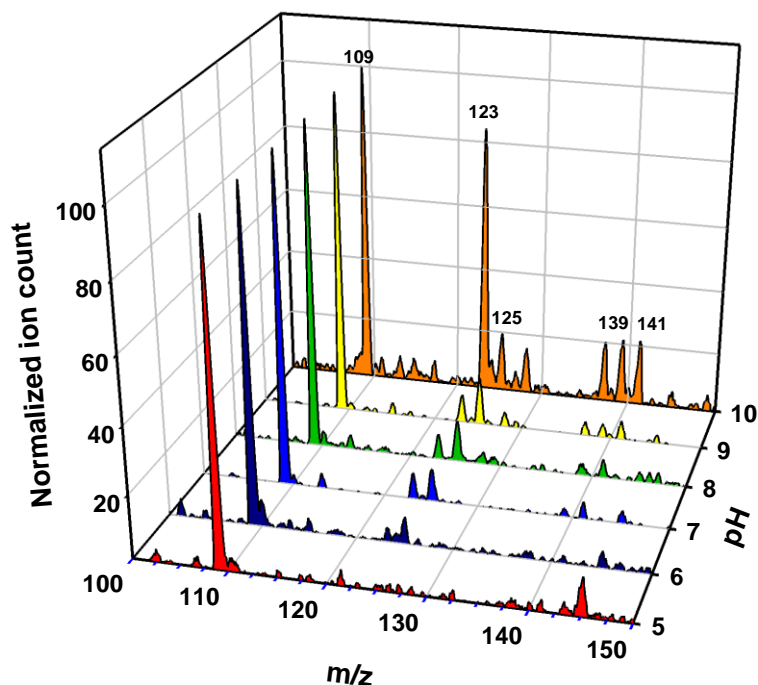
Figure S1. ESI-MS spectra of aerosolized solutions of 25 μM catechol exposed to 3.18 ppmv $O_3(g)$ at variable pH.

Predominant products in the direct ozonolysis of catechol at the air-water interface

Under acidic conditions OH-initiated chemistry does not contribute considerably to the production of polyhydroxylated aromatic hydrocarbons such as tetrahydroxybenzenes. Therefore, experiments at pH 5 and 6 (Figure S1, Supporting Information) are useful to quantify the maximum contribution of *cis,cis*-muconic acid to the peak at *m/z* 141. The mean normalized ion count at *m/z* 141 at pH 5 and 6 is $I_{141,O_3} = 2.32 \pm 0.03$ nM^{-1} of *cis,cis*-muconic acid. In contrast, experiments at pH 8 and 9 display contributions from both $O_3(g)$ and HO$^\bullet$ competing reactions, and the mean normalized ion count is $I_{141,O_3+HO} = 1.83 \times I_{141,O_3}$. Therefore, the ion count at high pH corresponding to the presence of tetrahydroxybenzene is given by the difference $\Delta I_{141} = 1.83 - 1.00 = 0.83$. In other words, a 55 % of the observed peak at pH 8 and 9 corresponds to *cis,cis*-muconic

acid. Therefore, spiked addition of *cis,cis*-muconic acid standard during experiments under the same conditions indicate that only a 55 % of $I_{141} \equiv 55\% \times 236$ nM (the total measured from spiked samples) = 129 nM *cis,cis*-muconic arises from the experiment at pH = 8 in Figure S1.

The pseudo-quantification of tetrahydroxybenzene is performed taking into account the response of the MS detector. A detector response factor linking the ratio of concentrations per normalized ion counts at pH = 8 in the presence of 25 μM catechol was established for *cis,cis*-muconic acid and 1,2,3-trihydroxybenzene (Acros, 99.7 %). In this case, 1,2,3-trihydroxybenzene was used as a representative analyte for the (commercially unavailable) tetrahydroxybenzenes produced *in situ* during the interfacial reaction. The previous assumption was based on measurements confirming that the MS detector gives a similar linear response for I_{109} and I_{125} with increasing catechol and 1,2,3-trihydroxybenzene concentration, respectively. The response factor β was:

$$\beta = \frac{I_{141,standard}}{I_{125,standard}} \simeq 0.25 \; \frac{nM \text{ cis,cis-muconic acid}}{nM \text{ tetrahydroxybenzenes}} \qquad \text{(Eq. 3.5)}$$

The equivalent concentration of *cis,cis*-muconic acid to tetrahydroxybenzenes can be retrieved from the experimental 45 % I_{141} signal remaining at pH = 8:

$$236 \, nM \, \times \, 45\% =$$

$106 \, nM$ equivalent cis,cis-muconic acid to tetrahydroxybenzenes   (Eq. 3.6)

after converting the concentration of 106 nM equivalent *cis,cis*-muconic acid to the actual

concentration of tetrahydroxybenzenes using the response factor *β*:

$$[\text{tetrahydroxybenzenes}] = \frac{106 \, nM \text{ cis,cis-muconic acid}}{0.25 \, \frac{nM \text{ cis,cis-muconic acid}}{nM \text{ tetrahydroxybenzenes}}}$$ (Eq. 3.7)

to obtain [tetrahydroxybenzenes] = 424 nM tetrahydroxybenzenes. Similarly, from the

high total [trihydroxybenzenes] = 2260 nM is evident that OH radicals quickly favor a

mechanism of production of polyhydroxylated aromatic compounds.

The quantification of the predominant products of direct ozonolysis was performed by

spiked addition of standards during ozonolysis. Aerosolized solutions of 25 μM catechol

at pH 8.0 were exposed to 3.18 ppmv O_3(g). The standards were prepared from oxalic

acid dihydrate (Mallinckrodt, 99.1 %), maleic acid (Sigma-Aldrich, 99.9%), glyoxylic

acid (Sigma-Aldrich, 50 wt. % in H_2O), pyruvic acid (Sigma-Aldrich, 99.1 %) as a

pseudo-standard to quantify 3-oxopropanoic acid, and *cis,cis*-muconic acid (Aldrich, 98.7

%). All analyses corresponded to experiments in which the normalized ion count of

products increased only by 1 to 3 times the intensity registered in the absence of the

spiked. Concentration of standards after spiked addition bracket the range from 50 nM to

2500 nM. The results indicate the presence of [glyoxylic acid] = 200 nM > [oxalic acid] = 174 nM > [*cis,cis*-muconic acid = 129 nM > 3-oxopropanoic acid] = 109 nM. Because [maleic acid] < 10 nM, it can be assumed that this species is quickly converted in glyoxylic acid.

Conversion of 1,2,4-trihydroxybenzene (THB) to 2-hydroxy-1,4-benzoquinone at variable pH

100 μM solutions of THB (Alfa Aesar, 99.2 %) were freshly prepared in degassed ultra-pure water (18.2 MΩ cm). An aliquot of 50 mL of the solution was adjusted to initial pH 5.06 (Thermo Scientific pH-meter) with 0.01 M HCl in an amber bottle. Solutions of 0.001-0.09 M NaOH were used to adjust the pH of the solution to the values reported in Figure S2. An aliquot of 3.5 mL of this pH-adjusted solution was transferred to a 10 mm path length fused silica cuvette (Starna Cells) to register the absorption spectra with an Evolution 220 UV-visible spectrophotometer equipped with a linear 8-cell changer (Thermo Scientific) cuvette holder.

Figure S2 shows that at pH 5.06 (black line) the UV-visible spectrum of the colorless solution of THB presents two peaks A and B with maximum wavelengths $\lambda_{max,A}$ = 194 nm and $\lambda_{max,B}$ = 287 nm, respectively. Small increments in pH were accompanied by a decrease in the intensity of peak B, representing the loss of THB. Simultaneously, as the pH increased and the solution turned pinkish orange (from the production of the quinone form in equilibrium), peaks C, D, and E appeared at $\lambda_{max,C}$ = 211 nm, $\lambda_{max,D}$ = 261 nM, and $\lambda_{max,E}$ = 486 nm, respectively. The inset in Figure S2 shows how the absorption maxima for peaks B and E can be can be used to monitor the inter-conversion of both

species at variable pH, as it has been observed in similar studies with denitrifying bacteria.[6]
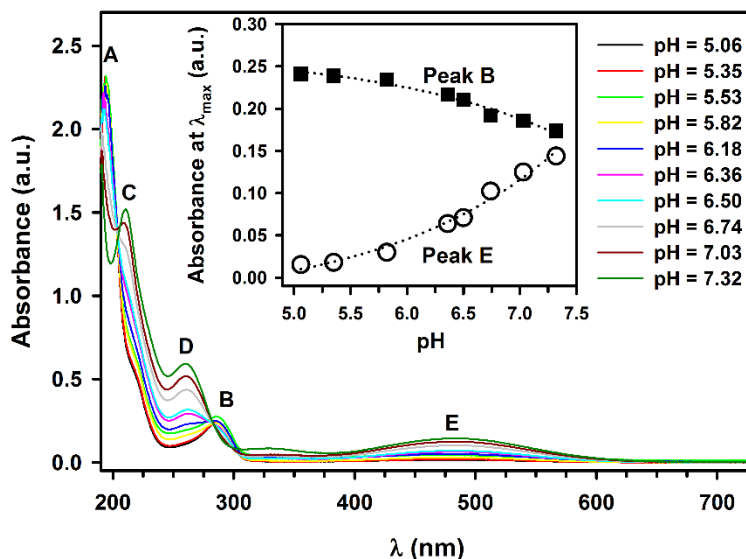
Figure S2. Conversion of 100 μM 1,2,4-trihydroxybenzene in 2-hydroxy-*p*-quinone at variable pH.

Ozonolysis of thin films of catechol studied by Fourier transform infrared (FTIR) spectroscopy

A Thermo Scientific FTIR spectrometer interfacing a Nicolet iZ10 module to an iN10 MX Infrared Imaging Microscope was used to study the heterogeneous ozonolysis of thin solid films of catechol. A fresh solution of catechol in acetone (British Drug Houses 99.97%) was freshly prepared before the experiment at a concentration of 2.0 mg mL^{-1}. A total of 500.0 μL of the solution was slowly deposited onto the circular ZnSe crystal (15 mm in diameter) of the 45° single-reflectance attenuated total reflectance (ATR) accessory (SpectraTech) by drop-wise addition, forming a stable film after two hours. A macro-loop program was used to collect spectra (64 scans, 4 cm^{-1} resolution) over time.

The loss of catechol O-H bands during ozonolysis was monitored in the absorbance mode at 3458 cm^{-1}. Spectra of thin films of *cis,cis*-muconic acid (Sigma-Aldrich ≥ 97.0%) were also registered for comparison purposes.

Experiments at high relative humidity RH ≥ 80% were conducted by mixing 0.8 L min^{-1} N$_2$(*g*) bubbled through ultrapure water with 0.2 L min^{-1} O$_3$(*g*) generated as described in the main text. Humidity measurements were registered in a mixing chamber with a relative humidity sensor (Fisher Scientific). A flow of 20 mL min^{-1} of this diluted O$_3$(*g*) was circulated through a homemade borosilicate glass cell covering the ATR crystal. A correction to the loss of catechol was applied by subtracting the loss of absorbance at 3458 cm^{-1} when humid UHP N$_2$(*g*) serving as zero air (control with no O$_3$(*g*)) was circulated under the same conditions.

The heterogeneous oxidation of catechol thin films proceeded promptly after addition of gaseous ozone at high relative humidity (RH). However, *cis,cis*-muconic acid, the previously unique identified product[7] appears to be embedded with other species and cannot explain the overall complexity of the spectrum after 2 hr of reaction with 4 ppmv O$_3$(*g*) at 81% RH. Herein, we suggest that the broadening of the O-H vibration bands at high RH levels previously suggested to indicate hydrogen bonding between catechol and adsorbed water molecules,[7] may actually correspond to the formation of the polyhydroxylated catechol products also observed by ESI-MS (see main text).

The spectra below for catechol and *cis,cis*-muconic acid thin films in Figure S3 agree with their crystalline structure features listed in Tables S1 and S2, respectively.
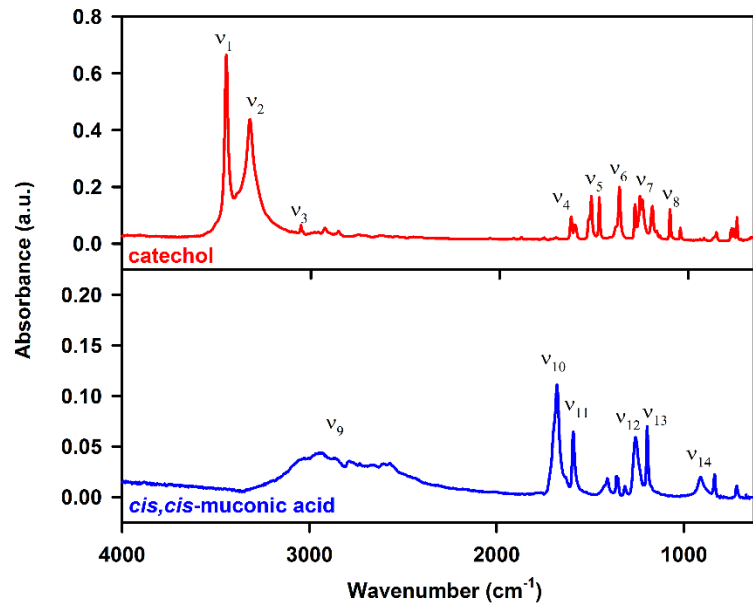
Figure S3. ATR-FTIR spectra of (red and top) catechol and (blue and bottom) *cis,cis*-muconic acid.

Table S1. Vibrational assignment of Catechol in the IR spectrum

Wavenumber (cm^{-1})	Strength	Assignment
3458 (ν_1)	S	O-H
3322 (ν_2)	S	O-H
3053 (ν_3)	W	=C-H
1619 (ν_4,) and 1513,1469 (ν_5)	W	C=C
1365 (ν_6)	M	C=C in aromatics
1256 (ν_7)	S	C-H
1094 (ν_8)	W	C-H

Key: S = Strong, M = Medium, and W = Weak

Table S2. Vibrational assignment of *cis,cis*-muconic acid in the IR spectrum

Wavenumber (cm^{-1})	Strength	Assignment
2936 (ν_9)	W	O-H
1675 (ν_{10})	S	C=O
1590 (ν_{11})	M	C=C
1259 (ν_{12})	W	C-H
1198 (ν_{13})	W	C-O
909 (ν_{14})	W	C-H

Key: S = Strong, M = Medium, and W = Weak

The decrease of the characteristic O-H stretching (ν_1) peak at 3458 cm^{-1} was used to monitor the loss of catechol in Figure S4. Several short experiments at high [O$_3$(g)] were performed at RH $\geq$ 80 %. For example, Figure S4 displays the loss of catechol exposed to [O$_3$(g)] = 2.12 $\times$ 10^{15} molecules cm^{-3} at 80% RH, and Figure S5 shows the relative reaction rate measured by extracting the CD-line (corrected absorbance) at 3458 cm^{-1} versus time. The corrected absorbance was measured using Omnic software (Thermo Scientific) from the A-B local baseline, to the left- and right-hand side of the peak, up to the maximum absorbance value or C-D line indicating the peak height depicted in Figure S4.
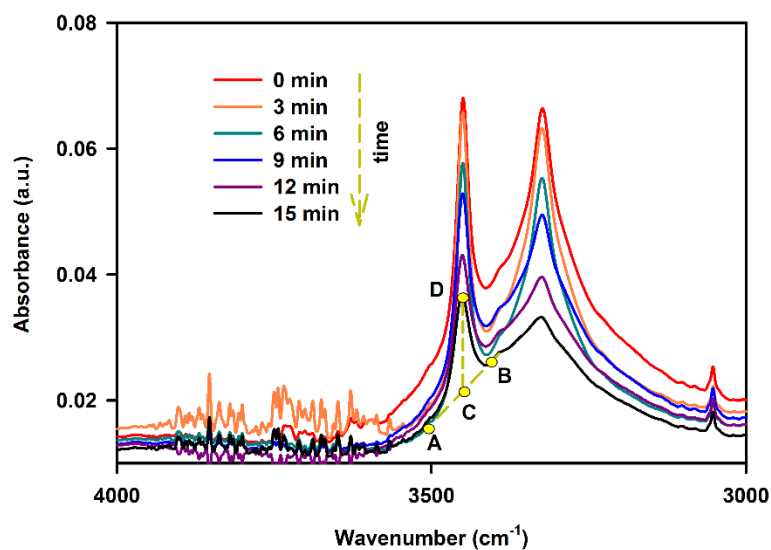
Figure S4. ATR-FTIR spectra of thin films of catechol exposed to $[O_3(g)] = 2.12 \times 10^{15}$ molecules cm^{-3} at 80 % RH.
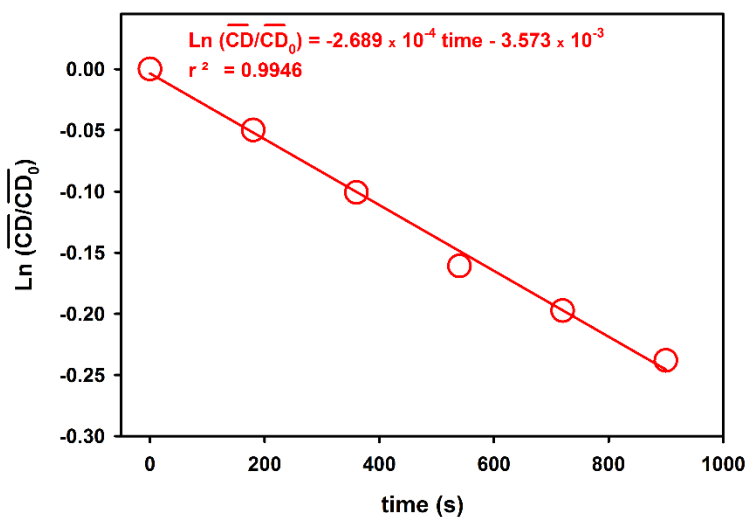
Figure S5. First-order decay of the CD-line of catechol at 3458 cm^{-1} relative to its initial value. Conditions: $[O_3(g)] = 2.12 \times 10^{15}$ molecules cm^{-3} and 80 % RH.

For high $[O_3(g)]$, the loss of catechol follows first order kinetics on the reactants[7] with rate constant k:

115

$-d$[catechol]$/dt = k$ [catechol] [$O_3(g)$] (Eq. 3.8)

Considering that for [$O_3(g)$] $= 2.12 \times 10^{15}$ molecules cm^{-3}, the level of this reactant remains constant in Figure S5, the equation simplifies to:

$-d$[catechol]$/dt = k'$ [catechol] (Eq. 3.9)

where k' is the pseudo-first order rate constant resulting from $k \times$ [$O_3(g)$]. The film of catechol disappeared in Figure S5 with a pseudo-first order rate constant $k' = 2.689 \times 10^{-4}$ s^{-1}. Therefore, for this high [$O_3(g)$], it only takes 43 min for a half of the catechol film to quickly disappear in the ATR setup.

Scheme S1. Proposed recycling of *o*-semiquinone radical into catechol at the air-water interface showing observed *m/z* values in blue font.

Scheme S1. Proposed recycling of *o*-semiquinone radical into catechol at the air-water interface showing observed *m/z* values in blue font.

References

1. Bailey, P. S. *Ozonation in Organic Chemistry*; Academic Press: New York, 1982; Vol. 2. p 272.

2. Mvula, E.; von Sonntag, C. Ozonolysis of Phenols in Aqueous Solution. *Org. Biomol. Chem.* **2003**, *1*, 1749-1756.

3. *CRC Handbook of Chemistry and Physics*, 93rd ed.; CRC Press/Taylor and Francis: Boca Raton, Fl., **2013**, p 2664.

4. Flyunt, R.; Leitzke, A.; Mark, G.; Mvula, E.; Reisz, E.; Schick, R.; von Sonntag, C. Determination of $^{\bullet}OH$, $O_2^{\bullet-}$, and Hydroperoxide Yields in Ozone Reactions in Aqueous Solution. *J. Phys. Chem. B* **2003**, *107*, 7242-7253.

5. Reisz, E.; Schmidt, W.; Schuchmann, H.-P.; von Sonntag, C. Photolysis of Ozone in Aqueous Solutions in the Presence of Tertiary Butanol. *Environ. Sci. Technol.* **2003**, *37*, 1941-1948.

6. Philipp, B.; Schink, B. Evidence of Two Oxidative Reaction Steps Initiating Anaerobic Degradation of Resorcinol (1,3-Dihydroxybenzene) by the Denitrifying Bacterium Azoarcus Anaerobius. *J. Bacteriol.* **1998**, *180*, 3644-3649.

7. Barnum, T. J.; Medeiros, N.; Hinrichs, R. Z. Condensed-Phase Versus Gas-Phase Ozonolysis of Catechol: A Combined Experimental and Ttheoretical Study. *Atmos. Environ.* **2012**, *55*, 98-106.

Chapter 4. Heterogeneous Oxidation of Catechol

Reproduced with permission from:
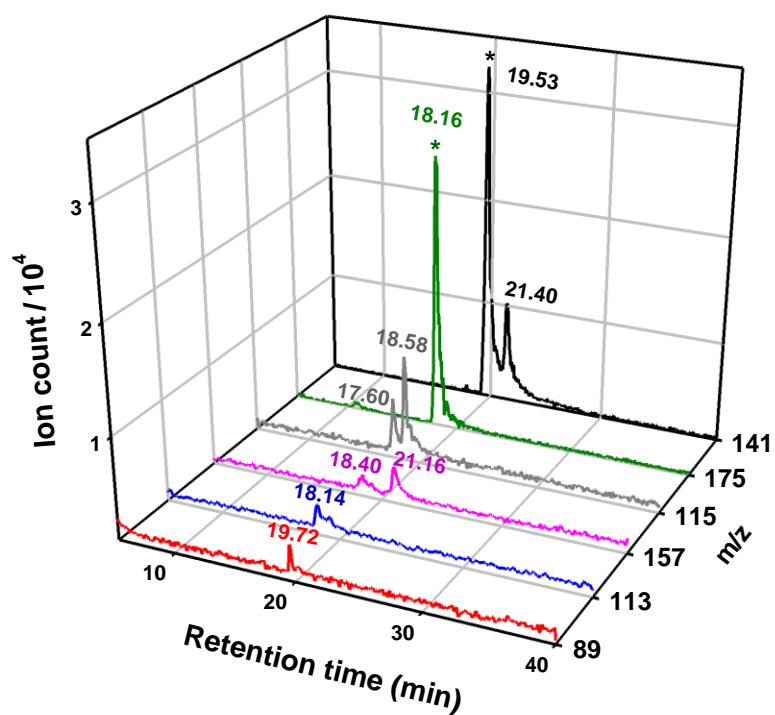
Scheme 4.1 Synopsis TOC

4.1 Synopsis

Natural and anthropogenic emissions of aromatic hydrocarbons from biomass burning, agro-industrial settings, and fossil fuel combustion contribute precursors to secondary aerosol formation (SOA). How these compounds are processed under humid tropospheric conditions is the focus of current attention to understand their environmental fate. This work shows how catechol thin films, a model for oxygenated aromatic hydrocarbons present in biomass burning and combustion aerosols, undergo heterogeneous oxidation at the air-solid interface under variable relative humidity (RH = 0-90%). The maximum reactive uptake coefficient of $O_3(g)$ by catechol $\gamma_{O_3} = (7.49 \pm 0.35) \times 10^{-6}$ occurs for 90 % RH. Upon exposure of *ca.* 104-μm thick catechol films to $O_3(g)$ mixing ratios between 230 ppbv and 25 ppmv, three main reaction pathways are observed. 1) The cleavage of the 1,2 carbon-carbon bond at the air-solid interface resulting in the formation of *cis,cis*-muconic acid via primary ozonide and hydroperoxide intermediates. Further direct ozonolysis of *cis,cis*-muconic yields glyoxylic, oxalic, crotonic, and maleic acids. 2) A second pathway is evidenced by the presence of Baeyer-Villiger oxidation products including glutaconic 4-hydroxy-2-butenoic, and 5-oxo-2-pentenoic acids during electrospray ionization (ESI) mass spectrometry (MS) and ion chromatography MS analyses. 3) Finally, indirect oxidation by in situ produced hydroxyl radical (HO•) results in the generation of semiquinone radical intermediates toward the synthesis of polyhydoxylated aromatic rings such as tri-, tetra-, and penta-hydroxybenzene. Remarkably, heavier polyhydroxylated biphenyl and terphenyl products present in the extracted oxidized films result from coupling reactions of semiquinones of catechol and its polyhydroxylated rings. The direct ozonolysis of 1,2,3- and 1,2,4-trihydroxybenezene

yields 2- and 3-hydroxy-cis,cis-muconic acid, respectively. The production of 2,4- or 3,4-dihdroxyhex-2-enedioic acid is proposed to result from the sequential processing of cis,cis-muconic acid, 2- and 3-hydroxy-cis,cis-muconic acid. Overall, these reactions contribute precursors to form aqueous SOA from aromatics in atmospheric aerosols and brown clouds.

4.2 Introduction

Aerosol particles absorb and scatter sunlight and act as condensation nuclei for clouds playing a key role in climate.[1] The production mechanisms and associated properties of secondary organic aerosols (SOA) from laboratory and field studies have been recently reviewed.[2-3] In situ aging of the species found in aerosols during atmospheric transport contributes to the chemical complexity that makes difficult to quantify organic species in aerosols.[4] The concentration of water soluble organic compounds (WSOC) in field measurements, e.g., glyoxylic, 3-oxopropoanoic, oxalic, and fumaric acids, suggests common natural formation mechanisms.[5] Because the high levels of WSOC quantified at dissimilar geographical locations can exceed typical urban pollution sources,[6-8] the identification of new chemical production mechanisms acting over emissions from natural processes is needed.

The composition of WSOC, atmospheric transport of biomass burning products, and photooxidation (e.g., of glyoxylic acid to generate oxalic acid) have been correlated at different sites.[6-8] Dihydroxybenzenes such as catechol are the most common gas-phase organic constituents (~50 ppbv) resulting from biomass burning,[9] pyrolysis and combustion.[10] Cloud water collected from brown clouds also contains aromatics such as

catechol rings substituted with methyl, carbonyl, and nitro groups.[11] The surfactant properties of these species favor their accommodation at interfaces of aerosols,[12] where they are prone to undergo photooxidation.[13]

A recent study has demanded the identification and quantification of products from catechol ozonolysis both in gas and particle phases.[14] In fact, the heterogeneous ozonolysis of catechol under ultrafast contact times[15-16] was examined in a previous study at the air-water interface of microdroplets.[17] Mass spectrometry (MS) analysis of the reaction products has revealed that different reaction channels are operative at the air-water interface, 1) oxidative cleavage of the aromatic ring, and 2) hydroxylation.[17-18] The cleavage of C(OH)-C(OH) bond of catechol yields *cis,cis*-muconic acid (MA)[19-20] and its lower molecular weight (LMW) carboxylic acid oxidation products.[17, 21] Attenuated total reflectance (ATR) Fourier transform infrared (FTIR) spectroscopy has been used to study the reaction of solid films under high relative humidity (RH) that yielded an uptake coefficient of ozone by catechol γ_{O_3} = 5.6 × 10^{-5} (RH = 81 %)[20] that is about 20-times larger than the value estimated at the air-water interface (γ_{O_3} = 2.73 × 10^{-6}).[17] Indeed, an explanation to this discrepancy justifies a new independent study to explore the values of γ_{O_3} at variable RH. The hydroxylation channel conducting to the production of semiquinone radicals explains the in situ interfacial formation of polyhydroxylated aromatic rings and chromophoric quinones in tropospheric particles.[17] However, the production of semiquinone radicals should also result in the formation of coupling aromatic products such as biphenyls during ozonolysis. Therefore, this work is focused on the identification of coupling products from catechol and in situ produced polyhydroxylated benzene rings during the heterogeneous ozonolysis of thin catechol

122

films. The results below provide new insights to understand the evolution of biomass burning and combustions emissions during atmospheric transport.

4.3 Experimental

4.3.1 Thin Film Preparation

Solutions of *ca.* 3.0 mg mL^{-1} catechol (Sigma-Aldrich, 99.9%) were prepared daily in isopropanol (Fisher Optima, 99.9%). A glass syringe with stainless steel plunger and needle (Hamilton, 705) was used for dropwise addition of 50 µL solution onto an infrared transparent optical window. Polished ZnSe or amorphous material transmitting infrared radiation (AMTIR) 2.0-mm thick optical windows with a diameter of 13.0 mm (PIKE) were used. After 3 h of solvent evaporation, dry films were confirmed to be stable by FTIR spectroscopy. The resulting film thickness measured by reflectance spectroscopy was *ca.* 104.5 (± 12.8) µm and contained *ca.* 150 µg of catechol deposited. Thin films of some candidate products were similarly prepared using *cis,cis*-muconic acid (Aldrich, 98.7%), maleic acid (Sigma-Aldrich, 99.9%), glyoxylic acid (Aldrich, 51.7 wt. % in water), oxalic acid (Sigma-Aldrich, 99.9%), 1,2,3-trihydroxybenzene (Acros, 99.7%), and 1,2,4-trihydroxybenzene (Alfa Aesar, 99.2%).

4.3.2 Ozonolysis of Thin Films

A customized ozone generation and monitoring system was used in all experiments.[16-17] Humid nitrogen was produced by passing $N_2(g)$ (Scott Gross, UHP) through a wash bottle containing ultra-pure water (18.2 MΩ cm, ELGA PURELAB flex, Veolia). The mixing ratio of dry $O_3(g)$ and humid $N_2(g)$ was controlled with flow meters (Aalborg). The relative humidity (RH) of the mixed gas (1.0 L min^{-1}) was monitored in a mixing

chamber with a remote hygrometer (Traceable) before flowing into a borosilicate glass flow-through reactor (3.785 L capacity) provided with a Teflon coated lid (Scheme 4.1). The gas was allowed to equilibrate for 1 h before introducing any samples into the reactor. UV-visible absorption measurements at wavelengths λ_1 = 250 nm and λ_2 = 300 nm were performed for a 1.0 L min^{-1} gas flow entering the chamber in a 10.00 cm pathlength fused silica cuvette (Starna Cell) before, during, and after the reaction and converted to [O$_3$(g)] using absorption cross sections $\sigma_{250\ nm}$ = 1.1 $\times$ 10^{-17} cm^2 molecule^{-1} and $\sigma_{300\ nm}$ = 3.9 $\times$ 10^{-19} cm^2 molecule^{-1}, respectively.[22] The standard deviation associated to measured [O$_3$(g)] during the reactions was below 2.50 %.

Scheme 4.2. Flow-through reactor system with mixing of dry and wet gases.
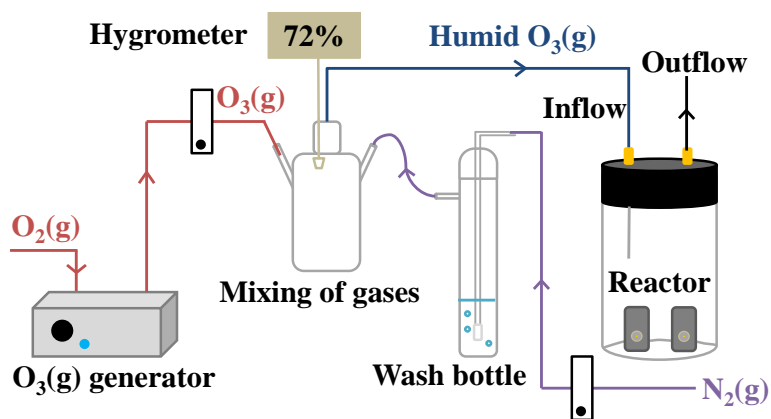
4.3.3 FTIR and UV-visible Monitoring

The spectroscopic changes associated to the oxidation of thin films were studied by FTIR spectroscopy. Optical windows with prepared films were mounted on stainless steel plates, placed in the reactor, and withdrawn for FTIR analysis at 20 min intervals of exposure to O$_3$(g), unless indicated otherwise. FTIR analysis was performed with a Nicolet iN10 infrared microscope (Thermo Scientific). A total of 64 scans were collected

and averaged in 1.5 min over the range 500–4000 cm^{-1} with 4 cm^{-1} resolution using an iZ10 FT-IR module connected to the infrared microscope. All samples were background subtracted using an empty optical window. Control experiments ensured that films exposed to humid air in the absence of $O_3(g)$ were chemically stable and that their loss by sublimation remained below 5.0 % during the timescale of experiments designed to gather kinetic information. Reported data are the average of duplicate experiments with error bars corresponding to one standard deviation. OMNIC software (Thermo Scientific) was utilized for FTIR spectroscopy, and for data processing. The CD line, or corrected peak heights after baseline correction as previously described,[17] is reported in all plots. Data analysis and fitting of rate constants was performed using SigmaPlot Software (Systat). UV-visible absorption measurements of films deposited on quartz optical windows followed the same procedure described above.

4.3.4 Film Extraction and Analysis

Each window with a film was extracted with 2.0 mL of selected solvents under sonication (Branson Ultrasonics) for 15 min. Extractions were performed using four different solvents: chloroform (Mallinckrodt, 99.8%), isopropanol, acetone (Fisher Scientific, 99.5%), or acetonitrile (Fisher Optima, 99.9%). After sonication, the samples were quantitatively transferred to 7.5 mL amber vials (Fisher Scientific) and dried by gently sparging $N_2(g)$. All samples were finally reconstituted with 1.0 mL methanol (Fisher Optima, 99.99%) unless stated otherwise. Control experiments showed that unreacted dry and humid catechol films extracts remain stable during the timescale of the reaction.

The analysis of reconstituted film extracts was performed by ESI MS in a MSQ Plus instrument (Thermo Scientific) operating in negative ion mode. Samples were injected into the calibrated ESI MS at a flow rate of 100 µL min^{-1} by mixing equal flows of the reconstituted sample in methanol and ultrapure water (18.2 MΩ-cm, Elga Purelab flex - Veolia). The ESI MS conditions were: drying gas temperature, 250 °C; nebulizer voltage, -1.9 kV; cone voltage, -50 V, and nebulizer pressure, 70 psi. Reported ion counts were background subtracted from the solvent and acquired over fixed intervals ($\geq$ 30 s).

Confirmation of the generation of carboxylic acids was obtained by ion chromatography (IC) MS analysis as described before.[23] For these analyses, dried film extracts were reconstituted in 1.5 mL water and injected with a Dionex AS autosampler into a Dionex ICS-2000 IC system. The IC was equipped with an IonPac AS11-HC column (2 × 250 mm), an AG11-HC guard column (2 × 50 mm), an ASRS-300 suppression module (2-mm), an eluent generator (EGC III) with KOH cartridge, and a CR-ATC anion trap column. The separation gradient applied a flow of 0.38 mL min^{-1} with an initial mobile phase of 1 mM KOH for 8 minutes followed by three linear increases of (1) 1.4 mM min^{-1} up to 15 mM, (2) 1.5 mM min^{-1} up to 30 mM, and (3) 3 mM min^{-1} up to 60 mM. After IC separation, the eluent was mixed with 0.12 mL min^{-1} methanol for identification of the mass to charge ratio (*m/z*) of separated components in the ESI MS (drying gas temperature, 450 °C; nebulizer voltage, -1.9 kV; cone voltage, -50 V, and nebulizer pressure, 70 psi). Chromeleon and Excalibur software were used to control and process data.

4.4 Results and Discussion

4.4.1 Oxidation of Catechol Films

Figure 4.1 shows FTIR spectra of catechol thin films (A) under ambient conditions and (B) after exposure to 230 ppbv $O_3(g)$ at 68 % RH for 24 h. All infrared spectroscopic features for pure catechol in Figure 4.1A are assigned to vibrational modes in Table S1 (Supporting Information). After exposure to $O_3(g)$ the features in Figure 4.1A for O-H stretching, C-C stretching, and C-H bending peaks of catechol at 3450 cm^{-1} (peak 1), 1365 cm^{-1} (peak 2), and 1095 cm^{-1} (peak 3), respectively, are lost in Figure 4.1B. Instead, new signals for C=O stretching at 1680 cm^{-1} (peak 4), C=C asymmetric stretching at 1585 cm^{-1} (peak 5), O-H stretching for carboxylic acid at 2400-3100 cm^{-1} (peak 6), and hydrogen bonded O-H stretching at ~3400 cm^{-1} (peak 7) become prominent in the ozonolysis products spectrum (Figure 12.1B).

Figure 4.1C displays the IR spectra, from top to bottom, of (blue trace) 1,2,4-trihydroxybenzene, (pink trace) 1,2,3-trihydroxybenzene, (green trace) *cis,cis*-muconic acid, (grey trace) maleic acid, (dark blue trace) oxalic acid, and (purple trace) glyoxylic acid, which represent candidate products from the previous ozonolysis study at the air-water interface.[17] The main features observed in Figure 4.1B, peaks 4-6, partially resemble those of *cis,cis*-muconic acid.[20] However, there is an additional level of complexity associated to peaks 4, 5 and 7, which cannot be explained by *cis,cis*-muconic acid alone. For example, maleic acid and both trihydroxybenzene species have features that might contribute significantly to peak 5, which is not observed in *cis,cis*-muconic acid,[20] to be as intense as peak 4. These species, combined with glyoxylic and oxalic acids may also explain the appearance of additional hydrogen bonded O-H stretching

modes giving rise to the broad peak centered at about 3400 cm⁻¹. Tables with the vibrational assignments for the oxidized film, *cis,cis*-muconic acid, maleic acid, glyoxylic acid, oxalic acid, 1,2,3- and 1,2,4-trihydroxybenzene are available in the Supporting Information (Tables S2-S8).
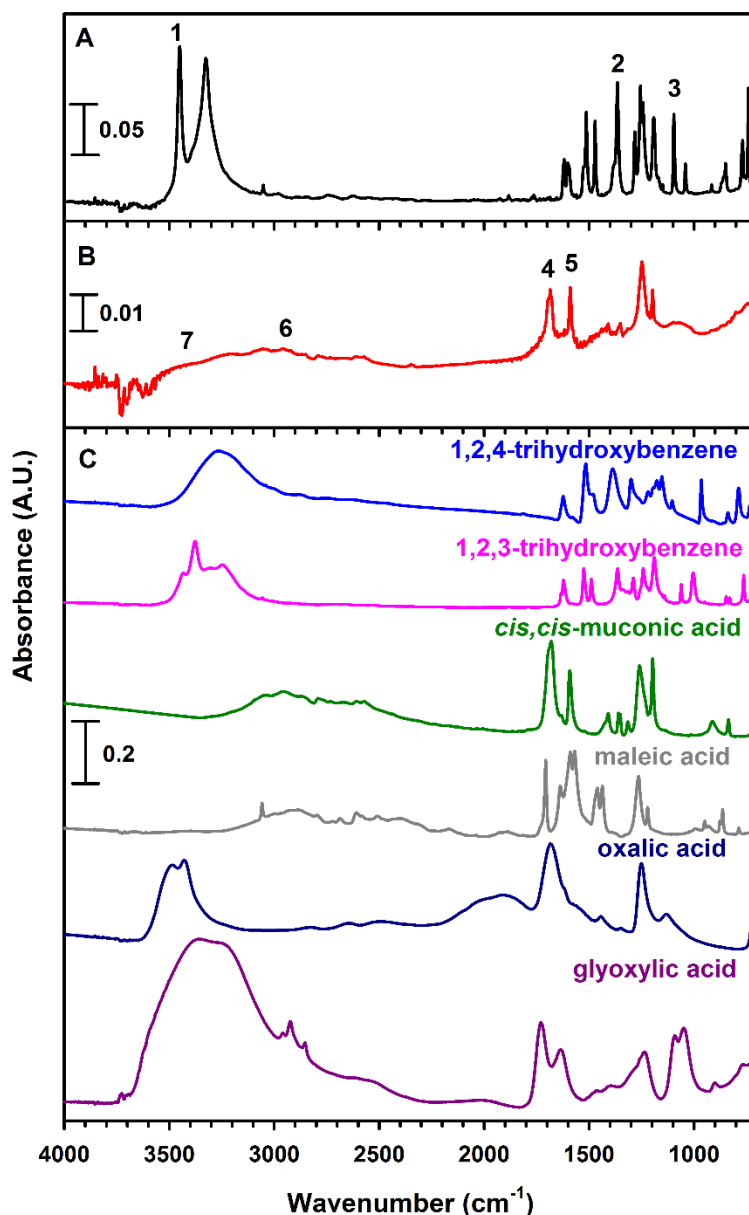
Figure 4.1. FTIR spectra of thin films of catechol (A) before and (B) after 24 h exposure to 230 ppbv $O_3(g)$ at 68 % relative humidity (RH). (C) Spectra for standards with features observed in oxidized films.

Detailed qualitative information of the products of catechol oxidation at the air-solid interface is gleaned from long lasting experiments (24 h exposure) at ozone levels approaching those typical of highly polluted urban environments (Figure 4.1).[24] However, this experiment is slow and yield kinetics results that may be biased due to the loss of catechol by sublimation occurring at long timescales. For example, a control experiment with pure $N_2(g)$ flow at 68 % RH shows a catechol loss by sublimation of 80 % after 24 h. Therefore, the experiments below are designed to constrain the sublimation loss of catechol during the reaction to be ≤ 5.0 % by increasing $[O_3(g)]$ to shorten their duration and provide valuable reaction rate constants.

Figure 4.2 shows the FTIR spectra of thin films with 150 μg catechol deposited, which are exposed to 23.6 ppmv $O_3(g)$ at 72 % RH for 3 hr. Ongoing work suggests a Langmuir-Hinshelwood mechanism is followed during the ozonolysis of catechol films.[25] The data in Figures 4.1 and 4.2 lays in the linear region of the hyperbola describing the dependence of the rate of reaction on $[O_3(g)]$. Monitoring the loss of peaks 1-3 and the appearance of peaks 4-6 allow us to register the corresponding oxidation of catechol and the development of organic acids and polyhydroxylated aromatics products, respectively. The similar product distribution to that obtained for 230 ppbv $O_3(g)$ (Figure 4.1) confirms that the information gathered for larger $[O_3(g)]$ does not affect the oxidation mechanism at the air-solid interface. Clearly, features of the primary product *cis,cis*-muconic acid are evident in Figure 4.2, as well as O-H (1410 cm⁻¹) and =C-H bending modes (1360 and 1320 cm⁻¹). Moreover, a defined peak centered at 3400 cm⁻¹ is visible together with distinct broadening stretches for C=O and C=C at 1680 and 1590 cm⁻¹, respectively.[26]
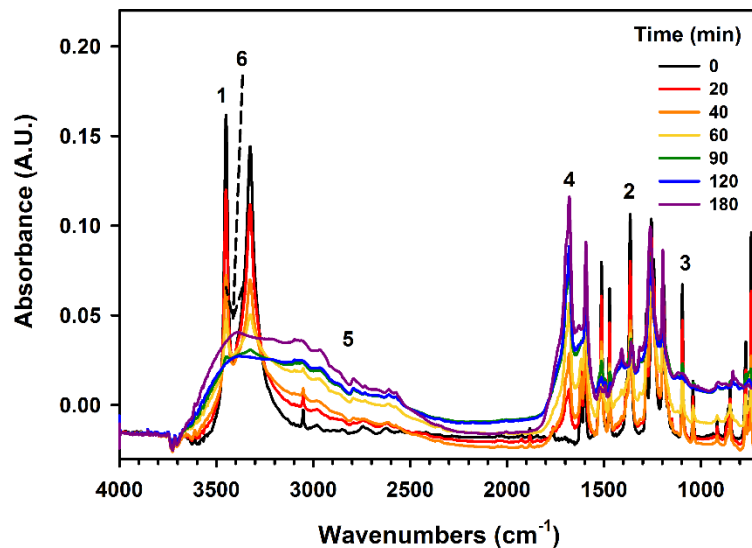
Figure 4.2. FTIR spectra showing the time series of catechol thin films exposed to 23.6 ppmv $O_3(g)$ at 72% RH. Peak labels 1-6 indicate characteristic peaks used to monitor reaction progress (see text).

The sharp peak clearly appearing at 1198 cm^{-1} in the FTIR spectra of Figures 4.1 and 4.2 for final oxidation times also corresponds to *cis,cis*-muconic acid vibrational modes. This peak is 8 cm^{-1} above the closest peak for catechol and cannot be confused with a reactant signal. In general, the common spectroscopic features of several candidate products in the infrared region prevent from assigning all products conclusively based on FTIR results. The critical need to resolve further the chemical composition of oxidized catechol conducted us to extract the films and analyze them by different techniques as described below.

4.4.2 Proposed Reaction Pathways Based on the Analysis of Extracted Films

Figure 4.3 shows ESI MS analyses of catechol films at 71% RH (blue) before and (red) after 3 h exposure to 29.3 ppmv $O_3(g)$, which were extracted in 1) acetonitrile, 2) acetone, 3) isopropanol, and 4) chloroform. The selection of these solvents with different properties ensures that peak identification of products is not affected by any artifacts

resulting from the extraction procedure itself. In addition, the possibility of methanol clustering of parent anions during infusion of all samples in 50:50 methanol:water solvent is discarded because the corresponding adducts would have an excess mass of +32 Da, which are absent in the MS spectra of Figure 4.3.

In the absence of ozone, (blue trace in Figure 4.3) only catechol (m/z 109) is detected as its monovalent ion corresponding to a general formula $C_6H_4(OH)O^-$. Numerous new product peaks are registered during the analysis of the oxidized film. Some of these products are the same observed during the ozonolysis of catechol at the air-water interface: glyoxylic acid (detected as glyoxylate ion with m/z 73), crotonic acid (m/z 85) or an isomer (e.g., 4-hydroxycrotonaldehyde), oxalic acid (m/z 89), maleinaldehydic acid (m/z 99), 4-hydroxy-2-butenoic acid (m/z 101), 5-oxo-3-pentenoic acid (m/z 113), maleic acid (m/z 115), glutaconic acid (m/z 129), and *cis,cis*-muconic acid (m/z 141). Because the origin of these species has been explained in detail previously,[17] the discussion below first summarizes those reactions (see Scheme 4.3) and then is focused on elucidating the pathways for the production of new molecules observed as anions at m/z 157, 175, 217, 249, 297, 311, and 325 amu (Figure 4.3).
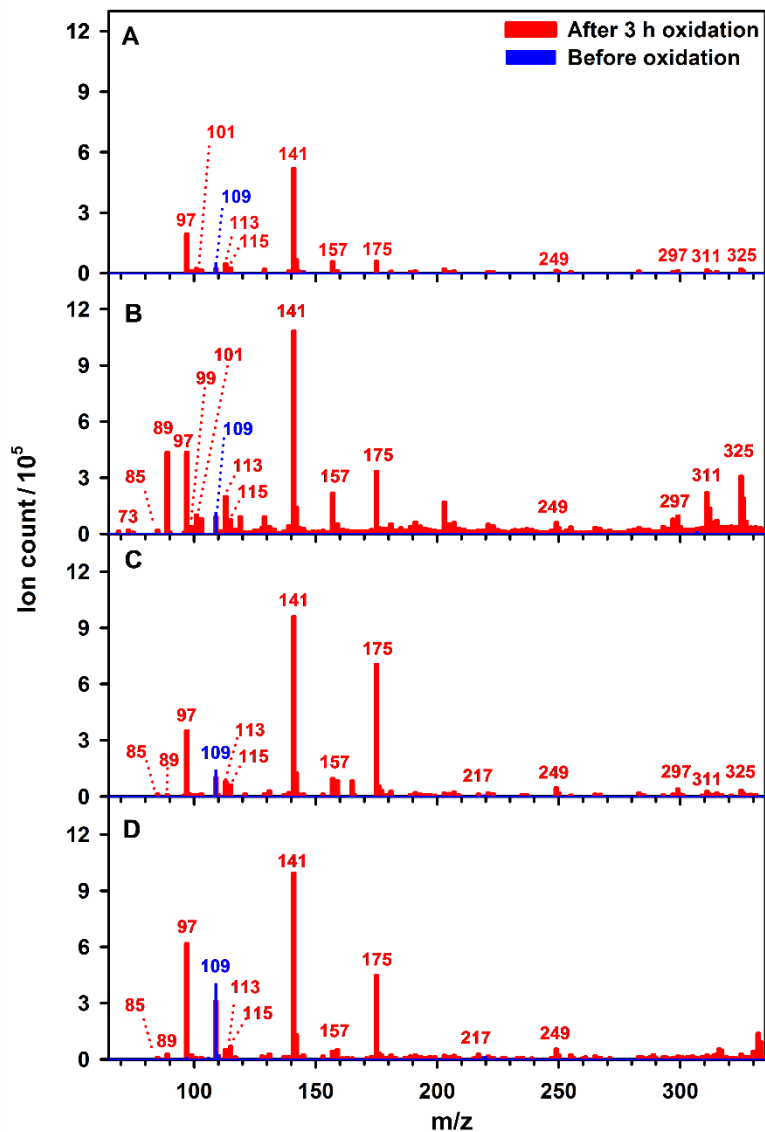
Figure 4.3. ESI MS of catechol thin films (blue trace) before and (red trace) after 3 hr exposure to 29.3 ppmv $O_3(g)$ at 71% RH extracted in (A) chloroform, (B) isopropanol, (C) acetone, and (D) acetonitrile.

A direct electrophilic attack of $O_3(g)$ to catechol[27] breaks the aromaticity between carbons 1 and 2. The sequential process starts with the formation of a primary ozonide precursor to a Criegee intermediate, which yields a hydroperoxide that is converted in *cis,cis*-muconic acid (*m/z* 141) and H_2O_2.[28] The primary direct ozonolysis product in

Scheme 4.3, *cis,cis*-muconic acid, is oxidized[29] to form maleinaldehydic acid (*m/z* 99), glyoxylic acid (*m/z* 73), maleic acid (*m/z* 115), and oxalic acid (*m/z* 89). Scheme 12.2 also summarizes the formation of 4-hydroxy-2-butenoic acid (*m/z* 101), 5-oxo-3-penteneoic acid (*m/z* 113), and glutaconic acid (*m/z* 129), resulting from Baeyer-Villiger (BV) oxidation of *cis,cis*-muconic acid.[17, 30]

Scheme 4.3. Products from catechol oxidation by O_3(g) and HO$^{\bullet}$ radical from Ref. [17]. The *m/z* values of species observed during ozonolysis at the air-solid interface are given in blue font.

glyoxylic acid
73

5-oxo-2-pentenoic acid
113

crotonic acid
85

oxalic acid
89

maleic acid
115

4-hydroxy-2-butenoic acid
101

glutaconic acid
129

O_3
H_2O_2
HO$^{\bullet}$

cis,cis-muconic acid
141

$\leftarrow H_2O + H_2O_2$

O_3

O_3 HO$^{\bullet}$

catechol
109

1,2,3- and 1,2,4-trihydroxybenzene

O_3/HO$^{\bullet}$

O_3 HO$^{\bullet}$

pentahydroxybenzene

tetrahydroxybenzenes
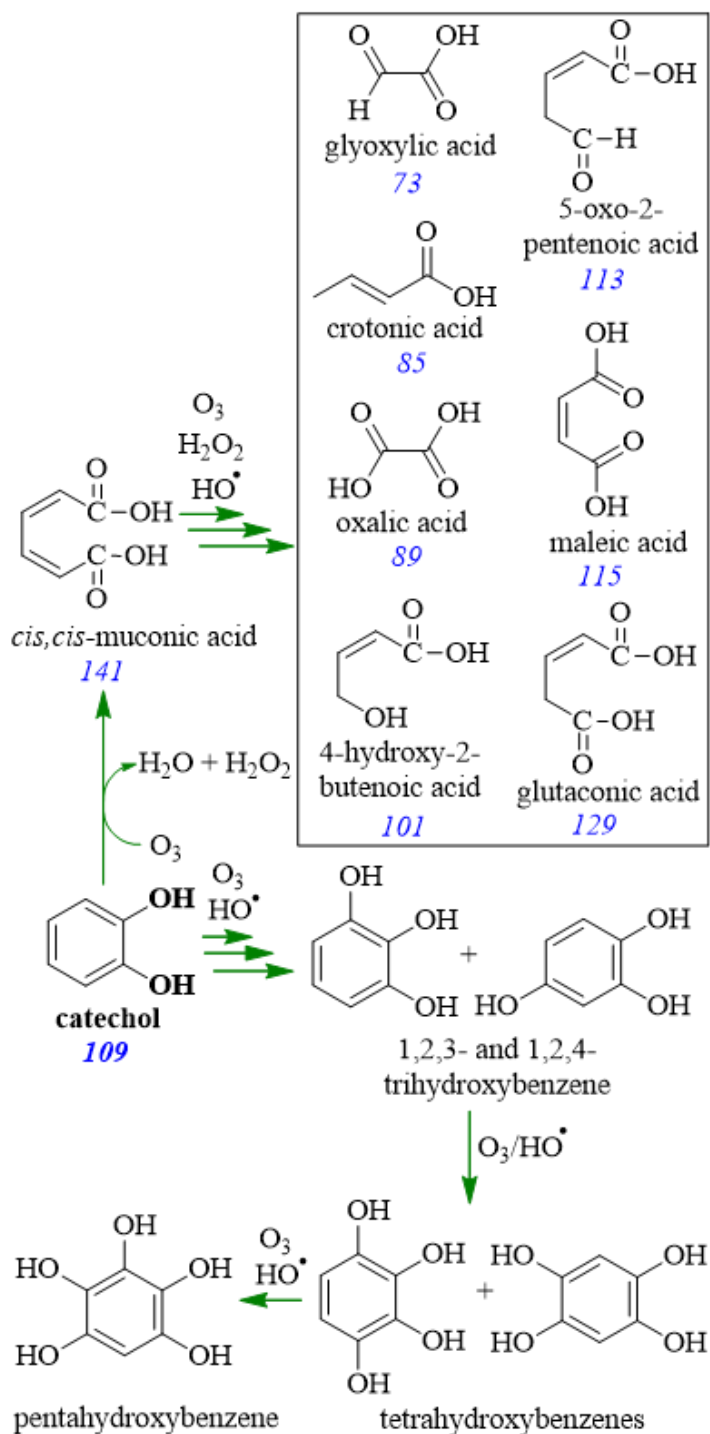
However, the appearance of new products with *m/z* 157 and 175 in Figure 4.3 has escaped detection in experiment at the air-water interface, [17] and requires new pathways describing their production. Thermodynamically favorable electron transfer between 1,2-dihydroxy-aromatics such as catechol and dissolved O_3 yields *o*-semiquinone and ozonide ($O_3^{\bullet-}$) radicals directly.[31] In the presence of water, the ozonide radical $O_3^{\bullet-}$ is quickly converted into $HO^{\bullet}$,[17] which contributes to the degradation of catechol with a rate constant $k_{HO^{\bullet}+\text{catechol}} = 1.1 \times 10^{10}\ M^{-1}s^{-1}$.[32] Similarly, produced polyhydroxylated species undergo reactions with $HO^{\bullet}$. In addition to electron transfer, the production of *o*-semiquinone radicals is also possible after $HO^{\bullet}$ attacks catechol forming trihydroxycyclohexadienyl radicals that undergo dehydration.[17]

Two channels for the production of the primary products from hydroxylation, 1,2,3- and 1,2,4-trihydroxybenzene, are possible.[17] The first channel results from the reaction of O_2 with 1,2,3- or 1,2,4-trihydroxycyclohexadienyl radicals intermediates that also release hydroperoxyl radicals ($HO_2^{\bullet}$).[17] The second reaction channel at the air-solid interface is the direct attack of O_3 to C_3 or C_6 of catechol that release $O_2(^1\Delta_g)$ en route to produce 1,2,3- and 1,2,4-trihydroxybenzene.[33-34] Once produced, trihydroxybenzenes can undergo similar reactions to those described above to sequentially form tetrahydroxybenzene and pentahydroxybenzene products (Scheme 4.3).[17]
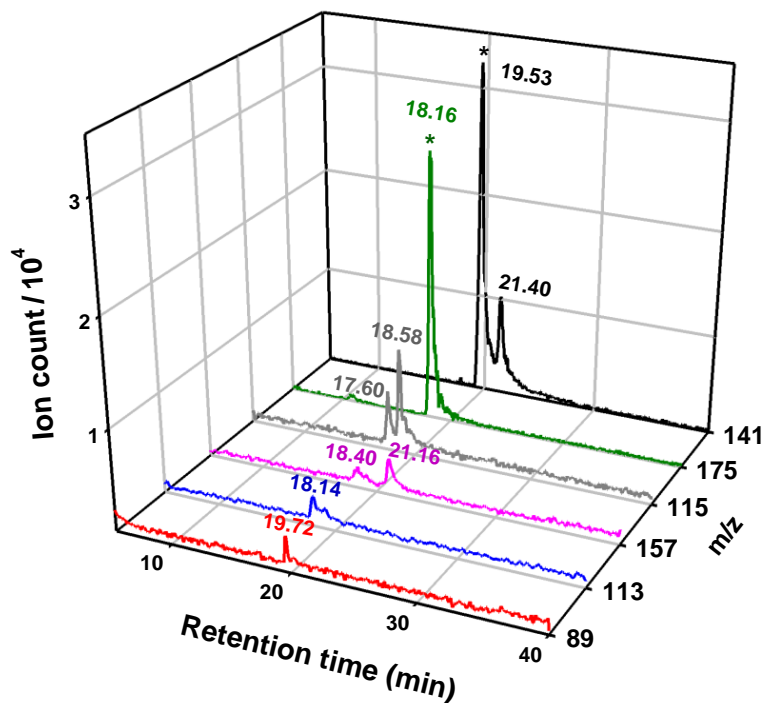
Figure 4.4. Extracted ion chromatograms during IC MS analysis of catechol film exposed to 29.3 ppmv $O_3(g)$ at 71% RH for 3 h. Peaks marked with an asterisk are scaled down 2-times.

The confirmation that several dicarboxylic acids are reaction products is obtained by IC MS analysis showing in Figure 4.4 the extracted ion chromatograms for the most abundant species with *m/z* 89, 113, 115, 141, 157, and 175. These species remained undetected during control experiments without ozone. The previously proposed mechanism of direct ozonolysis of catechol at the air-water interface is useful to guide the assignment of previously identified anionic products in Figures 4.3 and 4.4 as displayed in Scheme 4.3 and summarized above.[17]

Among the new molecules in Figures 4.3 and 4.4 are 2-hydroxyhexa-2,4-dienedioic acid and/or 3-hydroxyhexa-2,4-dienedioic acid (both *m/z* 157), and 2,4- or 3,4-dihydroxyhex-2-enedioic acid (*m/z* 175). These species can be explained based on the

indirect oxidation of catechol and its primary oxidation products. Direct ozonolysis of previously produced trihydroxybenzene precursors forms aliphatic species with neutral mass 158 Da such as 2-hydroxyhexa-2,4-dienedioic acid and 3-hydroxyhexa-2,4-dienedioic acid (Scheme 4.4). The hydration of a double bond from 2- or 3- hydroxy-muconic acids occurs in the presence of oxidants, freshly formed carboxylic acids, and water on the reactive surface. The mechanism of hydration of 2- and 3-hydroxy-*cis,cis*-muconic acid in Scheme 4.4 is acid catalyzed by the carboxylic acids formed during direct ozonolysis (Scheme 4.3), which facilitates the production of the species with *m/z* 175, such as 2,4- or 3,4-dihdroxyhex-2-enedioic acid. Alternatively, the two step addition of HO• to cis,cis-muconic acid (not included in Scheme 4.3) may result in the production of species with mass 176 Da. The proposed mechanism of indirect oxidation by in situ produced HO• at the air water interface[17] rationalizes the generation of *o*-semiquinone radicals precursor needed in several reactions conducting to the species in Figure 4.3. Radical coupling of semiquinone functionalities is involved in the production of condensed polyphenol rings. The *o*-semiquinone radicals have been shown to exist at the air-water interface[17] and should be able to undergo coupling reactions.

Dihydroxy-biphenyl isomeric species with *m/z* 217 in Figure 4.3 formed by coupling reactions can by represented by molecules such as [1,1'-biphenyl]-2,2',3,3'-tetraol, [1,1'-biphenyl]-3,3',4,4'-tetraol, [1,1'-biphenyl]-2,3,3',4'-tetraol (Scheme 4.5). The low intensity of this peak with *m/z* 217 indicates that reactive biphenyls are quickly consumed in the production of heavier coupling products. The related generation of crosslinks among two catechol rings in aqueous solutions has been identified during the catalytic oxidation with biomimetic iron-porphyrin by NMR spectroscopy.[35] In agreement with

previous studies,[35] the coupling reaction is proposed to preferentially form C-C bonds over the alternative aryloxy products with C-O-C groups.

Scheme 4.4. Proposed reactions producing species with *m/z* 157 and 175. The *m/z* values of species observed during ozonolysis at the air-solid interface are given in blue font.
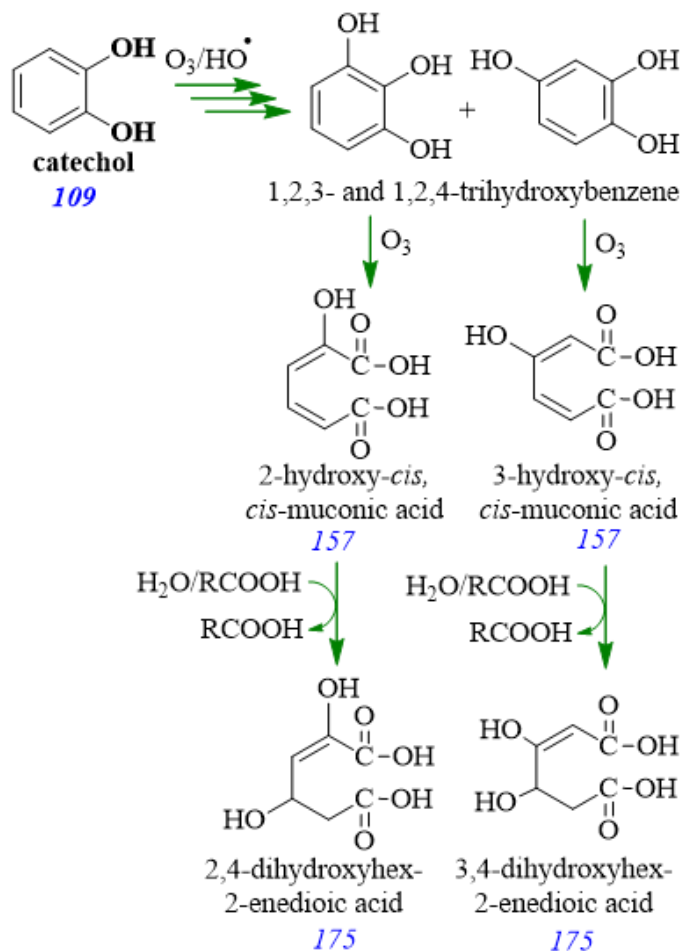
Figure 4.5 shows the UV-visible spectrum of catechol, 1,2,3- and 1,2,-4-trihydroxybenzene, which display $\pi \rightarrow \pi^*$ transitions at $\lambda = 274.1$, 267.1, and 290.2 nm, respectively. However these three polyphenols do not absorb visible light. Figure 4.5 also displays the spectrum of oxidized catechol.
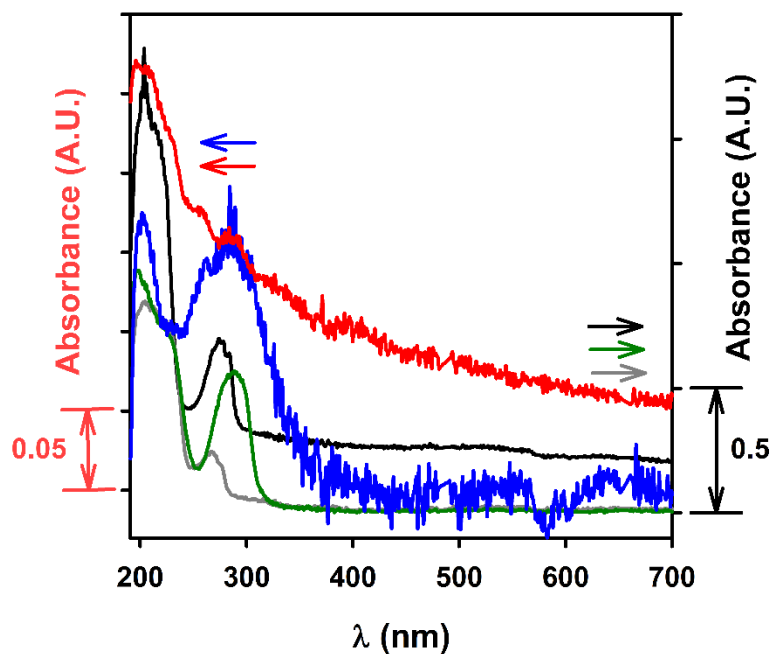
Figure 4.5. UV-visible absorption spectrum of thin films of (black) catechol, (grey) 1,2,3-trihydroxybenzene, (green) 1,2,4-trihydroxybenzene, (blue) *cis,cis*-muconic acid, and (red) oxidized catechol after 3 h under 23.6 ppmv $O_3(g)$ and 70 % RH.

Figure 4.5 also shows that *cis,cis*-muconic acid alone cannot explain the various transitions recorded. The peaks at $\lambda = 260$, 324, and 407 nm in the UV-visible absorption spectrum for the oxidized film are due to presence of crosslinks from dimers and trimers of catechol and trihydroxybenzenes.[36] Similarly, the peak at *m/z* 325 in the ESI MS of Figure 4.3 corresponds to a terphenyl arising from the combination of the semiquinone radicals of diphenyls and catechol (Scheme 4.5). Among the candidate products, three isomers displayed in Scheme 4.4 are [1,1':4',1"-terphenyl]-2',3,3',3",4,4"-hexaol, [1,1':4',1"-terphenyl]-2,2',2",3,3',3"-hexaol, and [1,1':4',1"-terphenyl]-2,2',3,3',3",4"-hexaol. The coupling of catechol monomer with formula mass 110 Da to form dimers (218 Da) and trimers (326 Da) displays the expected characteristic pattern with a consecutive weight loss of 2 Da per each new ring-carbon to ring-carbon bond.[37]

The species with *m/z* 249 in Figure 4.3 are assigned to a mixture of hexahydroxy-biphenyls such as [1,1'-biphenyl]-2,2',3,3',4,4'-hexaol, or any isomer such as those displayed in Scheme 4.5 to exemplify a few of them. Their production implies the combination of two semiquinone radicals from trihydroxybenzenes. Similarly, the production of tetra- and penta-hydroxybenzenes precursors of their respective semiquinone radicals results in the generation of [1,1'-biphenyl]-2,2',3,3',4,5,5',6,6'-nonaol or [1,1'-biphenyl]-2,2',3,3',4,4',5,5',6-nonaol, the candidate products in Scheme 4.6 with *m/z* 297. The production of 2,2',3',5,5',6,6'-heptahydroxy-[1,1'-biphenyl]-3,4-dione with *m/z* 311 is presented in Scheme 4.6 as the result of further oxidation of both species with *m/z* 297. Finally, it is possible to compare the efficiency of the four different solvents during the extraction procedure of oxidized films based on their increasing polarities: chloroform (1.04 D) < isopropanol (1.56 D) < acetone (2.88 D) < acetonitrile (3.93 D).[38] The hydroxyl group in isopropanol forms strong solvent solute interactions to favorably dissolve the polyhydroxylated biphenyl and terphenyl products. In general, the higher polarity solvents appear to be associated with an enhancement in the ion count of carboxylic acids in Figure 4.3.

Scheme 4.5. Proposed reactions producing tetrahydroxy-biphenyls and hexahydroxy-terphenyls. The *m/z* values of species observed during ozonolysis at the air-solid interface are given in blue font.
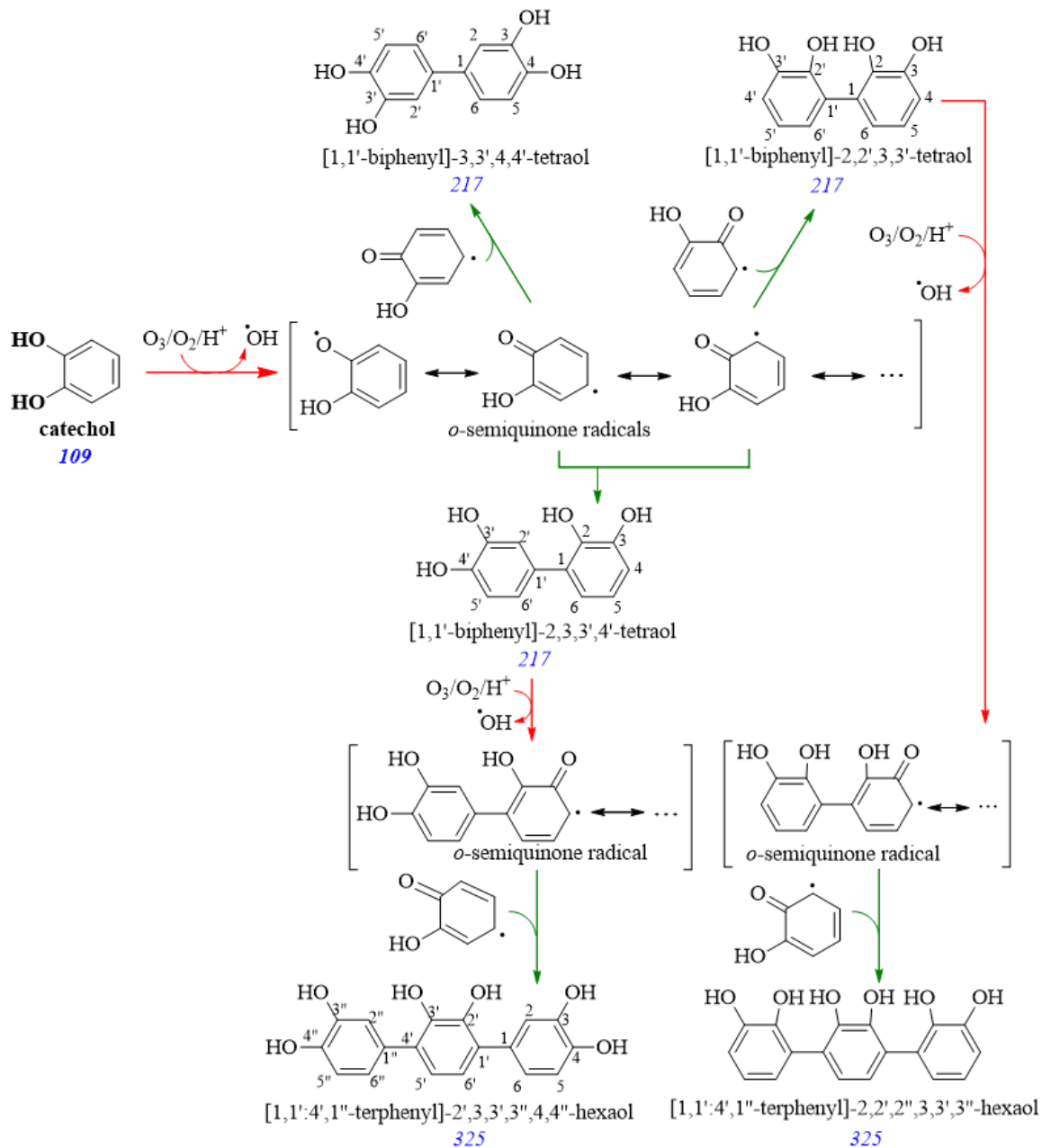
Scheme 4.6. Proposed reactions producing hexa- and nona-hydroxy-biphenyls. The *m/z* values of species observed during ozonolysis at the air-solid interface are given in blue font.
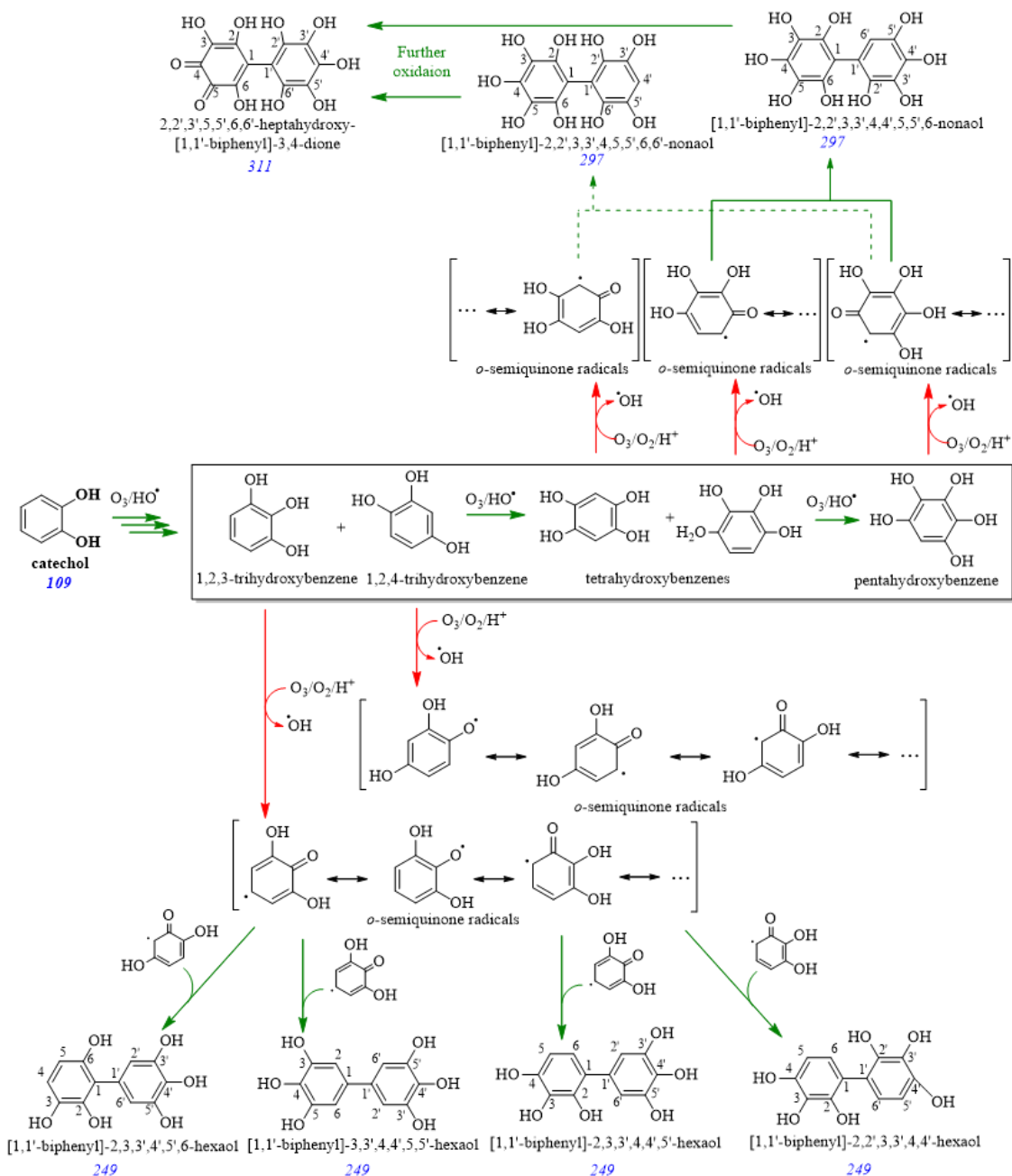
The lack of any major peak pairs in the FTIR spectra of oxidized films (Figure 4.2) with comparable intensity in the 1050-1260 cm^{-1} interval for C-O-C stretches, indicates

that oxyphenylene products are not the dominant coupling products during the ozonolysis of catechol at the air-solid interface.[39] More specifically, the absorbance for peaks located at ~1120 (a broad feature) and ~1220 cm^{-1}, common features for two aromatic rings bound to a common oxygen atom,[40] is very low, which demonstrates that if oxydiphenylenes are formed, they are much less abundant than biphenyl and triphenyl products. The previous analysis assumed that the combination of semiquinone radicals continuously produced during the reaction originates the products observed. However, a similar conclusion could be driven by considering the attack of the reactive radical species to abundant catechol molecules in the proximity of the solid film. Although Figures 4.3 and 4.4 display data for 71 % relative humidity, the relative abundance of the various products is generally enhanced as RH rises. Further studies are underway to characterize this dependence.

4.4.3 Effect of RH on γ_{O_3}

The loss of catechol and production of *cis,cis*-muconic acid during film oxidation under variable RH is displayed in Figure 4.6 for an $O_3(g)$ mixing ratio of 24.5 ppmv between 0 and 90 % RH. The presence of water alters the rate of reaction at the air-solid interface in agreement with related studies.[20] The normalized concentration of catechol to its initial value [catechol]/[catechol]$_0$ is obtained from the change of the CD line relative to its initial value CD$_0$ line in panel A of Figure 4.6. For this purpose, the loss of C(Ar)=C(Ar) stretching of catechol at 1363 cm^{-1} is used to fit a 3-parameters exponential decay equation $[\text{catechol}] = [catechol]_0 + a\, e^{-k_{catechol+O_3}\, t}$, where a is the pre-exponential constant and $k_{catechol+O_3}$ is the reaction rate constant.

Figure 4.6B shows the relative growth of [*cis,cis*-muconic acid] at time t relative to its final concentration [*cis,cis*-muconic acid]$_{inf}$ obtained from an extrapolation of the C=O stretching at 1680 cm^{-1} as $t \rightarrow \infty$, CD$_{inf}$ line. The fitted curves in Figure 4.6B correspond to 2-parameters exponential growth curves of the form [*cis,cis*-muconic acid]/ [*cis,cis*-muconic acid]$_{inf}$ $= 1 - e^{-k_{cs,cis\text{-muconic acid}}t}$, where the pseudo-first order rate constant $k_{cis,cis\text{-muconic acid}}$ and [*cis,cis*-muconic acid]$_{inf}$ are the fitted parameters. Both pseudo-first order rate constants, $k_{catechol+O_3}$ and $k_{cis,cis\text{-muconic acid}}$, at variable RH are available in Table S9 (Supporting Information).
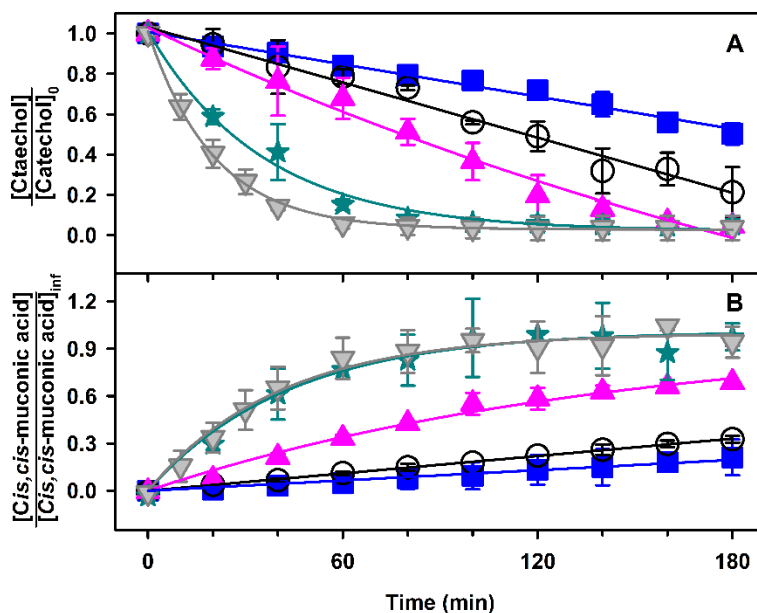
Figure 4.6. (A) Normalized loss of catechol (peak 2 in Figure 4.2) and (B) relative production of *cis,cis*-muconic acid (peak 4 in Figure 4.2) over 3 hr exposure to 24.5 ppmv O$_3$(g) at (blue squares) 0 %, (black open circles) 29 %, (pink triangles) 48 %, (teal stars) 72 %, and (grey triangles) 90% RH.

The data in Figure 4.6, for [O$_3$(g)] $= 6 \times 10^{14}$ molecules cm^{-3} is within the low concentration range that shows a linear dependence of the rate constant with [O$_3$(g)] in

the Langmuir-Hinshelwood mechanism.[25] Therefore, in the presence of water, the ozonolysis of catechol at the air-solid interface (Figure 4.6) follows a first order kinetic in both ozone and catechol concentrations.[41] A possible explanation for the enhanced reaction rates observed in Figure 4.3A for higher RH is related the orientation of catechol's O-H groups toward the interface. These O-H groups provide sites for water adsorption to the film that facilitates the attack to the vicinal C_1-C_2 bond resulting in the production of *cis,cis*-muconic acid (Scheme 4.3). Similarly, the reaction forming the C=O groups of *cis,cis*-muconic acid becomes more important with increasing RH (Figure 4.6B). For the two highest RH tested of 71 and 90 %, the production of *cis,cis* muconic acid levels off after 1.5 hr, conditions under which other carboxylic acids such as glyoxylic and maleic acids are observed by ESI MS analysis. Overall, these results imply that water facilitates the formation of carboxylic acids during the heterogeneous oxidation of catechol. Once formed, carboxylic acids can act as a source of protons for acid catalysis, which reaches a converging maximum above a threshold of ~70 % RH.

The reactive uptake coefficient of $O_3(g)$ by catechol, γ_{O_3}, is calculated based on equation 4.1:[42]

$$\gamma_{O_3} = \frac{4RT}{v_{O_3}} \delta \frac{k_{catechol+O_3}}{P_{O_3}} [\text{catechol}] \qquad \text{(Eq. 4.1)}$$

and plotted in Figure 4.7. This equation accounts for the fraction of reactive collisions relative to the total rate of collisions obtained from kinetic theory of gases. In equation 4.1, $R = 8.314$ J K^{-1} mol^{-1} is the gas constant, $v_{O_3} = 394$ m s^{-1} is the mean thermal velocity of $O_3(g)$ at T = 298 K, $k_{catechol+O_3}(s^{-1})$ are the measured values (Table S9), the partial

pressure of ozone $P_{O_3}(Pa)$ is known from UV absorption spectroscopy, the effective film thickness $\delta = 8.4 \times 10^{-8}$ m is estimated for a uniform surface coverage of catechol (8.20×10^{17} molecules) deposited over the IR-transparent crystal of area $S_A = 1.32 \times 10^{-4}$ m^2 , and [catechol] = 1.217×10^4 molecules m^{-3} based on catechol density of 1340 kg m^{-3} and formula mass of 110.1×10^{-3} kg mol^{-1}.
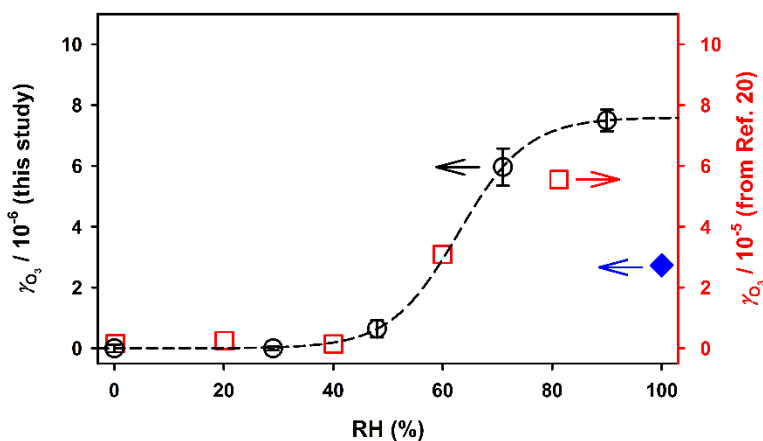
Figure 4.7. Reactive uptake coefficient of $O_3(g)$ by catechol thin film at variable RH. Measured (black circle) in this study for 24.5 ppmv $O_3(g)$ and (red square), in Ref. [20] for 4 ppmv $O_3(g)$, and (solid blue diamond) at the air-water interface in Ref. [17].

The large flow of $O_3(g)$ into the reactor favors a turbulent flow, which together with the very small reaction probabilities measured ($<10^{-5}$) indicate that the diffusion of $O_3(g)$ to the surface is not a limiting factor in this reactor. For comparison, Figure 4.7 also includes reactive uptake coefficients estimated at the air-water interface[17] (expressed as RH = 100 %) and reported in the literature[20] under similar conditions. Remarkably the trends of both studies in Figure 4.7 (black circles and red squares) match closely each other but their vertical scale is shifted an order of magnitude clearly reflecting a difference in the calculation of γ_{O_3}. For example, at 90 % RH the maximum $\gamma_{O_3} = (7.49 \pm$

0.35) $\times$ 10^{-6} measured for 24.5 ppmv O$_3$(g) in this study is 7.5-times smaller than the value from Ref. 20 (5.6 $\times$ 10^{-5} for 4 ppm O$_3$(g) at RH = 81 %), but only 2.7-times larger than the one estimated at the air-water interface.[17] In principle, this comparison suggests a smaller upper limit for the uptake coefficient of ozone by catechol to be used for modeling the behavior of the emissions from combustion and biomass burning under humid conditions. However, considering that γ_{O_3} should vary with [O$_3$(g)] following a Langmuir-Hinshelwood dependence from $k_{catechol+O_3}$, the reported discrepancy for γ_{O_3} could simply reflect the ~6-times ratio in concentrations used in both studies. In order to gain further insight about this system, future experimental work should aim to determine the Langmuir Hinshelwood dependence of the reaction rate constant on [O$_3$(g)].

4.5 Atmospheric Implications and Conclusions

This work shows how catechol, a model compound emitted during biomass burning and combustion emissions, is used to study the heterogeneous processing of the oxygenated fraction of aromatic hydrocarbons under variable RH. Similar chemical processing is expected for other aromatic surfaces in contact with the atmosphere (e.g., urban films, aerosols, etc.). After primary oxidation of aromatic surfaces by HO$^\bullet$, the sequential production of 1-hydroxy- and 1,2-dihydroxy-substituted aromatics should continue in a similar fashion to the one described in this work.

In this experimental system, ozone driven oxidation of catechol in the presence of water vapor leads to the generation of o-semiquinone radicals and secondary oxidants, including HO$^\bullet$, HO$_2^\bullet$, and H$_2$O$_2$, which further promote the aging of organic material.

Similar processes could occur in atmospheric aerosols generated by combustion and biomass burning. The products identified in this study demonstrate that heterogeneous reactions can provide oxidants and radicals to the atmosphere.[17] The competitive production of polyhydroxylated biphenyls and terphenyls proceeds at the air-solid interface together with the cleavage of the C_1-C_2 bond of catechol by ozonolysis. The absorptivity of model oxidized organic material representing these emissions becomes pronounced at $\lambda > 290$ nm. In addition, the gradual increase in absorptivity with decreasing wavelength, when transitioning from the visible to the UV, directly resembles the behavior of atmospheric brown carbon.[43-46] The prompt oxidation of aromatic species by abundant $HO^{\bullet}$ generates polyphenols that are prone to undergo direct ozonolysis to form carboxylic acids as a competitive aging mechanism at the air-solid interface in the presence of water molecules. The products detected in this study are consistent with the charge transfer complexes recently reported in water-extracted ambient particulate matter collected in Athens, Georgia.[47] Even in dry desert environments (e.g. Mojave and Great Basin Desert), where the range of RH is between ~15 % and ~72 % (comparable to the global-mean RH = 77 %),[48] γ_{O_3} will depend strongly on humidity as described above.

For particles of surface A with a mean diameter of 100-nm covered by catechol molecules, the reaction rate with $[O_3(g)]$ $= 2.46 \times 10^{12}$ molecules cm^{-3} relative to that with $[OH(g)] = 1.6 \times 10^6$ molecules cm^{-3} is:[49]

$$(\gamma_{O_3}[O_3(g)]\, v_{O_3} A/4)/(\gamma_{OH}[OH(g)]\, v_{OH} A/4) = 6.9 \qquad \text{(Eq. 4.2)}$$

where room temperature is assumed, γ_{O_3} = 7.49 × 10^{-6} for RH = 90 %, γ_{OH} = 1 is employed as an upper limit, and the mean thermal velocity of OH radicals is v_{OH} = 661 $m\ s^{-1}$. Therefore, ozonolysis may be at least 7-times faster than the loss of catechol by HO$^{\bullet}$ during interfacial reactions. Moreover, the heterogeneous processing of hydroxylated aromatics by this mechanism is expected to become important in the absence of HO$^{\bullet}$ during nighttime.

Overall, pollution plumes with tropospheric residence time of ~1 week against deposition,[50] contribute to the oxidative aging of aromatics during transport. These aging mechanisms produce low volatility species[51] such as oxalic acid and low molecular weight oxocarboxylic and unsaturated dicarboxylic acids found in SOA.[9, 11] Monitoring reactions occurring at surfaces contributes to enhance the understanding of key heterogeneous processes,[52-53] while contributing reaction mechanisms to explain atmospheric observations. Heterogeneous reactions provide a connection between the processing of combustion and biomass burning emissions and the ubiquitous generation of brown carbon species[54] resulting from pathways not yet considered in atmospheric models.

4.6 Acknowledgement

4.7 References

1. Boucher, O.; Randall, D.; Artaxo, P.; Bretherton, C.; Feingold, G.; Forster, P.; Kerminen, V.-M.; Kondo, Y.; Liao, H.; Lohmann, U.; Rasch, P.; Satheesh, S. K.; Sherwood, S.; Stevens, B.; X.Y. Zhang, X. Y. Clouds and Aerosols. In *Climate Change 2013: The Physical Science Basis. Contribution of Working Group I to the Fifth Assessment Report of the Intergovernmental Panel on Climate Change*, Stocker, T. F.;

Qin, D.; Plattner, G.-K.; Tignor, M.; Allen, S. K.; Boschung, J.; Nauels, A.; Xia, Y.; Bex, V.; Midgley, P. M., Eds. Cambridge University Press: Cambridge, United Kingdom and New York, NY, USA, 2013.

2. Hallquist, M.; Wenger, J. C.; Baltensperger, U.; Rudich, Y.; Simpson, D.; Claeys, M.; Dommen, J.; Donahue, N. M.; George, C.; Goldstein, A. H.; Hamilton, J. F.; Herrmann, H.; Hoffmann, T.; Iinuma, Y.; Jang, M.; Jenkin, M. E.; Jimenez, J. L.; Kiendler-Scharr, A.; Maenhaut, W.; McFiggans, G.; Mentel, T. F.; Monod, A.; Prevot, A. S. H.; Seinfeld, J. H.; Surratt, J. D.; Szmigielski, R.; Wildt, J. The Formation, Properties and Impact of Secondary Organic Aerosol: Current and Emerging Issues. *Atmos. Chem. Phys.* **2009**, *9*, 5155-5236.

3. Finlayson-Pitts, B. J. Reactions at Surfaces in the Atmosphere: Integration of Experiments and Theory as Necessary (but Not Necessarily Sufficient) for Predicting the Physical Chemistry of Aerosols. *Phys. Chem. Chem. Phys.* **2009**, *11*, 7760-7779.

4. Rudich, Y.; Donahue, N. M.; Mentel, T. F. Aging of Organic Aerosol: Bridging the Gap between Laboratory and Field Studies. *Annu. Rev. Phys. Chem.* **2007**, *58*, 321-352.

5. Mkoma, S. L.; Kawamura, K. Molecular Composition of Dicarboxylic Acids, Ketocarboxylic Acids, α-Dicarbonyls and Fatty Acids in Atmospheric Aerosols from Tanzania, East Africa During Wet and Dry Seasons. *Atmos. Chem. Phys.* **2013**, *13*, 2235-2251.

6. Kawamura, K.; Tachibana, E.; Okuzawa, K.; Aggarwal, S. G.; Kanaya, Y.; Wang, Z. F. High Abundances of Water-Soluble Dicarboxylic Acids, Ketocarboxylic Acids and α-Dicarbonyls in the Mountaintop Aerosols over the North China Plain During Wheat Burning Season. *Atmos. Chem. Phys.* **2013**, *13*, 8285-8302.

7. Kundu, S.; Kawamura, K.; Andreae, T. W.; Hoffer, A.; Andreae, M. O. Molecular Distributions of Dicarboxylic Acids, Ketocarboxylic Acids and α-Dicarbonyls in Biomass Burning Aerosols: Implications for Photochemical Production and Degradation in Smoke Layers. *Atmos. Chem. Phys.* **2010**, *10*, 2209-2225.

8. Yang, L.; Nguyen, D. M.; Jia, S.; Reid, J. S.; Yu, L. E. Impacts of Biomass Burning Smoke on the Distributions and Concentrations of C_2–C_5 Dicarboxylic Acids and Dicarboxylates in a Tropical Urban Environment. *Atmos. Environ.* **2013**, *78*, 211-218.

9. Veres, P.; Roberts, J. M.; Burling, I. R.; Warneke, C.; de Gouw, J.; Yokelson, R. J. Measurements of Gas-Phase Inorganic and Organic Acids from Biomass Fires by Negative-Ion Proton-Transfer Chemical-Ionization Mass Spectrometry. *J. Geophys. Res.-Atmos.* **2010**, *115*, D23302

10. Adounkpe, J.; Aina, M.; Mama, D.; Sinsin, B. Gas Chromatography Mass Spectrometry Identification of Labile Radicals Formed During Pyrolysis of Catechol, Hydroquinone, and Phenol through Neutral Pyrolysis Product Mass Analysis. *ISRN Environ. Chem.* **2013**, *2013*, Article ID 930573, 1-8.

11. Desyaterik, Y.; Sun, Y.; Shen, X.; Lee, T.; Wang, X.; Wang, T.; Collett, J. L. Speciation of "Brown" Carbon in Cloud Water Impacted by Agricultural Biomass Burning in Eastern China. *J. Geophys. Res.-Atmos.* **2013**, *118*, 7389-7399.

12. Dharaiya, N.; Bahadur, P. Phenol Induced Growth in Triton X-100 Micelles: Effect of pH and Phenols' Hydrophobicity. *Colloid Surf. A* **2012**, *410*, 81-90.

13. Latif, M. T.; Brimblecombe, P. Surfactants in Atmospheric Aerosols. *Environ. Sci. Technol.* **2004**, *38*, 6501-6506.

14. Zein, A. E.; Coeur, C.; Obeid, E.; Lauraguais, A.; Fagniez, T. Reaction Kinetics of Catechol (1,2-Benzenediol) and Guaiacol (2-Methoxyphenol) with Ozone. *J. Phys. Chem. A* **2015**, *119*, 6759-6765.

15. Guzman, M. I.; Athalye, R. R.; Rodriguez, J. M. Concentration Effects and Ion Properties Controlling the Fractionation of Halides During Aerosol Formation. *J. Phys. Chem. A* **2012**, *116*, 5428-5435.

16. Pillar, E. A.; Guzman, M. I.; Rodriguez, J. M. Conversion of Iodide to Hypoiodous Acid and Iodine in Aqueous Microdroplets Exposed to Ozone. *Environ. Sci. Technol.* **2013**, *47*, 10971-10979.

17. Pillar, E. A.; Camm, R., C.; Guzman, M. I. Catechol Oxidation by Ozone and Hydroxyl Radicals at the Air–Water Interface. *Environ. Sci. Technol.* **2014**, *48*, 14352-14360.

18. Guzman, M. I.; Pillar, E. A. Ozonation of Aromatic Hydrocarbon Probes at the Air-Water Interface In *248th ACS National Meeting & Exposition*, American Chemical Society: San Francisco, CA, 2014; pp COLL-93.

19. Woodill, L. A.; O'Neill, E. M.; Hinrichs, R. Z. Impacts of Surface Adsorbed Catechol on Tropospheric Aerosol Surrogates: Heterogeneous Ozonolysis and Its Effects on Water Uptake. *J. Phys. Chem. A* **2013**, *117*, 5620-5631.

20. Barnum, T. J.; Medeiros, N.; Hinrichs, R. Z. Condensed-Phase Versus Gas-Phase Ozonolysis of Catechol: A Combined Experimental and Theoretical Study. *Atmos. Environ.* **2012**, *55*, 98-106.

21. Ofner, J.; Krüger, H. U.; Zetzsch, C. Time Resolved Infrared Spectroscopy of Formation and Processing of Secondary Organic Aerosol. *Z. Phys. Chem.* **2010**, *224*, 1171-1183.

22. Sander, S. P.; Abbatt, J.; Barker, J. R.; Burkholder, J. B.; Friedl, R. R.; Golden, D. M.; Huie, R. E.; Kolb, C. E.; Kurylo, M. J.; Moortgat, G. K.; Orkin, V. L.; Wine, P. H. Chemical Kinetics and Photochemical Data for Use in Atmospheric Studies: Evaluation Number 17 Jet Propulsion Laboratory, California Institute of Technology, Pasadena, CA, http://jpldataeval.jpl.nasa.gov: 2011 (accessed June 7, 2015).

23. Zhou, R.; Guzman, M. I. Co$_2$ Reduction under Periodic Illumination of Zns. *J. Phys. Chem. C* **2014**, *118*, 11649-11656.

24. Han, S.-q.; Zhang, M.; Zhao, C.-s.; Lu, X.-q.; Ran, L.; Han, M.; Li, P.-y.; Li, X.-j. Differences in Ozone Photochemical Characteristics between the Megacity Tianjin and Its Rural Surroundings. *Atmos. Environ.* **2013**, *79*, 209-216.

25. Pillar, E. A.; Guzman, M. I. *Ozonolysis of Catechol at the Gas-Solid Interface*, 250^{t}h ACS National Meeting & Exposition, Boston, MA, August 16-20, 2015; American Chemical Society, Boston, MA, 2015; p CODEN:69TVIX.

26. Sŏhár, P.; Varsányi, G. Y. An IR Spectroscopic Study of Muconate Isomers. *J. Mol. Struct.* **1968**, *1*, 437-448.

27. Mvula, E.; von Sonntag, C. Ozonolysis of Phenols in Aqueous Solution. *Org. Biomol. Chem.* **2003**, *1*, 1749-1756.

28. Bailey, P. S. *Ozonation in Organic Chemistry*; Academic Press: New York, 1982; Vol. 2. p 272.

29. Ramseier, M. K.; von Gunten, U. Mechanisms of Phenol Ozonation-Kinetics of Formation of Primary and Secondary Reaction Products. *Ozone Sci. Eng.* **2009**, *31*, 201-215.

30. ten Brink, G. J.; Arends, I. W. C. E.; Sheldon, R. A. The Baeyer−Villiger Reaction: New Developments toward Greener Procedures. *Chem. Rev.* **2004**, *104*, 4105-4124.

31. Flyunt, R.; Leitzke, A.; Mark, G.; Mvula, E.; Reisz, E.; Schick, R.; von Sonntag, C. Determination of $^{\bullet}$OH, O$_2^{\bullet-}$, and Hydroperoxide Yields in Ozone Reactions in Aqueous Solution. *J. Phys. Chem. B* **2003**, *107*, 7242-7253.

32. Buxton, G. V.; Greenstock, C. L.; Helman, W. P.; Ross, A. B. Critical Review of Rate Constants for Reactions of Hydrated Electrons, Hydrogen Atoms and Hydroxyl Radicals ($^{\bullet}$OH/$^{\bullet}$O$^-$) in Aqueous Solution. *J. Phys. Chem. Ref. Data* **1988**, *17*, 513-886.

33. von Sonntag, C.; von Gunten, U. *Chemistry of Ozone in Water and Wastewater Treatment: From Basic Principles to Applications*; IWA Publishing, 2012, p 302.

34. Iwaki, R.; Kamiya, I. Chemiluminescent Reaction between Polyphenols and Ozone in Acetic Acid. *B. Chem. Soc. Jpn.* **1969**, *42*, 855-863.

35. Šmejkalová, D.; Conte, P.; Piccolo, A. Structural Characterization of Isomeric Dimers from the Oxidative Oligomerization of Catechol with a Biomimetic Catalyst. *Biomacromolecules* **2007**, *8*, 737-743.

36. Kandaswami, C.; Subra Rao, P. V.; Nair, P. M.; Vaidyanathan, C. S. Oxidation of Catechol in Higher Plants. I. Enzymic Conversion of Catechol to 3,4,3',4'-Tetrahydroxydiphenyl. *Can. J. Biochem.* **1969**, *47*, 375-377.

37. Yang, J.; Cohen Stuart, M. A.; Kamperman, M. Jack of All Trades: Versatile Catechol Crosslinking Mechanisms. *Chem. Soc. Rev.* **2014**, *43*, 8271-8298.

38. *CRC Handbook of Chemistry and Physics*, 93rd ed.; CRC Press/Taylor and Francis: Boca Raton, Fl., **2013**, p 2664.

39. Sun, X.; Bai, R.; Zhang, Y.; Wang, Q.; Fan, X.; Yuan, J.; Cui, L.; Wang, P. Laccase-Catalyzed Oxidative Polymerization of Phenolic Compounds. *Appl Biochem Biotechnol* **2013**, *171*, 1673-1680.

40. Mita, N.; Tawaki, S.-i.; Uyama, H.; Kobayashi, S. Laccase-Catalyzed Oxidative Polymerization of Phenols. *Macromolec. Biosci.* **2003**, *3*, 253-257.

41. Gurol, M. D.; Nekouinaini, S. Kinetic Behavior of Ozone in Aqueous Solutions of Substituted Phenols. *Ind. Eng. Chem. Fund.* **1984**, *23*, 54-60.

42. Hung, H.-M.; Ariya, P. Oxidation of Oleic Acid and Oleic Acid/Sodium Chloride(*aq*) Mixture Droplets with Ozone: Changes of Hygroscopicity and Role of Secondary Reactions. *J. Phys. Chem. A* **2007**, *111*, 620-632.

43. Rincón, A. G.; Guzmán, M. I.; Hoffmann, M. R.; Colussi, A. J. Optical Absorptivity Versus Molecular Composition of Model Organic Aerosol Matter. *J. Phys. Chem. A* **2009**, *113*, 10512-10520.

44. Rincón, A. G.; Guzmán, M. I.; Hoffmann, M. R.; Colussi, A. J. Thermochromism of Model Organic Aerosol Matter. *J. Phys. Chem. Lett.* **2010**, *1*, 368-373.

45. Saleh, R.; Robinson, E. S.; Tkacik, D. S.; Ahern, A. T.; Liu, S.; Aiken, A. C.; Sullivan, R. C.; Presto, A. A.; Dubey, M. K.; Yokelson, R. J.; Donahue, N. M.; Robinson, A. L. Brownness of Organics in Aerosols from Biomass Burning Linked to Their Black Carbon Content. *Nat. Geosci.* **2014**, *7*, 647-650.

46. Hecobian, A.; Zhang, X.; Zheng, M.; Frank, N.; Edgerton, E. S.; Weber, R. J. Water-Soluble Organic Aerosol Material and the Light-Absorption Characteristics of Aqueous Extracts Measured over the Southeastern United States. *Atmos. Chem. Phys.* **2010**, *10*, 5965-5977.

47. Phillips, S. M.; Smith, G. D. Light Absorption by Charge Transfer Complexes in Brown Carbon Aerosols. *Environ. Sci. Technol. Lett.* **2014**, *1*, 382-386.

48. Hartmann, D. L. *Global Physical Climatology*; Academic Press, 1994, p 411.

49. George, I. J.; Abbatt, J. P. D. Heterogeneous Oxidation of Atmospheric Aerosol Particles by Gas-Phase Radicals. *Nat. Chem.* **2010**, *2*, 713-722.

50. Seinfeld, J. H.; Pandis, S. N. *Atmospheric Chemistry and Physics: From Air Pollution to Climate Change*, 2nd ed.; Wiley: New York, 2006, p 1232.

51. Saleh, R.; Hennigan, C. J.; McMeeking, G. R.; Chuang, W. K.; Robinson, E. S.; Coe, H.; Donahue, N. M.; Robinson, A. L. Absorptivity of Brown Carbon in Fresh and Photo-Chemically Aged Biomass-Burning Emissions. *Atmos. Chem. Phys.* **2013**, *13*, 7683-7693.

52. Dubowski, Y.; Vieceli, J.; Tobias, D. J.; Gomez, A.; Lin, A.; Nizkorodov, S. A.; McIntire, T. M.; Finlayson-Pitts, B. J. Interaction of Gas-Phase Ozone at 296 K with Unsaturated Self-Assembled Monolayers: A New Look at an Old System. *J. Phys. Chem. A* **2004**, *108*, 10473-10485.

53. George, C.; Ammann, M.; D'Anna, B.; Donaldson, D. J.; Nizkorodov, S. A. Heterogeneous Photochemistry in the Atmosphere. *Chem. Rev.* **2015**, *115*, 4218-4258.

54. Laskin, A.; Laskin, J.; Nizkorodov, S. A. Chemistry of Atmospheric Brown Carbon. *Chem. Rev.* **2015**, *115*, 4335-4382.

4.8. Supporting Information for Heterogeneous Oxidation of Catechol

Table S1. Vibrational assignment for catechol film

Wavenumber (cm^{-1})	Intensity^a	Assignment^b
3450	s	ν(O-H)
3323	s	ν(O-H)
3051	m	ν(C-H)
1618, 1595	m, m	ν(C=C)
1512	s	ν(C=C)
1471	s	ν(C=C)
1363	s	ν(C=C)
1255	s	δ(C-H)
1190	s	δ(O-H)
1095	s	δ(C-H)
1041	s	δ(C-H)
918	w	ρ(C-H)
849	m	ρ(C-H)
769	s	ν(C=C)
741	s	ρ(C-H)

^{a} w = weak; m = medium; s = strong.
^{b} ν = stretching; δ = in plane bending; ρ = out of plane bending.
All assignments are based on theoretical and experimental studies.[1]

Table S2. Vibrational assignments for oxidized film

Wavenumber (cm^{-1})	Intensity[a]	Assignment[b]
3393	m	ν(O-H)
3100 - 2500	w,b	ν(O-H)
1737	sh	ν(C=O)
1694	sh	ν(C=O)
1679	s	ν(C=O)
1632	w	ν(C=C)
1594	s	ν(C=C)
1520	w	ν(C=C)
1408	m	δ(C=C)
1355,1315	m, m	δ(C=C-H)
1262, 1197	s, s	ν(C-O)
1216	w	δ(C=C-H)
1118	w	ν(C-O)
835	m	ρ(C=C-H)

[a] w = weak; m = medium; s = strong; sh = shoulder; b = broad.
[b] ν = stretching; δ = in plane bending; ρ = out of plane bending.

Table S3. Vibrational assignment of *cis,cis*-muconic acid

Wavenumber (cm^{-1})	Intensity[a]	Assignment[b]
3300 - 2200	m, br	ν(O-H)
1680	s	ν(C=O)
1635	sh	ν(C=C)
1591	s	ν(C=C)
1408	m	δ(C=C)
1355, 1316	m, m	δ(C=C-H)
1258, 1197	s, s	ν(C-O)
914	w	ρ(O-H)

[a] w = weak; m = medium; s = strong; sh = shoulder; br = broad.
[b] ν = stretching; δ = in plane bending; ρ = out of plane bending.
Assignments based on experimental results.[2]

Table S4. Vibrational assignment of maleic acid

Wavenumber (cm⁻¹)	Intensity[a]	Assignment[b]
3059	m	ν(C-H)
3200 - 2100	m, b	ν(O-H)
1708	s	ν(C=O)
1637	w	ν(C=C)
1579	s	ν(C=C)
1461	m	δ(C-O-H)
1436	m	δ(C=C-H)
1264	s	ν(C-O)
1221	m	δ(C=C-H)
950	w	ν(C=C)
871	m	ρ(C-H)

[a] w = weak; m = medium; s = strong; b = broad.
[b] ν = stretching; δ = in plane bending; ρ = out of plane bending.
Assignments based on experimental and theoretical results.[3]

Table S5. Vibrational assignment of glyoxylic acid.

Wavenumber (cm^{-1})	Intensity^a	Assignment^b
3700-2250	vs, br	ν(O-H)
1727	vs	ν(C=O)
1630	m	ν_{as}(O-C-O)
1231	s	ν(C-O) + δ(O-H)
1087, 1043	s, vs	δ(C-C-H)

^{a} w = weak; m = medium; s = strong; br = broad.
^{b} ν = stretching; δ = in plane bending; ρ = out of plane bending.
Assignments based on experimental results.[4]

Table S6. Vibrational assignment of oxalic acid

Wavenumber (cm^{-1})	Intensity^a	Assignment^b
3458	vs	ν(O-H)
1684	vs	ν_{as}(O-C-O)
1251	vs	ν_s(C-O) +
		δ(O-C-O)
1133	m	ν(C-OH)
725	s	δ(O-C-O)

^{a} w = weak; m = medium; s = strong.
^{b} ν = stretching; δ = in plane bending; ρ = out of plane bending.
Assignments based on experimental results.[4]

Table S7. Vibrational assignment of 1,2,3-trihydroxybenzene

Wavenumber (cm^{-1})	Intensity^a	Assignment^b
3375	s	ν(O-H)
3245	s	ν(O-H)
3056	w	ν(C-H)
1633	sh	ν(C=C)
1622	s	ν(C=C)
1525	s	ν(C=C)
1488	s	δ(C-O-H)
1363	s	δ(O-H)
1290	s	δ(C-O-H)
1243	s	δ(C-H)
1190	s	δ(C=C-H)
1061	m	ν(C=C)
1004	s	ρ (C=C-H)
847	w	ρ (C=C-H)
830	w	ρ(C=C-O)
764	m	ν(C=C)
805	s	ρ(=C-O-H)

^{a} w = weak; m = medium; s = strong; sh = shoulder.
^{b} ν = stretching; δ = in plane bending; ρ = out of plane bending.
Assignments based on experimental and theoretical results.[5]

Table S8. Vibrational assignment of 1,2,4-trihydroxybenzene

Wavenumber (cm⁻¹)	Intensity[a]	Assignment[b]
3256	s	ν(O-H)
1622	m	ν(C=C)
1577	sh	ν(C=C)
1514	sh	ν(C=C)
1386	s	δ(O-H)
1300	s	δ(C-O-H)
839	m	δ(C-O-H)
790	s	ρ(C-H)

[a] w = weak; m = medium; s = strong; sh = shoulder.
[b] ν = stretching; δ = in plane bending; ρ = out of plane bending.
Assignments based on experimental and theoretical results.[6]

Table S9. Pseudo-first order rate constants (k) and associated standard deviations (s) for the decay of catechol and production of *cis,cis*-muconic acid at variable RH extracted from the equations $[\text{catechol}] = [catechol]_0 + e^{-k_{catechol+O_3} \, t}$ and $[\textit{cis,cis}\text{-muconic acid}]/[\textit{cis,cis}\text{-muconic acid}]_{\text{inf}} = \left(1 - e^{-k_{\textit{cis,cis}\text{-muconic acid}} \, t}\right)$.

RH (%)	$k_{catechol+O_3}$ (s^{-1})	$k_{\textit{cis,cis}\text{-muconic acid}}$ (s^{-1})
0	2.156×10^{-8}	1.958×10^{-10}
29	3.260×10^{-8}	3.057×10^{-9}
48	5.471×10^{-5}	1.105×10^{-4}
71	4.863×10^{-4}	3.867×10^{-4}
90	8.183×10^{-4}	4.133×10^{-4}

References

1. Ramirez, F. J.; Navarrete, J. T. L. Normal Coordinate and Rotational Barrier Calculations on 1,2-Dihydroxybenzene. *Vib. Spectrosc.* **1993**, *4*, 321-334.

2. Sŏhár, P.; Varsányi, G. Y. An IR Spectroscopic Study of Muconate Isomers. *J. Mol. Struct.* **1968**, *1*, 437-448.

3. Maçôas, E. M. S.; Fausto, R.; Lundell, J.; Pettersson, M.; Khriachtchev, L.; Räsänen, M. A Matrix Isolation Spectroscopic and Quantum Chemical Study of Fumaric and Maleic Acid. *J. Phys. Chem. A* **2001**, *105*, 3922-3933.

4. Niculescu, M.; Ledeţi, I.; Bîrzescu, M. New Methods to Obtain Carboxylic Acids by Oxidation Reactions of 1,2-Ethanediol with Metallic Nitrates. *J. Organomet. Chem.* **2014**, *767*, 108-111.

5. Mustafa, C. Vibrational Spectroscopy of Pyrogallol with a Glance on the Problems of Formation of a Dimer. *Res. J. Chem. Environ.* **2013**, *17*, 117-128.

6. Etaiw, S. E. H.; Werida, A. H. Three-Dimensional Organotin–Hexacyanoferrate Polymers as Effective Oxidizing Reagents Towards Phenols. *Appl. Organomet. Chem.* **2010**, *24*, 805-808.

Chapter 5. Oxidation of Substituted Catechols at the Air-Water Interface: Production of Carboxylic Acids, Quinones, and Polyphenols

Scheme 5.**1** Synopsis TOC

5.1 Synopsis

Anthropogenic activities contribute benzene, toluene and anisole to the environment, which in the atmosphere are converted into the respective phenols, cresols, and methoxyphenols by fast gas-phase reaction with hydroxyl radicals (HO$^•$). Further processing of the latter species by HO$^•$ decreases their vapor pressure as a second hydroxyl group is incorporated to accelerate their oxidative aging at interfaces and in aqueous particles. This work shows how catechol, pyrogallol, 3-methylcatechol, 4-methylcatechol, and 3-methoxycatechol −all proxies for oxygenated aromatics derived from benzene, toluene and anisole− react at the air-water interface with increasing $O_3(g)$ during τ_c ~1 μs contact time and contrasts their potential for electron transfer and *in situ* production of HO$^•$ using structure-activity relationships. A unifying mechanism is provided to explain the oxidation of the five proxies, which includes the generation of semiquinone radicals. Functionalization in the presence of HO$^•$ results in the formation of polyphenols and hydroxylated quinones. Instead, fragmentation produces polyfunctional low molecular weight carboxylic acids after oxidative cleavage of the aromatic bond with two vicinal hydroxy groups to yield substituted *cis,cis*-muconic acids. The generation of maleinaldehydic, maleic, pyruvic, glyoxylic, and oxalic acids confirms the potential of oxy-aromatics to produce light-absorbing aqueous secondary organic aerosols (AqSOA) in the troposphere.

5.2 Introduction

Chemical and physical processes resulting in the generation of secondary organic aerosol (SOA) particles that scatter and absorb sunlight, and serve as ice and cloud

condensation nuclei play an important role on Earth's radiation fluxes.[1] Aromatic species emitted to the atmosphere during fossil fuel combustion and biomass burning (e.g., wildfires) processes provide phenol precursors for SOA formation through competing fragmentation and functionalization oxidation reactions.[2-3] Previous work has explored the catalytic effect played by interfaces and the role of variable relative humidity (RH) during the atmospheric oxidation of phenols, e.g., by $O_3(g)$ and hydroxyl radicals $HO^•$.[2-6] A combination of analytical methods –infrared spectroscopy, mass spectrometry (MS), and chromatography– employed in the laboratory revealed the importance of competitive oxidation mechanisms.[2-3] The production of several reactive oxygen species (ROS) including the formation of semiquinone radicals has been demonstrated,[2-3] suggesting that aromatics provide a significant missing mechanism for the production of low-volatility species found in aerosols.[2-3] Furthermore, the common products identified during offline analysis of reactions lasting a few hours and *in situ* studies under a few microseconds contact time (τ_c), validated a flow-through ultra-fast interfacial oxidation MS setup for inspecting reactions at the air-water interface.[2-3]

Combustion and biomass burning emissions provide the two main aromatic species to the atmosphere that total 5.6 and 6.9 Tg C y^{-1} of benzene and toluene, respectively.[7] It was previously explained that the oxidative processing of benzene by hydroxyl radicals ($HO^•$) consecutively yields phenol (reaction R1, Scheme 5.2) and dihydroxybenzenes such as catechol (reaction R2) with gas phase rate constants $k_{R1;benzene+HO^•} = 1.2 \times 10^{-12}$ cm^3 $molec^{-1}$ s^{-1},[8] and $k_{R2;phenol+HO^•} = 2.7 \times 10^{-11}$ cm^3 $molec^{-1}$ s^{-1},[9] respectively.[2-3] The aromatic structures and names, the ring functionalization reactions (e.g., numbered as reaction R1, R2, etc.), the products formed and their *m/z* values are introduced in Scheme

5.2 and Tables S1 and S2 (Supporting Information). By analogy to the reactivity observed for benzene, reactions R1 and R2 also comprehend that toluene ($k_{R1;toluene+HO^{\bullet}}$ = 5.6 × 10^{-12} cm^3 molec^{-1} s^{-1})[8] can generate methylphenols (*p*-, *m*-, and *o*-cresols) and dihydroxytoluenes (e.g., $k_{R2;2\text{-methylphenol}+HO^{\bullet}}$ = 4.3 × 10^{-11} cm^3 molec^{-1} s^{-1})[10] such as 3- or 4-methylcatechol, respectively. In addition, by consecutive hydrogen abstractions from the –CH$_3$ group of toluene, reactions R3a and R3b show that benzaldehyde and benzoic acid can be produced. In general phenols and dihydroxybenzenes[11] with methoxy (–OCH$_3$), methyl (–CH$_3$), carbonyl (C=O), and carboxylic acid (–COOH) substituents groups (-R) are ubiquitous aromatic species in the atmosphere, as proved from the analysis of cloud water that has scavenged combustion and biomass burning emissions.[12] The surfactant properties[13-14] of these polyfunctional phenols makes them especially susceptible to undergo oxidations as they accommodate at the air-water interface or partition into aqueous particles (reaction R4).[2-3]

Scheme 5.2. Proposed sequential oxidation mechanisms of (**black bold font**) **benzene**, (**blue bold font**) **toluene**, and (**red bold font**) **anisole** in the (purple font and reactions) gas-phase by hydroxyl radicals, which continue at the (green font and reactions) air-water interface and in aqueous particles after partitioning of the corresponding substituted catechols. The names of the products are color coded to the corresponding precursors. Complete lists of produced polyphenols and their corresponding quinones redox pair are available in Tables S1 and S2 (Supporting Information) with the observed m/z values.

benzene: $R_{1,2}$ = -H
toluene: R_1 = -CH$_3$, R_2 = -H
anisole: R_1 = -OCH$_3$, R_2 = -H

phenol: $R_{1,2}$ = -H
o-cresol: R_1 = -CH$_3$, R_2 = -H
p-cresol: R_2 = -CH$_3$, R_1 = -H
guaicol: R_1 = -OCH$_3$, R_2 = -H

catechol: $R_{1,2}$ = -H
3-methylcatechol: R_1 = -CH$_3$, R_2 = -H
4-methylcatechol: R_2 = -CH$_3$, R_1 = -H
3-methoxycatechol: R_1 = -OCH$_3$, R_2 = -H

benzaldehyde → benzoic acid

pyrogallol: R_1 = -H
4-methylpyrogallol: R_1 = -CH$_3$
4-methoxypyrogallol: R_1 = -OCH$_3$

tetrahydroxybenzene: R_1 = -H
4-methyl-5-hydroxypyrogallol: R_1 = -CH$_3$
4-methoxy-5-hydroxypyrogallol: R_1 = -OCH$_3$

pentahydroxybenzene: R_1 = -H
pentahydroxytoluene: R_1 = -CH$_3$
pentahydroxyanisole: R_1 = -OCH$_3$

benzenehexol

[a]Names in bold colored fonts match precursors and products.

170

In this work, the interfacial oxidation of a series of substituted catechols found in the environment is contrasted to understand their reactivity and potential for electron transfer during ultrafast contact ($\tau_c \sim 1~\mu s$) and detection ($\tau_d \sim 1$ ms) times.[2, 15-16] Electron density donating substituents of the aromatic ring alter the reactivity of each molecule relative to catechol. Mass spectral data confirms the interfacial production of short lived species can proceed through two pathways: 1) functionalization of the aromatic ring by hydroxylation and 2) fragmentation of the aromatic ring and intermediates by ozone $O_3(g)$ driven oxidative cleavage.[2-3] The first pathway implies that semiquinone radicals are formed *en route* to more hydroxylated aromatic and quinone products. In the alternate pathway, the fragmentation of unsaturated C=C bonds provides polyfunctional low molecular weight carboxylic acids[2-3] widely found in tropospheric aerosols.[17]

5.3 Experimental Section

5.3.1 Sample Preparation

Solutions of catechol (Sigma-Aldrich, 99.9%), pyrogallol (Acros, 99.7%), 3-methylcatechol (TCI, 99.8%), 3-methoxycatechol (Aldrich, 99.7%), and 4-methylcatechol (Acros, 97.6%) were freshly prepared in degassed ultrapure water (18.2 $M\Omega$ cm, Elga Purelab flex, Veolia) and infused into a calibrated ESI-MS (Thermo Scientific, MSQ Plus) operating in the negative ionization mode. Stock solutions of ca. 5.00 mM were diluted to 100.0 μM final concentration after adjusting the pH with 0.01 M NaOH (Fisher, 99.3%) as measured with a calibrated pH-meter (Mettler Toledo). Figures report the percent normalized anion count ($I_{m/z}$) at specific mass-to-charge (m/z) ratios for experiments at pH 7.80. While the oxidations were explored in the atmospheric relevant

pH range 5-10, reporting the results at pH 7.8 provides an example case that demonstrates the complexity of all the chemistry observed. Anthropogenic biomass burning emissions from agricultural practices often coincide with increased ammonia (NH_3) emissions from livestock and fertilizers,[18-19] what explains why fine particulate matter around agricultural regions can be predominately alkaline.[20-23] For example, in most of the Midwest Region and the Pacific coast of the United States, where agriculture is a primary economic activity, NH_3 emissions are estimated to be sufficient to neutralize all acidic components.[21] Thus, even fine aerosols can be neutral or slightly basic, which indicates the experiments reported are of atmospheric relevance. All experiments are performed by duplicate.

5.3.2 Oxidation of Substituted Catechols

The ESI-MS flow through reactor to investigate ultrafast oxidations at the air-water interface has been described in depth.[15-16] The 100 µM aqueous solution of the selected substituted catechol undergoes pneumatically assisted aerosolization to form a fine mist of micrometer size droplets at ambient pressure. A spark discharge generator (Ozone Solutions) acting over a 0.5 L min^{-1} flow of $O_2(g)$ (Scott-Gross, UHP) produces $O_3(g)$, which is quantified in a 10-cm path length cuvette (Starna cell) by UV absorption spectrophotometry (Evolution Array UV-Visible Spectrophotometer, Thermo Scientific) after dilution with 0.0-5.0 L min^{-1} $N_2(g)$ (Scott Gross, UHP) in a flow-through borosilicate chamber (3.785 L capacity).[24] In the final stage, $O_3(g)$ is diluted 61-times with the $N_2(g)$ nebulizing gas (12.0 L min^{-1}). The interface of the microdroplets containing substituted catechols encounters a 0.2 L min^{-1} flow of 0 ppbv $\leq [O_3(g)] \leq 3$ ppmv during a few microseconds.[15-16] If oxidized species are produced, they are observed

as anions by mass spectrometer at specific *m/z* values (reported in the text, figures and schemes) in less than 1 ms after their formation.[15-16] The experimental conditions employed were the same used during the previous study with catechol and trihydroxybenzenes:[2] Nebulizer pressure, 70 psi; nebulizer voltage, -1.9 kV; cone voltage, -50 V; and drying gas temperature, 250 °C. Reported $I_{m/z}$ values correspond to solvent background subtracted raw data acquired at fixed time intervals (e.g., time $\geq$ 30 s).

The conversion of terephthalic acid (Acros, 99.0%) to 2-hydroxyterephthalic acid (TCI, 98.3%) with a rate constant $k_{\text{terephthalic acid+HO}^{\bullet}} = 4 \times 10^9$ M^{-1} s^{-1} was used for *in situ* quantification of HO$^{\bullet}$ at the air-water interface.[25] The reaction of 100 μM 1) pyrogallol, 2) 4-methylcatechol, 3) 3-methylcatechol, and 4) 3-methoxycatechol with 2.7 ppmv O$_3$(*g*) was studied at pH 7.8 in the presence of 5 μM terephthalic acid. The characteristic product peak at *m/z* 181 for 2-hydroxyterephthalic acid was used to quantify the production of HO$^{\bullet}$ by standard addition after subtracting the background produced during controls under 1 atm N$_2$(*g*).

5.4 Results and Discussion

5.4.1 Reactions of Substituted Catechols at the Air-Water Interface

The interfacial oxidation of 100 μM substituted catechols was examined in the absence of O$_3$(*g*) or in its presence for mixing ratios of 0.223, 0.989, 1.760, and 2.420 ppm. For example, Figure 5.1 shows ESI mass spectra of aerosolized aqueous solutions of (top) pyrogallol and (bottom) 3-methoxycatechol at pH 7.8 impinged by a flow of 0.2 L min^{-1} of 0 ppb, 223 ppb, and 2.42 ppm O$_3$(*g*). Both traces in the absence of O$_3$(*g*) display the

anions of pyrogallol (m/z 125) and methoxycatechol (m/z 139). For comparison, experiments with catechol (m/z 109) have been studied in detail.[2] The direct oxidation of catechol by $O_3(g)$ has been shown to produce: glyoxylic acid (m/z 73), oxalic acid (m/z 89), maleinaldehydic acid (m/z 99), 5-oxo-3-pentenoic acid (m/z 113), maleic acid (m/z 115), 3-hydroxy-o-quinone or 4-hydroxy-o-quinone (m/z 123), 1,2,3- and 1,2,4-tryhydroxybenzenes (m/z 125), glutaconic acid (m/z 129), 3,4-dihydroxy-o-quinone or 3,6-dihydroxy-o-quinone (m/z 139), cis,cis-muconic acid, 1,2,3,4- and 1,2,4,5-tetrahydroxybenzene (m/z 141), 3,4,5-trihydroxy-o-quinone and 3,4,6-trihydroxy-o-quinone (m/z 155), pentahydroxybenzene (m/z 157), and benzenehexol (m/z 173).[2]
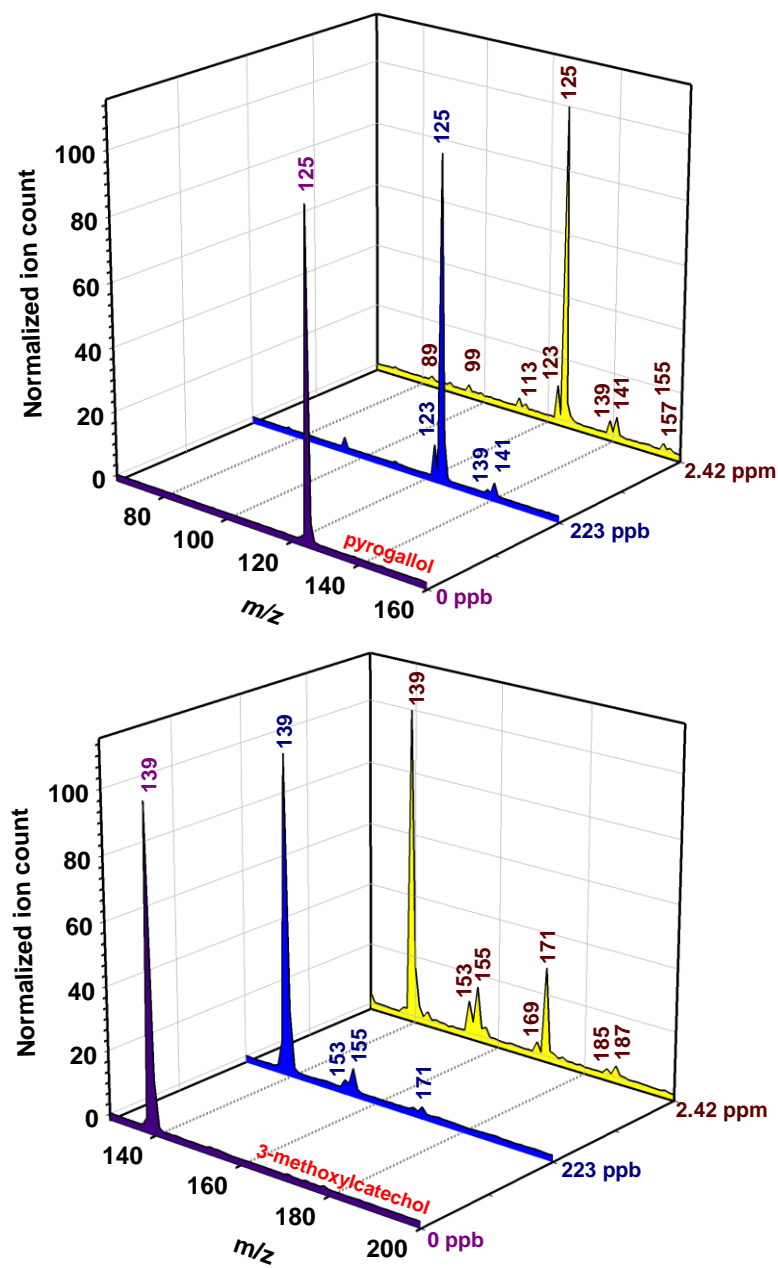
Figure 5.1. Spectra of ESI-MS of 100 µM solutions of (top) pyrogallol and (bottom) 3-methoxycatechol at pH 7.8 exposed to a 0.200 L min⁻¹ flow of (purple trace) 1 atm $N_2(g)$, (blue trace) 223 ppb $O_3(g)$, and (yellow trace) 2.42 ppm $O_3(g)$. Ion count values are normalized percentages relative to the most intense peak in each mass spectra, I_{125} for pyrogallol and I_{139} for 3-methoxycatechol.

Following the oxidation channels exhibited by catechol, it is possible to assign the

products for pyrogallol in Figure 5.1 to also be oxalic acid (*m/z* 89), maleinaldehydic acid

(*m/z* 99), 5-oxo-3-pentenoic acid (*m/z* 113), 3- and 4-hydroxy-*o*-quinones (*m/z* 123), 3,4-dihydroxy-*o*-quinone (*m/z* 139), 1,2,3,4-tetrahydroxybenzenes and 2-hydroxy-*cis,cis*-muconic acid (both *m/z* 141), 3,4,5-trihydroxy-*o*-quinone (*m/z* 155), and pentahydroxybenzene (*m/z* 157). Similarly, Figure 5.1 shows that 3-methoxycatechol (*m/z* 139) is oxidized to give the hydroxylated products 4-methoxypyrogallol or 3-methoxy-4-hydroxycatechol (*m/z* 155) and their corresponding quinone pairs, e.g., 3-methoxy-6-hydroxy-*o*-quinone and 3-methoxy-4-hydroxy-*o*-quinone (*m/z* 153); 4-methoxy-5-hydroxy-pyrogallol or 3-methoxy-4,5-dihydroxycatechol (*m/z* 171) and their corresponding quinones pairs, e.g., 3-methoxy-4,6-dihydroxy-*o*-quinone and 3-methoxy-4,5-dihydroxy-*o*-quinone (*m/z* 169); 4-methoxy-5,6-dihydroxy-pyrogallol (*m/z* 187) and its corresponding 3-methoxy-4,5,6-trihydroxy-*o*-quinone (*m/z* 185). When comparing the pairs at *m/z* 155 and 153, *m/z* 171 and 169, and *m/z* 187 and 185, for oxidized 3-methoxycatechol (Figure 5.1), it is obvious that the peak for the dihydroxylated product of 3-methoxycatechol at *m/z* 171 largely exceeds the expected value from correlation to the peak at *m/z* 169. For these quinone/hydroquinone pairs (signals separated by 2 amu), it is obvious that the peak at *m/z* 171 displays a large contribution of other species, which is 2-methoxymuconic acid, the major product from aromatic ring cleavage.

Figure 5.2 displays the ESI mass spectra for aerosolized solutions of (top) 3-methylcatechol and (bottom) 4-methylcatechol under the same conditions listed for Figure 5.1. Both traces in the absence of $O_3(g)$ display the anion for methylcatechol (*m/z* 123) and a small peak for its dihydrate (*m/z* 159), a feature also exhibited by catechol. Some of the products observed during the oxidation of both methylcatechols are oxalic acid (*m/z* 89); maleinaldehydic acid (*m/z* 99); 4-methyl-*o*-quinone (*m/z* 121) (no 3-

methyl-*o*-quinone is registered probably due to steric impediments); 3-methyl-4-hydroxy- and 3-hydroxy-4-methyl- and 4-methyl-5-hydroxy-*o*-quinone (*m/z* 137); 3-methyl-4-hydroxy-catechol, 4-methylpyrogallol and 4-methyl-5-hydroxy-catechol (*m/z* 139); 3-methyl-4,5-dihydroxy- and 3,5-dihydroxy-4-methyl-*o*-quinone (*m/z* 153); 2-methyl-*cis,cis*-muconic acid (*m/z* 155); 3-methyl-4,5-dihydroxy- and 3,5-dihydroxy-4-methyl-catechols (*m/z* 155); 4-methyl-3,5,6-trihydroxy-*o*-quinone (*m/z* 171); and 3-methyl-4,5,6-trihydroxy- and 3,5,6-trihydroxy-4-methyl-catechols (*m/z* 173).
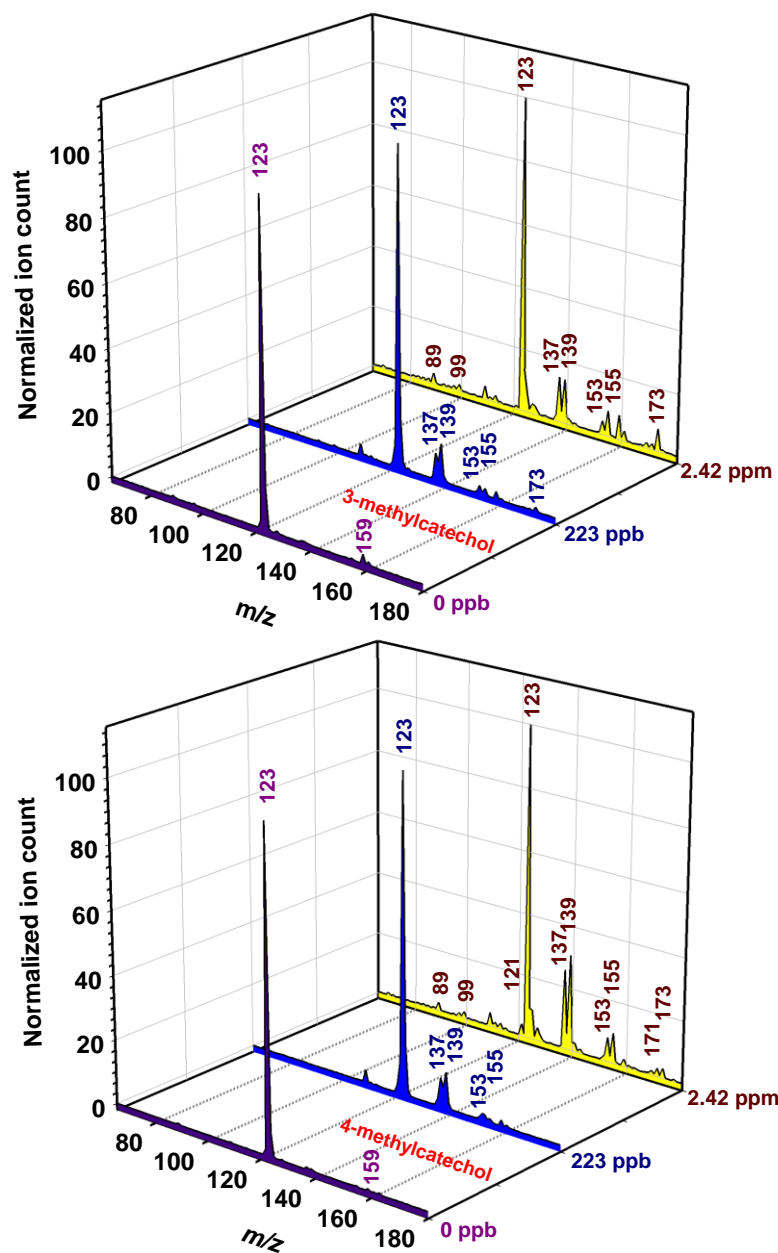
Figure 5.2. Spectra of ESI-MS of 100 μM solutions of (top) 3-methylcatechol and (bottom) 4-methylcatechol at pH 7.8 exposed to a 0.200 L min^{-1} flow of (purple trace) 1 atm $N_2(g)$, (blue trace) 223 ppb $O_3(g)$, and (yellow trace) 2.42 ppm $O_3(g)$. Ion count values are normalized percentages relative to I_{123}, the most intense peak in each mass spectrum.

Figure 5.3 gathers information from experiments with increasing $[O_3(g)]$ displaying the

exponential drop of $I_{m/z}$ for pyrogallol, 3-methylcatechol, 4-methylcatechol, and 3-

178

methoxycatechol. In agreement with previous work with catechol,[2] the information in Figure 5.3 suggests the first-order reaction on $[O_3]$ for all the substituted catechols studied takes place within $\tau_c \approx 1$ μs. Indeed, the reaction with $O_3(g)$ molecules occurs at the outermost layers of the interface of a few nanometers thickness without diffusion limitations while replenishment of the organic molecule from the core is facilitated.[2, 16]
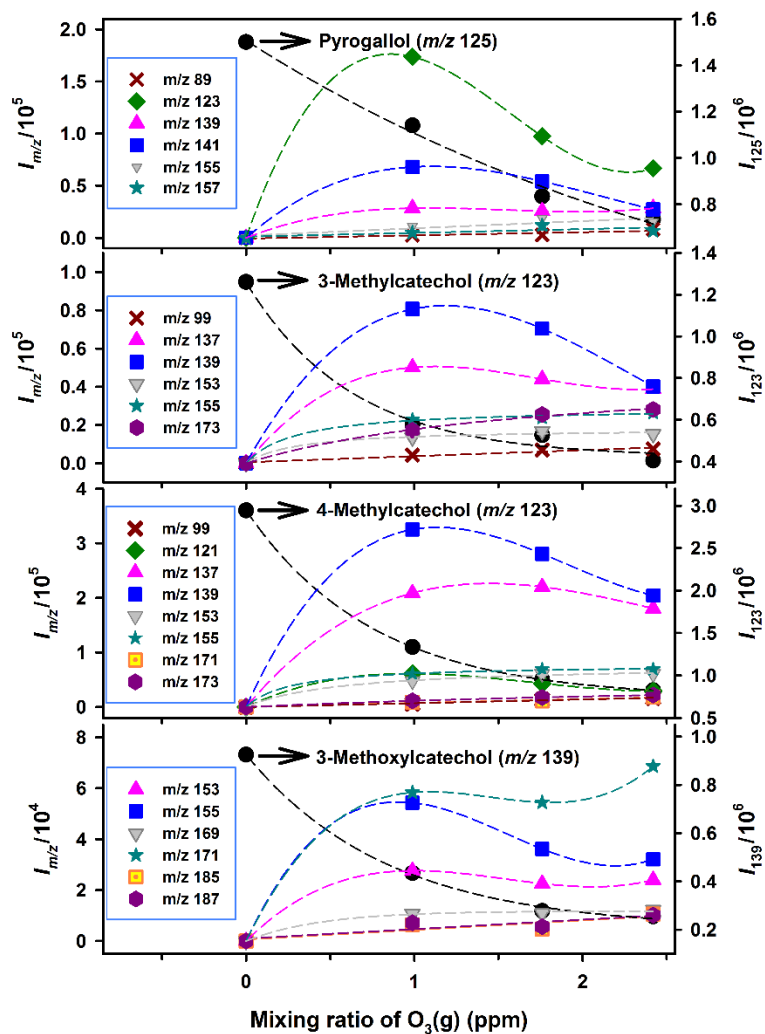
Figure 5.3. Ion count, $I_{m/z}$, of pyrogallol (*m/z* 125), 3-methylcatechol (*m/z* 123), 4-methylcatechol (*m/z* 123), 3-methoxycatechol (*m/z* 139), and the respective oxidation products from exposing aerosolized solutions of each compound to increasing mixing ratios of $O_3(g)$. Dashed lines connecting points are meant to guide the eye and do not represent curve fittings.

5.4.2 Electron and Proton Transfers

The speciation of the substituted catechols in Figures 5.1 and 5.2 can be calculated using both pK_{a1} and pK_{a2} for these weak diprotic species (H_2Q) and its intermediate form (HQ^-):

$$H_2Q \rightleftharpoons HQ^- + H^+, \text{pK}_{a1,} \qquad\qquad \text{(Eq. 5.1)}$$

$$HQ^- \rightleftharpoons HQ^{2-} + H^+, \text{pK}_{a2} \qquad\qquad \text{(Eq. 5.2)}$$

While this information is available for catechol and pyrogallol,[22] the instability of this class of compounds precludes access to experimental values of the other acid dissociation constants. However, theoretical methods capable of accurately predicting pK_{a1} and pK_{a2} values have been developed.[26-28] Thus, Table 5.1 combines the experimental and theoretical values for pK_{a1} and pK_{a2}, which can be used to solve the speciation of the H_2Q species vs pH. For example, at working pH 7.8, the fractions of fully associated catechols, $\alpha_{H_2Q} \geq 0.95$, and its intermediate monoprotic acid, $\alpha_{HQ^-} \leq 0.05$, are reported in Table 5.1. Clearly, the diprotic catechols are the dominant species available for the oxidations displayed in Figures 5.1 and 5.2.

Table 5.1.

Name	M.W. (amu)	pK_{a1}	pK_{a2}	$\alpha_{H_2Q}{}^{d}$	$\alpha_{HQ^-}{}^{d}$	$E_{H_2Q^{•+}/I}$ (V)^e	ΔE (V)^h	$\Delta G°$ (kJ mol^{-1})^g
Catechol	110.11	9.34[a]	12.60[a]	0.972	0.028	0.53[f]	0.48	-46.31
Pyrogallol	126.11	9.12[a]	11.19[a]	0.954	0.046	0.47[c,g]	0.54	-52.10
4-Methyl catechol	124.14	9.59[b]	12.69[c]	0.983	0.017	0.42[c]	0.59	-56.93
3-Methyl catechol	124.14	9.59[b]	12.66[c]	0.984	0.016	0.42[c]	0.59	-56.93
3-Methoxy catechol	140.14	9.59[c]	12.69[c]	0.984	0.016	0.33[c]	0.68	-65.61

[a]Experimental values,[26, 29] [b]predicted using ChemAxon,[27-28] [c]calculated using linear free energy relationships,[26, 30 31] [d]at working pH 7.8, [e]for the diprotic form H$_2$Q, [f]at pH 7.0, [g]accounting the equivalent -OH groups in carbons 1 and 3, [h]$\Delta E = E_{O_3/O_3^{•-}} - E_{H_2Q^{•+}/H_2Q}$, and $E_{O_3/O_3^{•-}} = 1.01$ V,[32] [g]$\Delta G° = -n\,F\,\Delta E$.

Under the oxidizing experimental conditions, the substituted catechols and/or their products can act as two-electron reductants, getting converted into the corresponding quinones by two coexisting pathways. The first pathway proceeds through initial electron transfer from the more abundant undissociated catechols to O$_3$ (reaction R5a). This electron transfer pathways is supported by the dominant fractions in equilibrium at pH 7.8, $\alpha_{H_2Q} \geq 0.95$ (Table 5.1), which continues by a fast proton transfer (reaction R5b). Reactions R5a + R5b are equivalent to the net loss of a hydrogen atom. However, direct

hydrogen atom transfer should be unfavorable in these molecular ensembles as exemplified by the ~10-times larger hydrogen bond dissociation energies, calculated from data in dimethylsulfoxide,[30] than the thermal energy available for the system. The second mechanism involves initial dissociation of the diprotic catechols followed by electron transfer (reactions R6a + R6b), which is less likely to be the dominant process given $\alpha_{HQ^-} \leq 0.05$ (Table 5.1). The equilibrium constant for reaction R6a corresponds to the first acid dissociation constant, K_{a1}. The self-reaction of two semiquinone radicals (HQ$^\bullet$) via reaction R7 finally produces a quinone (Q) while regenerating a substituted catechol: 2 HQ$^\bullet$ → Q + H$_2$Q. Analogously, the cross-reaction between two different semiquinone radicals also generates a quinone: $HQ_i^\bullet + HQ_j^\bullet \rightarrow Q_i + H_2Q_j$ (reaction R8).

The electron donating capacity of the substituents and their position relative to the –OH groups should be considered together with molecular specific properties (e.g., redox potentials and first and second proton dissociation constants) to understand why reactions R5a + R5b are favored herein. Table 5.1 also lists the 1 electron redox potentials of the semiquione radical cation (HQ$^{\bullet+}$) and undissociated substituted catechol pairs, $E_{HQ^{\bullet+}/H_2Q}$, which except for catechol reported at pH 7[31] are predicted using structure-activity relationships derived from computational methods.[30] The linear dependence of the redox potentials vs the normal hydrogen electrode (NHE) on the sum of the Hammett substituents parameters (σ) available in the literature is given by equation 3:[30]

$$E_{HQ^{\bullet+}/H_2Q} = 1.85 \sum_i \sigma_i + 0.46 \qquad \text{(Eq. 5.3)}$$

Table 5.1 reports the positive $\Delta E = E_{O_3/O_3^{\bullet-}} - E_{H_2Q^{\bullet+}/H_2Q}$ for electron transfer (reaction R5a) between the substituted catechols and dissolved O_3 ($E_{O_3/O_3^{\bullet-}} = 1.01$ V). The ΔE values correspond to thermodynamically favorable processes as indicated in Table 5.1 by the calculated $\Delta G^\circ = -nF\Delta E$, where $n = 1$ and $F = 96.485$ kJ mol^{-1} V^{-1} is the Faraday constant. From the increasing ΔE values in Table 5.1, it is observed that electron transfer occurs more easily following the trend catechol < pyrogallol < 4-methylcatechol = 3-methylcatechol < 3-methoxycatechol. In other words, the decreasing $E_{H_2Q^{\bullet+}/H_2Q}$ observed with these electron donating groups favors electron transfer from H_2Q to O_3 (reaction R5a). The directly generated semiquinone radicals $H_2Q^{\bullet+}$ (p$K_{a1} \sim$ -1)[33] promptly release a proton (reaction R5b), while the ozonide radical anion $O_3^{\bullet-}$ from reaction R5a coexists in equilibrium R9a with very basic $O^{\bullet-}$ (p$K_a = 11.8$).[34] Therefore, for environmentally relevant atmospheric waters and other aqueous systems (pH < 10) and in present experiments, $O^{\bullet-}$ is quickly converted into $HO^{\bullet}$ (equilibrium R9b). In consequence, this work also provides an opportunity to understand how $HO^{\bullet}$ continues the oxidation of substituted catechols at the air-water interface, in aqueous aerosols, and other relevant water media.

5.4.3 Reactions of the Substituted Catechols with HO$^{\bullet}$

In addition to reactions R7 and R8, the semiquinone radicals can also be produced by the attack of HO$^{\bullet}$ to the catechols (reaction R10) that generates resonance stabilized cyclohexadienyl radicals capable of undergoing fast acid or base catalyzed elimination of water (reaction R11). For instance, reaction R10 for unsubstituted catechol proceeds at pH 9 with a large rate constant $k_{HO^{\bullet}+catechol} = 1.1 \times 10^{10} M^{-1}s^{-1}$.[35] The rate constant for the aqueous reaction of pyrogallol, 3-methoxycatechol, 3- and 4-methylcatechol with

HO$^{\bullet}$ should be larger than for catechol due to the presence of electron donating groups.[36] For example, the reaction rates constants for 3-methylcatechol and 4-methylcatechol with HO$^{\bullet}$ (available in the gas phase) are 1.9 and 1.5 times larger than for catechol.[37] Comparable oxidation conditions are supported by experiments under fixed 100 μM concentration for each substituted catechol at pH 7.8 reacting with 2.7 ppmv O$_3$(g), which constrain the produced [HO$^{\bullet}$]$_{interface}$ = 1.1 (± 0.3) 10^{13} radicals cm^{-3}. Thus, the attack of HO$^{\bullet}$ to the activated rings should also be expected to be $\geq 2 \times 10^4$ times larger than for the corresponding reaction with O$_3$ ($k_{O_3+catechol} = 5.2 \times 10^5\ M^{-1}s^{-1}$ at pH 7).[38] Once HO$^{\bullet}$ is produced, it can also directly abstract a hydrogen atom from H$_2$Q to form HQ$^{\bullet}$. Under typical atmospheric conditions, the competitive fate of the cyclohexadienyl radicals is fast O$_2$ addition[39] forming a peroxy radical that decomposes into a hydroxylated product releasing hydroperoxyl radical (HO$_2^{\bullet}$) by reaction R12.[40] Thus, reaction R12 represents the formation of pyrogallol (*m/z* 125) from catechol; 3-methyl-4-hydroxycatechol, 4-methylpyrogallol, and 4-methyl-5-hydroxycatechol (*all* m/z 139) from 3- and 4-methylcatechol; and 4-methoxypyrogallol and 3-methoxy-4-hydroxycatechol (both with *m/z* 155) from anisole. It is particularly interesting to compare the relative ion count for the first hydroxylated products (*m/z* 139) of both methylcatechols studied. The fact that I_{139} for 4-methylcatechol is about twice larger than for 3-methylcatechol in experiments with 2.42 ppmv O$_3$ (Figure 5.2), and that their α_{H_2Q}, α_{HQ^-}, and $E_{H_2Q^{\bullet+}/H_2Q}$ (Table 5.1) are practically identical (Table 5.1) for both species, suggests that the efficiency for electron transfer must not be the cause for this discrepancy. Indeed, the presence of a vicinal –CH$_3$ causes steric hindrance that could

decrease the reactivity of 3-methylcatechol relative to 4-methylcatechol for this electron transfer initiated processes.

The quick production of HQ$^\bullet$ and HO$^\bullet$ is also reflected in Figure 5.3 showing the profiles of each species for increasing [O$_3$(g)]. For example, the top panel of Figure 5.3 shows how pyrogallol (m/z 125) generates a large production of 1) 3- and 4-hydroxy-o-quinones (m/z 123) likely from self-reaction R7 and 2) tetrahydroxybenzenes (m/z 141) via the sequence represented by reaction R13. Reaction R7 can also be invoked for the considerable production of 4-methyl-o-quinone (m/z 121) from 4-methylcatechol in Figure 5.3. Interestingly, reaction R7 is not observed in the cases of 3-methylcatechol and 3-methoxycatechol, showing the steric hindrance introduced by –CH$_3$ and –OCH$_3$ groups in position 3 (next to the bond with both –OH groups). In addition, reaction R13 also explains the large production of 1) 3-methyl-4,5-dihydroxycatechol and 4-methyl-3,5-dihydroxycatechol (both m/z 155) from 3-methyl-4-hydroxycatechol, 4-methylpyrogallol, and 4-methyl-5-hydroxycatechol; and 2) 4-methoxy-5-hydroxypyrogallol and 3-methoxy-4,5-dihydroxycatechol (both m/z 171) from 4-methoxypyrogallol and 3-methoxy-4-hydroxycatechol (both m/z 155). Alternatively, another very likely mechanism for incorporation of –OH to the catechols (not displayed in Scheme 5.2) is the direct reaction with O$_3$ at positions 3 and 6 that eliminates O$_2$($^1\Delta_g$).[2, 41-42]

In general, the maximum $I_{m/z}$ values for the products from the first electrophilic addition of HO$^\bullet$ to the substituted catechols via reaction R13 dominates the composition of products (see blue squares in Figure 5.3). However, pyrogallol is an exception due to its extraordinarily ability to form 3- and 4-hydroxy-o-quinones (m/z 123). For increasing [O$_3$(g)], $I_{m/z}$ of the monohydroxylated products starts to decay, indicating further

oxidation occurs. Interestingly, I_{171} for 3-methoxycatechol (see teal stars in Figure 5.3) keeps growing instead of decaying for higher $[O_3(g)]$. This anomaly clearly indicates that 2-methoxymuconic acid originated from oxidative cleavage of the aromatic ring contributes further to the peak intensity than the isomeric second hydroxylation product of 3-methoxycatechol. Otherwise, less intense growing patterns are observed from reactions R13 and R14 for $I_{m/z}$ of the respective second and third hydroxylation products (see teal stars in Figure 5.3). Reaction R14 represents a third generation product with a new –OH group added to 1) tetrahydroxybenzenes (*m/z* 141) to form pentrahydroxybenzene (*m/z* 157), 2) 3-methyl-4,5-dihydroxycatechol and 4-methyl-3,5-dihydroxycatechol (both *m/z* 155) to form 3-methyl-4,5,6-trihydroxycatechol and 4-methyl-3,5,6-trihydroxycatechol (both *m/z* 171), and 3) 4-methoxy-5-hydroxypyrogallol and 3-methoxy-4,5-dihydroxycatechol (both *m/z* 171) to form 4-methoxy-5,6-dihydroxypyrogallol (*m/z* 187). The conversion pentahydroxybenzene into benzenehexol (reaction R15) represents a fourth generation aqueous product from catechol (Table S1, Supporting Information).[2]

The reactions for the production of all the quinones experimentally observed in Figures 5.1 and 5.2 can be explained to proceed analogously to self-reaction R7 and/or cross-reaction R8. An alternate pathway for their production is the elimination of H_2O_2 after O_3 attack to vacant positions 3 and 4 of the substituted catechols.[2] These complex reactions likely proceed through a cyclic ozonide intermediate.[38] The structures for the quinones named above for *m/z* 121, 123, 137, 139, 153, 155, 169, and 171 are provided in Table S1 (Supporting Information) together with the corresponding precursors. Figure 5.3 shows

the profiles of these quinones are slightly less intense than the corresponding H_2Q species 2 amu heavier but generally resemble each other's behavior with increasing $[O_3(g)]$.

5.4.4 Oxidative Cleavage of Substituted Catechols

While the substituted catechols react at the air-water interface generating a distribution of products dominated by the functionalized aromatic rings described in Scheme 5.2, fragmentation of the bond between C_1 and C_2 by electrophilic O_3 generates polyfunctional carboxylic acids. The small ion count for the representative fragmentation products with *m/z* 89 and 99 included in Figure 5.3 is expected because these secondary oxidation products cannot accumulate during the short τ_c in the setup.[16] The detailed analysis explaining the mechanism of reaction for catechol[2] should also be applicable to its substituted counterparts. Catechol, pyrogallol, both methylcatechols, and 3-methoxycatechol undergo a series of oxidative fragmentations summarized in Scheme 5.3 to yield muconic acid (*m/z* 141), 2-hydroxymuconic acid (*m/z* 157), 2- and 3-methylmuconic acid (*m/z* 155), and 2-methoxymuconic acid (*m/z* 171), respectively.

The produced substituted muconic acids result from an ozonide that is sequentially converted into a Criegee intermediate, and a hydroperoxide that also releases H_2O_2.[2] Scheme 5.3 also shows that further fragmentation by O_3 and *in situ* generated H_2O_2 produces glyoxylic (*m/z* 73), crotonic (*m/z* 85), pyruvic (*m/z* 87), 3-oxopropanoic (*m/z* 87), oxalic (*m/z* 89), maleinaldehydic (*m/z* 99), 4-hydroxy-2-butenoic (*m/z* 101), 5-oxo-3-pentenoic (*m/z* 113), maleic (*m/z* 115), and glutaconic (*m/z* 129).[2] While the majority of the compounds (e.g., glyoxylic and oxalic acids) could be originated from all the catechols, the color coding in Scheme 5.3 clearly indicates that pyruvic acid only arises from the oxidation of the methylcatechols. Thus, together with the pathways from

isoprene photooxidation,[22, 43] the oxidative channel for the oxidation of methylated aromatics such as toluene producing cresols (reactions R1 and R2) is responsible for the production of this important tropospheric compound.

The common oxidative fate of the low molecular weight carboxylic acids is to continue getting oxidized *en route* to form CO, CO_2, oxalic acid and formic acid. Interestingly, glyoxylic acid was the most abundant product during the oxidation of catechol at the air-water interface lasting $\tau_c \sim 1$ μs.[2] Glyoxylic acid can be oxidized to form oxalic acid (*m/z* 89),[2] but photooxidation in water yield CO, CO_2, formic acid, glyoxal, and a small amount of tartaric acid.[23] Both pyruvic and glyoxylic acid also yield these common products by Baeyer–Villiger (BV) oxidation in the presence of *in situ* generated H_2O_2.[2] In addition, a comparison of the reactivity of both methylcatechols shows that the –CH_3 group in position 3 creates an electron richer vicinal carbon-carbon bond with –OH groups and enhances fragmentation by electrophilic O_3. The previous fact can be visualized in Figure 5.2 as well as by the brown crosses for *m/z* 99 in the center panel of Figure 5.3. Consequently, a slight increase in the number of low molecular weight carboxylic acids is observed for 3-methylcatechol relative to 4-methylcatechol. Finally, it is possible to consider the attack of HO$^•$ to the substituted catechols followed by the addition of O_2 to form an endoperoxide that will add a second O_2. The peroxide formed can decompose contributing quinones and mainly low molecular weight carbonyls and carboxylic acids. For example, the production of glyoxal, glyoxylic acid, oxalic acid, methylglyoxal, and pyruvic acid from both methylcatechols can proceed through this channel.

Scheme 5.3. Products and Observed *m/z* Values from Substituted Catechols Oxidation by O_3 and H_2O_2 Following the Mechanisms from Ref. 2.[a]

R_1
OH
R_2
OH

catechol: $R_{1,2}$ = -H (*m/z* 109)
pyrogallol: R_1 = -OH, R_2 = -H (*m/z* 125)
3-methylcatechol: R_1 = -CH$_3$, R_2 = -H (*m/z* 123)
4-methylcatechol: R_2 = -CH$_3$, R_1 = -H (*m/z* 123)
3-methoxycatechol: R_1 = -OCH$_3$, R_2 = -H (*m/z* 139)

O_3
$H_2O + H_2O_2$

R_1
R_2 COOH
COOH

muconic acid: $R_{1,2}$ = -H (*m/z* 141)
2-hydroxymuconic acid: R_1 = -OH, R_2 = -H (*m/z* 157)
2-methylmuconic acid: R_1 = -CH$_3$, R_2 = -H (*m/z* 155)
3-methylmuconic acid: R_2 = -CH$_3$, R_1 = -H (*m/z* 155)
2-methoxymuconic acid: R_1 = -OCH$_3$, R_2 = -H (*m/z* 171)

O_3
H_2O_2
HO·

glyoxylic acid
m/z 73

pyruvic acid
m/z 87

oxalic acid
m/z 89

crotonic acid
m/z 85

3-oxopropanoic acid
m/z 87

maleinaldehydic acid
m/z 99

4-hydroxy-2-butenoic acid
m/z 101

5-oxo-2-pentenoic acid
m/z 113

maleic acid
m/z 115

glutaconic acid
m/z 129

[a]Names in bold colored fonts match precursors and products.

5.4.5 Implications

This laboratory study contributes to characterizing the evolution of combustion and biomass burning emissions, an important subject to understand how the surface of carbonaceous materials is affected during interfacial oxidations that can potentially alter the morphology of particles that play a role in the direct radiative effect.[44] The most important process governing the initial oxidation of aromatic species in the atmosphere is controlled by the presence of HO•. The results from ultra-fast experiments analyzed by mass spectrometry reveal the identity of low volatility reaction products. Quinones (Table S2, Supporting Information) and polyphenols reactive intermediates coexist at the air-water interface, where low molecular weight carboxylic acids found in brown clouds are produced. The quick oxidation of all substituted catechols proceeds by competing functionalization and fragmentation reactions. Although for acidic hygroscopic particles containing sulfate a lower amount of hydroxyl radical should be generated *in situ* by the electron transfer mechanism presented, the reactions of phenols with this radical will proceed as reported here regardless of the source of HO•. Thus, the studied phenols, available on the surface of tropospheric particles, should react with impinging HO• produced in the gas phase through the same pathways presented.

The proposed pathways agree with observations previously made for catechol at the air-water and air-solid interface under variable relative humidity,[2-3] which generate more hydrophilic products that partition into the aqueous phase. In addition, photochemical oxidation should also contribute to the degradation of aromatics in the aqueous phase.[45] However, the substituted catechols display an enhancement in their reactivity due to the ring activating functional groups. Similarly, the functionalized rings with more –OH

groups are also highly activated toward fragmentation and should be relevant intermediates in the degradation of aromatics emitted during combustion and biomass burning. In addition, this information can also be applied to support the similar chemical processing of particulate matter with diameter < 1 μm (PM_1) from the greater London area in winter 2012.[46] This PM_1 contains non-volatile organics associated with refractory black carbon that could originate either from combustion or biomass burning emissions. Finally, this work also explains typical degradation pathways that aromatic pollutants derived from benzene, toluene, and anisole in water media and at the air-water interface.

5.5 Acknowledgement

5.6 References

1. Boucher, O.; Randall, D.; Artaxo, P.; Bretherton, C.; Feingold, G.; Forster, P.; Kerminen, V.-M.; Kondo, Y.; Liao, H.; Lohmann, U.; Rasch, P.; Satheesh, S. K.; Sherwood, S.; Stevens, B.; X.Y. Zhang, X. Y. Clouds and Aerosols. In *Climate Change 2013: The Physical Science Basis. Contribution of Working Group I to the Fifth Assessment Report of the Intergovernmental Panel on Climate Change*, Stocker, T. F.; Qin, D.; Plattner, G.-K.; Tignor, M.; Allen, S. K.; Boschung, J.; Nauels, A.; Xia, Y.; Bex, V.; Midgley, P. M., Eds. Cambridge University Press: Cambridge, United Kingdom and New York, NY, USA, 2013.

2. Pillar, E. A.; Camm, R. C.; Guzman, M. I. Catechol Oxidation by Ozone and Hydroxyl Radicals at the Air–Water Interface. *Environ. Sci. Technol.* **2014**, *48*, 14352-14360.

3. Pillar, E. A.; Zhou, R.; Guzman, M. I. Heterogeneous Oxidation of Catechol. *J. Phys. Chem. A* **2015**, *119*, 10349-10359.

4. O'Neill, E. M.; Kawam, A. Z.; Van Ry, D. A.; Hinrichs, R. Z. Ozonolysis of Surface-Adsorbed Methoxyphenols: Kinetics of Aromatic Ring Cleavage vs. Alkene Side-Chain Oxidation. *Atmos. Chem. Phys.* **2014**, *14*, 47-60.

5. Barnum, T. J.; Medeiros, N.; Hinrichs, R. Z. Condensed-Phase Versus Gas-Phase Ozonolysis of Catechol: A Combined Experimental and Theoretical Study. *Atmos. Environ.* **2012**, *55*, 98-106.

6. Woodill, L. A.; O'Neill, E. M.; Hinrichs, R. Z. Impacts of Surface Adsorbed Catechol on Tropospheric Aerosol Surrogates: Heterogeneous Ozonolysis and Its Effects on Water Uptake. *J. Phys. Chem. A* **2013**, *117*, 5620-5631.

7. Henze, D. K.; Seinfeld, J. H.; Ng, N. L.; Kroll, J. H.; Fu, T. M.; Jacob, D. J.; Heald, C. L. Global Modeling of Secondary Organic Aerosol Formation from Aromatic Hydrocarbons: High- Vs. Low-Yield Pathways. *Atmos. Chem. Phys.* **2008**, *8*, 2405-2420.

8. Atkinson, R.; Arey, J. Atmospheric Degradation of Volatile Organic Compounds. *Chem. Rev.* **2003**, *103*, 4605-4638.

9. Calvert, J. G.; Atkinson, R.; Becker, K. H.; Kamens, R. M.; Seinfeld, J. H.; Wallington, T. J.; Yarwood, G. *The Mechanisms of Atmospheric Oxidation of the Aromatic Hydrocarbons*; Oxford University Press: New York, USA, 2002, p 566.

10. Atkinson, R.; Aschmann, S. M. Rate Constants for the Gas-Phase Reactions of the OH Radical with the Cresols and Dimethylphenols at $296 \pm 2K$. *Int. J. Chem. Kinet.* **1990**, *22*, 59-67.

11. Veres, P.; Roberts, J. M.; Burling, I. R.; Warneke, C.; de Gouw, J.; Yokelson, R. J. Measurements of Gas-Phase Inorganic and Organic Acids from Biomass Fires by Negative-Ion Proton-Transfer Chemical-Ionization Mass Spectrometry. *J. Geophys. Res. Atmos.* **2010**, *115*, D23302.

12. Desyaterik, Y.; Sun, Y.; Shen, X.; Lee, T.; Wang, X.; Wang, T.; Collett, J. L. Speciation of "Brown" Carbon in Cloud Water Impacted by Agricultural Biomass Burning in Eastern China. *J. Geophys. Res. Atmos.* **2013**, *118*, 7389-7399.

13. Latif, M. T.; Brimblecombe, P. Surfactants in Atmospheric Aerosols. *Environ. Sci. Technol.* **2004**, *38*, 6501-6506.

14. Dharaiya, N.; Bahadur, P. Phenol Induced Growth in Triton X-100 Micelles: Effect of pH and Phenols' Hydrophobicity. *Colloid Surf. A* **2012**, *410*, 81-90.

15. Guzman, M. I.; Athalye, R. R.; Rodriguez, J. M. Concentration Effects and Ion Properties Controlling the Fractionation of Halides During Aerosol Formation. *J. Phys. Chem. A* **2012**, *116*, 5428-5435.

16. Pillar, E. A.; Guzman, M. I.; Rodriguez, J. M. Conversion of Iodide to Hypoiodous Acid and Iodine in Aqueous Microdroplets Exposed to Ozone. *Environ. Sci. Technol.* **2013**, *47*, 10971-10979.

17. Kawamura, K.; Tachibana, E.; Okuzawa, K.; Aggarwal, S. G.; Kanaya, Y.; Wang, Z. F. High Abundances of Water-Soluble Dicarboxylic Acids, Ketocarboxylic Acids and α-

Dicarbonyls in the Mountaintop Aerosols over the North China Plain During Wheat Burning Season. *Atmos. Chem. Phys.* **2013**, *13*, 8285-8302.

18. Andreae, M. O.; Merlet, P. Emission of Trace Gases and Aerosols from Biomass Burning. *Glob. Biogeochem. Cycles* **2001**, *15*, 955-966.

19. Alves, C. A.; Gonçalves, C.; Pio, C. A.; Mirante, F.; Caseiro, A.; Tarelho, L.; Freitas, M. C.; Viegas, D. X. Smoke Emissions from Biomass Burning in a Mediterranean Shrubland. *Atmos. Environ.* **2010**, *44*, 3024-3033.

20. Parmar, R. S.; Satsangi, G. S.; Kumari, M.; Lakhani, A.; Srivastava, S. S.; Prakash, S. Study of Size Distribution of Atmospheric Aerosol at Agra. *Atmos. Environ.* **2001**, *35*, 693-702.

21. Paulot, F.; Jacob, D. J. Hidden Cost of U.S. Agricultural Exports: Particulate Matter from Ammonia Emissions. *Environ. Sci. Technol.* **2014**, *48*, 903-908.

22. Carlton, A. G.; Turpin, B. J.; Lim, H.-J.; Altieri, K. E.; Seitzinger, S. Link between Isoprene and Secondary Organic Aerosol (SOA): Pyruvic Acid Oxidation Yields Low Volatility Organic Acids in Clouds. *Geophys. Res. Lett.* **2006**, *33*, 06822.

23. Eugene, A. J.; Xia, S.-S.; Guzman, M. I. Aqueous Photochemistry of Glyoxylic Acid. *J. Phys. Chem. A* **2016**, *120*, 3817-3826.

24. Sander, S. P.; Abbatt, J.; Barker, J. R.; Burkholder, J. B.; Friedl, R. R.; Golden, D. M.; Huie, R. E.; Kolb, C. E.; Kurylo, M. J.; Moortgat, G. K.; Orkin, V. L.; Wine, P. H. Chemical Kinetics and Photochemical Data for Use in Atmospheric Studies: Evaluation Number 17 Jet Propulsion Laboratory, California Institute of Technology, Pasadena, CA, http://jpldataeval.jpl.nasa.gov: 2011.

25. Charbouillot, T.; Brigante, M.; Mailhot, G.; Maddigapu, P. R.; Minero, C.; Vione, D. Performance and Selectivity of the Terephthalic Acid Probe for OH as a Function of Temperature, pH and Composition of Atmospherically Relevant Aqueous Media. *J. Photoch. Photobiol. A* **2011**, *222*, 70-76.

26. Perrin, D. D.; Dempsey, B.; Serjeant, E. P. *pKa Prediction for Organic Acids and Bases*; Chapman and Hall: London, 1981. p 146.

27. Wishart, D. S.; Jewison, T.; Guo, A. C.; Wilson, M.; Knox, C.; Liu, Y.; Djoumbou, Y.; Mandal, R.; Aziat, F.; Dong, E.; Bouatra, S.; Sinelnikov, I.; Arndt, D.; Xia, J.; Liu, P.; Yallou, F.; Bjorndahl, T.; Perez-Pineiro, R.; Eisner, R.; Allen, F.; Neveu, V.; Greiner, R.; Scalbert, A. HMDB 3.0—the Human Metabolome Database in 2013. *Nucleic Acids Res.* **2013**, *41*, D801-D807.

28. Wishart, D. S.; Knox, C.; Guo, A. C.; Shrivastava, S.; Hassanali, M.; Stothard, P.; Chang, Z.; Woolsey, J. Drugbank: A Comprehensive Resource for in Silico Drug Discovery and Exploration. *Nucleic Acids Res.* **2006**, *34*, D668-D672.

29. *CRC Handbook of Chemistry and Physics*, 93rd ed.; CRC Press/Taylor and Francis: Boca Raton, Fl., **2013**, p 2664.

30. Zhu, X.-Q.; Wang, C.-H.; Liang, H. Scales of Oxidation Potentials, pK$_a$, and BDE of Various Hydroquinones and Catechols in DMSO. *J. Org. Chem.* **2010**, *75*, 7240-7257.

31. Steenken, S.; Neta, P. Electron Transfer Rates and Equilibriums between Substituted Phenoxide Ions and Phenoxyl Radicals. *J. Phys. Chem.* **1979**, *83*, 1134-1137.

32. Flyunt, R.; Leitzke, A.; Mark, G.; Mvula, E.; Reisz, E.; Schick, R.; von Sonntag, C. Determination of $^\bullet$OH, O$_2^{\bullet-}$, and Hydroperoxide Yields in Ozone Reactions in Aqueous Solution. *J. Phys. Chem. B* **2003**, *107*, 7242-7253.

33. Steenken, S.; Neta, P. Properties of Phenoxyl Radicals. In *The Chemistry of Phenols*, Rappoport, Z., Ed. John Wiley & Sons: New York, 2003; p 1000.

34. Elliot, A. J.; McCracken, D. R. Effect of Temperature on O$^{\bullet-}$ Reactions and Equilibria: A Pulse Radiolysis Study. *Rad. Phys. Chem.* **1989**, *33*, 69-74.

35. Buxton, G. V.; Greenstock, C. L.; Helman, W. P.; Ross, A. B. Critical Review of Rate Constants for Reactions of Hydrated Electrons, Hydrogen Atoms and Hydroxyl Radicals ($^\bullet$OH/$^\bullet$O$^-$) in Aqueous Solution. *J. Phys. Chem. Ref. Data* **1988**, *17*, 513-886.

36. Schwarzenbach, R. P.; Gschwend, P. M.; Imboden, D. M. *Environmental Organic Chemistry*, 2nd ed.; Wiley, **2005**. p 1328.

37. Olariu, R. I.; Barnes, I.; Becker, K. H.; Klotz, B. Rate Coefficients for the Gas-Phase Reaction of OH Radicals with Selected Dihydroxybenzenes and Benzoquinones. *Int. J. Chem. Kinet.* **2000**, *32*, 696-702.

38. Mvula, E.; von Sonntag, C. Ozonolysis of Phenols in Aqueous Solution. *Org. Biomol. Chem.* **2003**, *1*, 1749-1756.

39. Mvula, E.; Schuchmann, M. N.; von Sonntag, C. Reactions of Phenol-OH-Adduct Radicals. Phenoxyl Radical Formation by Water Elimination Vs. Oxidation by Dioxygen. *J. Chem. Soc. Perk. T. 2* **2001**, 264-268.

40. Adams, G. E.; Michael, B. D. Pulse Radiolysis of Benzoquinone and Hydroquinone. Semiquinone Formation by Water Elimination from Trihydroxy-Cyclohexadienyl Radicals. *T. Faraday Soc.* **1967**, *63*, 1171-1180.

41. von Sonntag, C.; von Gunten, U. *Chemistry of Ozone in Water and Wastewater Treatment: From Basic Principles to Applications*; IWA Publishing, 2012, p 302.

42. Iwaki, R.; Kamiya, I. Chemiluminescent Reaction between Polyphenols and Ozone in Acetic Acid. *B. Chem. Soc. Jpn.* **1969**, *42*, 855-863.

43. Guenther, A.; Jiang, X.; Heald, C. L.; Sakulyanontvittaya, T.; Duhl, T.; Emmons, L. K.; Wang, X. The Model of Emissions of Gases and Aerosols from Nature Version 2.1 (MEGAN2. 1): An Extended and Updated Framework for Modeling Biogenic Emissions. *Geosci. Model Dev.* **2012**, *5*, 1471-1492.

44. Saleh, R.; Adams, P. J.; Donahue, N. M.; Robinson, A. L. The Interplay between Assumed Morphology and the Direct Radiative Effect of Light-Absorbing Organic Aerosol. *Geophys. Res. Lett.* **2016**, *43*, 8735-8743.

45. Vione, D.; Maurino, V.; Minero, C.; Pelizzetti, E.; Harrison, M. A. J.; Olariu, R.-I.; Arsene, C. Photochemical Reactions in the Tropospheric Aqueous Phase and on Particulate Matter. *Chem. Soc. Rev.* **2006**, *35*, 441-453.

46. Xu, L.; Williams, L. R.; Young, D. E.; Allan, J. D.; Coe, H.; Massoli, P.; Fortner, E.; Chhabra, P.; Herndon, S.; Brooks, W. A.; Jayne, J. T.; Worsnop, D. R.; Aiken, A. C.; Liu, S.; Gorkowski, K.; Dubey, M. K.; Fleming, Z. L.; Visser, S.; Prevot, A. S. H.; Ng, N. L. Wintertime Aerosol Chemical Composition, Volatility, and Spatial Variability in the Greater London Area. *Atmos. Chem. Phys.* **2016**, *16*, 1139-1160.

5.7 Supporting Information For: Oxidation of Substituted Catechols at the Air-Water Interface: Production of Carboxylic Acids, Quinones, and Polyphenols

Content   **Page**

Justification of the pH Conditions Examined
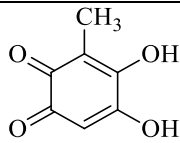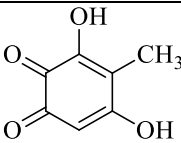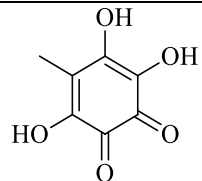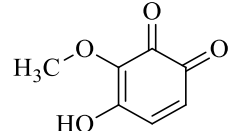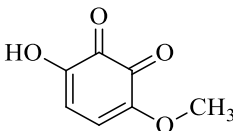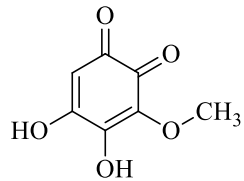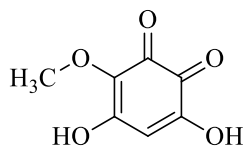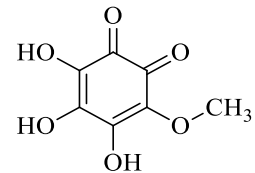
While the oxidations were explored in the atmospheric relevant pH range 5-10, reporting the results at pH 7.8 provides an example case that demonstrates the complexity of all the chemistry observed. Although many atmospheric studies are commonly aimed to reproduce highly acidic aerosol conditions, there is considerable evidence demonstrating that basic particles exist in the atmosphere. For example, particulate matter with a dimeter less than 2.5 μm ($PM_{2.5}$) collected in and around agricultural regions is predominately alkaline.[1, 2] Importantly, anthropogenic biomass burning emissions from agricultural practices (slash and burn, controlled burns, etc.) often coincide with increased ammonia (NH_3) emissions from livestock and fertilizers.[3, 4] Once these species are emitted to the atmosphere, they can effectively neutralize available nitric and sulfuric acids from industrial emissions.[5, 6] Recent work has shown that in most of the Midwest Region and the Pacific coast of the United States, where agriculture is a primary economic activity, NH_3 emissions are estimated to be sufficient to neutralize all acidic components.[2] Therefore, the experiments outlined are representative of true atmospheric conditions because even fine aerosols can be neutral or slightly basic. Indeed, for atmospheric particles occurring under the basic conditions described, a high ionic strength is expected due to presence of ammonium salts. Importantly, our work has demonstrated that for increasing ionic strength (e.g., for a series sodium halides) the solubility of gaseous ozone at the air-water interface is enhanced.[7] Therefore, for a higher dissolved ozone level, the probability for electron transfer induced $HO^\bullet$ production should also growth. In summary, the oxidation of the substituted catechols in aerosols with higher ionic strength is expected to also be enhanced.

Table S1. Complete List of Products Resulting from the Mechanism in Scheme 1 with Species Observed Indicated by their *m/z* Values

Parent	1st Generation	2nd Generation	*m/z⁻*	3rd Generation	*m/z⁻*	4th Generation	*m/z⁻*	5th Generation	*m/z*
Benzene	Phenol	Catechol	109	Pyrogallol	125	Tetrahydroxybenzenes	141	Pentahydroxybenzene	157
Toluene	o-Cresol	3-Methylcatechol	123	3-Methyl-4-hydroxycatechol	139	3-Methyl-4,5-dihydroxycatechol	155	Pentahydroxytoluene	171
Toluene	p-Cresol	4-Methylcatechol	123	4-Methylpyrogallol	139	5-Methyl-1,2,3,4-tetrahydroxybenzene	155		
				4-Methyl-5-hydroxycatechol	139	4-Methyl-3,5-dihydroxycatechol			
Anisole	Guaicol	3-Methoxycatechol	139	3-Methoxy-4-hydroxycatechol	155	3-Methoxy-4,5-dihydroxycatechol	171	Pentahydroxyanisole	187
			139	4-Methoxypyrogallol	155	4-Methoxy-5-hydroxypyrogallol	171		

Table S2. Produced Quinones and their Initial Precursors from Scheme 1.

m/z	Product 1	Product 2	Product 3	Precursor(s)
123	3-Hydroxy-*o*-quinone	4-Hydroxy-*o*-quinone		Catechol and Pyrogallol
139	3,4-Dihydroxy-*o*-quinone	3,6-Dihydroxy-*o*-quinone		Catechol and Pyrogallol
155	3,4,5-Trihydroxy-*o*-quinone	3,4,6-Trihydroxy-*o*-quinone		Catechol and Pyrogallol
121	4-methyl-*o*-quinone			4-Methylcatechol
137	3-methyl-4-hydroxy-*o*-quinone	4-methyl-3-hydroxy-*o*-quinone	4-methyl-5-hydroxy-*o*-quinone	3-Methylcatechol and 4-Methylcatechol

199

153	3-methyl-4,5-dihydroxy-*o*-quinone	4-methyl-3,5-dihydroxy-*o*-quinone	3-Methylcatechol and 4-Methylcatechol
171	4-methyl-3,5,6-trihydroxy-*o*-quinone		3-Methylcatechol and 4-Methylcatechol
153	3-methoxy-4-hydroxy-*o*-quinone	3-methoxyl-6-hydroxy-*o*-quinone	3-Methoxycatechol
169	3-methoxy-4,5-dihydroxy-*o*-quinone	3-methoxyl-4,6-dihydroxy-*o*-quinone	3-Methoxycatechol
185	3-methoxy-4,5,6-trihydroxy-*o*-quinone		3-Methoxycatechol

References

1. Parmar, R. S.; Satsangi, G. S.; Kumari, M.; Lakhani, A.; Srivastava, S. S.; Prakash, S. Study of Size Distribution of Atmospheric Aerosol at Agra. *Atmos. Environ.* **2001,** *35* (4), 693-702.

2. Paulot, F.; Jacob, D. J. Hidden Cost of U.S. Agricultural Exports: Particulate Matter from Ammonia Emissions. *Environ. Sci. Technol.* **2014,** *48* (2), 903-908.

3. Andreae, M. O.; Merlet, P. Emission of Trace Gases and Aerosols from Biomass Burning. *Glob. Biogeochem. Cycles* **2001,** *15* (4), 955-966.

4. Alves, C. A.; Gonçalves, C.; Pio, C. A.; Mirante, F.; Caseiro, A.; Tarelho, L.; Freitas, M. C.; Viegas, D. X. Smoke Emissions from Biomass Burning in a Mediterranean Shrubland. *Atmos. Environ.* **2010,** *44* (25), 3024-3033.

5. Carlton, A. G.; Turpin, B. J.; Lim, H.-J.; Altieri, K. E.; Seitzinger, S. Link between Isoprene and Secondary Organic Aerosol (SOA): Pyruvic Acid Oxidation Yields Low Volatility Organic Acids in Clouds. *Geophys. Res. Lett.* **2006,** *33* (6), 06822.

6. Eugene, A. J.; Xia, S.-S.; Guzman, M. I. Aqueous Photochemistry of Glyoxylic Acid. *J. Phys. Chem. A* **2016,** *120* (21), 3817-3826.

7. Pillar, E. A.; Guzman, M. I.; Rodriguez, J. M. Conversion of Iodide to Hypoiodous Acid and Iodine in Aqueous Microdroplets Exposed to Ozone. *Environ. Sci. Technol.* **2013,** *47* (19), 10971-10979.

Chapter 6. Conclusion and Future Directions

6.1 Synopsis

This chapter presents the integrated conclusion of the experimental work performed which includes three emerging common themes regardless of the reaction or phase under study. The first segment relates to how ozone is an important player in tropospheric chemistry by cycling radicals and other trace atmospheric species. The second section recounts how the oxidation of organic aerosols by trace species such as ozone can dramatically alter their composition while increasing hygroscopicity and ultraviolet/visible absorptivity. The last component integrates the use of advanced instrumentation and reactors to reveal mechanistic information of model aerosols in laboratory settings. Finally, some open questions that arose while undertaking this work and possible experimental routes to survey them are outlined.

6.2 Conclusion

The use of advanced instrumentation and reactors has enabled this work to push the boundaries of current knowledge about how aerosols undergo oxidation at atmospheric interfaces. Electrospray mass spectrometry has been a fundamental tool for studying surface chemistry by actually examining the structure of the interfacial region and reactions occurring in this boundary region.[1-3] The experiments studying the oxidation of iodide (Chapter 2), catechol (Chapter 3), and substituted catechols (Chapter 5) represent cutting edge measurements enabled by creating and validating a customized technique to observe the products of chemical aging at the air-water interface.[4-6] The use of FTIR,

202

mass spectrometry, and chromatography to characterize aerosol proxies reacting at the air-solid interface in experiments under variable humidity conditions relevant to the environment has been demonstrated (Chapter 4). The setup utilized a flow through reactor to provide the reactive uptake coefficient of ozone on catechol films (Chapter 4) under variable humidity conditions and elucidated the formation of biphenyl and terphenyl rings.[7] This detailed work will inspire future chamber and field studies to examine the product mixtures resulting from these mechanisms and for inclusion in the next generation of computational models to predict the effects of aerosols on climate.

Another commonality between these studies has been the selection of ozone as a potent tropospheric oxidizer. This secondary pollutant is formed through a series of gas phase reactions[8-10] and is available to oxidize several species as demonstrated in this dissertation. When O_3 reacts with I^- or substituted catechols, a wide range of reactive intermediates are produced alongside the oxidized products.[4-7] The generation of radicals can further propagate chain reactions through previously unexpected channels, as evidenced by the hydroxylation pathway observed during the ozonolysis of catechol.[5-7] Both inorganic and organic systems interacting with ozone reveal important insights for predicting how increasing tropospheric pollution could impact atmospheric composition. Elevated emissions of VOCs and NO_x in urban areas favor high O_3 levels, and thus impact the oxidation mechanism of aerosols surfaces.[10]

Finally, this thesis has shown how to design laboratory studies to collect and interpret data of oxidative aging contributions to the complexity of organic aerosols. Aerosol and cloud water samples collected on different geographical location often display similarities in composition despite significant differences in parent species.[11-14] The mechanisms

presented in this thesis explain the processing of different organic atmospheric precursors, which are found in both biomass burning[15] and anthropogenic emissions,[16] likely proceed through similar pathways.[5-7] These studies have demonstrated how oxy-aromatics can generate a rich product mixture that absorbs more light, form better nuclei to form clouds, and partition into clouds easily.[5-7] The experiments in Chapters 3 and 4 established that the absorptivity of oxidative products grows in the visible region both in films and aqueous solutions, contributing to the "browning" of aerosols during the aging process.[17] The highly oxidized products contain carboxylic acid and hydroxyl moieties that justify the extremely hygroscopic nature of this class of aerosols from aromatic precursors.[18, 19] These products easily partition into cloud waters and serve as precursors to the formation of humic-like materials.[20, 21]

6.3 Future Directions

While the work presented in this dissertation significantly advanced the understanding of how the aging of aerosols by O_3, $HO^\bullet$, and H_2O_2 proceeds at interfaces through utilizing conventional methodologies in new ways, some new questions that deserve further investigation have emerged. For instance, it would be informative to further investigate how organic surfactants and molecules coating the exterior of aerosol particles affect the distribution of and identity of products observed in Chapter 2.[22] Future experiments should these organic moieties will interact with large species, such as I_2, that tend to salt out towards the interface.[1] Dissolved organic matter extracted from coastal seawater samples as well as long saturated organic acids can enhance I_2 production by donating protons to the interfacial region and thus favor the triiodide channel.[23, 24]

Solutions containing equimolar amounts of NaI and organics can be injected in the reactor described in Chapter 2 to analyze if there is an enhancement of I_2 production. It is anticipated that several optimizations of the setup are needed to determine the ideal ratio of organic to iodide, working temperature, pH, etc.

In Chapters 3 and 4, the presented work proposed that Baeyer-Villager (BV) oxidation of unsaturated dicarboxylic acids generated some of the unexpected oxo- and carboxylic acids observed[5, 7] during the oxidation of benzenediols in water.[25, 26] While the production of H_2O_2 and sequential losses of CO_2 from the carbon chain are strong indicators of this chemistry, it would be interesting to tackle this experimentally in the future. A set up could be devised to detect CO_2 and to provide additional support for the BV chemistry proposed. In order to monitor the evolution of CO_2 and other volatile species that might be produced from BV chemistry and escape into the gas phase, an infrared gas cell could be utilized. This approach would provide additional validation of the proposed BV pathway that was unable to be achieved with mass spectrometry studies.

In Chapter 4, the effect of relative humidity on the reactive uptake coefficient was examined at ~ 24 ppmv O_3. While this can underscore the role water is playing in facilitating the reaction with ozone on the surface, it does not provide information about the kind of adsorption mechanism. The interaction between a gas and analytes on the surface of an aerosol can be described via different adsorption mechanisms, resulting in a different set of rate laws and adsorption isotherms to describe the scenario. In the case of the reaction between ozone and catechol, there two possible descriptions of the heterogeneous reaction at the air-solid interface. In the first of these, the Langmuir-Hinshelwood mechanism, ozone would be adsorbed on the surface of the film and then

react with catechol.[27] In the Eley-Rideal mechanism, gas-phase ozone would react with catechol, forming adsorbed products directly. In both cases, gas-phase products can be desorbed afterwards and monitored in the infrared.[27]

Based on the principles of the Langmuir-Hinshelwood mechanism, it is expected that at low ozone concentrations the reaction rate should be directly proportional to [O$_3$] × [catechol].[28] If the surface available sites are saturated with ozone and ozone concentration keeps increasing, the reaction rate (k_I) should eventually level off to a maximum value (k_{max}^I). The values of k_{max}^I, k_I, ozone gas to surface equilibrium constant (K_{O_3}), thermal velocity of ozone, and ozone concentration can then be utilized to construct a relationship between ozone concentration and apparent reactive uptake (γ). This information would be extremely useful for predicting the uptake of ozone by catechol thin films under environmentally relevant concentrations that aerosols would encounter during transport. Efforts to examine if film composition and morphology is being impacted as a function of [O$_3$] under variable relative humidity would also be important.

When working with *o*-cresols and their derivatives such as methylcatechols, they can undergo two electron oxidations to form highly reactive species called quinone methides. A two electron oxidation can transform the alcohol and methyl substituents into a carbonyl and a methide respectively. This structure is highly unstable and is expected to react with water to create a primary alcohol,[29] suggesting that methides have not been the species detected in Chapter 5 despite having the same mass as the first hydroxylation product, 4-methylpyrogallol. An interesting experiment could utilize deuterium-labeled

methyl groups of the methylcatechols to check if a quinone methide is being formed with the loss of one deuterium atom that can be easily registered as a mass shift.

Other advancements in mass spectrometry could further enhance the experimental capabilities of systems that were explored in the laboratory. Aerosol mass spectrometry (AMS) was developed for real-time field and laboratory characterization of aerosol particles.[30] Briefly, particles are pumped from the environment or aerosol chamber into an ion trap where they are collected and held by an electromagnetic field until they are injected into an ionization chamber interfaced to a time-of-flight mass spectrometer. However, this instrument can suffer losses of information regarding the original aerosol constituents because of thermal degradation from the thermal desorption used to vaporization or extreme fragmentation imparted from hard ionization sources, such as electron impact.[31] Some work has been done to develop programs and computer algorithms to analyze the fragmentation patterns[32] produced by this type of instrument as well as to distinguish between isomeric fragments and different functional groups,[31] but it would be difficult to glean mechanistic data from this approach. So it might be worthwhile to develop an aerosol mass spectrometer that could permit the *in situ* generation of aerosols that can be captured by an ion trap, oxidized, and then later ionized and analyzed by mass spectrometry. Ion traps used for aerosol studies can be placed prior to soft ionization sources, such as electrospray, so that the structure of constituents is retained during analysis.[33] This could be a worthy investment to study processes discussed in earlier chapters over longer time scales.

While many experiments could be outlined here to address the open questions, many other challenges remain. The development of new methods, instrumentation, and

laboratory studies to investigate atmospheric interfaces is a rich research area capable of

bearing fruits for many years to come.

6.4 References

1. Guzman, M. I.; Athalye, R. R.; Rodriguez, J. M. Concentration Effects and Ion Properties Controlling the Fractionation of Halides During Aerosol Formation. *J. Phys. Chem. A* **2012,** *116* (22), 5428-5435.

2. Enami, S.; Hoffmann, M. R.; Colussi, A. J. How Phenol and α-Tocopherol React with Ambient Ozone at Gas/Liquid Interfaces. *J. Phys. Chem. A* **2009,** *113* (25), 7002-7010.

3. Enami, S.; Vecitis, C. D.; Cheng, J.; Hoffmann, M. R.; Colussi, A. J. Global Inorganic Source of Atmospheric Bromine. *J. Phys. Chem. A* **2007,** *111* (36), 8749-8752.

4. Pillar, E. A.; Guzman, M. I.; Rodriguez, J. M. Conversion of Iodide to Hypoiodous Acid and Iodine in Aqueous Microdroplets Exposed to Ozone. *Environ. Sci. Technol.* **2013,** *47* (19), 10971-10979.

5. Pillar, E. A.; Camm, R. C.; Guzman, M. I. Catechol Oxidation by Ozone and Hydroxyl Radicals at the Air–Water Interface. *Environ. Sci. Technol.* **2014,** *48* (24), 14352-14360.

6. Pillar, E. A.; Guzman, M. I. Oxidation of Substituted Catechols at the Air–Water Interface: Production of Carboxylic Acids, Quinones, and Polyphenols. *Environ. Sci. Technol.* **2017,** *51*, 4951-4959.

7. Pillar, E. A.; Zhou, R.; Guzman, M. I. Heterogeneous Oxidation of Catechol. *J.Phys. Chem. A* **2015,** *119* (41), 10349-10359.

8. Monks, P. S.; Archibald, A. T.; Colette, A.; Cooper, O.; Coyle, M.; Derwent, R.; Fowler, D.; Granier, C.; Law, K. S.; Mills, G. E.; Stevenson, D. S.; Tarasova, O.; Thouret, V.; von Schneidemesser, E.; Sommariva, R.; Wild, O.; Williams, M. L. Tropospheric Ozone and Its Precursors from the Urban to the Global Scale from Air Quality to Short-Lived Climate Forcer. *Atmos. Chem. Phys.* **2015,** *15* (15), 8889-8973.

9. Sillman, S. The Relation between Ozone, NO_x and Hydrocarbons in Urban and Polluted Rural Environments. *Atmos. Environ.* **1999,** *33* (12), 1821-1845.

10. Atkinson, R. Atmospheric Chemistry of VOCs and NO_x. *Atmos. Environ.* **2000,** *34* (12), 2063-2101.

11. Desyaterik, Y.; Sun, Y.; Shen, X.; Lee, T.; Wang, X.; Wang, T.; Collett, J. L. Speciation of "Brown" Carbon in Cloud Water Impacted by Agricultural Biomass Burning in Eastern China. *J. Geophys. Res. Atmos.* **2013,** *118* (13), 7389-7399.

12. Kanakidou, M.; Seinfeld, J. H.; Pandis, S. N.; Barnes, I.; Dentener, F. J.; Facchini, M. C.; Van Dingenen, R.; Ervens, B.; Nenes, A.; Nielsen, C. J.; Swietlicki, E.; Putaud, J. P.; Balkanski, Y.; Fuzzi, S.; Horth, J.; Moortgat, G. K.; Winterhalter, R.; Myhre, C. E. L.; Tsigaridis, K.; Vignati, E.; Stephanou, E. G.; Wilson, J. Organic Aerosol and Global Climate Modelling: A Review. *Atmos. Chem. Phys.* **2005,** *5* (4), 1053-1123.

13. Kawamura, K.; Tachibana, E.; Okuzawa, K.; Aggarwal, S. G.; Kanaya, Y.; Wang, Z. F. High Abundances of Water-Soluble Dicarboxylic Acids, Ketocarboxylic Acids and α-Dicarbonyls in the Mountaintop Aerosols over the North China Plain During Wheat Burning Season. *Atmos. Chem. Phys.* **2013,** *13* (16), 8285-8302.

14. Hoque, M.; Kawamura, K.; Seki, O.; Hoshi, N. Spatial Distributions of Dicarboxylic Acids, ω-Oxoacids, Pyruvic Acid and α-Dicarbonyls in the Remote Marine Aerosols over the North Pacific. *Mar. Chem.* **2015,** *172*, 1-11.

15. Veres, P.; Roberts, J. M.; Burling, I. R.; Warneke, C.; de Gouw, J.; Yokelson, R. J. Measurements of Gas-Phase Inorganic and Organic Acids from Biomass Fires by Negative-Ion Proton-Transfer Chemical-Ionization Mass Spectrometry. *J. Geophys. Res. Atmos.* **2010,** *115*, D23302.

16. Henze, D. K.; Seinfeld, J. H.; Ng, N. L.; Kroll, J. H.; Fu, T. M.; Jacob, D. J.; Heald, C. L. Global Modeling of Secondary Organic Aerosol Formation from Aromatic Hydrocarbons: High- vs. Low-Yield Pathways. *Atmos. Chem. Phys.* **2008,** *8* (9), 2405-2420.

17. Andreae, M. O.; Gelencsér, A. Black Carbon or Brown Carbon? The Nature of Light-Absorbing Carbonaceous Aerosols. *Atmos. Chem. Phys.* **2006,** *6* (10), 3131-3148.

18. Liu, J.; Li, Z. Estimation of Cloud Condensation Nuclei Concentration from Aerosol Optical Quantities: Influential Factors and Uncertainties. *Atmos. Chem. Phys.* **2014,** *14* (1), 471-483.

19. Kravitz, B.; Wang, H.; Rasch, P. J.; Morrison, H.; Solomon, A. B. Process-Model Simulations of Cloud Albedo Enhancement by Aerosols in the Arctic. *Phil. Trans. R. Soc. A* **2014,** *372* (2031).

20. Lin, P.; Engling, G.; Yu, J. Z. Humic-Like Substances in Fresh Emissions of Rice Straw Burning and in Ambient Aerosols in the Pearl River Delta Region, China. *Atmos. Chem. Phys.* **2010,** *10* (14), 6487-6500.

21. Hoffer, A.; Gelencsér, A.; Guyon, P.; Kiss, G.; Schmid, O.; Frank, G. P.; Artaxo, P.; Andreae, M. O. Optical Properties of Humic-Like Substances (Hulis) in Biomass-Burning Aerosols. *Atmos. Chem. Phys.* **2006,** *6* (11), 3563-3570.

22. You, Y.; Renbaum-Wolff, L.; Carreras-Sospedra, M.; Hanna, S. J.; Hiranuma, N.; Kamal, S.; Smith, M. L.; Zhang, X.; Weber, R. J.; Shilling, J. E.; Dabdub, D.; Martin, S. T.; Bertram, A. K. Images Reveal That Atmospheric Particles Can Undergo Liquid–Liquid Phase Separations. *Proc. Natl. Acad. Sci.* **2012,** *109* (33), 13188-13193.

23. Shaw, M. D.; Carpenter, L. J. Modification of Ozone Deposition and I_2 Emissions at the Air–Aqueous Interface by Dissolved Organic Carbon of Marine Origin. *Environ. Sci. Technol.* **2013,** *47* (19), 10947-10954.

24. Hayase, S.; Yabushita, A.; Kawasaki, M.; Enami, S.; Hoffmann, M. R.; Colussi, A. J. Weak Acids Enhance Halogen Activation on Atmospheric Water's Surfaces. *J. Phys. Chem. A* **2011,** *115* (19), 4935-4940.

25. von Sonntag, C.; von Gunten, U., *Chemistry of Ozone in Water and Wastewater Treatment*. IWA Publishing: 2012; p 302.

26. Mvula, E.; von Sonntag, C. Ozonolysis of Phenols in Aqueous Solution. *Org. Biomol. Chem.* **2003,** *1* (10), 1749-1756.

27. Grassian, V. H., *Environmental Catalysis*. Taylor & Francis: New York, 2005; p 701.

28. Steinfeld, J. I.; Francisco, J. S.; Hase, W. L., *Chemical Kinetics and Dynamics*. 2nd ed.; Prentice Hall Engelwood Cliffs, New Jersey, 1989; p 560.

29. Sugumaran, M. Reactivities of Quinone Methides versus *o*-Quinones in Catecholamine Metabolism and Eumelanin Biosynthesis. *Int. J. Mol. Sci.* **2016,** *17* (9), 1576-1599.

30. Jayne, J. T.; Leard, D. C.; Zhang, X.; Davidovits, P.; Smith, K. A.; Kolb, C. E.; Worsnop, D. R. Development of an Aerosol Mass Spectrometer for Size and Composition Analysis of Submicron Particles. *Aerosol Sci. Technol.* **2000,** *33* (1-2), 49-70.

31. Fachinger, J. R. W.; Gallavardin, S. J.; Helleis, F.; Fachinger, F.; Drewnick, F.; Borrmann, S. The Ion Trap Aerosol Mass Spectrometer: Field Intercomparison with the TOF-AMS and the Capability of Differentiating Organic Compound Classes Via MS-MS. *Atmos. Meas. Tech.* **2017,** *10* (4), 1623-1637.

32. Allan, J. D.; Delia, A. E.; Coe, H.; Bower, K. N.; Alfarra, M. R.; Jimenez, J. L.; Middlebrook, A. M.; Drewnick, F.; Onasch, T. B.; Canagaratna, M. R.; Jayne, J. T.; Worsnop, D. R. A Generalised Method for the Extraction of Chemically Resolved Mass Spectra from Aerodyne Aerosol Mass Spectrometer Data. *J. Aerosol Sci.* **2004,** *35* (7), 909-922.

33. Vogel, A. L.; Äijälä, M.; Brüggemann, M.; Ehn, M.; Junninen, H.; Petäjä, T.; Worsnop, D. R.; Kulmala, M.; Williams, J.; Hoffmann, T. Online Atmospheric Pressure Chemical Ionization Ion Trap Mass Spectrometry (APCI-IT-Ms^n) for Measuring Organic Acids in Concentrated Bulk Aerosol - a Laboratory and Field Study. *Atmos. Meas. Tech.* **2013,** *6* (2), 431-443.

BIBLIOGRAPHY

Adams, G. E.; Michael, B. D. Pulse Radiolysis of Benzoquinone and Hydroquinone. Semiquinone Formation by Water Elimination from Trihydroxy-Cyclohexadienyl Radicals. *T. Faraday Soc.* **1967**, *63*, 1171-1180.

Adounkpe, J.; Aina, M.; Mama, D.; Sinsin, B. Gas Chromatography Mass Spectrometry Identification of Labile Radicals Formed During Pyrolysis of Catechol, Hydroquinone, and Phenol through Neutral Pyrolysis Product Mass Analysis. *ISRN Environ. Chem.* **2013**, *2013*, Article ID 930573, 1-8.

Albrecht, B. A. Aerosols, Cloud Microphysics, and Fractional Cloudiness. *Science* **1989**, *245* (4923), 1227-1230.

Alexander, B.; Park, R. J.; Jacob, D. J.; Li, Q. B.; Yantosca, R. M.; Savarino, J.; Lee, C. C. W.; Thiemens, M. H. Sulfate Formation in Sea-Salt Aerosols: Constraints from Oxygen Isotopes. *J. Geophys. Res. Atmos.* **2005**, *110* (D10), D10307.

Allan, J. D.; Delia, A. E.; Coe, H.; Bower, K. N.; Alfarra, M. R.; Jimenez, J. L.; Middlebrook, A. M.; Drewnick, F.; Onasch, T. B.; Canagaratna, M. R.; Jayne, J. T.; Worsnop, D. R. A Generalised Method for the Extraction of Chemically Resolved Mass Spectra from Aerodyne Aerosol Mass Spectrometer Data. *J. Aerosol Sci.* **2004,** *35* (7), 909-922.

Alves, C. A.; Gonçalves, C.; Pio, C. A.; Mirante, F.; Caseiro, A.; Tarelho, L.; Freitas, M. C.; Viegas, D. X. Smoke Emissions from Biomass Burning in a Mediterranean Shrubland. *Atmos. Environ.* **2010**, *44*, 3024-3033.

AMAP. *The Impact of Black Carbon on the Arctic Climate*; Arctic Monitoring and Assessment Programme (AMAP): Oslo, 2011.

Ammann, M.; Klimont, Z.; Wagner, F. Regional and Global Emissions of Air Pollutants: Recent Trends and Future Scenarios. *Annu. Rev. Environ. Resour.* **2013**, *38* (1), 31-55.

Ammann, M.; Pöschl, U. Kinetic Model Framework for Aerosol and Cloud Surface Chemistry and Gas-Particle Interactions - Part 2: Exemplary Practical Applications and Numerical Simulations. Atmos. Chem. Phys. 2007, 7 (23), 6025-6045.

Andreae, M. O. Aerosols before Pollution. *Science* **2007**, *315* (5808), 50-51.

Andreae, M. O.; Gelencsér, A. Black Carbon or Brown Carbon? The Nature of Light-Absorbing Carbonaceous Aerosols. *Atmos. Chem. Phys*. **2006**, *6* (10), 3131-3148.

Andreae, M. O.; Merlet, P. Emission of Trace Gases and Aerosols from Biomass Burning. *Glob. Biogeochem. Cycles* **2001**, *15*, 955-966.

Arangio, A. M.; Slade, J. H.; Berkemeier, T.; Pöschl, U.; Knopf, D. A.; Shiraiwa, M. Multiphase Chemical Kinetics of OH Radical Uptake by Molecular Organic Markers of

Biomass Burning Aerosols: Humidity and Temperature Dependence, Surface Reaction, and Bulk Diffusion. *J. Phys. Chem. A* **2015**, *119* (19), 4533-4544.

Atkins, P.; de Paula, J. *Elements of Physical Chemistry*, 6th ed.; W. H. Freeman: New York, 2013, p 630.

Atkinson, R. Atmospheric Chemistry of VOCs and NO_x. *Atmos. Environ.* **2000,** *34* (12), 2063-2101.

Atkinson, R.; Arey, J. Atmospheric Degradation of Volatile Organic Compounds. *Chem. Rev.* **2003**, *103* (12), 4605-4638.

Atkinson, R.; Aschmann, S. M. Rate Constants for the Gas-Phase Reactions of the OH Radical with the Cresols and Dimethylphenols at $296 \pm 2K$. *Int. J. Chem. Kinet.* **1990**, *22*, 59-67.

Augugliaro, V.; Rizzuti, L. The pH Dependence of the Ozone Absorption Kinetics in Aqueous Phenol Solutions. *Chem. Eng. Sci.* **1978**, *33*, 1441-1447.

Bailey, P. S. *Ozonation in Organic Chemistry*; Academic Press: New York, 1982; Vol. 2. p 272.

Barnum, T. J.; Medeiros, N.; Hinrichs, R. Z. Condensed-Phase versus Gas-Phase Ozonolysis of Catechol: A Combined Experimental and Theoretical Study. *Atmos. Environ.* **2012**, *55*, 98-106.

Barrie, L. A.; Bottenheim, J. W.; Schnell, R. C.; Crutzen, P. J.; Rasmussen, R. A. Ozone Destruction and Photochemical Reactions at Polar Sunrise in the Lower Arctic Atmosphere. *Nature* **1988,** *334* (6178), 138-141.

Barsanti, K. C.; Pankow, J. F. Thermodynamics of the Formation of Atmospheric Organic Particulate Matter by Accretion Reactions—Part 1: Aldehydes and Ketones. Atmos. Environ. **2004**, 38 (26), 4371-4382.

Benson, S. W. *The Foundations of Chemical Kinetics*. McGraw-Hill: New York, 1960; p 736.

Bertram, T. H.; Thornton, J. A.; Riedel, T. P. An Experimental Technique for the Direct Measurement of N_2O_5 Reactivity on Ambient Particles. *Atmos. Meas. Tech.* **2009**, *2* (1), 231-242.

Bhattacharyya, I.; Maze, J. T.; Ewing, G. E.; Jarrold, M. F. Charge Separation from the Bursting of Bubbles on Water. *J. Phys. Chem. A* **2011,** *115* (23), 5723-5728.

Bichsel, Y.; von Gunten, U. Hypoiodous Acid: Kinetics of the Buffer-Catalyzed Disproportionation. *Water Res.* **2000,** *34* (12), 3197-3203.

Bichsel, Y.; von Gunten, U. Oxidation of Iodide and Hypoiodous Acid in the Disinfection of Natural Waters. *Environ. Sci. Technol.* **1999,** *33* (22), 4040-4045.

Bielski, B. H. J.; Cabelli, D. E.; Arudi, R. L.; Ross, A. B. Reactivity of HO_2/O_2^- Radicals in Aqueous Solution. *J. Phys. Chem. Ref. Data* **1985**, *14*, 1041-1100.

Blanchard, D. C. Electrically Charged Drops from Bubbles in Sea Water and Their Meteorological Significance. *J. Meteorology* **1958,** *15* (4), 383-396.

Bond, T. C. Spectral Dependence of Visible Light Absorption by Carbonaceous Particles Emitted from Coal Combustion. *Geophys. Res. Lett.* **2001**, *28* (21), 4075-4078.

Boucher, O.; Randall, D.; Artaxo, P.; Bretherton, C.; Feingold, G.; Forster, P.; Kerminen, V.-M.; Kondo, Y.; Liao, H.; Lohmann, U.; Rasch, P.; Satheesh, S. K.; Sherwood, S.; Stevens, B.; Zhang, X. Y., Clouds and Aerosols. In *Climate Change 2013: The Physical Science Basis. Contribution of Working Group I to the Fifth Assessment Report of the Intergovernmental Panel on Climate Change*, Stocker, T. F.; Qin, D.; Plattner, G.-K.; Tignor, M.; Allen, S. K.; Boschung, J.; Nauels, A.; Xia, Y.; Bex, V.; Midgley, P. M., Eds. Cambridge University Press: Cambridge, United Kingdom and New York, NY, USA, 2013; pp 571–658.

Bratsch, S. G. Standard Electrode Potentials and Temperature Coefficients in Water at 298.15 K. *J. Phys. Chem. Ref. Data* **1989,** *18* (1), 1-21.

Brook, R. D.; Rajagopalan, S. Particulate Matter, Air Pollution, and Blood Pressure. *J. Am. Soc. Hypertens.* **2009**, *3* (5), 332-350.

Buxton, G. V.; Greenstock, C. L.; Helman, W. P.; Ross, A. B. Critical Review of Rate Constants for Reactions of Hydrated Electrons, Hydrogen Atoms and Hydroxyl Radicals ($^•OH/^•O^-$) in Aqueous Solution. *J. Phys. Chem. Ref. Data* **1988**, *17*, 513-886.

Caloz, F.; Fenter, F. F.; Tabor, K. D.; Rossi, M. J. Paper I: Design and Construction of a Knudsen-Cell Reactor for the Study of Heterogeneous Reactions over the Temperature Range 130–750 K: Performances and Limitations. *Rev. Sci. Instrum.* **1997**, *68* (8), 3172-3179.

Calvert, J. G.; Atkinson, R.; Becker, K. H.; Kamens, R. M.; Seinfeld, J. H.; Wallington, T. J.; Yarwood, G. *The Mechanisms of Atmospheric Oxidation of the Aromatic Hydrocarbons*; Oxford University Press: New York, USA, 2002, p 566.

Canagaratna, M. R.; Jayne, J. T.; Jimenez, J. L.; Allan, J. D.; Alfarra, M. R.; Zhang, Q.; Onasch, T. B.; Drewnick, F.; Coe, H.; Middlebrook, A.; Delia, A.; Williams, L. R.; Trimborn, A. M.; Northway, M. J.; DeCarlo, P. F.; Kolb, C. E.; Davidovits, P.; Worsnop, D. R. Chemical and Microphysical Characterization of Ambient Aerosols with the Aerodyne Aerosol Mass Spectrometer. *Mass Spectrom. Rev.* **2007**, *26* (2), 185-222.

Canonica, S.; Kohn, T.; Mac, M.; Real, F. J.; Wirz, J.; von Gunten, U. Photosensitizer Method to Determine Rate Constants for the Reaction of Carbonate Radical with Organic Compounds. *Environ. Sci. Technol.* **2005**, *39* (23), 9182-9188.

Cappa, C. D.; Che, D. L.; Kessler, S. H.; Kroll, J. H.; Wilson, K. R. Variations in Organic Aerosol Optical and Hygroscopic Properties Upon Heterogeneous OH Oxidation. *J. Geophys. Res. Atmos.* **2011**, *116* (D15), D15204.

Carlton, A. G.; Turpin, B. J.; Lim, H.-J.; Altieri, K. E.; Seitzinger, S. Link between Isoprene and Secondary Organic Aerosol (SOA): Pyruvic Acid Oxidation Yields Low Volatility Organic Acids in Clouds. *Geophys. Res. Lett.* **2006**, *33*, 06822.

Carpenter, L. J.; Hopkins, J. R.; Jones, C. E.; Lewis, A. C.; Parthipan, R.; Wevill, D. J.; Poissant, L.; Pilote, M.; Constant, P. Abiotic Source of Reactive Organic Halogens in the Sub-Arctic Atmosphere? *Environ. Sci. Technol.* **2005,** *39* (22), 8812-8816.

Carpenter, L. J.; MacDonald, S. M.; Shaw, M. D.; Kumar, R.; Saunders, R. W.; Parthipan, R.; Wilson, J.; Plane, J. M. C. Atmospheric Iodine Levels Influenced by Sea Surface Emissions of Inorganic Iodine. *Nature Geosci.* **2013**, *6* (2), 108-111.

Chan, A. W. H.; Kroll, J. H.; Ng, N. L.; Seinfeld, J. H. Kinetic Modeling of Secondary Organic Aerosol Formation: Effects of Particle- and Gas-Phase Reactions of Semivolatile Products. *Atmos. Chem. Phys.* **2007**, *7* (15), 4135-4147.

Charbouillot, T.; Brigante, M.; Mailhot, G.; Maddigapu, P. R.; Minero, C.; Vione, D. Performance and Selectivity of the Terephthalic Acid Probe for OH as a Function of Temperature, pH and Composition of Atmospherically Relevant Aqueous Media. *J. Photoch. Photobiol. A* **2011**, *222*, 70-76.

Cheng, J.; Hoffmann, M. R.; Colussi, A. J. Anion Fractionation and Reactivity at Air/Water:Methanol Interfaces. Implications for the Origin of Hofmeister Effects. *J. Phys. Chem. B* **2008,** *112* (24), 7157-7161.

Cheng, J.; Vecitis, C. D.; Hoffmann, M. R.; Colussi, A. J. Experimental Anion Affinities for the Air/Water Interface. *J. Phys. Chem. B* **2006,** *110* (51), 25598-25602.

Chung, C. E.; Ramanathan, V.; Decremer, D. Observationally Constrained Estimates of Carbonaceous Aerosol Radiative Forcing. *Proc. Natl. Acad. Sci.* **2012**, *109* (29), 11624-11629.

Cody, R. B. Electrospray Ionization Mass Spectrometry: History, Theory, and Instrumentation. In *Applied Electrospray Mass Spectrometry*, 1st ed.; Pramanik, B. N.; Ganguly, A. K.; Gross, M. L., Eds. Taylor & Francis: New York, 2002; p 464.

CRC Handbook of Chemistry and Physics. 93rd ed.; CRC Press/Taylor and Francis: Boca Raton, Fl., **2013**; p 2664.

Criegee, R. Mechanism of Ozonolysis. *Angew. Chem. Int. Ed.* **1975**, *14*, 745-752.

Crowley, J. N.; Ammann, M.; Cox, R. A.; Hynes, R. G.; Jenkin, M. E.; Mellouki, A.; Rossi, M. J.; Troe, J.; Wallington, T. J. Evaluated Kinetic and Photochemical Data for Atmospheric Chemistry: Volume V – Heterogeneous Reactions on Solid Substrates. *Atmos. Chem. Phys.* **2010**, *10* (18), 9059-9223.

Davidovits, P.; Kolb, C. E.; Williams, L. R.; Jayne, J. T.; Worsnop, D. R. Update 1 Of: Mass Accommodation and Chemical Reactions at Gas−Liquid Interfaces. *Chem. Rev.* **2011**, *111* (4).

Davidovits, P.; Worsnop, D. R.; Jayne, J. T.; Kolb, C. E.; Winkler, P.; Vrtala, A.; Wagner, P. E.; Kulmala, M.; Lehtinen, K. E. J.; Vesala, T.; Mozurkewich, M. Mass Accommodation Coefficient of Water Vapor on Liquid Water. *Geophys. Res. Lett.* **2004**, *31* (L22), L22111.

DeCarlo, P. F.; Kimmel, J. R.; Trimborn, A. M.; Northway, M. J.; Jayne, J. T.; Aiken, A. C.; Gonin, M.; Fuhrer, K.; Horvath, T.; Docherty, K. S.; Worsnop, D. R.; Jimenez, J. L. Field-Deployable, High-Resolution, Time-of-Flight Aerosol Mass Spectrometer. *Anal. Chem.* **2006**, *78* (24), 8281-8289.

Denman, K. L.; Brasseur, G.; Chidthaisong, A.; Ciais, P.; Cox, P. M.; Dickinson, R. E.; Hauglustaine, D.; Heinze, C.; Holland, E.; Jacob, D.; Lohmann, U.; Ramachandran, S.; da Silva Dias, P. L.; S.C.;, W.; Zhang, X., Couplings between Changes in the Climate System and Biogeochemistry. In *Climate Change 2007: The Physical Science Basis. Contribution of Working Group I to the Fourth Assessment Report of the Intergovernmental Panel on Climate Change*, Solomon, S.; Qin, D.; Manning, M.; Chen, Z.; Marquis, M.; Averyt, K. B.; Tignor, M.; Miller, H. L., Eds. Cambridge University Press: Cambridge, United Kingdom and New York, NY, USA, 2007.

Desyaterik, Y.; Sun, Y.; Shen, X.; Lee, T.; Wang, X.; Wang, T.; Collett, J. L. Speciation of "Brown" Carbon in Cloud Water Impacted by Agricultural Biomass Burning in Eastern China. *J. Geophys. Res. Atmos.* **2013**, *118*, 7389-7399.

Doherty, R. M.; Wild, O.; Shindell, D. T.; Zeng, G.; MacKenzie, I. A.; Collins, W. J.; Fiore, A. M.; Stevenson, D. S.; Dentener, F. J.; Schultz, M. G.; Hess, P.; Derwent, R. G.; Keating, T. J. Impacts of Climate Change on Surface Ozone and Intercontinental Ozone Pollution: A Multi-Model Study. *J. Geophys. Res. Atmos.* **2013**, *118* (9), 3744-3763.

Docherty, K. S.; Ziemann, P. J. Reaction of Oleic Acid Particles with NO_3 Radicals: Products, Mechanism, and Implications for Radical-Initiated Organic Aerosol Oxidation. *J. Phys. Chem. A* **2006**, *110* (10), 3567-3577.

Dharaiya, N.; Bahadur, P. Phenol Induced Growth in Triton X-100 Micelles: Effect of pH and Phenols' Hydrophobicity. *Colloid Surf. A* **2012**, *410*, 81-90.

Ding, F.; Hu, Z.; Zhong, Q.; Manfred, K.; Gattass, R. R.; Brindza, M. R.; Fourkas, J. T.; Walker, R. A.; Weeks, J. D. Interfacial Organization of Acetonitrile: Simulation and Experiment. *J. Phys. Chem. C* **2010,** *114* (41), 17651-17659.

Dubowski, Y.; Vieceli, J.; Tobias, D. J.; Gomez, A.; Lin, A.; Nizkorodov, S. A.; McIntire, T. M.; Finlayson-Pitts, B. J. Interaction of Gas-Phase Ozone at 296 K with Unsaturated Self-Assembled Monolayers: A New Look at an Old System. *J. Phys. Chem. A* **2004**, *108*, 10473-10485.

Duplissy, J.; DeCarlo, P. F.; Dommen, J.; Alfarra, M. R.; Metzger, A.; Barmpadimos, I.; Prevot, A. S. H.; Weingartner, E.; Tritscher, T.; Gysel, M.; Aiken, A. C.; Jimenez, J. L.; Canagaratna, M. R.; Worsnop, D. R.; Collins, D. R.; Tomlinson, J.; Baltensperger, U. Relating Hygroscopicity and Composition of Organic Aerosol Particulate Matter. *Atmos. Chem. Phys*. **2011**, *11* (3), 1155-1165.

Eigen, M.; Kustin, K. The Kinetics of Halogen Hydrolysis. *J. Am. Chem. Soc.* **1962,** *84* (8), 1355-1361.

Elliot, A. J.; McCracken, D. R. Effect of Temperature on O$^{\bullet-}$ Reactions and Equilibria: A Pulse Radiolysis Study. *Rad. Phys. Chem.* **1989**, *33*, 69-74.

Enami, S.; Hoffmann, M. R.; Colussi, A. J. How Phenol and α-Tocopherol React with Ambient Ozone at Gas/Liquid Interfaces. *J. Phys. Chem. A* **2009,** *113* (25), 7002-7010.

Enami, S.; Hoffmann, M. R.; Colussi, A. J. Proton Availability at the Air/Water Interface. *J. Phys. Chem. Lett.* **2010,** *1* (10), 1599-1604.

Enami, S.; Vecitis, C. D.; Cheng, J.; Hoffmann, M. R.; Colussi, A. J. Electrospray Mass Spectrometric Detection of Products and Short-Lived Intermediates in Aqueous Aerosol Microdroplets Exposed to a Reactive Gas. *J. Phys. Chem. A* **2007,** *111* (50), 13032-13037.

Enami, S.; Vecitis, C. D.; Cheng, J.; Hoffmann, M. R.; Colussi, A. J. Global Inorganic Source of Atmospheric Bromine. *J. Phys. Chem. A* **2007,** *111* (36), 8749-8752.

Enami, S.; Vecitis, C. D.; Cheng, J.; Hoffmann, M. R.; Colussi, A. J. Mass Spectrometry of Interfacial Layers During Fast Aqueous Aerosol/Ozone Gas Reactions of Atmospheric Interest. *Chem. Phys. Lett.* **2008,** *455* (4–6), 316-320.

Etaiw, S. E. H.; Werida, A. H. Three-Dimensional Organotin–Hexacyanoferrate Polymers as Effective Oxidizing Reagents towards Phenols. *Appl. Organomet. Chem.* **2010**, *24*, 805-808.

Eugene, A. J.; Guzman, M. I. Reactivity of Ketyl and Acetyl Radicals from Direct Solar Actinic Photolysis of Aqueous Pyruvic Acid. *J. Phys. Chem. A* **2017**, *121*, 2924-2935.

Eugene, A. J.; Xia, S.-S.; Guzman, M. I. Aqueous Photochemistry of Glyoxylic Acid. *J. Phys. Chem. A* **2016**, *120* (21), 3817-3826.

Eugene, A. J.; Xia, S.-S.; Guzman, M. I. Negative Production of Acetoin in the Photochemistry of Aqueous Pyruvic Acid. *Proc. Natl. Acad. Sci.* **2013**, *110* (46), E4274-E4275.

Fachinger, J. R. W.; Gallavardin, S. J.; Helleis, F.; Fachinger, F.; Drewnick, F.; Borrmann, S. The Ion Trap Aerosol Mass Spectrometer: Field Intercomparison with the TOF-AMS and the Capability of Differentiating Organic Compound Classes via MS-MS. *Atmos. Meas. Tech.* **2017,** *10* (4), 1623-1637.

Finlayson-Pitts, B. J. Halogens in the Troposphere. *Anal. Chem.* **2009,** *82* (3), 770-776.

Finlayson-Pitts, B. J. Reactions at Surfaces in the Atmosphere: Integration of Experiments and Theory as Necessary (but Not Necessarily Sufficient) for Predicting the Physical Chemistry of Aerosols. *Phys. Chem. Chem. Phys.* **2009**, *11* (36), 7760-7779.

Flanner, M. G. Arctic Climate Sensitivity to Local Black Carbon. *J. Geophys. Res. Atmos.* **2013**, *118* (4), 1840-1851.

Flyunt, R.; Leitzke, A.; Mark, G.; Mvula, E.; Reisz, E.; Schick, R.; von Sonntag, C. Determination of $^{\bullet}OH$, $O_2^{\bullet-}$, and Hydroperoxide Yields in Ozone Reactions in Aqueous Solution. *J. Phys. Chem. B* **2003**, *107*, 7242-7253.

Forster, P.; Ramaswamy, V.; Artaxo, P.; Berntsen, T.; Betts, R.; Fahey, D. W.; Haywood, J.; Lean, J.; Lowe, D. C.; Myhre, G.; Nganga, J.; Prinn, R.; Raga, G.; Schulz, M.; Van Dorland, R., Changes in Atmospheric Constituents and in Radiative Forcing. In *Climate Change 2007: The Physical Science Basis. Contribution of Working Group I to the Fourth Assessment Report of the Intergovernmental Panel on Climate Change*, Solomon, S.; Qin, D.; Manning, M.; Chen, Z.; Marquis, M.; Averyt, K. B.; Tignor, M.; Miller, H. L., Eds. Cambridge University Press: Cambridge, United Kingdom and New York, NY, USA, 2007.

Fu, P.; Kawamura, K.; Usukura, K.; Miura, K. Dicarboxylic Acids, Ketocarboxylic Acids and Glyoxal in the Marine Aerosols Collected During a Round-the-World Cruise. *Mar. Chem.* **2013**, *148*, 22-32.

Fukushi, K.; Watanabe, K.; Takeda, S.; Wakida, S. I.; Yamane, M.; Higashi, K.; Hiiro, K. Determination of Bromide Ions in Seawater by Capillary Zone Electrophoresis Using Diluted Artificial Seawater as the Buffer Solution. *J. Chromatogr. A* **1998,** *802* (1), 211-217.

Garland, J. A.; Curtis, H. Emission of Iodine from the Sea Surface in the Presence of Ozone. *J. Geophys. Res. Oceans* **1981,** *86* (C4), 3183-3186.

Garrett, B. C.; Schenter, G. K.; Morita, A. Molecular Simulations of the Transport of Molecules across the Liquid/Vapor Interface of Water. *Chem. Rev.* **2006**, *106* (4), 1355-1374.

George, I. J.; Abbatt, J. P. D. Heterogeneous Oxidation of Atmospheric Aerosol Particles by Gas-Phase Radicals. *Nature Chem.* **2010**, *2* (9), 713-722.

George, C.; Ammann, M.; D'Anna, B.; Donaldson, D. J.; Nizkorodov, S. A. Heterogeneous Photochemistry in the Atmosphere. *Chem. Rev.* **2015**, *115*, 4218-4258.

Gligorovski, S.; Strekowski, R.; Barbati, S.; Vione, D. Environmental Implications of Hydroxyl Radicals ($^{\bullet}OH$). *Chem. Rev.* **2015**, *115* (24), 13051–13092.

Graber, E. R.; Rudich, Y. Atmospheric Hulis: How Humic-Like Are They? A Comprehensive and Critical Review. *Atmos. Chem. Phys.* **2006**, *6*, 729-753.

Grassian, V. H. *Environmental Catalysis*. Taylor & Francis: New York, 2005; p 701.

Guenther, A.; Jiang, X.; Heald, C. L.; Sakulyanontvittaya, T.; Duhl, T.; Emmons, L. K.; Wang, X. The Model of Emissions of Gases and Aerosols from Nature Version 2.1 (MEGAN2. 1): An Extended and Updated Framework for Modeling Biogenic Emissions. *Geosci. Model Dev.* **2012**, *5*, 1471-1492.

Guenther, A.; Karl, T.; Harley, P.; Wiedinmyer, C.; Palmer, P. I.; Geron, C. Estimates of Global Terrestrial Isoprene Emissions Using MEGAN (Model of Emissions of Gases and Aerosols from Nature). *Atmos. Chem. Phys.* **2006**, *6* (11), 3181-3210.

Gurol, M. D.; Nekouinaini, S. Kinetic Behavior of Ozone in Aqueous Solutions of Substituted Phenols. *Ind. Eng. Chem. Fund.* **1984**, *23*, 54-60.

Guzman, M. I.; Athalye, R. R.; Rodriguez, J. M. Concentration Effects and Ion Properties Controlling the Fractionation of Halides During Aerosol Formation. *J. Phys. Chem. A* **2012**, *116* (22), 5428-5435.

Guzmán, M. I.; Colussi, A. J.; Hoffmann, M. R. Photoinduced Oligomerization of Aqueous Pyruvic Acid. *J. Phys. Chem. A* **2006**, *110* (10), 3619-3626.

Guzman, M. I.; Pillar, E. A. Ozonation of Aromatic Hydrocarbon Probes at the Air-Water Interface In *248th ACS National Meeting & Exposition*, American Chemical Society: San Francisco, CA, 2014; pp COLL-93.

Hallquist, M.; Wenger, J. C.; Baltensperger, U.; Rudich, Y.; Simpson, D.; Claeys, M.; Dommen, J.; Donahue, N. M.; George, C.; Goldstein, A. H.; Hamilton, J. F.; Herrmann, H.; Hoffmann, T.; Iinuma, Y.; Jang, M.; Jenkin, M. E.; Jimenez, J. L.; Kiendler-Scharr, A.; Maenhaut, W.; McFiggans, G.; Mentel, T. F.; Monod, A.; Prévôt, A. S. H.; Seinfeld, J. H.; Surratt, J. D.; Szmigielski, R.; Wildt, J. The Formation, Properties and Impact of Secondary Organic Aerosol: Current and Emerging Issues. *Atmos. Chem. Phys.* **2009**, *9* (14), 5155-5236.

Han, S.-q.; Zhang, M.; Zhao, C.-s.; Lu, X.-q.; Ran, L.; Han, M.; Li, P.-y.; Li, X.-j. Differences in Ozone Photochemical Characteristics between the Megacity Tianjin and Its Rural Surroundings. *Atmos. Environ.* **2013**, *79*, 209-216.

Hao, C.; March, R. E.; Croley, T. R.; Smith, J. C.; Rafferty, S. P. Electrospray Ionization Tandem Mass Spectrometric Study of Salt Cluster Ions. Part 1— Investigations of Alkali Metal Chloride and Sodium Salt Cluster Ions. *J. Mass. Spec.* **2001,** *36* (1), 79-96.

Hartmann, D. L. *Global Physical Climatology*; Academic Press, 1994, p 411.

Hayase, S.; Yabushita, A.; Kawasaki, M. Iodine Emission in the Presence of Humic Substances at the Water's Surface. *J. Phys. Chem. A* **2012,** *116* (24), 5779-5783.

Hayase, S.; Yabushita, A.; Kawasaki, M.; Enami, S.; Hoffmann, M. R.; Colussi, A. J. Heterogeneous Reaction of Gaseous Ozone with Aqueous Iodide in the Presence of Aqueous Organic Species. *J. Phys. Chem. A* **2010,** *114* (19), 6016-6021.

Hayase, S.; Yabushita, A.; Kawasaki, M.; Enami, S.; Hoffmann, M. R.; Colussi, A. J. Weak Acids Enhance Halogen Activation on Atmospheric Water's Surfaces. *J. Phys. Chem. A* **2011,** *115* (19), 4935-4940.

Heald, C. L.; Jacob, D. J.; Park, R. J.; Russell, L. M.; Huebert, B. J.; Seinfeld, J. H.; Liao, H.; Weber, R. J. A Large Organic Aerosol Source in the Free Troposphere Missing from Current Models. *Geophys. Res. Lett.* **2005**, *32* (18), L18809.

Hecobian, A.; Zhang, X.; Zheng, M.; Frank, N.; Edgerton, E. S.; Weber, R. J. Water-Soluble Organic Aerosol Material and the Light-Absorption Characteristics of Aqueous Extracts Measured over the Southeastern United States. *Atmos. Chem. Phys.* **2010**, *10*, 5965-5977.

Henze, D. K.; Seinfeld, J. H.; Ng, N. L.; Kroll, J. H.; Fu, T. M.; Jacob, D. J.; Heald, C. L. Global Modeling of Secondary Organic Aerosol Formation from Aromatic Hydrocarbons: High- Vs. Low-Yield Pathways. *Atmos. Chem. Phys.* **2008**, *8*, 2405-2420.

Hoffer, A.; Gelencsér, A.; Guyon, P.; Kiss, G.; Schmid, O.; Frank, G. P.; Artaxo, P.; Andreae, M. O. Optical Properties of Humic-Like Substances (Hulis) in Biomass-Burning Aerosols. *Atmos. Chem. Phys.* **2006,** *6* (11), 3563-3570.

Hoque, M.; Kawamura, K.; Seki, O.; Hoshi, N. Spatial Distributions of Dicarboxylic Acids, ω-Oxoacids, Pyruvic Acid and α-Dicarbonyls in the Remote Marine Aerosols over the North Pacific. *Mar. Chem.* **2015,** *172*, 1-11.

House, J. E.; House, K. A., *Descriptive Inorganic Chemistry*. 2nd ed.; Academic Press: Burlington, 2010; p 592.

Hunt, S. W.; Roeselová, M.; Wang, W.; Wingen, L. M.; Knipping, E. M.; Tobias, D. J.; Dabdub, D.; Finlayson-Pitts, B. J. Formation of Molecular Bromine from the Reaction of Ozone with Deliquesced NaBr Aerosol: Evidence for Interface Chemistry. *J. Phys. Chem. A* **2004,** *108* (52), 11559-11572.

Huang, R. J.; Seitz, K.; Buxmann, J.; Pöhler, D.; Hornsby, K. E.; Carpenter, L. J.; Platt, U.; Hoffmann, T. *In Situ* Measurements of Molecular Iodine in the Marine Boundary Layer: The Link to Macroalgae and the Implications for O_3, IO, OIO and NO_x. *Atmos. Chem. Phys.* **2010,** *10* (10), 4823-4833.

Huang, R. J.; Thorenz, U. R.; Kundel, M.; Venables, D. S.; Ceburnis, D.; Ho, K. F.; Chen, J.; Vogel, A. L.; Küpper, F. C.; Smyth, P. P. A.; Nitschke, U.; Stengel, D. B.; Berresheim, H.; O'Dowd, C. D.; Hoffmann, T. The Seaweeds *Fucus Vesiculosus* and *Ascophyllum Nodosum* Are Significant Contributors to Coastal Iodine Emissions. *Atmos. Chem. Phys.* **2013,** *13* (10), 5255-5264.

Huheey, J. E.; Keiter, E. A.; Keiter, R. L., *Inorganic Chemistry: Principles of Structure and Reactivity*. Pearson Education 1993.

Hung, H.-M.; Ariya, P. Oxidation of Oleic Acid and Oleic Acid/Sodium Chloride(*aq*) Mixture Droplets with Ozone: Changes of Hygroscopicity and Role of Secondary Reactions. *J. Phys. Chem. A* **2007**, *111*, 620-632.

Iribarne, J. V.; Thomson, B. A. On the Evaporation of Small Ions from Charged Droplets. *J. Chem. Phys.* **1976**, *64* (6), 2287-2294.

Iwaki, R.; Kamiya, I. Chemiluminescent Reaction between Polyphenols and Ozone in Acetic Acid. *B. Chem. Soc. Jpn.* **1969**, *42*, 855-863.

Jacobs, D. J., *Introduction to Atmospheric Chemistry*. Princeton University Press: Princeton, New Jersey, 1999; p 280.

Jayne, J. T.; Leard, D. C.; Zhang, X.; Davidovits, P.; Smith, K. A.; Kolb, C. E.; Worsnop, D. R. Development of an Aerosol Mass Spectrometer for Size and Composition Analysis of Submicron Particles. *Aerosol Sci. Technol.* **2000,** *33* (1-2), 49-70.

Johnson, D.; Utembe, S. R.; Jenkin, M. E.; Derwent, R. G.; Hayman, G. D.; Alfarra, M. R.; Coe, H.; McFiggans, G. Simulating Regional Scale Secondary Organic Aerosol Formation During the Torch 2003 Campaign in the Southern UK. *Atmos. Chem. Phys.* **2006**, *6* (2), 403-418.

Kandaswami, C.; Subra Rao, P. V.; Nair, P. M.; Vaidyanathan, C. S. Oxidation of Catechol in Higher Plants. I. Enzymic Conversion of Catechol to 3,4,3',4'-Tetrahydroxydiphenyl. *Can. J. Biochem.* **1969**, *47*, 375-377.

Kanakidou, M.; Seinfeld, J. H.; Pandis, S. N.; Barnes, I.; Dentener, F. J.; Facchini, M. C.; Van Dingenen, R.; Ervens, B.; Nenes, A.; Nielsen, C. J.; Swietlicki, E.; Putaud, J. P.; Balkanski, Y.; Fuzzi, S.; Horth, J.; Moortgat, G. K.; Winterhalter, R.; Myhre, C. E. L.; Tsigaridis, K.; Vignati, E.; Stephanou, E. G.; Wilson, J. Organic Aerosol and Global Climate Modelling: A Review. *Atmos. Chem. Phys.* **2005,** *5* (4), 1053-1123.

Kaiser, J. W.; Heil, A.; Andreae, M. O.; Benedetti, A.; Chubarova, N.; Jones, L.; Morcrette, J. J.; Razinger, M.; Schultz, M. G.; Suttie, M.; van der Werf, G. R. Biomass Burning Emissions Estimated with a Global Fire Assimilation System Based on Observed Fire Radiative Power. *Biogeosci.* **2012**, *9* (1), 527-554.

Katrib, Y.; Biskos, G.; Buseck, P. R.; Davidovits, P.; Jayne, J. T.; Mochida, M.; Wise, M. E.; Worsnop, D. R.; Martin, S. T. Ozonolysis of Mixed Oleic-Acid/Stearic-Acid Particles: Reaction Kinetics and Chemical Morphology. *J. Phys. Chem. A* **2005**, *109* (48), 10910-10919.

Kawamura, K.; Tachibana, E.; Okuzawa, K.; Aggarwal, S. G.; Kanaya, Y.; Wang, Z. F. High Abundances of Water-Soluble Dicarboxylic Acids, Ketocarboxylic Acids and α-Dicarbonyls in the Mountaintop Aerosols over the North China Plain During Wheat Burning Season. *Atmos. Chem. Phys.* **2013**, *13* (16), 8285-8302.

Kim, C.; Hsieh, Y.-L. Wetting and Absorbency of Nonionic Surfactant Solutions on Cotton Fabrics. *Colloids Surf. A Physicochem. Eng. Asp.* **2001,** *187–188*, 385-397.

Kolb, C. E.; Cox, R. A.; Abbatt, J. P. D.; Ammann, M.; Davis, E. J.; Donaldson, D. J.; Garrett, B. C.; George, C.; Griffiths, P. T.; Hanson, D. R.; Kulmala, M.; McFiggans, G.; Pöschl, U.; Riipinen, I.; Rossi, M. J.; Rudich, Y.; Wagner, P. E.; Winkler, P. M.; Worsnop, D. R.; O' Dowd, C. D. An Overview of Current Issues in the Uptake of Atmospheric Trace Gases by Aerosols and Clouds. *Atmos. Chem. Phys.* **2010**, *10* (21), 10561-10605.

Kolsaker, P.; Bernatek, E.; Johanson, R.; Hytta, R. Glyoxylic Acid as a Reductant in Ozonolysis. *Acta Chem. Scand.* **1973**, *27*, 1526-1530.

Konstantinova, M. L.; Razumovskii, S. D.; Zaikov, G. E. Kinetics and Mechanism of the Reaction of Ozone with Phenol in Alkaline Media. *B. Acad. Sci. USSR, Div. Chem. Sci.* **1991**, *40*, 266-270.

Kravitz, B.; Wang, H.; Rasch, P. J.; Morrison, H.; Solomon, A. B. Process-Model Simulations of Cloud Albedo Enhancement by Aerosols in the Arctic. *Phil. Trans. R. Soc. A* **2014**, 372 (2031), 20140052.

Kroll, J. H.; Seinfeld, J. H. Chemistry of Secondary Organic Aerosol: Formation and Evolution of Low-Volatility Organics in the Atmosphere. *Atmos. Environ.* **2008**, *42* (16), 3593-3624.

Kroll, J. H.; Smith, J. D.; Che, D. L.; Kessler, S. H.; Worsnop, D. R.; Wilson, K. R. Measurement of Fragmentation and Functionalization Pathways in the Heterogeneous Oxidation of Oxidized Organic Aerosol. *Phys. Chem. Chem. Phys.* **2009**, *11* (36), 8005-8014.

Kundu, S.; Kawamura, K.; Andreae, T. W.; Hoffer, A.; Andreae, M. O. Molecular Distributions of Dicarboxylic Acids, Ketocarboxylic Acids and α-Dicarbonyls in Biomass Burning Aerosols: Implications for Photochemical Production and Degradation in Smoke Layers. *Atmos. Chem. Phys.* **2010**, *10*, 2209-2225.

Kupc, A.; Winkler, P. M.; Vrtala, A.; Wagner, P. E. Unusual Temperature Dependence of Heterogeneous Nucleation of Water Vapor on Ag Particles. *Aerosol Sci. Technol.* **2013**, *47* (9), i-iv.

Last, D. J.; Najera, J. J.; Percival, C. J.; Horn, A. B. A Comparison of Infrared Spectroscopic Methods for the Study of Heterogeneous Reactions Occurring on Atmospheric Aerosol Proxies. *Phys. Chem. Chem. Phys.* **2009**, *11* (37), 8214-8225.

Laskin, A.; Laskin, J.; Nizkorodov, S. A. Chemistry of Atmospheric Brown Carbon. *Chem. Rev.* **2015**, *115*, 4335-4382.

Latif, M. T.; Brimblecombe, P. Surfactants in Atmospheric Aerosols. *Environ. Sci. Technol.* **2004**, *38*, 6501-6506.

Lathière, J.; Hauglustaine, D. A.; Friend, A. D.; De Noblet-Ducoudré, N.; Viovy, N.; Folberth, G. A. Impact of Climate Variability and Land Use Changes on Global Biogenic Volatile Organic Compound Emissions. *Atmos. Chem. Phys.* **2006**, *6* (8), 2129-2146.

Leng, C.; Hiltner, J.; Pham, H.; Kelley, J.; Mach, M.; Zhang, Y.; Liu, Y. Kinetics Study of Heterogeneous Reactions of Ozone with Erucic Acid Using an ATR-IR Flow Reactor. *Phys. Chem. Chem. Phys.* **2014**, *16* (9), 4350-4360.

Levy, H.; Horowitz, L. W.; Schwarzkopf, M. D.; Ming, Y.; Golaz, J.-C.; Naik, V.; Ramaswamy, V. The Roles of Aerosol Direct and Indirect Effects in Past and Future Climate Change. *J. Geophys. Res. Atmos.* **2013**, *118* (10), 4521-4532.

Li, Y. J.; Cheong, G. Y. L.; Lau, A. P. S.; Chan, C. K. Acid-Catalyzed Condensed-Phase Reactions of Limonene and Terpineol and Their Impacts on Gas-to-Particle Partitioning in the Formation of Organic Aerosols. *Environ. Sci. Technol.* **2010**, *44* (14), 5483-5489.

Li, Y. Q.; Davidovits, P.; Kolb, C. E.; Worsnop, D. R. Mass and Thermal Accommodation Coefficients of $H_2O(g)$ on Liquid Water as a Function of Temperature. *J. Phys. Chem. A* **2001**, *105* (47), 10627-10634.

Liao, J.; Sihler, H.; Huey, L. G.; Neuman, J. A.; Tanner, D. J.; Friess, U.; Platt, U.; Flocke, F. M.; Orlando, J. J.; Shepson, P. B.; Beine, H. J.; Weinheimer, A. J.; Sjostedt, S. J.; Nowak, J. B.; Knapp, D. J.; Staebler, R. M.; Zheng, W.; Sander, R.; Hall, S. R.; Ullmann, K. A Comparison of Arctic BrO Measurements by Chemical Ionization Mass Spectrometry and Long Path-Differential Optical Absorption Spectroscopy. *J. Geophys. Res. Atmos.* **2011,** *116*, D00R02.

Liggio, J.; Li, S.-M.; Brook, J. R.; Mihele, C. Direct Polymerization of Isoprene and α-Pinene on Acidic Aerosols. *Geophys. Res. Lett.* **2007**, *34* (5), L05814.

Lin, C.-C. Volatility of Iodine in Dilute Aqueous Solutions. *J. Inorg. Nucl. Chem.* **1981,** *43* (12), 3229-3238.

Lin, P.; Engling, G.; Yu, J. Z. Humic-Like Substances in Fresh Emissions of Rice Straw Burning and in Ambient Aerosols in the Pearl River Delta Region, China. *Atmos. Chem. Phys.* **2010,** *10* (14), 6487-6500.

Liu, J.; Li, Z. Estimation of Cloud Condensation Nuclei Concentration from Aerosol Optical Quantities: Influential Factors and Uncertainties. *Atmos. Chem. Phys.* **2014**, *14* (1), 471-483.

Liu, J.; Scheuer, E.; Dibb, J.; Ziemba, L. D.; Thornhill, K. L.; Anderson, B. E.; Wisthaler, A.; Mikoviny, T.; Devi, J. J.; Bergin, M.; Weber, R. J. Brown Carbon in the Continental Troposphere. *Geophys. Res. Lett.* **2014**, *41* (6), 2191-2195.

Liu, W.-T.; Zhang, L.; Shen, Y. R. Interfacial Structures of Methanol:Water Mixtures at a Hydrophobic Interface Probed by Sum-Frequency Vibrational Spectroscopy. *J. Chem. Phys.* **2006,** *125* (14), 144711-144716.

Maçôas, E. M. S.; Fausto, R.; Lundell, J.; Pettersson, M.; Khriachtchev, L.; Räsänen, M. A Matrix Isolation Spectroscopic and Quantum Chemical Study of Fumaric and Maleic Acid. *J. Phys. Chem. A* **2001**, *105*, 3922-3933.

Magi, L.; Schweitzer, F.; Pallares, C.; Cherif, S.; Mirabel, P.; George, C. Investigation of the Uptake Rate of Ozone and Methyl Hydroperoxide by Water Surfaces. *J. Phys. Chem. A* **1997,** *101* (27), 4943-4949.

Markus, Y. *Ion Properties*. Marcel Dekker: New York, 1997; p 272.

Martinelango, P. K.; Tian, K.; Dasgupta, P. K. Perchlorate in Seawater - Bioconcentration of Iodide and Perchlorate by Various Seaweed Species. *Anal. Chim. Acta* **2006,** *567* (1), 100-107.

McCabe, J.; Abbatt, J. P. D. Heterogeneous Loss of Gas-Phase Ozone on n-Hexane Soot Surfaces: Similar Kinetics to Loss on Other Chemically Unsaturated Solid Surfaces. *J. Phys. Chem. C* **2009**, *113* (6), 2120-2127.

McMurdo, C. J.; Ellis, D. A.; Webster, E.; Butler, J.; Christensen, R. D.; Reid, L. K. Aerosol Enrichment of the Surfactant PFO and Mediation of the Water−Air Transport of Gaseous PFOA. *Environ. Sci. Technol.* **2008,** *42* (11), 3969-3974.

Mita, N.; Tawaki, S.-i.; Uyama, H.; Kobayashi, S. Laccase-Catalyzed Oxidative Polymerization of Phenols. *Macromolec. Biosci.* **2003**, *3*, 253-257.

Mkoma, S. L.; Kawamura, K. Molecular Composition of Dicarboxylic Acids, Ketocarboxylic Acids, α-Dicarbonyls and Fatty Acids in Atmospheric Aerosols from Tanzania, East Africa During Wet and Dry Seasons. *Atmos. Chem. Phys.* **2013**, *13* (4), 2235-2251.

Mmereki, B. T.; Donaldson, D. J. Direct Observation of the Kinetics of an Atmospherically Important Reaction at the Air−Aqueous Interface. *J. Phys. Chem. A* **2003,** *107* (50), 11038-11042.

Mochida, M.; Kawamura, K.; Umemoto, N.; Kobayashi, M.; Matsunaga, S.; Lim, H. J.; Turpin, B. J.; Bates, T. S.; Simoneit, B. R. T. Spatial Distributions of Oxygenated Organic Compounds (Dicarboxylic Acids, Fatty Acids, and Levoglucosan) in Marine Aerosols over the Western Pacific and Off the Coast of East Asia: Continental Outflow of Organic Aerosols During the Ace-Asia Campaign. *J. Geophys. Res. Atmos.* **2003**, *108*, 8638.

Moise, T.; Flores, J. M.; Rudich, Y. Optical Properties of Secondary Organic Aerosols and Their Changes by Chemical Processes. *Chem. Rev*. **2015**, *115* (10), 4400-4439.

Monks, P. S.; Archibald, A. T.; Colette, A.; Cooper, O.; Coyle, M.; Derwent, R.; Fowler, D.; Granier, C.; Law, K. S.; Mills, G. E.; Stevenson, D. S.; Tarasova, O.; Thouret, V.; von Schneidemesser, E.; Sommariva, R.; Wild, O.; Williams, M. L. Tropospheric Ozone and Its Precursors from the Urban to the Global Scale from Air Quality to Short-Lived Climate Forcer. *Atmos. Chem. Phys.* **2015,** *15* (15), 8889-8973.

Morris, J. W.; Davidovits, P.; Jayne, J. T.; Jimenez, J. L.; Shi, Q.; Kolb, C. E.; Worsnop, D. R.; Barney, W. S.; Cass, G. Kinetics of Submicron Oleic Acid Aerosols with Ozone: A Novel Aerosol Mass Spectrometric Technique. *Geophys. Res. Lett.* **2002**, *29* (9), 711-714.

Murphy, D. M.; Fahey, D. W. An Estimate of the Flux of Stratospheric Reactive Nitrogen and Ozone into the Troposphere. *J. Geophys. Res. Atmos.* **1994,** *99* (D3), 5325-5332.

Mustafa, C. Vibrational Spectroscopy of Pyrogallol with a Glance on the Problems of Formation of a Dimer. *Res. J. Chem. Environ.* **2013**, *17*, 117-128.

Mvula, E.; Schuchmann, M. N.; von Sonntag, C. Reactions of Phenol-OH-Adduct Radicals. Phenoxyl Radical Formation by Water Elimination vs. Oxidation by Dioxygen. *J. Chem. Soc. Perk. T. 2* **2001**, 264-268.

Mvula, E.; von Sonntag, C. Ozonolysis of Phenols in Aqueous Solution. *Org. Biomol. Chem.* **2003**, *1*, 1749-1756.

Myhre, G.; Samset, B. H.; Schulz, M.; Balkanski, Y.; Bauer, S.; Berntsen, T. K.; Bian, H.; Bellouin, N.; Chin, M.; Diehl, T.; Easter, R. C.; Feichter, J.; Ghan, S. J.; Hauglustaine, D.; Iversen, T.; Kinne, S.; Kirkevåg, A.; Lamarque, J. F.; Lin, G.; Liu, X.; Lund, M. T.; Luo, G.; Ma, X.; van Noije, T.; Penner, J. E.; Rasch, P. J.; Ruiz, A.; Seland, Ø.; Skeie, R. B.; Stier, P.; Takemura, T.; Tsigaridis, K.; Wang, P.; Wang, Z.; Xu, L.; Yu, H.; Yu, F.; Yoon, J. H.; Zhang, K.; Zhang, H.; Zhou, C. Radiative Forcing of the Direct Aerosol Effect from Aerocom Phase Ii Simulations. *Atmos. Chem. Phys.* **2013**, *13* (4), 1853-1877.

Naik, V.; Horowitz, L. W.; Fiore, A. M. Impact of Preindustrial to Present-Day Changes in Short-Lived Pollutant Emissions on Atmospheric Composition and Climate Forcing. *J. Geophys. Res. Atmos.* **2013**, *118* (14), 8086-8110.

Najera, J. J.; Percival, C. J.; Horn, A. B. Infrared Spectroscopic Studies of the Heterogeneous Reaction of Ozone with Dry Maleic and Fumaric Acid Aerosol Particles. *Phys. Chem. Chem. Phys.* **2009**, *11* (40), 9093-9103.

Neta, P.; Huie, R. E.; Ross, A. B. Rate Constants for Reactions of Inorganic Radicals in Aqueous Solution. *J. Phys. Chem. Ref. Data* **1988**, *17*, 1027-1284.

Niculescu, M.; Ledeţi, I.; Bîrzescu, M. New Methods to Obtain Carboxylic Acids by Oxidation Reactions of 1,2-Ethanediol with Metallic Nitrates. *J. Organomet. Chem.* **2014**, *767*, 108-111.

O'Brien, R. E.; Wang, B.; Kelly, S. T.; Lundt, N.; You, Y.; Bertram, A. K.; Leone, S. R.; Laskin, A.; Gilles, M. K. Liquid–Liquid Phase Separation in Aerosol Particles: Imaging at the Nanometer Scale. *Environ. Sci. Technol.* **2015**, *49* (8), 4995-5002.

O'Dowd, C. D.; Jimenez, J. L.; Bahreini, R.; Flagan, R. C.; Seinfeld, J. H.; Hameri, K.; Pirjola, L.; Kulmala, M.; Jennings, S. G.; Hoffmann, T. Marine Aerosol Formation from Biogenic Iodine Emissions. *Nature* **2002,** *417* (6889), 632-636.

Ofner, J.; Krüger, H. U.; Zetzsch, C. Time Resolved Infrared Spectroscopy of Formation and Processing of Secondary Organic Aerosol *Z. Phys. Chem.* **2010**, *224*, 1171-1183.

Olariu, R. I.; Barnes, I.; Becker, K. H.; Klotz, B. Rate Coefficients for the Gas-Phase Reaction of OH Radicals with Selected Dihydroxybenzenes and Benzoquinones. *Int. J. Chem. Kinet.* **2000**, *32*, 696-702.

Oldridge, N. W.; Abbatt, J. P. D. Formation of Gas-Phase Bromine from Interaction of Ozone with Frozen and Liquid NaCl/NaBr Solutions: Quantitative Separation of Surficial Chemistry from Bulk-Phase Reaction. *J. Phys. Chem. A* **2011,** *115* (12), 2590-2598.

O'Neill, E. M.; Kawam, A. Z.; Van Ry, D. A.; Hinrichs, R. Z. Ozonolysis of Surface-Adsorbed Methoxyphenols: Kinetics of Aromatic Ring Cleavage vs. Alkene Side-Chain Oxidation. *Atmos. Chem. Phys.* **2014**, *14*, 47-60.

Paasonen, P.; Asmi, A.; Petaja, T.; Kajos, M. K.; Aijala, M.; Junninen, H.; Holst, T.; Abbatt, J. P. D.; Arneth, A.; Birmili, W.; van der Gon, H. D.; Hamed, A.; Hoffer, A.; Laakso, L.; Laaksonen, A.; Richard Leaitch, W.; Plass-Dulmer, C.; Pryor, S. C.; Raisanen, P.; Swietlicki, E.; Wiedensohler, A.; Worsnop, D. R.; Kerminen, V.-M.; Kulmala, M. Warming-Induced Increase in Aerosol Number Concentration Likely to Moderate Climate Change. *Nature Geosci.* **2013**, *6* (6), 438-442.

Palmer, D. A.; Ramette, R. W.; Mesmer, R. E. The Hydrolysis of Iodine: Equilibria at High Temperatures. *J. Nucl. Mater.* **1985,** *130* (0), 280-286.

Pankow, J. F. An Absorption Model of the Gas/Aerosol Partitioning Involved in the Formation of Secondary Organic Aerosol. *Atmos. Environ.* **1994**, *28* (2), 189-193.

Pankow, J. F.; Asher, W. E. Simpol.1: A Simple Group Contribution Method for Predicting Vapor Pressures and Enthalpies of Vaporization of Multifunctional Organic Compounds. *Atmos. Chem. Phys. Discuss.* **2007**, *7* (4), 11839-11894.

Parmar, R. S.; Satsangi, G. S.; Kumari, M.; Lakhani, A.; Srivastava, S. S.; Prakash, S. Study of Size Distribution of Atmospheric Aerosol at Agra. *Atmos. Environ.* **2001**, *35*, 693-702.

Paulot, F.; Jacob, D. J. Hidden Cost of U.S. Agricultural Exports: Particulate Matter from Ammonia Emissions. *Environ. Sci. Technol.* **2014**, *48*, 903-908.

Perrin, D. D.; Dempsey, B.; Serjeant, E. P. *pKa Prediction for Organic Acids and Bases*; Chapman and Hall: London, 1981. p 146.

Petersen, P. B.; Saykally, R. J. Probing the Interfacial Structure of Aqueous Electrolytes with Femtosecond Second Harmonic Generation Spectroscopy. *J. Phys. Chem. B* **2006,** *110* (29), 14060-14073.

Petters, M. D.; Kreidenweis, S. M. A Single Parameter Representation of Hygroscopic Growth and Cloud Condensation Nucleus Activity. *Atmos. Chem. Phys.* **2007**, *7* (8), 1961-1971.

Philipp, B.; Schink, B. Evidence of Two Oxidative Reaction Steps Initiating Anaerobic Degradation of Resorcinol (1,3-Dihydroxybenzene) by the Denitrifying Bacterium Azoarcus Anaerobius. *J. Bacteriol.* **1998**, *180*, 3644-3649.

Phillips, S. M.; Smith, G. D. Light Absorption by Charge Transfer Complexes in Brown Carbon Aerosols. *Environ. Sci. Technol. Lett.* **2014**, *1*, 382-386.

Pillar, E. A.; Camm, R. C.; Guzman, M. I. Catechol Oxidation by Ozone and Hydroxyl Radicals at the Air–Water Interface. *Environ. Sci. Technol.* **2014**, *48* (24), 14352-14360.

Pillar, E. A.; Eugene, A. J.; Guzman, M. I. *In Preparation.* **2016**.

Pillar, E. A.; Guzman, M. I. Oxidation of Substituted Catechols at the Air–Water Interface: Production of Carboxylic Acids, Quinones, and Polyphenols. *Environ. Sci. Technol.* **2017**, *51*, 4951-4959.

Pillar, E. A.; Guzman, M. I. *Ozonolysis of Catechol at the Gas-Solid Interface*, 250th ACS National Meeting & Exposition, Boston, MA, August 16-20, 2015; American Chemical Society, Boston, MA, 2015; p CODEN:69TVIX.

Pillar, E. A.; Guzman, M. I.; Rodriguez, J. M. Conversion of Iodide to Hypoiodous Acid and Iodine in Aqueous Microdroplets Exposed to Ozone. *Environ. Sci. Technol.* **2013**, *47* (19), 10971-10979.

Pillar, E. A.; Zhou, R.; Guzman, M. I. Heterogeneous Oxidation of Catechol. *J. Phys. Chem. A* **2015**, *119* (41), 10349-10359.

Platt, U.; Honninger, G. The Role of Halogen Species in the Troposphere. *Chemosphere* **2003,** *52* (2), 325-338.

Pope, C. A.; Burnett, R. T.; Thun, M. J. Lung Cancer, Cardiopulmonary Mortality, and Long-Term Exposure to Fine Particulate Air Pollution. *J. Am. Med. Assoc.* **2002**, *287* (9), 1132-1141.

Pöschl, U.; Rudich, Y.; Ammann, M. Kinetic Model Framework for Aerosol and Cloud Surface Chemistry and Gas-Particle Interactions - Part 1: General Equations, Parameters, and Terminology. *Atmos. Chem. Phys.* **2007**, *7* (23), 5989-6023.

Pósfai, M.; Axisa, D.; Tompa, É.; Freney, E.; Bruintjes, R.; Buseck, P. R. Interactions of Mineral Dust with Pollution and Clouds: An Individual-Particle TEM Study of Atmospheric Aerosol from Saudi Arabia. *Atmos. Res.* **2013**, *122*, 347-361.

Pusede, S. E.; Steiner, A. L.; Cohen, R. C. Temperature and Recent Trends in the Chemistry of Continental Surface Ozone. *Chem. Rev.* **2015**, *115* (10), 3898-3918.

Quinlan, M. A.; Reihs, C. M.; Golden, D. M.; Tolbert, M. A. Heterogeneous Reactions on Model Polar Stratospheric Cloud Surfaces: Reaction of Dinitrogen Pentoxide on Ice and Nitric Acid Trihydrate. *J. Phys. Chem.* **1990**, *94* (8), 3255-3260.

Rader, D. J.; Grasser, T. W.; Castaneda, J. N.; Trott, W. M.; Torczynski, J. R. *Measurements of Thermal Accommodation Coefficients*. United States. Department of Energy: 2005.

Ramanathan, V.; Carmichael, G. Global and Regional Climate Changes Due to Black Carbon. *Nature Geosci.* **2008**, *1* (4), 221-227.

Ramirez, F. J.; Navarrete, J. T. L. Normal Coordinate and Rotational Barrier Calculations on 1,2-Dihydroxybenzene. *Vib. Spectrosc.* **1993**, *4*, 321-334.

Ramseier, M. K.; von Gunten, U. Mechanisms of Phenol Ozonation-Kinetics of Formation of Primary and Secondary Reaction Products. *Ozone Sci. Eng.* **2009**, *31*, 201-215.

Read, K. A.; Mahajan, A. S.; Carpenter, L. J.; Evans, M. J.; Faria, B. V. E.; Heard, D. E.; Hopkins, J. R.; Lee, J. D.; Moller, S. J.; Lewis, A. C.; Mendes, L.; McQuaid, J. B.; Oetjen, H.; Saiz-Lopez, A.; Pilling, M. J.; Plane, J. M. C. Extensive Halogen-Mediated Ozone Destruction over the Tropical Atlantic Ocean. *Nature* **2008,** *453* (7199), 1232-1235.

Reeser, D. I.; Donaldson, D. J. Influence of Water Surface Properties on the Heterogeneous Reaction between $O_3(g)$ and $I^-(aq)$. *Atmos. Environ.* **2011,** *45* (34), 6116-6120.

Reisz, E.; Schmidt, W.; Schuchmann, H.-P.; von Sonntag, C. Photolysis of Ozone in Aqueous Solutions in the Presence of Tertiary Butanol. *Environ. Sci. Technol.* **2003**, *37*, 1941-1948.

Reiter, R. Charges on Particles of Different Size from Bubbles of Mediterranean Sea Surf and from Waterfalls. *J. Geophys. Res. Atmos.* **1994,** *99* (D5), 10807-10812.

Rhim, J. A. Equilibrium Concentration and Overall Henry's Law Constant of the Dissolved Ozone. *Env. Eng. Res.* **2004,** *9* (2), 88-95.

Rincón, A. G.; Guzmán, M. I.; Hoffmann, M. R.; Colussi, A. J. Optical Absorptivity Versus Molecular Composition of Model Organic Aerosol Matter. *J. Phys. Chem. A* **2009**, *113* (39), 10512-10520.

Rincón, A. G.; Guzmán, M. I.; Hoffmann, M. R.; Colussi, A. J. Thermochromism of Model Organic Aerosol Matter. *J. Phys. Chem. Lett.* **2010**, *1* (1), 368-373.

Rischbieter, E.; Stein, H.; Schumpe, A. Ozone Solubilities in Water and Aqueous Salt Solutions. *J. Chem. Eng. Data* **2000,** *45* (2), 338-340.

Robinson, A. L.; Donahue, N. M.; Shrivastava, M. K.; Weitkamp, E. A.; Sage, A. M.; Grieshop, A. P.; Lane, T. E.; Pierce, J. R.; Pandis, S. N. Rethinking Organic Aerosols: Semivolatile Emissions and Photochemical Aging. *Science* **2007**, *315* (5816), 1259-1262.

Rosen, M. J. *Surfactants and Interfacial Phenomena*. 3rd ed.; Wiley: Hoboken, 2004; p 444.

Roth, J. A.; Sullivan, D. E. Solubility of Ozone in Water. *Ind. Eng. Chem. Fund.* **1981,** *20* (2), 137-140.

Rotstayn, L. D.; Collier, M. A.; Chrastansky, A.; Jeffrey, S. J.; Luo, J. J. Projected Effects of Declining Aerosols in RCP4.5: Unmasking Global Warming? *Atmos. Chem. Phys.* **2013**, *13* (21), 10883-10905.

Rouvière, A.; Ammann, M. The Effect of Fatty Acid Surfactants on the Uptake of Ozone to Aqueous Halogenide Particles. *Atmos. Chem. Phys.* **2010,** *10* (23), 11489-11500.

Rouvière, A.; Sosedova, Y.; Ammann, M. Uptake of Ozone to Deliquesced KI and Mixed KI/NaCl Aerosol Particles. *J. Phys. Chem. A* **2010,** *114* (26), 7085-7093.

Rudich, Y.; Donahue, N. M.; Mentel, T. F. Aging of Organic Aerosol: Bridging the Gap between Laboratory and Field Studies. *Ann. Rev. Phys. Chem.* **2007**, *58* (1), 321-352.

Ryder, O. S.; Campbell, N. R.; Morris, H.; Forestieri, S.; Ruppel, M. J.; Cappa, C. D.; Tivanski, A.; Prather, K.; Bertram, T. H. Role of Organic Coatings in Regulating N_2O_5 Reactive Uptake to Sea Spray Aerosol. *J. Phys. Chem. A* **2015**, *119* (48), 11683-11692.

Sage, A. M.; Weitkamp, E. A.; Robinson, A. L.; Donahue, N. M. Reactivity of Oleic Acid in Organic Particles: Changes in Oxidant Uptake and Reaction Stoichiometry with Particle Oxidation. *Phys. Chem. Chem. Phys.* **2009**, *11* (36), 7951-7962.

Saiz-Lopez, A.; Plane, J. M. C.; Baker, A. R.; Carpenter, L. J.; von Glasow, R.; Gómez Martín, J. C.; McFiggans, G.; Saunders, R. W. Atmospheric Chemistry of Iodine. *Chem. Rev.* **2011,** *112* (3), 1773-1804.

Saiz-Lopez, A.; von Glasow, R. Reactive Halogen Chemistry in the Troposphere. *Chem. Soc. Rev.* **2012,** *41* (19), 6448-6472.

Sakamoto, Y.; Yabushita, A.; Kawasaki, M.; Enami, S. Direct Emission of I_2 Molecule and IO Radical from the Heterogeneous Reactions of Gaseous Ozone with Aqueous Potassium Iodide Solution. *J. Phys. Chem. A* **2009,** *113* (27), 7707-7713.

Sakata, K.; Sakaguchi, A.; Tanimizu, M.; Takaku, Y.; Yokoyama, Y.; Takahashi, Y. Identification of Sources of Lead in the Atmosphere by Chemical Speciation Using X-Ray Absorption near-Edge Structure (XANES) Spectroscopy. *J. Environ. Sci.* **2014**, *26* (2), 343-352.

Saleh, R.; Adams, P. J.; Donahue, N. M.; Robinson, A. L. The Interplay between Assumed Morphology and the Direct Radiative Effect of Light-Absorbing Organic Aerosol. *Geophys. Res. Lett.* **2016**, *43*, 8735-8743.

Saleh, R.; Hennigan, C. J.; McMeeking, G. R.; Chuang, W. K.; Robinson, E. S.; Coe, H.; Donahue, N. M.; Robinson, A. L. Absorptivity of Brown Carbon in Fresh and Photo-Chemically Aged Biomass-Burning Emissions. *Atmos. Chem. Phys.* **2013**, *13*, 7683-7693.

Saleh, R.; Robinson, E. S.; Tkacik, D. S.; Ahern, A. T.; Liu, S.; Aiken, A. C.; Sullivan, R. C.; Presto, A. A.; Dubey, M. K.; Yokelson, R. J.; Donahue, N. M.; Robinson, A. L. Brownness of Organics in Aerosols from Biomass Burning Linked to Their Black Carbon Content. *Nature Geosci.* **2014**, *7*, 647-650.

Sander, S. P.; Abbatt, J.; Barker, J. R.; Burkholder, J. B.; Friedl, R. R.; Golden, D. M.; Huie, R. E.; Kolb, C. E.; Kurylo, M. J.; Moortgat, G. K.; Orkin, V. L.; Wine, P. H., Chemical Kinetics and Photochemical Data for Use in Atmospheric Studies: Evaluation Number 17. In Jet Propulsion Laboratory, California Institute of Technology, Pasadena, CA, http://jpldataeval.jpl.nasa.gov: 2011.

Sanderson, M. G.; Jones, C. D.; Collins, W. J.; Johnson, C. E.; Derwent, R. G. Effect of Climate Change on Isoprene Emissions and Surface Ozone Levels. *Geophys. Res. Lett*. **2003**, *30* (18), 1936-1940.

Satsangi, P. G.; Yadav, S. Characterization of $PM_{2.5}$ by X-Ray Diffraction and Scanning Electron Microscopy–Energy Dispersive Spectrometer: It's Relation with Different Pollution Sources. *Int. J. Environ. Sci. Technol.* **2014**, *11* (1), 217-232.

Saunders, R. W.; Kumar, R.; MacDonald, S. M.; Plane, J. M. C. Insights into the Photochemical Transformation of Iodine in Aqueous Systems: Humic Acid Photosensitized Reduction of Iodate. *Environ. Sci. Technol.* **2012,** *46* (21), 11854-11861.

Schwarzenbach, R. P.; Gschwend, P. M.; Imboden, D. M. *Environmental Organic Chemistry*, 2nd ed.; Wiley, **2005**. p 1328.

Seinfeld, J. H.; Pandis, S. N. *Atmospheric Chemistry and Physics: From Air Pollution to Climate Change.* 2nd ed.; Wiley: 2006; p 1232.

Setyan, A.; Song, C.; Merkel, M.; Knighton, W. B.; Onasch, T. B.; Canagaratna, M. R.; Worsnop, D. R.; Wiedensohler, A.; Shilling, J. E.; Zhang, Q. Chemistry of New Particle Growth in Mixed Urban and Biogenic Emissions – Insights from CARES. *Atmos. Chem. Phys*. **2014**, *14* (13), 6477-6494.

Sharpless, C. M.; Aeschbacher, M.; Page, S. E.; Wenk, J.; Sander, M.; McNeill, K. Photooxidation-Induced Changes in Optical, Electrochemical, and Photochemical Properties of Humic Substances. *Environ. Sci. Technol.* **2014**, *48* (5), 2688-2696.

Shaw, M. D.; Carpenter, L. J. Modification of Ozone Deposition and I_2 Emissions at the Air–Aqueous Interface by Dissolved Organic Carbon of Marine Origin. *Environ. Sci. Technol.* **2013,** *47* (19), 10947-10954.

Sillman, S. The Relation between Ozone, NO_x and Hydrocarbons in Urban and Polluted Rural Environments. *Atmos. Environ.* **1999,** *33* (12), 1821-1845.

Simpson, W. R.; von Glasow, R.; Riedel, K.; Anderson, P.; Ariya, P.; Bottenheim, J.; Burrows, J.; Carpenter, L. J.; Frieß, U.; Goodsite, M. E.; Heard, D.; Hutterli, M.; Jacobi, H. W.; Kaleschke, L.; Neff, B.; Plane, J.; Platt, U.; Richter, A.; Roscoe, H.; Sander, R.; Shepson, P.; Sodeau, J.; Steffen, A.; Wagner, T.; Wolff, E. Halogens and Their Role in Polar Boundary-Layer Ozone Depletion. *Atmos. Chem. Phys.* **2007,** *7* (16), 4375-4418.

Slade, J. H.; Knopf, D. A. Multiphase OH Oxidation Kinetics of Organic Aerosol: The Role of Particle Phase State and Relative Humidity. *Geophys. Res. Lett.* **2014**, *41*, 5297-5306.

Šmejkalová, D.; Conte, P.; Piccolo, A. Structural Characterization of Isomeric Dimers from the Oxidative Oligomerization of Catechol with a Biomimetic Catalyst. *Biomacromolecules* **2007**, *8*, 737-743.

Sŏhár, P.; Varsányi, G. Y. An IR Spectroscopic Study of Muconate Isomers. *J. Mol. Struct.* **1968**, *1*, 437-448.

Sokolik, I. N.; Winker, D. M.; Bergametti, G.; Gillette, D. A.; Carmichael, G.; Kaufman, Y. J.; Gomes, L.; Schuetz, L.; Penner, J. E. Introduction to Special Section: Outstanding Problems in Quantifying the Radiative Impacts of Mineral Dust. *J. Geophys. Res. Atmos.* **2001**, *106* (D16), 18015-18027.

Standard Reference Database 69: The NIST Chemistry Webbook. In Mallard, W. G.; Linstrom, P. J. Eds. National Institute of Standards and Technology: http://webbook.nist.gov. Gaithersburg, MD, 2000; Vol. 2012.

Steenken, S.; O'Neill, P. Oxidative Demethoxylation of Methoxylated Phenols and Hydroxybenzoic Acids by the Hydroxyl Radical. An in Situ Electron Spin Resonance, Conductometric Pulse Radiolysis and Product Analysis Study. *J. Phys. Chem.* **1977**, *81*, 505-508.

Steenken, S.; Neta, P. Electron Transfer Rates and Equilibriums between Substituted Phenoxide Ions and Phenoxyl Radicals. *J. Phys. Chem.* **1979**, *83*, 1134-1137.

Steenken, S.; Neta, P. Properties of Phenoxyl Radicals. In *The Chemistry of Phenols*, Rappoport, Z. Ed. John Wiley & Sons: New York, 2003; p 1000.

Steinfeld, J. I.; Francisco, J. S.; Hase, W. L., *Chemical Kinetics and Dynamics*. 2nd ed.; Prentice Hall Engelwood Cliffs, New Jersey, 1989; p 560.

Stumm, W.; Morgan, J. J., *Aquatic Chemistry*. 3rd ed.; Wiley: 1996; p 1040.

Sugumaran, M. Reactivities of Quinone Methides versus *o*-Quinones in Catecholamine Metabolism and Eumelanin Biosynthesis. *Int. J. Mol. Sci.* **2016,** *17* (9), 1576-1599.

Sun, X.; Bai, R.; Zhang, Y.; Wang, Q.; Fan, X.; Yuan, J.; Cui, L.; Wang, P. Laccase-Catalyzed Oxidative Polymerization of Phenolic Compounds. *Appl Biochem Biotechnol* **2013**, *171*, 1673-1680.

ten Brink, G. J.; Arends, I. W. C. E.; Sheldon, R. A. The Baeyer−Villiger Reaction: New Developments toward Greener Procedures. *Chem. Rev.* **2004**, *104*, 4105-4124.

Thomas, J. L.; Jimenez-Aranda, A.; Finlayson-Pitts, B. J.; Dabdub, D. Gas-Phase Molecular Halogen Formation from NaCl and NaBr Aerosols: When Are Interface Reactions Important? *J. Phys. Chem. A* **2006,** *110* (5), 1859-1867.

Tomas, A.; Olariu, R. I.; Barnes, I.; Becker, K. H. Kinetics of the Reaction of O_3 with Selected Benzenediols. *Int. J. Chem. Kinet.* **2003**, *35*, 223-230.

Tosca, M. G.; Randerson, J. T.; Zender, C. S. Global Impact of Smoke Aerosols from Landscape Fires on Climate and the Hadley Circulation. *Atmos. Chem. Phys.* **2013**, *13* (10), 5227-5241.

Troy, R. C.; Kelley, M. D.; Nagy, J. C.; Margerum, D. W. Non-Metal Redox Kinetics: Iodine Monobromide Reaction with Iodide Ion and the Hydrolysis of IBr. *Inorg. Chem.* **1991,** *30* (25), 4838-4845.

Updyke, K. M.; Nguyen, T. B.; Nizkorodov, S. A. Formation of Brown Carbon Via Reactions of Ammonia with Secondary Organic Aerosols from Biogenic and Anthropogenic Precursors. *Atmos. Environ.* **2012**, *63*, 22-31.

Usher, C. R.; Michel, A. E.; Grassian, V. H. Reactions on Mineral Dust. *Chem. Rev.* **2003**, *103* (12), 4883-4940.

van Elk, E. P. Gas-Liquid Reactions - Influence of Bulk and Mass Transfer on Process Performance. Ph.D., University of Twente, Enschede, 2001.

Veres, P.; Roberts, J. M.; Burling, I. R.; Warneke, C.; de Gouw, J.; Yokelson, R. J. Measurements of Gas-Phase Inorganic and Organic Acids from Biomass Fires by Negative-Ion Proton-Transfer Chemical-Ionization Mass Spectrometry. *J. Geophys. Res.-Atmos.* **2010**, *115*.

Vesala, T.; Kulmala, M.; Rudolf, R.; Vrtala, A.; Wagner, P. E. Models for Condensational Growth and Evaporation of Binary Aerosol Particles. *J. Aerosol Sci.* **1997**, *28* (4), 565-598.

Vieceli, J.; Roeselová, M.; Potter, N.; Dang, L. X.; Garrett, B. C.; Tobias, D. J. Molecular Dynamics Simulations of Atmospheric Oxidants at the Air−Water Interface: Solvation and Accommodation of OH and O_3. *J. Phys. Chem. B* **2005**, *109* (33), 15876-15892.

Vione, D.; Maurino, V.; Minero, C.; Pelizzetti, E.; Harrison, M. A. J.; Olariu, R.-I.; Arsene, C. Photochemical Reactions in the Tropospheric Aqueous Phase and on Particulate Matter. *Chem. Soc. Rev.* **2006**, *35* (5), 441-453.

Vogel, A. L.; Äijälä, M.; Brüggemann, M.; Ehn, M.; Junninen, H.; Petäjä, T.; Worsnop, D. R.; Kulmala, M.; Williams, J.; Hoffmann, T. Online Atmospheric Pressure Chemical Ionization Ion Trap Mass Spectrometry (APCI-IT-MS^n) for Measuring Organic Acids in Concentrated Bulk Aerosol - a Laboratory and Field Study. *Atmos. Meas. Tech.* **2013,** *6* (2), 431-443.

von Glasow, R. Atmospheric Chemistry: Sun, Sea, and Ozone Destruction. *Nature* **2008,** *453* (7199), 1195-1196.

von Schneidemesser, E.; Monks, P. S.; Allan, J. D.; Bruhwiler, L.; Forster, P.; Fowler, D.; Lauer, A.; Morgan, W. T.; Paasonen, P.; Righi, M.; Sindelarova, K.; Sutton, M. A.

Chemistry and the Linkages between Air Quality and Climate Change. *Chem. Rev.* **2015**, *115* (10), 3856-3897.

von Sonntag, C.; von Gunten, U. *Chemistry of Ozone in Water and Wastewater Treatment.* IWA Publishing: 2012. p 302.

Wagner, P. E. A Constant-Angle Mie Scattering Method (CAMS) for Investigation of Particle Formation Processes. *J. Colloid Interface Sci.* **1985**, *105* (2), 456-467.

Wang, Y.; Shen, L.; Wu, S.; Mickley, L.; He, J.; Hao, J. Sensitivity of Surface Ozone over China to 2000–2050 Global Changes of Climate and Emissions. *Atmos. Environ.* **2013**, *75*, 374-382.

Washenfelder, R. A.; Attwood, A. R.; Brock, C. A.; Guo, H.; Xu, L.; Weber, R. J.; Ng, N. L.; Allen, H. M.; Ayres, B. R.; Baumann, K.; Cohen, R. C.; Draper, D. C.; Duffey, K. C.; Edgerton, E.; Fry, J. L.; Hu, W. W.; Jimenez, J. L.; Palm, B. B.; Romer, P.; Stone, E. A.; Wooldridge, P. J.; Brown, S. S. Biomass Burning Dominates Brown Carbon Absorption in the Rural Southeastern United States. *Geophys. Res. Lett.* **2015**, *42* (2), 653-664.

Whitby, K. T. The Physical Characteristics of Sulfur Aerosols. *Atmos. Environ.* **1978**, *12* (1–3), 135-159.

Wiedinmyer, C.; Tie, X.; Guenther, A.; Neilson, R.; Granier, C. Future Changes in Biogenic Isoprene Emissions: How Might They Affect Regional and Global Atmospheric Chemistry? *Earth Interact.* **2006**, *10* (3), 1-19.

Williams, M. B.; Michelsen, R. R. H.; Axson, J. L.; Iraci, L. T. Uptake of Acetone, Acetaldehyde and Ethanol in Cold Sulfuric Acid Solutions Containing Organic Material: Carbon Accretion Mechanisms. *Atmos. Environ. 2010*, *44* (9), 1145-1151.

Wishart, D. S.; Jewison, T.; Guo, A. C.; Wilson, M.; Knox, C.; Liu, Y.; Djoumbou, Y.; Mandal, R.; Aziat, F.; Dong, E.; Bouatra, S.; Sinelnikov, I.; Arndt, D.; Xia, J.; Liu, P.; Yallou, F.; Bjorndahl, T.; Perez-Pineiro, R.; Eisner, R.; Allen, F.; Neveu, V.; Greiner, R.; Scalbert, A. HMDB 3.0—the Human Metabolome Database in 2013. *Nucleic Acids Res.* **2013**, *41*, D801-D807.

Wishart, D. S.; Knox, C.; Guo, A. C.; Shrivastava, S.; Hassanali, M.; Stothard, P.; Chang, Z.; Woolsey, J. Drugbank: A Comprehensive Resource for in Silico Drug Discovery and Exploration. *Nucleic Acids Res.* **2006**, *34*, D668-D672. 194

Wong, G. T. F.; Zhang, L. S. Seasonal Variations in the Speciation of Dissolved Iodine in the Chesapeake Bay. *Estuar. Coast. Shelf Sci.* **2003,** *56* (5-6), 1093-1106.

Woodhouse, M. T.; Mann, G. W.; Carslaw, K. S.; Boucher, O. Sensitivity of Cloud Condensation Nuclei to Regional Changes in Dimethyl-Sulphide Emissions. *Atmos. Chem. Phys.* **2013**, *13* (5), 2723-2733.

Woodill, L. A.; O'Neill, E. M.; Hinrichs, R. Z. Impacts of Surface Adsorbed Catechol on Tropospheric Aerosol Surrogates: Heterogeneous Ozonolysis and Its Effects on Water Uptake. *J. Phys. Chem. A* **2013**, *117*, 5620-5631.

World Health Organization. *Review of Evidence on Health Aspects of Air Pollution (Revihaap) Project*; Copenhagen, 2013.

Worsnop, D. R.; Shi, Q.; Jayne, J. T.; Kolb, C. E.; Swartz, E.; Davidovits, P. Gas-Phase Diffusion in Droplet Train Measurements of Uptake Coefficients. *J. Aerosol Sci.* **2001**, *32* (7), 877-891.

Worsnop, D. R.; Zahniser, M. S.; Kolb, C. E.; Gardner, J. A.; Watson, L. R.; Van Doren, J. M.; Jayne, J. T.; Davidovits, P. The Temperature Dependence of Mass Accommodation of Sulfur Dioxide and Hydrogen Peroxide on Aqueous Surfaces. *J. Phys. Chem.* **1989**, *93* (3), 1159-1172.

Wren, S. N.; Donaldson, D. J. Glancing-Angle Raman Spectroscopic Probe for Reaction Kinetics at Water Surfaces. *Phys. Chem. Chem. Phys.* **2010,** *12* (11), 2648-2654.

Wu, S.; Mickley, L. J.; Jacob, D. J.; Rind, D.; Streets, D. G. Effects of 2000–2050 Changes in Climate and Emissions on Global Tropospheric Ozone and the Policy-Relevant Background Surface Ozone in the United States. *J. Geophys. Res. Atmos.* **2008**, *113* (D18), D18312.

Xu, L.; Williams, L. R.; Young, D. E.; Allan, J. D.; Coe, H.; Massoli, P.; Fortner, E.; Chhabra, P.; Herndon, S.; Brooks, W. A.; Jayne, J. T.; Worsnop, D. R.; Aiken, A. C.; Liu, S.; Gorkowski, K.; Dubey, M. K.; Fleming, Z. L.; Visser, S.; Prevot, A. S. H.; Ng, N. L. Wintertime Aerosol Chemical Composition, Volatility, and Spatial Variability in the Greater London Area. *Atmos. Chem. Phys.* **2016**, *16*, 1139-1160.

Yamamoto, Y.; Niki, E.; Shiokawa, H.; Kamiya, Y. Ozonation of Organic Compounds. 2. Ozonation of Phenol in Water. *J. Org. Chem.* **1979**, *44*, 2137-2142.

Yang, J.; Cohen Stuart, M. A.; Kamperman, M. Jack of All Trades: Versatile Catechol Crosslinking Mechanisms. *Chem. Soc. Rev.* **2014**, *43*, 8271-8298.

Yang, L.; Nguyen, D. M.; Jia, S.; Reid, J. S.; Yu, L. E. Impacts of Biomass Burning Smoke on the Distributions and Concentrations of C_2–C_5 Dicarboxylic Acids and Dicarboxylates in a Tropical Urban Environment. *Atmos. Environ.* **2013**, *78*, 211-218.

You, Y.; Renbaum-Wolff, L.; Carreras-Sospedra, M.; Hanna, S. J.; Hiranuma, N.; Kamal, S.; Smith, M. L.; Zhang, X.; Weber, R. J.; Shilling, J. E.; Dabdub, D.; Martin, S. T.; Bertram, A. K. Images Reveal That Atmospheric Particles Can Undergo Liquid–Liquid Phase Separations. *Proc. Natl. Acad. Sci.* **2012,** *109* (33), 13188-13193.

14. Zein, A. E.; Coeur, C.; Obeid, E.; Lauraguais, A.; Fagniez, T. Reaction Kinetics of Catechol (1,2-Benzenediol) and Guaiacol (2-Methoxyphenol) with Ozone. *J. Phys. Chem. A* **2015**, *119*, 6759-6765.

Zhang, R.; Wang, G.; Guo, S.; Zamora, M. L.; Ying, Q.; Lin, Y.; Wang, W.; Hu, M.; Wang, Y. Formation of Urban Fine Particulate Matter. *Chem. Rev.* **2015**, *115* (10), 3803-3855.

Zheng, G.; He, K.; Duan, F.; Cheng, Y.; Ma, Y. Measurement of Humic-Like Substances in Aerosols: A Review. *Environ. Pollut.* **2013**, *181*, 301-314.

Zhou, R.; Guzman, M. I. CO_2 Reduction under Periodic Illumination of ZnS. *J. Phys. Chem. C* **2014**, *118*, 11649-11656.

Zhu, X.-Q.; Wang, C.-H.; Liang, H. Scales of Oxidation Potentials, pKa, and BDE of Various Hydroquinones and Catechols in DMSO. *J. Org. Chem.* **2010**, *75*, 7240-7257.

Ziemann, P. J. Aerosol Products, Mechanisms, and Kinetics of Heterogeneous Reactions of Ozone with Oleic Acid in Pure and Mixed Particles. *Faraday Discuss.* **2005**, *130*, 469-490.

EDUCATION

- Mercyhurst College (Sept 2005 – Nov 2009)

  o Bachelor of Science (GPA: 3.77) - Biochemistry and Forensic Science

  o Latin Honors Graduate – Magna Cum Laude

PROFESSIONAL EXPERIENCE

- Research Assistant at the University of Kentucky (December 2011 – present): Guzman Group

  o Mass spectrometry studies of the reactivity of halides with ozone at the air-water interface

  o Studies of the reactivity of phenols with ozone at the air-water and air-solid interfaces

  o Development of trace gas sensing system for field studies onboard unmanned aerial vehicles

- Teaching Assistant at the University of Kentucky – Department of Chemistry

  o Teaching Assistant – Organic Chemistry Lab I (CHE 231; Fall 2011, Spring 2015, Spring 2017, Summer II 2017) and II (CHE 233; Spring 2012); General Chemistry I Recitation (CHE 105; Fall 2012)

  o Guest Lecturer – Environmental Chemistry (CHE 565) 1 lecture each - Spring 2016 and 2017; Atmospheric Chemistry (CHE 580); 2 lectures - Fall 2016. Instructor for both courses: Dr. Marcelo I. Guzman

AWARDS, FELLOWSHIPS, AND HONORS

- University of Kentucky Department of Chemistry Outstanding Graduate Research Award - Spring 2016

- University of Kentucky Women's Club Fellowship – December 2015

- Selection of "Heterogeneous Oxidation of Catechol" for Atmospheric Physical Chemistry Special Issue of *Journal of Physical Chemistry A*

- American Geophysical Union Outstanding Student Paper Award – December 2013

- Naff Symposium Student Poster Competition – First Place, April 2013

- Max Steckler Fellowship – Awarded Yearly since 2012

- University of Kentucky Department of Chemistry Fast Start Award – May 2012

PUBLICATIONS

- Pillar, E.A.; Guzman, M.I. Oxidation of Substituted Catechols at the Air-Water Interface: Production of Carboxylic Acids, Quinones, and Polyphenols. *Environmental Science and Technology*. **2017**, *51*, 4951.

- Pillar, E.A.; Zhou, R.; Guzman, M.I. Heterogeneous Oxidation of Catechol. *Journal of Physical Chemistry A*. **2015**, *115*, 10349.

- Pillar, E.A.; Camm, R.C.; Guzman, M.I. Catechol Oxidation by Ozone and Hydroxyl Radicals at the Air-Water Interface. *Environmental Science & Technology,* **2014**, *48*, 14352.

- Pillar, E.A.; Guzman, M.I.; Rodriguez, J.M. Conversion of Iodide to Hypoiodous Acid and Iodine in Aqueous Microdroplets Exposed to Ozone. *Environmental Science & Technology,* **2013**, *47*, 10971.

ORAL PRESENTATIONS

- Pillar, E.A; Guzman, M.I. Ozonolysis of Catechol at the Gas-Solid Interface. Central Regional Meeting of the American Chemical Society, Covington, KY, May 18, 2016.

- Pillar, E.A; Guzman, M.I. Ozonolysis of Catechol at the Gas-Solid Interface. 250th National Meeting of the American Chemical Society, Boston, MA, August 18, 2015.

- Pillar, E.A; Guzman, M.I. Transformation of Chlorinated Pesticides at the Air-Water Interface. Southeastern Regional Meeting of the American Chemical Society, Nashville, TN, October 16, 2014.

- Guzman, M.I; Pillar, E.A. Oxidation of Polyphenols at the Air-Water Interface. Southeastern Regional Meeting of the American Chemical Society, Nashville, TN, October 16, 2014.

- Pillar, E.A; Guzman, M.I. Heterogeneous Reactions of Ozone with Aqueous Iodide. Southeastern Regional Meeting of the American Chemical Society, Atlanta, GA, November 2013.

POSTER PRESENTATIONS

- Pillar, E.A.; Schuyler, T.J.; Bailey, S.C.C.; Guzman, M.I. Development of an Economic, Portable Sensor Network for the Monitoring of Trace Tropospheric Gases. 6th Annual Tracy Farmer Institute Sustainability Forum, Lexington, KY, December 1, 2016.

- Pillar, E.A.; Kaindu, J.; Guzman, M.I. Development of an Economic, Portable Sensor Network for the Monitoring of Trace Tropospheric Gases. 14th Annual International Global Atmospheric Chemistry Science Conference, Breckenridge, CO, September 27, 2016.

- Guzman, M.I.; Pillar E.A. Catechol Oxidation by Ozone and Hydroxyl Radicals at the Air-Water Interface. Kentucky EPSCoR Annual Conference, Lexington, KY, May 22, 2015.

- Pillar, E.A.; Guzman, M.I. Ozonolysis of Catechol at the Gas-Solid Interface. 41st Annual Naff Symposium on Chemistry and Molecular Biology, Lexington, KY, March 6, 2015.

- Pillar, E.A.; Guzman, M.I. Heterogeneous Reactions of Ozone with Aqueous Iodide. American Geophysical Union Fall Meeting, San Francisco, CA, December 9, 2013.

- Guzman, M.I.; Pillar E.A. Ozone Loss Catalyzed by Iodide at the Air-Water Interface. Kentucky EPSCoR Annual Conference, Lousiville, KY, October 17, 2013.

- Pillar, E.A.; Guzman, M.I. Heterogeneous Reactions of Ozone with Aqueous Iodide. 39th Annual Naff Symposium on Chemistry and Molecular Biology, Lexington, KY, April 12, 2013.

ARTICLES AND PRESS RELEASES

- Aromatic pollutants emitted during combustion and wood burning contribute to the formation of brown clouds. https://phys.org/news/2017-05-aromatic-pollutants-emitted-combustion-wood.html

- NSF Awards $6 Million to UK and Three Partner Schools to Develop Weather Research Drones. https://chem.as.uky.edu/nsf-awards-6-million-uk-and-three-partner-schools-develop-weather-research-drones

- Secondary oxidants produced during heterogeneous processing of aromatic pollutants by gaseous ozone. http://phys.org/news/2015-10-secondary-oxidants-heterogeneous-aromatic-pollutants.html

- How the complexity of interfacial chemistry translates into atmospheric changes. http://phys.org/news/2014-12-complexity-interfacial-chemistry-atmospheric.html

- Rarified Air: Liz Pillar. https://chem.as.uky.edu/rarefied-air-liz-pillar

SCIENCE OUTREACH

- Science Demonstrator at the Carnegie Science Center (Feb 2011- June 2011)

  o Present and assist with science demonstration shows geared towards K–12 students

- Participant in K–12 outreach with the Guzman Group and the Chemistry Graduate Student Association

  o Coordinate and present demonstrations geared towards elementary and middle schoolers as a part of the annual National Chemistry Week Demonstration Show in the third week of October for the years 2011, 2012, 2013, 2015, and 2016.

  o Gave building and laboratories tour, and answered questions as part of STEM camp for Hope Hill Youth Services & Family Connection Inc., underprivileged girls, grades 7-12 (Summer 2015)

  o Co-mentored underrepresented high school senior student (Jimmy Kaindu) participating in research experience at UK (2015-2016 school year).

  o Provided a hands-on chromatography activity during the Summer Science Camp for middle schoolers as an immersive experience in STEM disciplines (Summer 2014).

- Facilitated a hands-on activity to demonstrate light absorption by chromophores at Winburn Middle School Science Night (Jan 17, 2013).